

Dissertation

Control of vibrations of civil engineering structures with special emphasis on tall buildings

ausgeführt zum Zwecke der Erlangung des akademischen Grades
eines Doktors der technischen Wissenschaften unter der Leitung von

o.Univ.Prof. Dipl.-Ing. Dr.techn. Dr.h.c. Franz Ziegler
E201
Institut für Allgemeine Mechanik

eingereicht an der Technischen Universität Wien
Fakultät für Bauingenieurwesen

von

Dipl.-Ing. Markus J. Hochrainer MSc.
1200 Wien, Universumstr. 12/25

Wien, Dezember 2001

Contents

1. FUNDAMENTALS	1
1.1. DYNAMIC BEHAVIOUR OF SINGLE-DEGREE-OF-FREEDOM SYSTEMS	1
1.1.1. EQUATION OF MOTION	1
1.2. EQUATIONS OF MOTION FOR LINEAR MDOF STRUCTURES	13
1.3. ENERGY CONSIDERATIONS	17
1.4. STATE TRANSFORMATIONS AND STATE SPACE REPRESENTATION	19
1.5. REFERENCES	22
2. OVERVIEW OF PASSIVE DEVICES FOR VIBRATION DAMPING	24
2.1. METALLIC DAMPERS	24
2.2. FRICTION DAMPERS	25
2.3. VISCOELASTIC DAMPERS	27
2.4. VISCOUS FLUID DAMPERS	28
2.5. DYNAMIC VIBRATION ABSORBERS	30
2.5.1. TUNED LIQUID DAMPERS	30
2.5.2. SEISMIC ISOLATION	33
2.6. TUNED MASS DAMPERS	37
2.6.1. BASIC EQUATIONS	38
2.6.2. DENHARTOG'S SOLUTION FOR OPTIMAL ABSORBER PARAMETER	40
2.6.3. STRUCTURAL IMPLEMENTATIONS	47
2.7. SMART MATERIALS	47
2.7.1. SHAPE MEMORY ALLOYS	48
2.7.2. PIEZOELECTRIC MATERIALS	49
2.7.3. ELECTORRHEOLOGICAL FLUID	51
2.7.4. MAGNETORHEOLOGICAL FLUID	51
2.8. REFERENCES	51

3. STATE OF THE ART REVIEW ON TUNED LIQUID COLUMN DAMPER	55
3.1. REFERENCES	67
4. MATHEMATICAL DESCRIPTION AND DISCUSSION OF THE GENERAL SHAPED TLCD	70
4.1. EQUATIONS OF MOTION FOR PLANE TLCD	70
4.1.1. DERIVATION OF THE EQUATION OF MOTION USING THE LAGRANGE EQUATIONS OF MOTION	72
4.1.2. BERNOULLI'S EQUATION FOR MOVING COORDINATE SYSTEMS	74
4.1.3. DERIVATION OF THE EQUATION OF MOTION APPLYING THE GENERALISED BERNOULLI EQUATION	78
4.2. REACTION FORCES AND MOMENTS FOR THE PLANE TLCD	79
4.3. DETERMINATION OF THE AIR SPRING EFFECT	82
4.4. GENERAL DISCUSSION OF THE TLCD'S DESIGN AND ITS ADVANTAGES	87
4.4.1. INFLUENCE OF GEOMETRY	87
4.4.2. INSTALLATION AND MAINTENANCE	88
4.4.3. IN SITU TESTING OF STRUCTURES	89
4.5. TORSIONAL TUNED LIQUID COLUMN DAMPER (TTLCD)	89
4.5.1. INTRODUCTION	89
4.5.2. EQUATION OF MOTION	90
4.5.3. FORCES AND MOMENTS	92
4.6. REFERENCES	95
5. OPTIMAL DESIGN OF TLCDS ATTACHED TO HOST STRUCTURES	97
5.1. ANALOGY BETWEEN TMD AND TLCD FOR SDOF HOST STRUCTURE	97
5.4.1. APPLICATION OF TMD-TLCD ANALOGY TO SDOF HOST STRUCTURE WITH TLCD ATTACHED	100
5.2. CONTROL OF MDOF HOST STRUCTURES BY TLCD	103
5.3. GENERAL REMARKS ON TMD-TLCD ANALOGY	107
5.4. REFERENCES	108

6. EQUATIONS OF MOTION OF LINEAR MDOF STRUCTURES	109
6.1. INTRODUCTION	109
6.2. GENERAL APPROACH	109
6.3. GENERAL APPROACH FOR FRAMED STRUCTURES	110
6.4. KINEMATIC CONSTRAINTS	112
6.5. STATIC CONDENSATION	113
6.6. MODAL TRUNCATION	114
6.7. MODAL REDUCTION	118
6.8. EXAMPLES	122
6.9. REFERENCES	123
 7. OPTIMISATION OF MULTIPLE TLCDs AND MDOF STRUCTURAL SYSTEMS IN THE STATE SPACE DOMAIN	 124
7.1. OPTIMISATION FOR FREE VIBRATION OF MDOF STRUCTURE WITH SEVERAL TLCD INSTALLED	126
7.2. FREQUENCY RESPONSE OPTIMISATION FOR MDOF STRUCTURES WITH SEVERAL TLCD INSTALLED	129
7.2.1. DETERMINATION OF A PERFORMANCE INDEX IN THE FREQUENCY DOMAIN	129
7.3. STOCHASTIC OPTIMISATION: MINIMUM VARIANCE	132
7.4. COMMENTS ON SYSTEMS WITH MULTIPLE INPUTS	135
7.5. COLOURED NOISE INPUT	135
7.6. REMARKS ON THE NUMERICAL OPTIMISATION AND CHOICE OF INITIAL CONDITIONS	138
7.7. REFERENCES	139
 8. ACTIVE DEVICES FOR VIBRATION DAMPING	 140
8.1. ACTIVE CONTROL	141
8.2. HYBRID CONTROL	142
8.3. SEMI ACTIVE CONTROL SYSTEMS	144
8.4. ACTIVE TUNED LIQUID COLUMN DAMPER (ATLCD)	145
8.4.1. STATE SPACE REPRESENTATION	149

8.5.	OPTIMAL CONTROL	150
8.6.	MODAL CONTROL	154
8.7.	POLYNOMIAL AND SWITCHING CONTROL LAWS	155
8.8.	REFERENCES	158

9.	APPLICATION TO REAL STRUCTURES AND NUMERICAL STUDIES	162
-----------	---	------------

9.1.	3D-BUILDING WITH TRANSLATIONAL AND TORSIONAL PASSIVE TLCD	162
9.2.	WIND EXCITED 47-STORY TALL BUILDING	176
9.2.1.	OPTIMAL TMD DESIGN	178
9.2.2.	TLCD DESIGN	180
9.2.3.	SIMULATION OF TURBULENT DAMPING	184
9.2.4.	DEVICE CONFIGURATION AND CONCLUDING REMARKS	185
9.3.	3-DOF BENCHMARK STRUCTURE	188
9.3.1.	INTRODUCTION	188
9.3.2.	TLCD DESIGN	189
9.3.3.	IMPLEMENTATION OF AN ACTIVE PRESSURE CONTROL	193
9.4.	76-STORY BENCHMARK STRUCTURE	200
9.4.1.	RESPONSE OF ORIGINAL BUILDING	203
9.4.2.	PASSIVE TLCD	206
9.4.3.	PERFORMANCE CRITERIA	213
9.5.	BENCHMARK CONTROL PROBLEM FOR SEISMICALLY EXCITED STRUCTURE	220
9.5.1.	TLCD DESIGN	223
9.5.2.	ACTIVE CONTROL	226
9.6.	REFERENCES	231

APPENDIX	233
-----------------	------------

A.	EQUIVALENT LINEARISATION	233
B.	LYAPUNOV EQUATION	235
C.	NOTATION	236

1. Fundamentals

Traditionally, most civil engineering structures have been designed and considered as static systems, but the development and application of modern protective elements demands a more precise analysis. Instead, buildings, towers or bridges must be considered as dynamic systems, allowing better mathematical modelling and a correct investigation of the dynamic behaviour. In this introductory section a simple structure is idealised as a single-degree-of-freedom (SDOF) system with a lumped mass on a supporting structure, thus representing the prototype of a spring-mass-dashpot system. Such a linear oscillator model permits the investigation of typical dynamic effects like free and forced vibration, the influence of damping and the resonance phenomenon. While such a simple model is useful for developing an understanding of the dynamic behaviour, most real structures must be represented by multiple-degree-of-freedom (MDOF) systems for better reproduction of the actual structural behaviour. After a basic treatment of single-degree-of-freedom systems, for which some general analysis procedures are outlined, the structural modelling is extended to multiple-degree-of-freedom systems where resonance phenomena, a system representation in state space description as well as basic concepts, like state transformations and modal analysis are discussed. The introduction is mainly influenced by presentations included in Ziegler¹, Soong and Dargush², Chopra³, Clough-Penzien⁴ and Magnus⁵.

1.1. Dynamic behaviour of single-degree-of-freedom systems

1.1.1. Equation of motion

The simplest model that demonstrates most essential response characteristics when subjected to dynamic loading is the single-degree-of-freedom system, for two simple models see Figure 1-1.

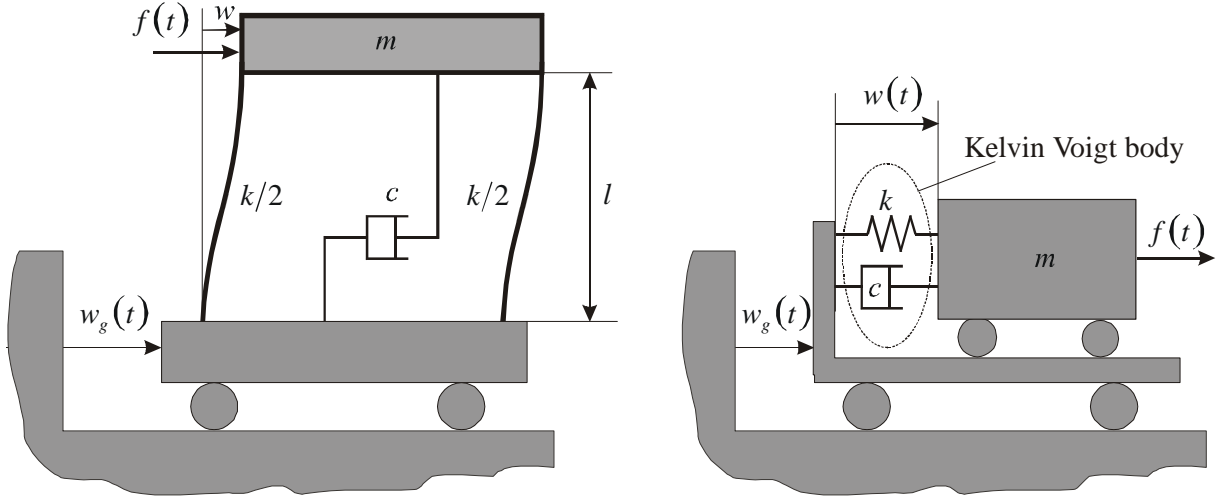


Figure 1-1: Single degree of freedom model excited by a (wind) force $f(t)$ and a ground motion $w_g(t)$: a) shear frame model b) mass-spring-dashpot system

It consists of a mass m concentrated on the roof level and is supported by a massless frame, providing a total linear elastic stiffness k to the system - the reduced stiffness due to the vertical loading of the column (P- Δ -effect) is included, and approximately reduces the unloaded column stiffness \bar{k} by $k = \bar{k} - 6mg/5l$, where g denotes the constant of gravity acceleration, see Ziegler⁶. A linear viscous damper, representing a simple model of material damping has the viscosity c and is in parallel connection to the Hookean spring thereby forming a Kelvin-Voigt body. The system is subjected to a seismic disturbance characterised by a spatially uniform, time-dependent ground acceleration \ddot{w}_g , and a time dependent single force $f(t)$. The lateral displacement $w(t)$, relative to the ground, describes the response of the excited system, and the absolute displacement is

$$w_t(t) = w_g(t) + w(t). \quad (1-1)$$

Assuming spring and damping forces linearly proportional to the displacement and the velocity, respectively, the equation of motion for this SDOF system follows directly from Newton's law and can be written as

$$m \ddot{w} + c \dot{w} + k w = -m \ddot{w}_g + f \quad (1-2)$$

in which the differentiation with respect to time is given by the superimposed dots, e.g. in the material description $\dot{x} = \frac{d x}{d t}$ or $\ddot{x} = \frac{d^2 x}{d t^2}$. If appropriate, the time argument is skipped in time dependent quantities to gain clarity in long expressions. It is often convenient to introduce the effective loading

$$f_{eff}(t) = -m \ddot{w}_g(t) + f(t), \quad (1-3)$$

so that it is not necessary to distinguish between force loading and ground excitation.

1.1.1.1. Free vibrations

A structure is said to perform free vibration if it is disturbed from its equilibrium position and then allowed to vibrate without any external dynamic excitation. In absence of any effective loading, the right hand terms of Eq. (1-2) vanish and it simplifies to the case of natural vibration. If the mass is given some initial displacement $w(0)$ and velocity $\dot{w}(0)$ the response of the SDOF system becomes

$$w_h(t) = w_1 \exp(-\zeta \omega_0 t) \cos(\omega_D t - \phi_1) \quad (1-4)$$

$$\tan \phi_1 = \frac{1}{(1-\zeta^2)^{1/2}} \frac{\frac{\dot{w}(0)}{\omega_0} + \zeta w(0)}{w(0)}, \quad w_1 = \left(\frac{w(0)}{1-\zeta^2} \left(w(0) + 2\zeta \frac{\dot{w}(0)}{\omega_0} \right) + \frac{1}{1-\zeta^2} \frac{\dot{w}(0)^2}{\omega_0^2} \right)^{1/2} \quad (1-5)$$

where ω_D and ζ represent the damped natural circular frequency and the nondimensional damping ratio given by

$$\omega_D = \omega_0 \sqrt{1-\zeta^2}, \quad \zeta = \frac{c}{2m\omega_0} < 1. \quad (1-6)$$

and ω_0 denotes the natural circular frequency of the undamped structure, defined as

$$\omega_0 = \sqrt{\frac{k}{m}} = 2\pi f_0 = \frac{2\pi}{T_0}, \quad (1-7)$$

Notice, that for $\zeta = 0$, the free vibration response Eq.(1-4) does not decay and in absence of dissipation the motion is characterised by the perpetual exchange of potential (strain) and

kinetic energies. Damping has the effect of lowering the natural circular frequency from ω_0 to ω_D and lengthening the natural period from T_0 to $T_D = 2\pi/\omega_D$. These effects are negligible for damping ratios ζ below 20%, a range that includes material damping of all civil engineering structures of interest. Increasing ζ to the critical damped value $\zeta = \zeta_{crit} = 1$ changes the response character completely, since ω_D becomes complex and the system response Eq. (1-4) loses its vibrational characteristics. Instead, the structural response of such an over-critically damped system is described by two decaying exponential functions, obtained from the sine and cosine functions with complex arguments. However, those highly damped systems do not occur in the elastic deformation range of civil engineering structures. Common damping ratios for steel, concrete and wooden structures are between $\zeta = 0.5\%$ and $\zeta = 3\%$, presuming linear elastic behaviour. Figure1-2 illustrates the SDOF system's displacement in natural vibration for various damping factors with the initial conditions $w_h(0) = w_0$ and $\dot{w}_h(0) = \omega_0 w_0$.

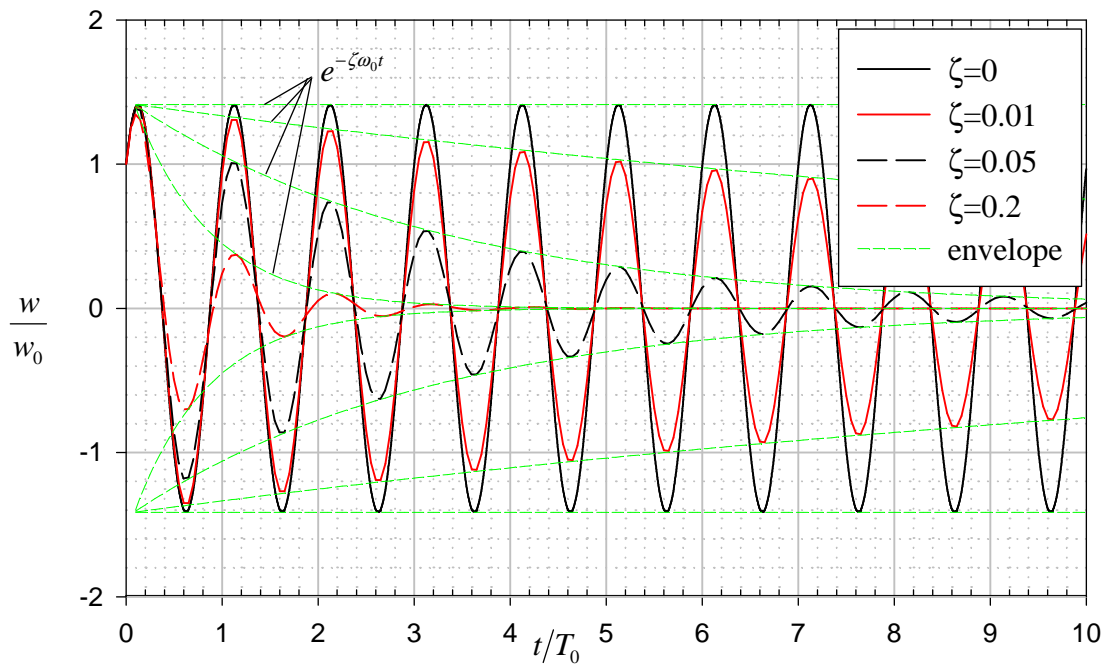


Figure1-2: Free vibration response for various damping ratios

1.1.1.2. Forced vibrations – time harmonic forcing

The response of SDOF systems to harmonic excitation is a classical topic in structural dynamics, not only because such excitations often occur in engineering systems, but because

the frequency response function provides indeed insight, how the system will respond to more general time dependent forces. At this point it is useful to distinguish between the excitation due to a pure force loading and the vibrations caused by a ground motion.

1.1.1.3. Force loading

Firstly, in the case of forced vibrations, let the ground acceleration \ddot{w}_g be put to zero, thus, effective forcing becomes $f_{eff} = f_0 \cos(\omega t)$. Consequently, a time-harmonic force of magnitude f_0 and frequency ν excites the SDOF model. This effective loading can also be described by the real part of the complex exponential function

$$f_{eff} = \begin{cases} \text{Re}(f_0 e^{i\nu t}) = f_0 \cos(\nu t) & \text{for } t \geq 0 \\ 0 & \text{for } t < 0 \end{cases} \quad (1-8)$$

with $i = \sqrt{-1}$ representing the imaginary unit. Due to the superposition principle, the total response can be given as sum of the homogenous and a particular solution

$$w(t) = w_h(t) + w_p(t), \quad (1-9)$$

Starting with homogenous initial conditions the solution of Eq.(1-2) due to the harmonic force is obtained in the complex form:

$$w(t) = w_1 \exp i(\nu t - \phi_1) + \exp(-\zeta \omega_0 t) w_2 \exp i(\omega_D t - \phi_2), \quad (1-10)$$

in which w_1 , w_2 , ϕ_1 and ϕ_2 denote amplitudes and phase angles, respectively, which are given by,

$$w_1 = \frac{f_0}{k} \frac{1}{\left((1-\gamma^2)^2 + (2\zeta\gamma)^2\right)^{1/2}}, \quad w_2 = \frac{w_1}{\sqrt{1-\zeta^2}} \quad (1-11)$$

$$\tan \phi_1 = \frac{2\gamma\zeta}{1-\gamma^2}, \quad \tan \phi_2 = \frac{\zeta}{(1-\zeta^2)^{1/2}} \frac{1+\gamma}{1-\gamma} \quad (1-12)$$

γ denotes the ratio of the forcing to the undamped natural frequency,

$$\gamma = \frac{\nu}{\omega_0}. \quad (1-13)$$

The first term appearing in Eq.(1-10) corresponds to the steady-state solution, whereas the second describes the transient response component, which might be responsible for peaks in the transient regime. Due to damping the amplitude of transient response decays and, after several periods, the steady-state term will cause the dominant response contribution.

Referring the steady state displacement amplitude w_1 to the static displacement w_{st} defines the response function, $A_d(\gamma)$, for real input

$$A_d(\gamma) = \frac{w_1(\gamma) \exp(-i\phi_1)}{w_{st}} = \left[(1 - \gamma^2) + 2i\zeta\gamma \right]^{-1}, \quad (1-14)$$

$$w_{st} = \frac{f_0}{k}. \quad (1-15)$$

The absolute value of $A_d(\gamma)$ is called amplitude response function and measures the amplitude magnification when compared to the static load case, whereas phase angle between the excitation and the response is described by the phase shift $\arg(A_d(\gamma))$. Both quantities are respectively given by

$$|A_d(\gamma)| = \left[(1 - \gamma^2)^2 + (2\zeta\gamma)^2 \right]^{-\frac{1}{2}}, \quad (1-16)$$

$$\arg(A_d(\gamma)) = \tan^{-1} \left[\frac{2\zeta\gamma}{1 - \gamma^2} \right], \quad (1-17)$$

and they are of vital interest for dynamic analysis. The amplitude response magnification can e.g. be used to determine local stress distributions to estimate the possibility of material fatigue, even within elastic limits: the admissible stress amplitude decreases with the number of load cycles according to Wöhler's curve, see e.g. Chwalla⁷

1.1.1.4. Ground excitation

The second loading case, by ground excitation, can be treated analogously, if the effective force excitation is given by the ground excitation forcing $f_{eff} = -v^2 w_g \cos(vt)$. Thus the solution can be given by Eq.(1-10), when replacing f_0 by f_{eff} .

When referring the steady state response to the ground excitation input w_g , it is possible to define the complex displacement frequency response function

$$A_d(\gamma_g) = \left[(1 - \gamma_g^2) + 2i\zeta\gamma_g \right]^{-1} \quad (1-18)$$

Again, the absolute values of $A_d(\nu)$ and the phase shift $\arg(A_d(\nu))$ are

$$|A_d(\gamma_g)| = \left[(1 - \gamma_g^2)^2 + (2\zeta\gamma_g)^2 \right]^{-\frac{1}{2}}, \quad \arg(A_d(\gamma_g)) = \tan^{-1} \left[\frac{2\zeta\gamma_g}{1 - \gamma_g^2} \right], \quad (1-19)$$

but in contrast to the force loading of Section 1.1.1.3 the reciprocal nondimensional excitation frequency γ_g is defined as

$$\gamma_g = \gamma^{-1} = \frac{\omega_0}{\nu}. \quad (1-20)$$

1.1.1.5. Resonant vibrations

Apparently, Eq.(1-14) and Eq.(1-18) are identical but the difference between the two excitation types lies in the definition of the non-dimensional frequency γ , namely of Eq.(1-13) and $\gamma_g = \gamma^{-1}$ of Eq.(1-20). As it is either defined by ν/ω_0 or reciprocally by ω_0/ν , the response functions are mirrored about the resonance frequency $\gamma = 1$. Besides the displacement response curve, the frequency response curves of the velocity $A_v(\gamma) = i\gamma A_d(\gamma)$ and of the acceleration $A_a(\gamma) = -\gamma^2 A_d(\gamma)$, are of equal importance, when characterising dynamic systems. It is understood, that γ_g has to be substituted in case of base excitation. All frequency response curves are represented parametrically with respect to the damping coefficient, in a fourfold logarithmic diagram named after Blake, see Figure 1-3a.

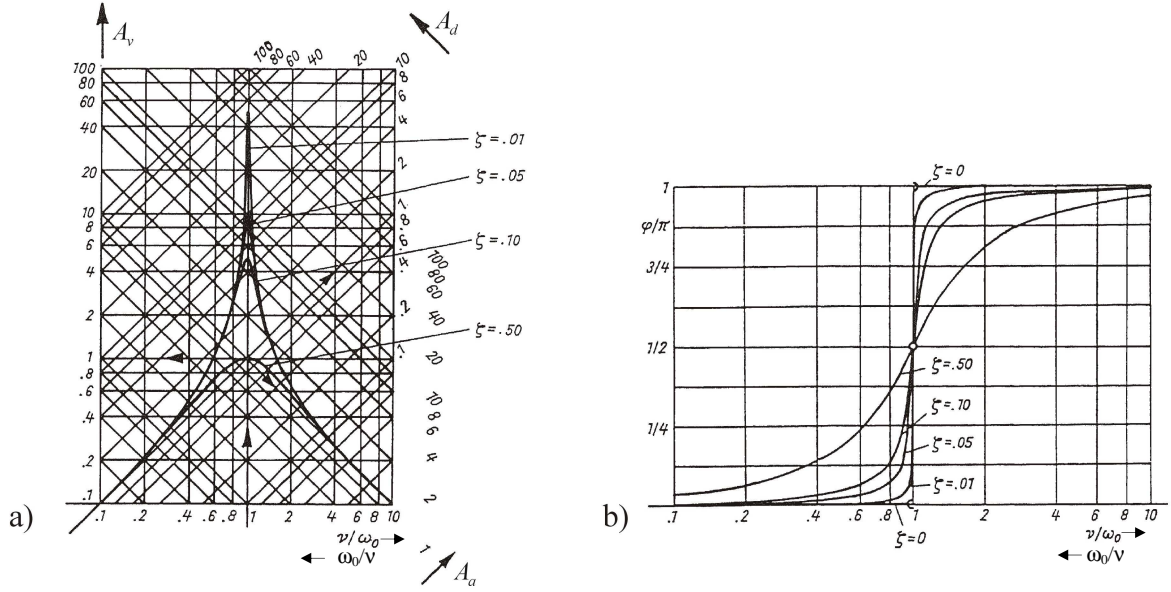


Figure 1-3: a) Blake's diagram: Amplitude frequency response function of displacement, velocity and acceleration b) Phase frequency response of the steady state vibrations, see Ziegler¹

Under steady state conditions, the maximum displacement magnification occurs at the resonance frequency ω_D and is given by

$$\max[A_d(\gamma)] = \frac{1}{2\zeta\sqrt{1-\zeta^2}}. \quad (1-21)$$

For weakly damped systems $\zeta < 0.2$ it can be approximated by $\max[A_d(\gamma)] = 1/2\zeta$. Figure 1-3b displays the phase frequency response curves parametrically with respect to the damping. The phase shift at resonance is always $\pi/2$, which is of practical value if a resonance has to be determined experimentally. The resonance magnification is only limited by damping, e.g. for $\zeta = 0.01$ the amplification factor is approximately 50 whereas for $\zeta = 0.2$ it decreases to 2.5, for structures with identical static behaviour. It is often helpful to work with a slightly modified notation of the frequency response function where absolute frequencies replace the non-dimensional frequencies γ or γ_g . The simple relation

$$H(v) = A_d\left(\frac{v}{\omega_0}\right), \quad (1-22)$$

$$H(v_g) = A_d\left(\frac{\omega_0}{v_g}\right),$$

can be utilised to obtain the frequency response function $H(\gamma)$ or $H(\gamma_g)$.

1.1.1.6. Transient resonant vibrations

If a resonant harmonic force excitation of amplitude f_0 is applied to a lightly damped SDOF system at rest, then the amplitudes w_1 and w_2 of Eq.(1-11), and the phase angles ϕ_1 and ϕ_2 of Eq.(1-12) can be approximated by

$$w_1 = w_2 \approx \frac{f_0}{k} \frac{1}{2\zeta}, \quad (1-23)$$

$$\phi_1 = \frac{\pi}{2}, \quad \phi_2 = -\frac{\pi}{2}$$

where $\omega_D \approx \omega_0$ and $\zeta \ll 1$. Inserting into Eq.(1-10) renders the resonant transient vibration response,

$$w_{res}(t) = \frac{f_0}{k} \frac{1}{2\zeta} (1 - \exp(-\zeta \omega_0 t)) \sin(\omega_0 t), \quad (1-24)$$

For an undamped system, $\zeta = 0$, Hospital's rule must be applied to obtain

$$w_{res}(t) = \frac{f_0}{k} \frac{\omega t}{2} \sin(\omega_0 t), \quad (1-25)$$

which describes an increasing unbounded vibration. For $\zeta > 0$ Figure1-4 visualises the transient vibration's envelope function. Another transient phenomenon for undamped SDOF oscillators is the beat-like-vibration, if the excitation and the natural frequency only differ slightly. In this case Eqs.(1-11) and (1-12) render $w_1 = w_2 = \frac{f_0}{k} \frac{1}{1-\gamma^2}$, and $\phi_1 = 0$, $\phi_2 = \pi$, respectively. Inserting into Eq.(1-10) and applying the additive theorem for harmonic functions renders

$$w_p(t) = -\frac{f_0}{k} \frac{1}{1-(\nu/\omega_0)^2} \sin\left(\frac{\nu - \omega_D}{2} t\right) \sin\left(\frac{\nu + \omega_D}{2} t\right). \quad (1-26)$$

Figure 1-1 displays such a beating vibration for an undamped system, $\zeta = 0$ and $|\nu - \omega| \ll \nu + \omega$.

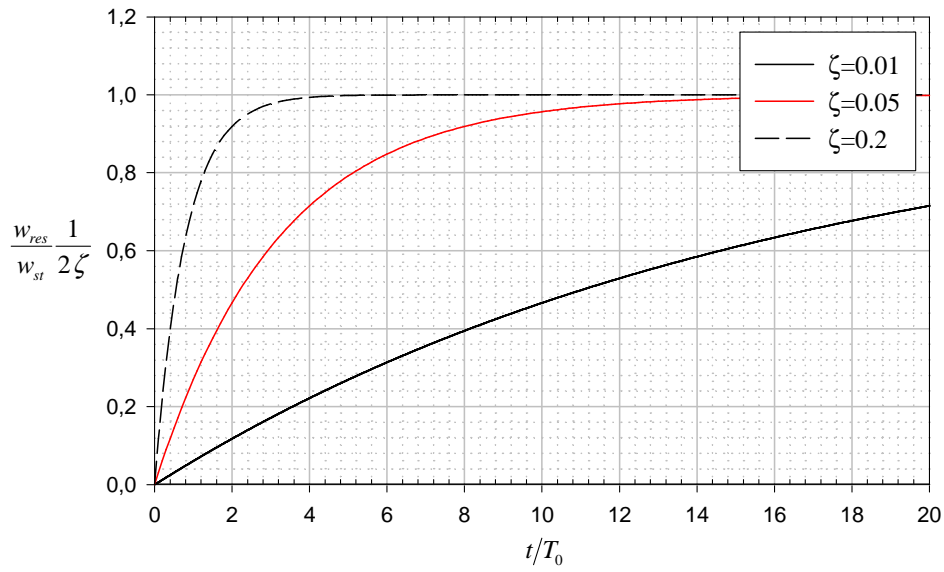
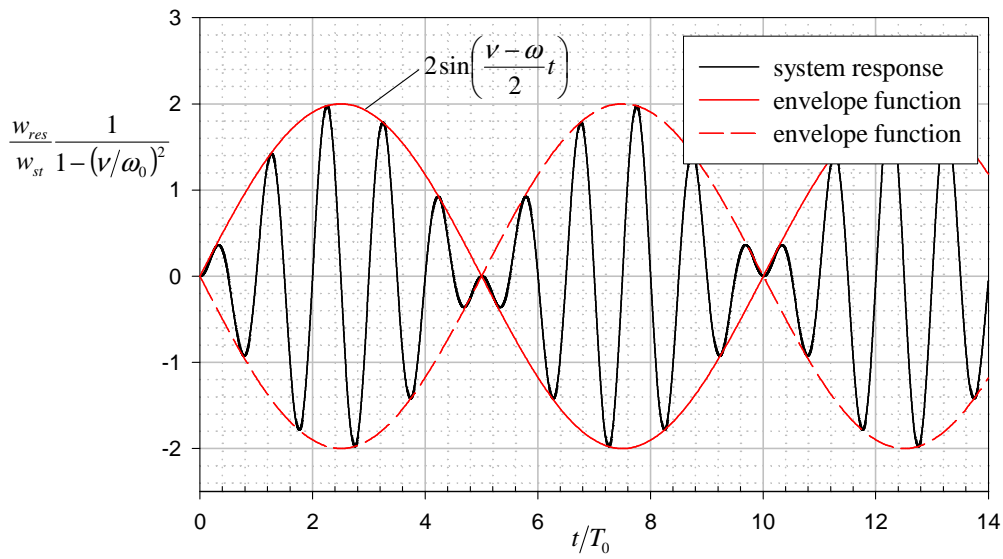


Figure1-4: Envelope functions of transient resonant vibrations

Figure1-5: Beat-like-vibration of SDOF oscillator with $\nu \approx \omega_0$

1.1.1.7. Arbitrary periodic forcing function

If the effective excitation is a periodic function $f_{\text{eff}}(t) = f_{\text{eff}}(t + T)$ with T defining the excitation period, it can be expanded in the complex Fourier time series,

$f_{eff}(t)/m = \sum_{n=-\infty}^{\infty} C_n \exp\left(\frac{2i\pi}{T} n t\right)$. The excitation may then be considered termwise, and the solutions given in Section 1.1.1.2 are applied to each term and finally, superposition allows to render the total response. This approach permits the investigation of all steady state vibration problems by summation of the individual contributions

$$w_p(t) = \sum_{n=-\infty}^{\infty} C_n H\left(n \frac{2\pi}{T}\right) \exp\left(\frac{2i\pi}{T} n t\right), \quad (1-27)$$

where $H(\gamma)$ denotes the amplitude response function for force excitation given by Eq.(1-22). If force loading and ground excitation are applied simultaneously, then both load cases can also be treated independently and superimposed to obtain the total response. In practice, the forcing is considered band-limited, and only a finite number of terms is involved in the above series representations.

1.1.1.8. Forced vibrations - non-periodic forcing function – transient response

Contrary to the discrete spectrum of a periodic force, the non-periodic forcing function $f_{eff}(t)$ has a continuous spectrum, according to the Fourier integral,

$$c(\omega) = \frac{1}{m} \int_{-\infty}^{\infty} f_{eff}(t) \exp(-i\omega t) dt, \quad (1-28)$$

with the continuous Fourier coefficients $c(\omega)$. The continuous formulation of the superposition principle in the frequency domain becomes

$$w(t) = \frac{1}{2\pi} \int_{-\infty}^{\infty} c(\omega) H(\omega) \exp(i\omega t) d\omega, \quad (1-29)$$

where $H(\omega)$ denotes the complex frequency response function, Eq.(1-22). The integrals in Eqs.(1-28) and (1-29) can be evaluated by means of the Fast Fourier Transform (FFT), see e.g. Walker⁸. The corresponding solution in the time domain for $t > 0$ is given by Duhamel's convolution integral, if homogeneous initial conditions of the structure at rest are assumed,

$$w(t) = \int_0^t f_{eff}(\tau) h(t-\tau) d\tau, \quad (1-30)$$

where the impulse response function $h(t - \tau)$ defines the displacement at time t due to a unit impulse force $f_{eff}(t) = \delta(t)$, acting at time τ . In terms of the frequency response function it is given by

$$h(t) = \frac{1}{2\pi m} \int_{-\infty}^{\infty} H(\omega) \exp(i\omega t) d\omega, \quad (1-31)$$

and becomes the Green's function of Eq.(1-2),

$$h(t) = \frac{e^{-\omega_0 \zeta t}}{m \omega_D} \sin \omega_D t \quad \text{for } \zeta < 1, \quad (1-32)$$

in the case of a SDOF oscillator. For simple excitations the integral expression Eq.(1-30) can be solved analytically with the aid of symbolic algebra programs. In general, the convolution integral must be solved numerically, a task which has become a standard problem in numerical mathematics. However, using the addition theorem, $\sin(t - \tau) = \cos \tau \sin t - \cos t \sin \tau$, simplifies the evaluation of Eq.(1-30).

1.1.1.9. Response with a passive damper attached

The previous section has shown the beneficial effects of passive energy dissipation by a linear viscous damper. However, there are many more mechanisms for energy dissipation like yielding, friction, radiation damping into the foundation or other types of energy transmission. Energy loss by those effects cause damping and can be incorporated into the mechanical model by a general damping element, typically described by a force-displacement relation. If the dynamic modulus, see e.g. Harris⁹, is the ratio between the force and the displacement,

$$\mathcal{D} = \frac{f}{w}, \quad (1-33)$$

then most damper and absorber configurations can be described by the integro-differential operator \mathcal{D} . In Figure 1-6 such a general damping device is added to the SDOF model. For its application to multiple story high rise buildings, see e.g. Lei¹⁰

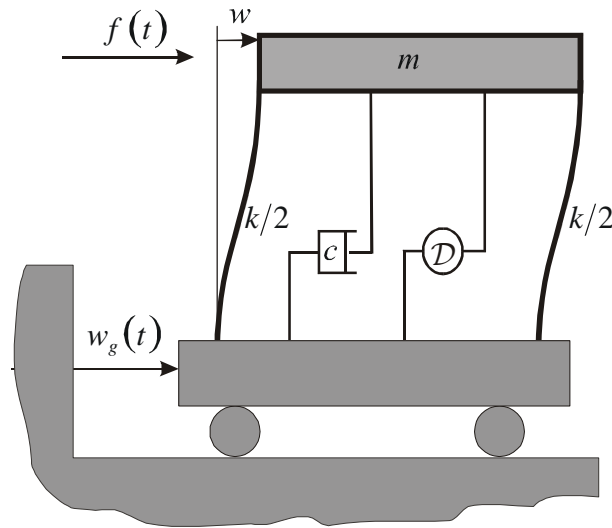


Figure 1-6: SDOF system with general damping device

Writing the force contribution of the device as $\mathcal{D} \cdot w$ permits various response characteristics including displacement, velocity and acceleration dependency. Neglecting the mass of the damping device the extension of Eq.(1-2) takes on the simple form

$$m \ddot{w} + c \dot{w} + k w + \mathcal{D} w = f_{eff}. \quad (1-34)$$

Only if the damping device is purely viscous the energy dissipation of the SDOF model is always increased which corresponds to an increase in the overall damping ratio. For all other types of damping devices only careful dynamic analysis can guarantee improved performance.

1.2. Equations of motion for linear MDOF structures

A proper mathematical idealisation of a physical construction is crucial for the development of vibration absorbers and the determination of the dynamic characteristics of any structure. Unfortunately it is rarely adequate to utilise a SDOF idealisation for the entire construction. Thus the dynamic investigations must be adapted for MDOF structures. Although the structural model can have several degrees of freedom, the structure-soil-structure interaction is not accommodated for, and the ground excitation in vertical direction is neglected throughout this dissertation. Figure 1-7 displays typical idealised lumped mass MDOF structures, a plane shear frame building, and a cantilevered shear-beam model.

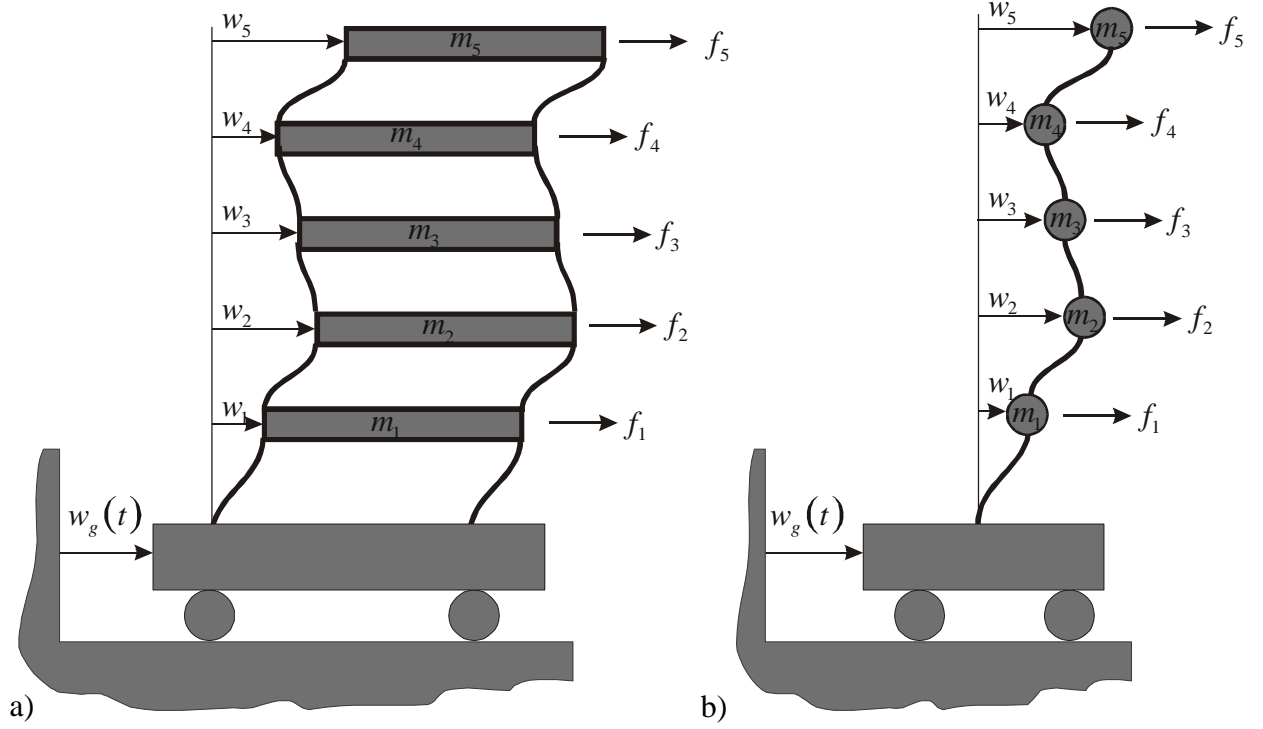


Figure 1-7: Multiple-story model: a) shear frame b) beam model, both in single point excitation and (wind) force loading

One of the most appropriate techniques for a MDOF discretisation of a continuous structure is the Finite Element Method (FEM), where, from a physical point of view, each structural member is mathematically represented by an element having the same mass, stiffness and damping characteristics as the original member. Those elements are assembled together, according to the physical construction, rendering a N -DOF system with a discrete set of variables. The mass, stiffness and damping matrices and a general displacement vector \mathbf{w} is generated during this process. Then, the N equations of motion for the discretised structural system, under uniform ground excitation and time varying forces, can be written analogous to Eq.(1-34), in matrix notation,

$$\mathbf{M} \ddot{\mathbf{w}} + \mathbf{C} \dot{\mathbf{w}} + \mathbf{K} \mathbf{w} + \mathbf{D} \mathbf{w} = -\mathbf{M} \mathbf{r}_s \ddot{w}_g + \mathbf{f}, \quad (1-35)$$

where \mathbf{M} , \mathbf{C} , \mathbf{K} and \mathbf{r}_s represent the mass, damping, stiffness matrices as well as the static influence vector, respectively. \ddot{w}_g and \mathbf{f} denote the ground excitation and the dynamic loading forces, respectively, which can be combined in an effective loading term $\mathbf{f}_{eff} = -\mathbf{M} \mathbf{r}_s \ddot{w}_g + \mathbf{f}$. If additional damping devices are installed, they can be treated analogous

to SDOF freedom systems by adding the vector expression $\mathcal{D}\mathbf{w}$, which again describes force-displacement relations, for a practical application, see again Lei¹⁰. In general, the stiffness matrix is symmetric ($k_{ij} = k_{ji}$) whereas such a property does not always exist for the mass matrix. For linear systems and linear energy dissipating devices it is convenient to incorporate $\mathcal{D}\mathbf{w}$ directly into the equations of motion, resulting in modified mass, stiffness and damping matrices. Due to the increased computational capacity of modern computers, it is possible to solve Eq.(1-35) directly. Nevertheless, deep insight can be gained and the required effort can be kept to a minimum if the equations are uncoupled via a modal transformation. As such a transformation is normally performed for the main structure, the additional damping terms $\mathcal{D}\mathbf{w}$ are not considered and Eq.(1-35) is solved for undamped free vibrations via the general solution $\mathbf{w}(t) = \boldsymbol{\varphi} e^{i\omega t}$. This renders the associated generalised eigenvalue problem,

$$(\mathbf{K} - \omega^2 \mathbf{M}) \boldsymbol{\varphi} = 0, \quad (1-36)$$

and there are numerous methods available to solve the generalised eigenvalue problem, see e.g. Stoe¹¹. An N -DOF system will have N nontrivial solutions of Eq.(1-36), where ω_i and $\boldsymbol{\varphi}_i$ denote the corresponding natural frequencies assumed to be well separated, and mode shape vectors, respectively. Normally the mode shape vectors are sorted according to their natural frequencies in ascending order, starting with the fundamental mode. When properly normalised the mode shapes satisfy the following orthogonality conditions

$$\boldsymbol{\varphi}_i^T \mathbf{M} \boldsymbol{\varphi}_j = \delta_{ij}, \quad (1-37)$$

$$\boldsymbol{\varphi}_i^T \mathbf{K} \boldsymbol{\varphi}_j = \begin{cases} \omega_i^2 & \text{for } i = j \\ 0 & \text{for } i \neq j \end{cases}, \quad (1-38)$$

where δ_{ij} represents the Kronecker Symbol. Introducing a linear transformation such that the original displacements \mathbf{w} are expressed by

$$\mathbf{w} = \boldsymbol{\Phi} \mathbf{q} \quad (1-39)$$

where the shape vectors $\boldsymbol{\varphi}_i$ form the columns of the modal matrix (square matrix) $\boldsymbol{\Phi} = [\boldsymbol{\varphi}_1, \dots, \boldsymbol{\varphi}_N]$. The modal vector \mathbf{q} contains the new generalised, so called principal

coordinates. Inserting Eq.(1-39) into Eq.(1-36) pre-multiplying with the transposed modal matrix Φ^T and applying Eqs.(1-37) and (1-38) render the following set of equations of motion in modal coordinates

$$\ddot{\mathbf{q}} + \Phi^T \mathbf{C} \Phi \dot{\mathbf{q}} + \Omega^2 \mathbf{q} = -\Phi^T \mathbf{M} \mathbf{r}_S \ddot{w}_g + \Phi^T \mathbf{f}, \quad (1-40)$$

where $\Omega^2 = \text{diag}(\omega_1^2, \dots, \omega_N^2)$. The simultaneous diagonalisation of a damped system is only possible, see e.g. Hütte¹², Müller¹³, if the condition

$$\mathbf{C} \mathbf{M}^{-1} \mathbf{K} = \mathbf{K} \mathbf{M}^{-1} \mathbf{C} \quad (1-41)$$

holds. This condition is valid for all modally damped systems, also referred to as classically damped systems. In such a situation the transformed damping matrix $\Phi^T \mathbf{C} \Phi$ is also of diagonal shape and the left hand side of the damped structural system, Eq.(1-40), decouples completely. Since very little is known about the actual damping conditions in a building, modal damping is frequently introduced into the equations of forced motion. The special case of the proportional Rayleigh damping

$$\mathbf{C} = \alpha_1 \mathbf{M} + \alpha_2 \mathbf{K}, \quad (1-42)$$

e.g., allows modal decoupling, but it can be generalised to the Caughey series, see Soong², p.22,

$$\mathbf{C} = \mathbf{M} \sum_{j=0}^{N-1} \alpha_j (\mathbf{M}^{-1} \mathbf{K})^j \quad (1-43)$$

Using the normalisation condition, Eq.(1-37), and expanding Eq.(1-43), renders

$$\Phi^T \mathbf{C} \Phi = \alpha_0 \Phi^T \mathbf{M} \Phi + \alpha_1 \Phi^T \mathbf{K} \Phi + \sum_{j=2}^{N-1} \alpha_j \Phi^T \mathbf{K} (\mathbf{M}^{-1} \mathbf{K})^j \Phi \quad (1-44)$$

$$= \alpha_0 \Phi^T \mathbf{M} \Phi + \alpha_1 \Phi^T \mathbf{K} \Phi$$

$$+ \sum_{j=2}^{N-1} \alpha_j \underbrace{\Phi^T \mathbf{K} \Phi}_{\Omega^2} \underbrace{\Phi^{-1} \mathbf{M}^{-1} (\Phi^{-1})^T}_{\mathbf{I}} \underbrace{\Phi^T \mathbf{K} \Phi}_{\Omega^2} \dots \underbrace{\Phi^{-1} \mathbf{M}^{-1} (\Phi^{-1})^T}_{\mathbf{I}} \underbrace{\Phi^T \mathbf{K} \Phi}_{d\Omega^2} \quad (1-45)$$

$$= \sum_{j=0}^{N-1} \alpha_j [\Omega^2]^j = \text{diag}(2\zeta_1 \omega_1, \dots, 2\zeta_1 \omega_1),$$

where ζ_j denote the modal damping ratios. Under the condition of separated natural frequencies Eq.(1-45) has a solution for the damping coefficients α_j . The damping matrix of a 3-DOF model, e.g., can be given by

$$\mathbf{C} = \mathbf{M} \sum_{j=0}^2 \alpha_j (\mathbf{M}^{-1} \mathbf{K})^j, \quad (1-46)$$

where

$$\begin{pmatrix} \alpha_0 \\ \alpha_1 \\ \alpha_2 \end{pmatrix} = 2 \begin{pmatrix} \omega_1^{-1} & \omega_1 & \omega_1^3 \\ \omega_2^{-1} & \omega_2 & \omega_2^3 \\ \omega_3^{-1} & \omega_3 & \omega_3^3 \end{pmatrix}^{-1} \begin{pmatrix} \zeta_1 \\ \zeta_2 \\ \zeta_3 \end{pmatrix}. \quad (1-47)$$

After the modal transformation is performed, the equations of motion simplify to a set of scalar equations, one for each mode j

$$\ddot{q}_j + 2\zeta_j q_j \omega_j + \omega_j^2 q_j = -\xi_g^j \ddot{w}_g + \boldsymbol{\phi}_j^T \mathbf{f}, \quad j = 1, 2, \dots, N \quad (1-48)$$

$$\xi_g^j = \boldsymbol{\phi}_j^T \mathbf{M} \mathbf{r}_s \quad (1-49)$$

where q_j and ξ_g^j denotes the modal coordinate and the participation factor of the ground acceleration, respectively. Besides the participation factor, the first excitation term depends on the spectral density of the ground excitation. The second excitation term depends on spatial distribution of \mathbf{f} and on time. Equation (1-48) is identical with a SDOF equation of motion with effective forcing, and consequently all methodology and phenomena developed and discussed in Section 1.1.1.1 to Section 1.1.1.9 are applicable. The major computational task is the determination of the natural frequencies and the mode shape vectors. For large systems, however, often only the structural modes within the lower frequency band need to be calculated, and a diagonalisation is performed before the dynamic analysis.

1.3. Energy considerations

Traditionally, the calculation of displacements, velocities, accelerations and forces has been of outmost interest during design and investigation of dynamic resistance. However, with the development of innovative concepts in passive energy dissipation a focus on energy as a design criterion has been developed. This line of attack puts the centre of attention towards

the need to dissipate structural energy instead of increasing the resistance to lateral loads. Energy considerations are very general in nature and appropriate to incorporate dynamic effects due to various load cases e.g. wind or seismic loading. The resulting formulation is suitable for a general discussion of energy dissipation and used in the chapter about the tuned liquid column damper (TLCD) design optimisation with performance indices, see Chapter 7. In the following section an energy formulation for the idealised SDOF and MDOF system is developed which may include one or more passive devices. A straightforward energy approach is the integration of the equations of motion over the entire displacement history. As a result one obtains, see Soong²,

$$E_{Kin} + E_D + E_S + E_P = E_I \quad (1-50)$$

where the individual energy expressions are given by

$$E_{kin} = \frac{1}{2} \dot{\mathbf{w}}^T \mathbf{M} \dot{\mathbf{w}}, \quad (1-51)$$

$$E_D = \int \dot{\mathbf{w}}^T \mathbf{C} \dot{\mathbf{w}} dt, \quad (1-52)$$

$$E_S = \int \mathbf{w}^T \mathbf{K} d\mathbf{w} = \frac{1}{2} \mathbf{w}^T \mathbf{K} \mathbf{w}, \quad (1-53)$$

$$E_P = \int (\mathcal{D} \mathbf{w})^T d\mathbf{w}, \quad (1-54)$$

$$E_I = -\int \ddot{\mathbf{w}}_g^T \mathbf{M} d\mathbf{w} + \int \mathbf{f}^T d\mathbf{w}. \quad (1-55)$$

The contributions on the left hand side of Eq. (1-50) represent the relative kinetic energy E_{kin} , the dissipative energy E_D caused by light material damping of the structure with viscous module, and the elastic strain energy E_S . E_P denotes the energy dissipated via the general damping device. From the law of conservation of mechanical energy it can be concluded that the sum of these energies balances the external input energy E_I , which comprises of the energy input due to seismic activity and the wind energy. From an energy perspective, one must attempt to minimise the amount of kinetic and strain energy by proper design. Two approaches are feasible. The first reduces the energy input into the structure, like base isolation, whereas the latter focuses on the application of additional energy dissipating mechanism in the structure, which is the central theme of this thesis. The main goal is to avoid

any damage caused by excessive loading (plastic deformation, overturning moments, P-Δ-effect, etc) of the main structure by the installation of energy consuming substructures.

1.4. State transformations and state space representation

The linear equations of motion of an arbitrary linear time invariant structural system are second order differential equations, resulting from conservation of momentum,

$$\mathbf{M} \ddot{\mathbf{w}} + \mathbf{C} \dot{\mathbf{w}} + \mathbf{K} \mathbf{w} = \mathbf{f}_{eff}, \quad (1-56)$$

with an effective load vector, $\mathbf{f}_{eff} = -\mathbf{M} \mathbf{r}_s \ddot{w}_g + \mathbf{f}$, see Section 1.1.1.7 for wind and seismic load. Often \mathbf{w} describes the absolute deformations, but many other sets of coordinates are possible, e.g. the relative story displacements. Any physically meaningful coordinates can be obtained from \mathbf{w} by the regular state transformation

$$\bar{\mathbf{w}} = \mathbf{T}^{-1} \mathbf{w}, \quad (1-57)$$

with the regular transformation matrix \mathbf{T} . A special case is the modal transformation where $\mathbf{T} = \mathbf{\Phi}$, yielding a diagonal mass and stiffness matrix when pre-multiplying with $\mathbf{\Phi}^T$. The equation of motion in transformed coordinates becomes

$$\mathbf{M} \mathbf{T} \ddot{\bar{\mathbf{w}}} + \mathbf{C} \mathbf{T} \dot{\bar{\mathbf{w}}} + \mathbf{K} \mathbf{T} \bar{\mathbf{w}} = \mathbf{f}_{eff} \quad (1-58)$$

Working with a set of first order differential equations often simplifies dynamic system analysis, and a suitable representation of Eq.(1-56) can be achieved by introducing a new state variable \mathbf{z} consisting of the displacements and velocities of the original system, Eq.(1-56):

$$\mathbf{z}(t) = \begin{pmatrix} \bar{\mathbf{w}} \\ \dot{\bar{\mathbf{w}}} \end{pmatrix}. \quad (1-59)$$

With this new state vector Eq.(1-56) can be rewritten as a system of first order differential equations:

$$\dot{\mathbf{z}}(t) = \begin{pmatrix} \mathbf{0} & \mathbf{I} \\ -\mathbf{T}^{-1}\mathbf{M}^{-1}\mathbf{K}\mathbf{T} & -\mathbf{T}^{-1}\mathbf{M}^{-1}\mathbf{C}\mathbf{T} \end{pmatrix} \mathbf{z}(t) + \begin{pmatrix} \mathbf{0} \\ \mathbf{T}^{-1}\mathbf{M}^{-1}\mathbf{f}_{eff}(t) \end{pmatrix}. \quad (1-60)$$

Eq.(1-60) is known as the state space representation of the dynamic system, Eq.(1-56). It is not limited to linear systems. The inversion of the mass matrix is always possible, unless the original set of equations, Eq.(1-56), contains algebraic equations which must be solved before performing the transformation. Any state space representation is equivalent to the equations of motion, but the reduction from a second to a first order system comes at the price that the new system dimensions are twice the original ones. Of course another state transformation $\bar{\mathbf{z}} = \bar{\mathbf{T}}\mathbf{z}$ can be applied if desired. State space representations have become widely used and appreciated, since many powerful mathematical tools can be applied directly, and it is the favourite description of dynamic system in control engineering. If necessary, the state space equations are extended by a so called ‘output equation’ which is a function of the state and the external excitation, for linear systems

$$\mathbf{y}(t) = \mathbf{C}\mathbf{z}(t) + \mathbf{D}\mathbf{f}_{eff}(t). \quad (1-61)$$

Such an output equation is particularly useful if one is not interested in all state variables but in particular output quantities, e.g. certain floor accelerations, velocities, displacements or a combination of those like shear forces or moments and torques.

In system analysis, Eqs.(1-60) and (1-61) are often written in a standardised form given by

$$\dot{\mathbf{z}}(t) = \mathbf{A}\mathbf{z}(t) + \mathbf{B}\mathbf{f}_{eff}(t), \quad (1-62)$$

$$\mathbf{y} = \mathbf{C}\mathbf{z}(t) + \mathbf{D}\mathbf{f}_{eff}(t),$$

where \mathbf{A} , \mathbf{B} , \mathbf{C} and \mathbf{D} are denoted system matrix, input, output and feed-through matrix, respectively. It is vital to be aware of the outstanding importance of the system matrix: all relevant information about dynamic behaviour e.g. free vibration response, damping and stability, pole location, is contained in \mathbf{A} . For that reason the system matrix plays the very central role in system analysis. Transforming Eq.(1-62) into the Laplace domain,

$$\mathcal{L}\{\dot{\mathbf{z}}(t)\} = \mathbf{f}(s) = \int_0^{\infty} \dot{\mathbf{z}}(t)e^{-st} dt, \text{ see e.g. Doetsch}^{14}, \text{ and solving for } \mathbf{Z}(s) \text{ yields}$$

$$\mathbf{Z}(s) = (s\mathbf{I} - \mathbf{A})^{-1} \mathbf{B}\mathbf{F}_{eff}(s) + (s\mathbf{I} - \mathbf{A})^{-1} \mathbf{z}(0), \quad (1-63)$$

$$\mathbf{Y}(s) = \left(\mathbf{C}(s\mathbf{I} - \mathbf{A})^{-1} \mathbf{B} + \mathbf{D} \right) \mathbf{F}_{eff}(s) + \mathbf{C}(s\mathbf{I} - \mathbf{A})^{-1} \mathbf{z}(0),$$

The inverse Laplace transformation is given by

$$\mathcal{L}^{-1}\{f(s)\} = f(t) = \frac{1}{2\pi i} \int_{\delta-i\infty}^{\delta+i\infty} f(s) e^{st} ds = \begin{cases} f(t) & \text{für } t > 0 \\ 0 & \text{für } t < 0 \end{cases} \quad (1-64)$$

where the complex variable s is defined by $s = \delta + i\nu$, and the state transition matrix $\Gamma(t)$ is defined as the inverse Laplace transformation of the resolvent matrix $\Gamma(s)$:

$$\Gamma(s) = (s\mathbf{I} - \mathbf{A})^{-1}, \quad (1-65)$$

$$\Gamma(t) = \mathcal{L}^{-1}\{\Gamma(s)\},$$

By means of the inverse Laplace transformation, Eq.(1-63), and the convolution theorem,

$$\mathcal{L}^{-1}\{f_1(s) \cdot f_2(s)\} = \int_0^t f_1(\tau) f_2(t-\tau) d\tau, \text{ the time domain solution can be given by}$$

$$\mathbf{z}(t) = \int_0^t \Gamma(t-\tau) \mathbf{B} \mathbf{f}_{eff}(\tau) d\tau + \Gamma(t) \mathbf{z}(0), \quad (1-66)$$

$$\mathbf{y}(t) = \int_0^t \mathbf{C} \Gamma(t-\tau) \mathbf{B} \mathbf{f}_{eff}(\tau) d\tau + \mathbf{D} \mathbf{f}_{eff}(t) + \mathbf{C} \Gamma(t) \mathbf{z}(0).$$

There are efficient numerical schemes to calculate the state transition matrix. One is using the Taylor series expansion, see e.g. Müller¹⁵, Ludyk¹⁶,

$$\Gamma(t) = e^{\mathbf{A}t} = \sum_{n=0}^{\infty} \frac{\mathbf{A}^n t^n}{n!}. \quad (1-67)$$

The system matrix uniquely defines the state transition matrix and this is another proof of the exceptional importance of \mathbf{A} . For linear systems a lot of system design and analysis is done in the frequency domain, due to the existence of the superposition principle. The input-output behaviour of dynamic systems, is usually described by the transfer function $\mathbf{H}(s)$, whose magnitude and phase angle are called the frequency response of the system. From Eq. (1-63) it follows directly that for homogenous initial conditions the frequency transfer function $\mathbf{H}(s)$ is given by

$$\mathbf{Y}(s) = \mathbf{H}(s) \mathbf{F}_{eff}(s), \quad \mathbf{H}(s) = \mathbf{C} (s \mathbf{I} - \mathbf{A})^{-1} \mathbf{B} + \mathbf{D}. \quad (1-68)$$

If the output $\mathbf{Y}(s)$ is a function of the state variables only (e.g. velocities and displacements), then $\mathbf{D} = 0$ and there is no direct dependence of $\mathbf{Y}(s)$ on the input. If furthermore, the output matrix \mathbf{C} is chosen to be the identity matrix, then the frequency response function simplifies to

$$\mathbf{H}(s) = (s \mathbf{I} - \mathbf{A})^{-1} \mathbf{B}. \quad (1-69)$$

Under the assumption that $\mathbf{H}(s)$ can still be computed if the real part of s is chosen to be zero, s becomes $s = i\nu$, and it can be written in the equivalent form $\mathbf{H}(i\nu) = (i\nu \mathbf{I} - \mathbf{A})^{-1} \mathbf{B}$. As it describes the system-response to a unit impulse excitation $\mathcal{L}\{\delta(t)\} = 1$, the corresponding time function of $\mathbf{H}(s)$ is normally referred to as the impulse response function, see Eq.(1-32) for SDOF oscillators. Since $\mathbf{H}(t) = \mathbf{0}$ for $t < 0$, the Fourier transformed, if existing (see Doetsch¹⁴), equals the Laplace transformed with

$$\mathcal{L}\{\mathbf{H}(t)\} = \mathbf{H}(s) = \int_0^{\infty} \mathbf{H}(t) e^{-st} dt \underset{s=i\nu}{=} \int_0^{\infty} \mathbf{H}(t) e^{-i\nu t} dt, \quad (1-70)$$

$$\mathcal{F}\{\mathbf{H}(t)\} = \mathbf{H}(\nu) = \int_{-\infty}^{\infty} \mathbf{H}(t) e^{-i\nu t} dt = \int_0^{\infty} \mathbf{H}(t) e^{-i\nu t} dt.$$

However, it has to be pointed out that, for general system analysis, the application of the Laplace transformation is much more powerful, when compared to the Fourier integral.

1.5. References

¹ Ziegler, F., *Mechanics of Solids and Fluids*, 2nd reprint of second edition, Springer, 1999.

² Soong, T.T., Dargush, G.F., *Passive Energy Dissipation Systems in Structural Engineering*, Wiley, Chichester England, 1997

³ Chopra, A.K., *Dynamics of Structures*, Prentice Hall, New Jersey, 1995

⁴ Clough, R.W., Penzien, J., *Dynamics of Structures*, 2nd edition, McGraw-Hill, 1993

⁵ Magnus, K., Popp, K., *Schwingungen*, 5th. ed., Teuber, Stuttgart, 1997

⁶ Ziegler, F., *Vorlesungen über Baudynamik*, lecture notes, Technical University of Vienna, 1979

- ⁷ Chwalla, E., *Introduction to Structural Mechanics, in German*, Stahlbau Verlag, Köln, 1954,
- ⁸ Walker, J.S., *Fast Fourier Transform*, CRC Press, 1991
- ⁹ Harris, M., Crede, C.E., *Shock and Vibration Handbook*, McGraw-Hill, 1961
- ¹⁰ Lei, Y., *Sure and Random Vibrations of Simple Dissipative Civil Engineering Steel Structures*, Dissertation and Report, Institute of Rational Mechanics, TU-Vienna, A-1040 Wien, Austria, 1994
- ¹¹ Stoer J., Burlisch R., *Numerische Mathematik 2*, 3rd edition, Springer Verlag, 1990
- ¹² Hütte, *Die Grundlagen der Ingenieurwissenschaften*, 29th edition Springer Verlag, 1991
- ¹³ Müller, P.C., *Stabilität und Matrizen*, Springer Verlag Berlin, 1977
- ¹⁴ Doetsch, G., *Anleitung zum praktischen Gebrauch der Laplace Transformation*, Oldenburg, 1956
- ¹⁵ Müller, P.C., *Stabilität und Matrizen*, Springer-Verlag, 1977
- ¹⁶ Ludyk, G., *Theoretische Regelungstechnik I*, Springer, 1995

2. Overview of passive devices for vibration damping

The purpose of this chapter is to review common structural control techniques and applications. It is restricted to passive energy absorbing devices, starting with well established damping devices like metallic dampers, friction dampers, viscoelastic dampers or viscous fluid dampers. Section 2.5 is conceptually concerned with dynamic vibration absorbers, including the description of tuned liquid damper and the shortly described idea of base isolation. Tuned mass damper are discussed in much more detail (Section 2.6) since the understanding of their working principle is the basis for the analysis of tuned liquid column dampers. The chapter ends with a short overview of smart materials used for structural control.

2.1. *Metallic Dampers*

One of the most effective mechanisms available for the dissipation of energy already accumulated in a structure, is through inelastic deformation of metals. In traditional steel structures the aseismic design relied on the plastic deformation (and post yield ductility) of structural members whereas the introduction of metallic yield dampers started with the concept of utilising separate metallic hysteretic dampers to absorb a major part of the external energy input to the structure. During the years a variety of such devices has been proposed, many of them using mild steel plates with triangular or hourglass shape so that yielding spreads evenly throughout the material. The dissipating effect is based on the nonlinear force-displacement behaviour, which typically contains hysteresis loops for energy dissipation, see Figure 2-1, where several load cycles with increasing amplitude displacement are displayed for the Ramberg-Osgood model, see Wen¹ for details. Many different designs and materials, such as lead and shape memory alloys, have been developed and evaluated, some with particularly desirable features like stable hysteretic behaviour, long term reliability and insensitivity to environmental temperature. The ongoing research has resulted in the development of several commercial products for both, new and retrofit construction projects. The inelastic deformation of metallic elements is the underlying dissipative mechanism for all different types and geometries of metallic dampers. In order to include these devices in the structural design, the expected hysteretic behaviour under arbitrary cyclic loading has to be

characterised. Ideally such a description would be based on the micro-mechanical theory of dislocations which determine the inelastic response, but since this approach is hardly feasible a phenomenological description of the processes is accepted. A common approach to describe the inelastic behaviour of metallic dampers starts with the selection of a basic hysteretic model, followed by a parameter identification, where curve fitting is utilised to match the model with experimental data, available from experiments. Additionally, scaling and material relationships can be determined by macroscopic mechanical analysis of the device.

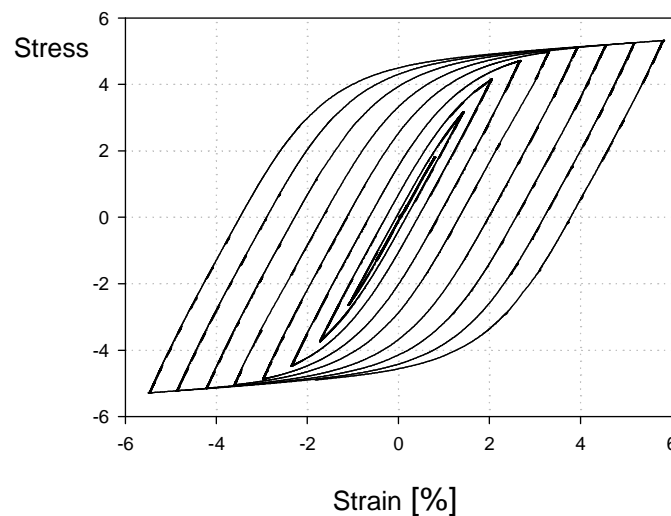


Figure 2-1: Force displacement response of hysteretic model, see Wen¹

Since its application in New Zealand 1980, reported in Sinner et al.², metallic yield dampers have been installed in various countries, including a 29-storey building in Italy, see Chiampi³, seismic retrofit installations in USA, see Perry et al.⁴ and Mexico, see Martinez-Romero⁵, and a number of installations in Japan.

2.2. Friction Dampers

Dry friction provides another excellent mechanism for energy dissipation, and plays an important role in automotive brakes. Based upon an analogy to the automotive brake, began the development of passive frictional dampers to improve the seismic response of structures. Although a variety of devices, differing in mechanical complexity and sliding materials, has been proposed, it is essential for all of them to avoid stick-slip phenomena which introduce high frequency excitation. A critical component is the sliding interface, because an improper composition of the interface layers causes corrosion and thus, an alteration of slipping

properties with time. As a consequence, compatible materials must be found to ensure a consistent coefficient of friction independent of environmental factors. One of the damper elements based upon the friction mechanism is the X-braced friction damper, shown in Figure 2-2, for both, a schematic view and an actually manufactured device, see Pall⁶. Those devices are not designed to operate during strong winds or moderate earthquakes. Instead maximum energy dissipation is guaranteed as slipping occurs at a predetermined optimum load before primary structural members start to yield. Typically, these devices provide good performance almost independently of the loading amplitude, frequency or load cycles.

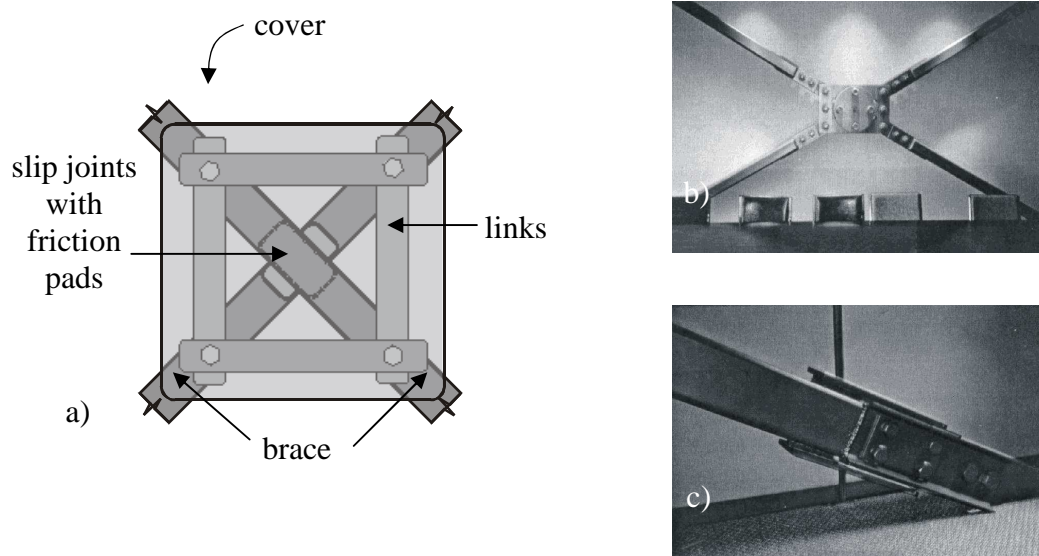


Figure 2-2: Pall Friction Damper, a) schematic view, b) exposed friction damper in X-bracing c) exposed friction damper in single diagonal [6]

Similar to metallic yield dampers most macroscopic hysteretic models for friction dampers are obtained from test data, generally assuming Coulomb friction with a constant coefficient of friction. Those relatively simple models are incorporated into an overall structural analysis, and the concept of equivalent damping as well as full nonlinear time domain analysis, see Lei^{7,8} have been performed. Both approaches show the effectiveness of friction dampers in reducing displacements, while maintaining comparable acceleration levels, when compared to the corresponding unbraced or conventionally braced structure. Friction dampers have been installed in several buildings, some as retrofits, some as new facilities, including structures in Canada and USA, see again Pall⁶.

However, the classical design is based on earthquake loading only, not taking strong winds and mild ground movements into consideration. To effectively mitigate all different excitations, a combination mechanism consisting of a frictional slider and a viscous damper in

series must be used, overcoming the problem of the threshold activation force which exists for all frictional dampers.

2.3. Viscoelastic Dampers

The metallic and frictional devices described so far, are mainly intended for seismic applications. On the other hand, some viscoelastic materials can be used to dissipate energy at all deformation levels. As a consequence viscoelastic materials can be applied in both wind and seismic protection. Since the 1950s, viscoelastic materials have been applied as vibration absorbing materials. With the installation of about 10.000 viscoelastic dampers to reduce wind induced vibrations, in each of the twin towers of the World Trade Center in New York in 1969, they gained civil engineering relevance, see Samali et al.⁹.

A typical viscoelastic damper used in civil engineering structures, is illustrated in Figure 2-3a. It consists of viscoelastic layers bonded together with steel plates. A corresponding force displacement diagram under harmonic excitation clearly shows the hysteretic character responsible for energy dissipation, and is given in Figure 2-3b. Viscoelastic dampers dissipate energy through shear deformation, and their energy absorbing behaviour strongly depends on the dynamic load and on environmental conditions, e.g. the vibration frequency, strain and ambient temperature. Nevertheless, the force displacement relationship is still linear and, unlike metallic and friction dampers, a linear structural system, with linear viscoelastic dampers added remains linear, with an increased overall viscous damping, as well as an augmented lateral stiffness. This fact greatly simplifies the analytical investigations for both, single-degree-of-freedom and multiple-degree-of-freedom-systems.

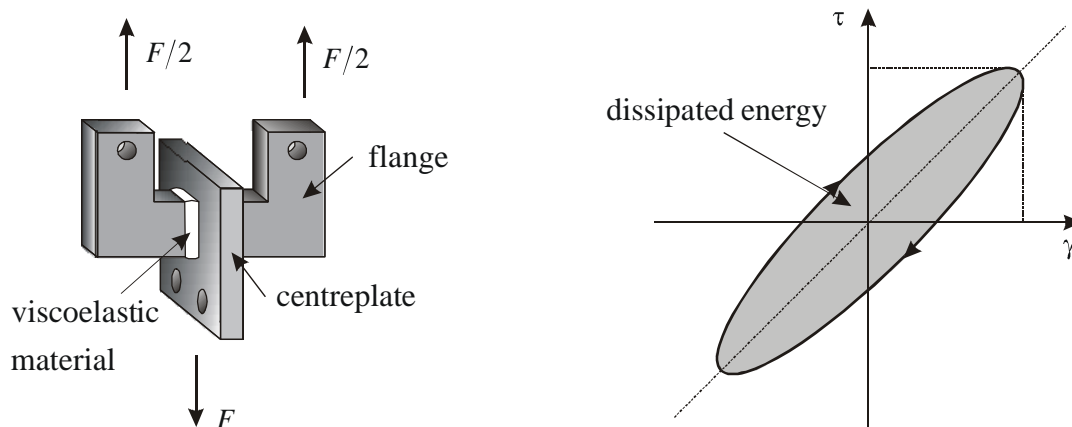


Figure 2-3: Viscoelastic damper, a) schematic view, b) corresponding hysteretic stress-strain curve, see e.g. Zhang¹⁰ or Tsai¹¹

Although originally designed for wind loading, further analytical and experimental studies have shown that viscoelastically damped structures have proven to be very resistant against a large range of earthquake ground motion intensity levels. Results indicate that viscoelastic dampers are effective in reducing the inelastic ductility demand of the test structure. Investigations have demonstrated the effectiveness of viscoelastic dampers for both, steel and reinforced concrete structures, and when compared against steel structures, reinforced concrete structures show inelastic response behaviour for smaller excitation levels leading to permanent deformation and damage. With proper installation of the dampers this damage can be significantly reduced or even eliminated.

Other than the World Trade Center, several buildings in USA and Taiwan, see again Samali⁹, are equipped with viscoelastic dampers to reduce wind induced vibrations, and also seismic retrofit projects have been undertaken.

2.4. Viscous Fluid Dampers

In the previous sections passive dampers were described which dissipate energy by inelastic deformation of solids. But fluids can also be used effectively in order to achieve a desired level of passive control. In fact the concept of a fluid damper for general shock and vibration reduction is well known. One very prominent example is, of course, the automotive shock absorber, where the damping effect results from the movement of a piston head with small orifices in a hydraulic fluid. Initiated by significant efforts, the development of fluid dampers for structural applications has reached the levels of both, retrofit and new implementations, mainly through a conversion of technology from heavy industry. The device shown in Figure 2-4a, see Makris et al.¹² is a cylindrical pot damper, where a piston deforms a thick, highly viscous substance, such as silicon gel, thereby dissipating energy. In order to maximise the energy dissipation density, materials with high viscosity have to be employed, which typically show both, frequency and temperature dependency. In a dashpot, see Figure 2-4b, see Taylor et al.¹³, which is another example of the uncomplicated viscous fluid dampers, the energy dissipation occurs by forcing a fluid, usually a compound of silicone or oil, to pass through small orifices in the piston. This effective method of energy conversion into heat allows high dissipation densities, even for less viscous fluids. However, to gain frequency independence, compactness in comparison to stroke and output force and insensitivity to output force a high level of sophistication is required.

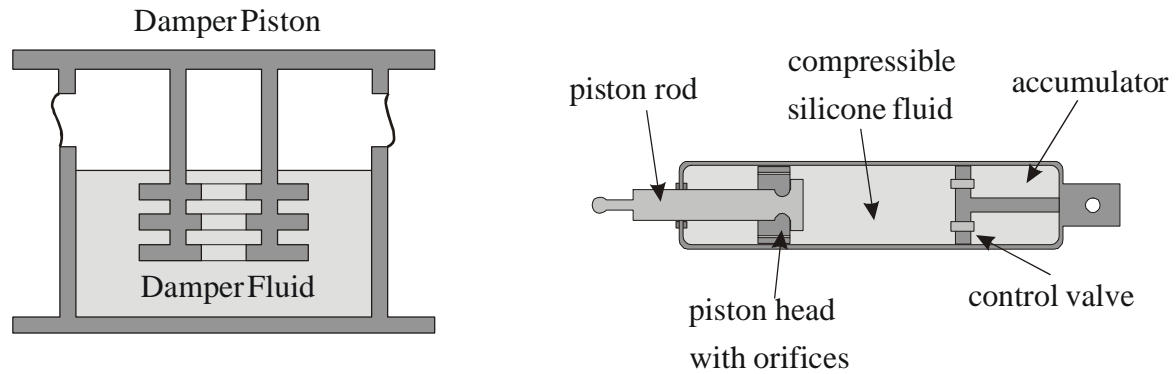


Figure 2-4: Viscous fluid damper a) cylindrical pot damper, see Makris et al.¹²
b) dashpot damper, see Taylor¹³

The damping devices described so far are small and local components which must be integrated within the hosting structure, typically in form of braces or vertical elements connecting adjacent floors. A different design concept involves the development of viscous damping wall (VDW). In this design, a steel plate, acting as piston, is moving in a narrow rectangular container, filled with a viscous fluid. In a typical installation in a frame bay, the steel plate is attached to the upper floor, while the container is fixed to the lower floor, see Yeung¹⁴.

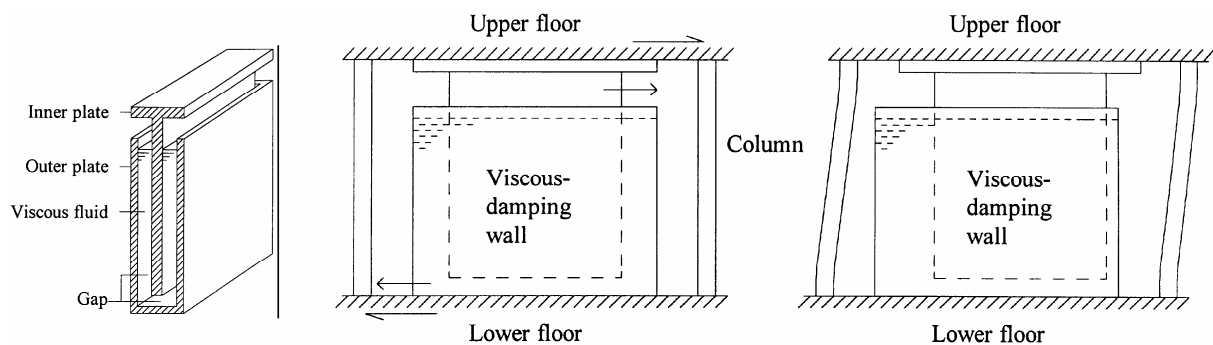


Figure 2-5: Viscous damping wall unit, Yeung¹⁴

Relative interstory motion shears the fluid and thus provides energy dissipation. If the deformed fluid is purely viscous (e.g. Newtonian), and the flow laminar, then the output force of the damper is directly proportional to the velocity of the piston. Hence, over a large frequency range the device behaves viscoelastic and is thus, often described by a Maxwell model. In recent years the development of viscous dampers has reached the level of structural installations. Housner et al.¹⁵ report, e.g. the seismic protection of a 1000m long bridge in

Italy, the application of viscous walls in tall buildings in Japan, and several implementations where viscous dampers are used as energy dissipating components for seismic base isolation.

2.5. Dynamic Vibration Absorbers

The concept of dynamic vibration absorbers differs from the damping mechanism utilised by the devices discussed in Section 2.1-2.4 because the vibration energy is not immediately dissipated, but transferred to a secondary system, typically consisting of some spring-mass-damper system. When designed correctly the energy dissipation occurs in this subsystem, thereby reducing the energy dissipation demand on the primary structural members, avoiding inelastic deformations and damage. Two basic types of dynamic vibration absorbers are already established in practice, see Soong³⁵. The first is the tuned mass damper which, in its simplest form, consists of an auxiliary mass-spring-dashpot system attached to the main structure. Pendulum type absorber also belong to this group. The second category is commonly labelled tuned liquid damper, and generally involves the dissipation of energy either through the sloshing of liquids in a container or, in case of the tuned liquid column damper (TLCD), via turbulence losses when the liquid is passing through orifices. Although dynamic vibration absorbers have often been proposed for aseismic design, the most important installations had the purpose of alleviating wind induced vibrations in high rise buildings. The hurdle still limiting the seismic applications include the high levels of damping that are normally required, detuning, if the host structure yields, and an inability to control higher mode responses.

2.5.1. Tuned Liquid Dampers

Tuned Liquid vibration absorbers can be split into two major groups, tuned liquid dampers (TLD) described in this section, and tuned liquid column dampers, which will be investigated in detail from Chapter 3 throughout the remainder of this thesis.

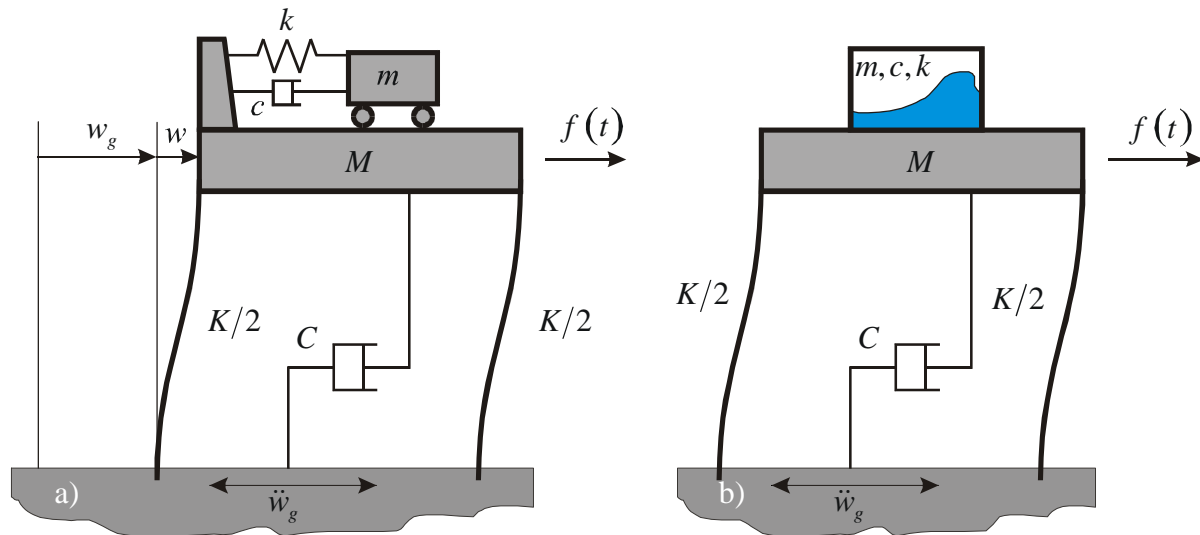


Figure 2-6: Comparison of dynamic vibration absorbers; a) tuned mass damper b) tuned sloshing damper

Figure 2-6a displays a schematic of the standard TMD attached to a SDOF model. In comparison, Figure 2-6b shows a specific type of TLD, the tuned sloshing damper. Particular advantages of this unit are firstly that the liquid supplies the secondary mass, secondly that the liquid provides viscous damping, primarily in the boundary layers, and thirdly, that the necessary restoring forces are provided in combination with gravity forces. Although performing a complicated motion, the system has characteristic frequencies which can be tuned for most favourable performance.

The idea of using TLD for structural control began in the mid-1980s, when Bauer¹⁶ suggested the use of rectangular tanks, completely filled with two immiscible fluids, similarly Rammerstorfer et al.¹⁷ investigated the response of storage tanks under earthquake loading, Heuer¹⁸ and Haßlinger et al.¹⁹ have studied the influence of a swimming pool on top of a building, and Hayek²⁰ has researched the vibrations of a liquid container during earthquakes. In Bauer¹⁶, the structural damping was achieved through the motion of the interface. The first TLD concepts were intended to reduce wind induced vibrations, followed by ideas to use them as well for the improvement of the structural seismic response. A schematic view of the proposed devices, see Modi et al.²¹, is given in Figure 2-7 a-c, and Figure 2-7d illustrates a real implementation of a TLD array at the Yokohama Marine Tower, see Tamura et al.²².

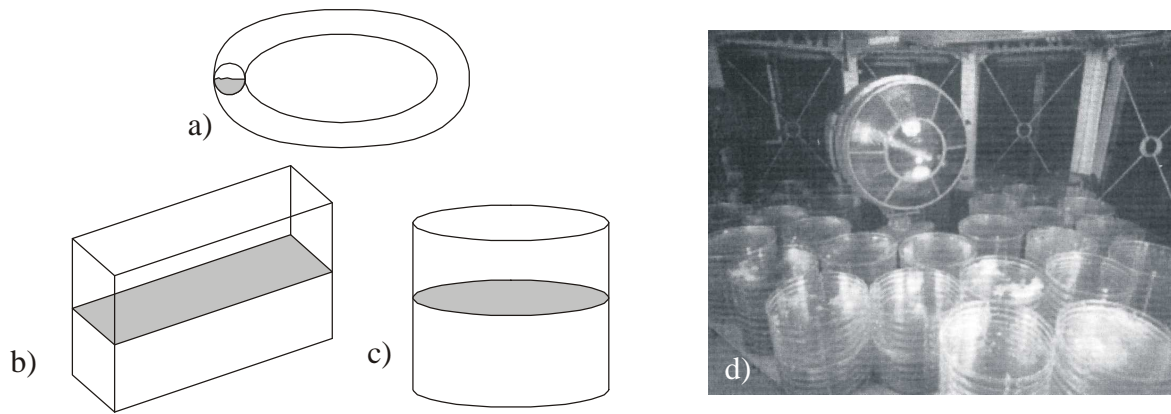


Figure 2-7: a) nutation damper b) rectangular TLD c) circular TLD d) TLD vessels on the Yokohama Marine Tower

As mentioned earlier, TLD operate on the same basic principles as TMDs. However, some of the drawbacks of TMD systems are not present in TLDs. Due to the simple physical concepts on which the restoring force is provided by gravity, no activation mechanism is necessary. As the system is operating all time, no complications due to an inadequate activation occur. All hardware requirements are surprisingly simple: the container is often made of polypropylene and commercially available, and the moving liquid is typically plain water. Normally, the fundamental frequencies, even of containers with characteristic dimensions of less than $1m$ are so low, that dozens of TLDs have to be installed. Whether they are stacked together to form a compact unit, or distributed, the installation is simple, even for temporarily installations in existing structures. From both, a mechanical and mathematical point of view the description of a TLD is quite involved. This distributed system has several natural frequencies and normally behaves strongly nonlinear, but for large oscillation amplitudes the system is rather insensitive to detuning between host and secondary structure. Therefore the water level at rest, the parameter which controls the fundamental sloshing frequency will not significantly modify the response during strong vibrations. Circular containers are used for symmetric structures with the same fundamental frequencies in the principal directions, and for unsymmetrical structures with different fundamental frequencies along the principal axis, tuning may be accomplished with a rectangular tank. One of the first structural implementations was at a steel frame airport tower at Nagasaki, see Tamura et al.²², consisting of 25 cylindrical TLD, each of which is a stacked arrangement of 7 layers of water. Free vibration tests revealed a five times increased critical damping ratio, when compared to the original structure, with a total water mass of only 0.59% of the entire structure. Similar results were obtained in a more recent implementation in the Yokohama marine tower, see again

Tamura et al.²² and Figure 2-7d, where 39 tuned sloshing dampers were installed, with a total water mass of 0.3% of the tower's mass. A study on comfort and serviceability on both towers reflects the beneficial action of the damper in the response of structures.

2.5.2. Seismic Isolation

The concept of seismic isolation was developed to mitigate all kinds of ground excitation, but on the other side, this damping method is not working for other types of loads e.g. for strong wind excitation or from unbalanced machinery. However, this is only a minor restriction for the success of seismic isolation in earthquake prone countries because seismic isolation is a highly appreciated concept to protect important structures from ground motion. The isolation system is typically installed at the foundation of a structure and is therefore often called base isolation system. The first ideas of base isolation date back to the beginning of the 20th century, see Naeim²³, but only since the development of proper high strength bearings, the concept of seismic isolation has become a practical reality. By means of its flexibility, the isolation system partially reflects the incident energy, before it is transmitted to the structure. Consequently, the energy dissipation demand of the structural system is reduced considerably, resulting in an increase of survivability.

Basically, modern seismic isolation systems can be divided into two groups: The most common type are cylindrical multiple-layer hard rubber (or elastomeric) bearings made by vulcanisation bonding of sheets of rubber to thin steel reinforcing plates, Figure 2-8a), see Chopra²⁴. These bearings are very stiff in the vertical direction and can carry the weight of the building while remaining very flexible horizontally, see Figure 2-8b). Because the natural damping of such a bearing is low, additional damping is usually provided by some form of mechanical damper. Commonly, lead plugs are included within the bearing, dissipating energy by yielding, or alternatively, any type external dampers, described in Section 2.1-2.4, can be added.

The second type of isolation system uses rollers or sliders between the foundation and the base of the structure. The shear force transmitted to the structure across the isolation interface is limited by keeping the friction coefficient as low as possible, but at the same time sufficiently high to sustain strong winds or small earthquakes without sliding. To limit the displacements, high tension springs or a concave dish for the rollers have to provide the restoring forces to return the structure to its equilibrium position, see Chopra²⁴. Whichever type of bearing is utilised, one has to ensure that there is enough space around the structure

(the isolation gap) to allow for the necessary large base displacements, which are typically about $0.4m$.

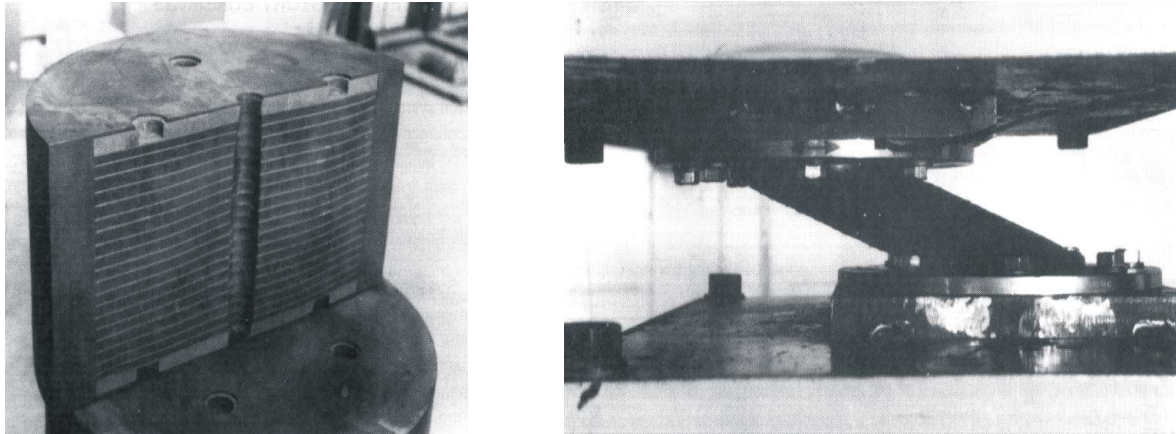


Figure 2-8: base isolation a) cross section of a laminated rubber bearing b) deformed laminated rubber bearing [24]

Base isolation uncouples the building or structure from the horizontal components of the ground motion and allows the simultaneous reduction of interstory drifts and floor acceleration by providing the necessary flexibility. The underlying idea is to cut down the fundamental structural frequency to be much lower than both, its fixed base frequency and the predominant frequencies of the earthquake. The mode shapes of a typical five storey civil engineering structure with constant column stiffness from floor 1-5 but with very low stiffness in the basement is displayed in Figure 2-9. Apparently, the first mode shape of the isolated building involves deformations mainly in the isolation system, keeping the structure above more or less rigid. The mode shape vectors of the higher modes are also excited, however, with very small participation factors, see Eq.(1-49). The isolation system does deflect the earthquake energy through the modified structural dynamics, rather than dissipating it. Nevertheless, a certain level of damping at the isolation level is beneficial to increase the first mode damping ratio and thus suppress resonance at the isolation frequency.

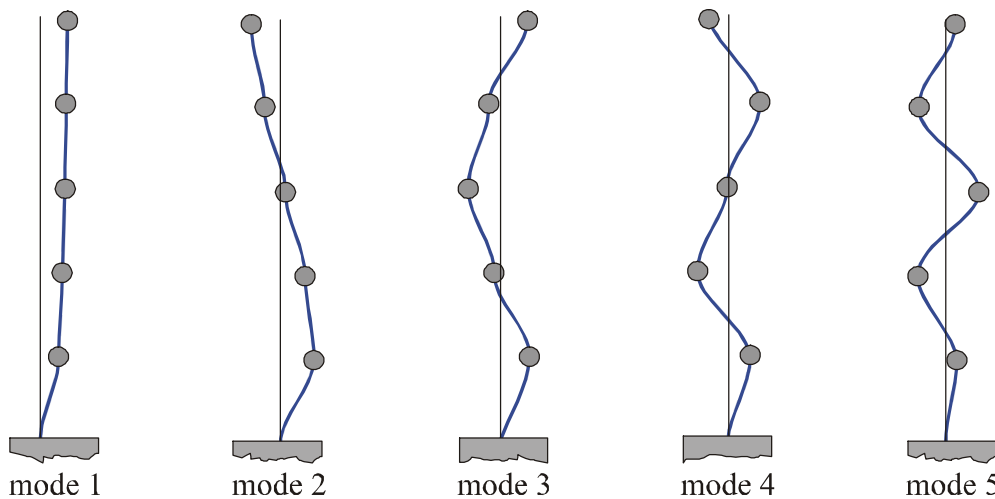


Figure 2-9: Base isolation: five story building with base isolation
(very low stiffness at ground level)

Although existing base isolation systems have proven to be very effective in vibration reduction it has to be mentioned that the predominant frequency content of the earthquake largely determines the beneficial influence of base isolation systems. Assume that the fundamental frequency of a base isolated building was decreased from 2,5 to 0.5Hz , thereby increasing the damping ratio from 2% to 10% due to energy dissipating devices installed at the isolation level. For such a building, Figure 2-10 shows the response spectrum of the 1985 Mexico City earthquake, with spectral ordinates for fixed-base and isolated building, see Chopra²⁴. Although the damping ratio was increased by a factor of five, the pseudo acceleration increased from $0.25g$ to $0.63g$ causing accelerations and a base shear that is approximately 2.5 times the base shear in the original building. This is due to the unusual spectrum of the recorded ground motion (caused by thick layers of alluvium), where the predominant frequencies are between 0.3 and 0.6Hz . Obviously the situation would be even worse, if the fundamental damping wouldn't have been increased to 10%.

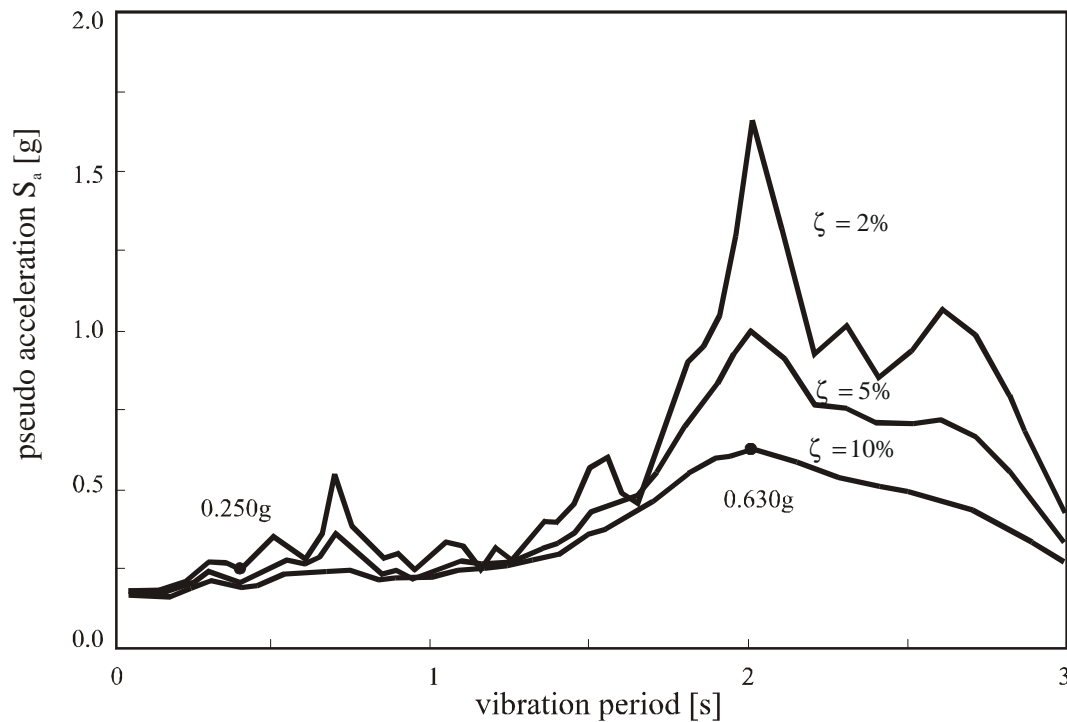


Figure 2-10: Response spectrum for ground motion recorded in Mexico City on September 19th, 1985, Chopra²⁴

Although base isolation systems can not guarantee an improved structural behaviour, it provides a widely accepted and appreciated alternative to fixed base design of structures. Clark²⁵, reports two structures in Japan, where the protection with base isolation systems has already been proven during earthquakes. As it is not necessary to strengthen an existing structure by adding new structural members seismic isolation is attractive for both, buildings which must remain functional after a major earthquake (e.g. hospitals, schools, emergency centres) and retrofit of existing structures that are brittle and weak. Actual implementations are numerous, many of them are listed in Naeim²³, including very prestigious buildings like the San Francisco City Hall or the Los Angeles City Hall (28 story), the Emergency Operations Centre (Los Angeles), or the Fire Command and Control Facility (Los Angeles). In Japan, where earthquake resistant design always had a high priority, the seismic isolation implementations started 1986 and at the time of the January 1995 Kobe earthquake about 80 systems were installed, see e.g. Kelly²⁶. In Europe base isolation is most actively studied and designed in Italy and France, but the first base isolated building of the world was completed in 1981 in New Zealand. Several other buildings followed, e.g. the outstanding retrofit of the New Zealand Parliament House, see Naeim²³.

2.6. Tuned Mass Dampers

The relatively new concept of utilising tuned mass dampers for structural control has its roots in the dynamic vibration absorbers, invented by Frahm²⁷ in 1909, see also DenHartog²⁸. The first vibration absorbers consisted of a small spring-mass system (stiffness k , mass m) attached to a large spring-mass system (stiffness K , mass M), as shown in Figure 2-11. Let the combination K , M be the schematic representation of a vibrating machine, with a harmonic force $f(t) = f_0 \sin(\nu t)$ acting on it. Under this simple load it can be shown that the main mass does not vibrate, if the natural frequency $\sqrt{k/m}$ of the absorber is chosen to be equal to the frequency ν of the disturbing force f . Much of the initial work has been focused on the restrictive assumption that a single operating frequency is in resonance with the fundamental frequency of the machine. Civil engineering structures however, are subjected to different types of environmental loads, which contain many frequency components. Thus, the performance of TMD is complex, and for multiple-degree-of-freedom less efficient than expected. The theory of damped and undamped vibration absorbers in absence of structural damping was first studied by DenHartog, who developed basic principles for proper selection of absorber parameters.

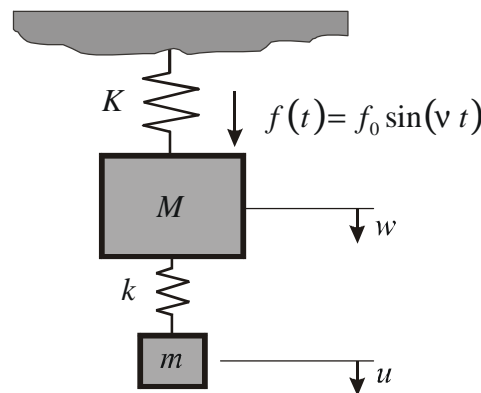


Figure 2-11: Undamped Absorber and Main Mass (Machine) subject to harmonic excitation (Frahm's Absorber, Frahm²⁷)

In order to increase the absorber's effectiveness in reducing the maximum dynamic response of the main system, the application of nonlinear spring elements was investigated with the aim of widening the tuning frequency range, see Soong³⁵: Roberson²⁹ applied a Duffing type spring and demonstrated that the 'suppression band' of the nonlinear system was much wider than that of a linear absorber. A different attempt to improve the performance of dynamic vibration absorbers was the application of materials with frequency dependent stiffness, see

Snowdon³⁰, which clearly was superior to the classical spring-dashpot type absorber. Soong³⁵ also reports that other investigators experimented with different configurations of TMD, e.g. a second undamped tuned mass added in parallel or triple-element absorbers, where a second spring is added in series with the damper. Both alternative configurations show a good vibration reduction behaviour, but are sensitive to variations in the tuning.

2.6.1. Basic equations

From a mechanical point of view, the model considered by DenHartog and Frahm is identical with that of a structure under a fundamental frequency vibration. Such a basic configuration is given by the SDOF model in Figure 2-12, where a ground acceleration \ddot{w}_g and an external wind force $f(t)$ excite the building. $f(t)$ as well as the structural mass M and stiffness K can also be modal quantities. By applying Newton's law to the free-body-diagrams of mass M and m , the equations of motion can be written directly as

$$(M + m)\ddot{w} + C\dot{w} + Kw = -(M + m)\ddot{w}_g + f(t) - m\ddot{u}. \quad (2-1)$$

$$m\ddot{u} + c\dot{u} + ku = -m(\ddot{w}_g + \ddot{w}) \quad (2-2)$$

It is seen from Eq.(2-2), that the influence of the dynamic absorber on the host structure is firstly a negligible increase in effective mass $M + m$ leading to a slightly decreased natural frequency, and secondly, an additional forcing term $m\ddot{u}$ which is responsible for the modified, normally improved, dynamic behaviour. Again, energy considerations can help to get a better insight into the absorber-host structure interaction. Assuming that the excitation terms on the right hand side of Eq.(2-2) are time-harmonic or alternatively stationary random inputs, Eq.(2-2) can be rewritten in form of energy or power balance

$$E[(M + m)\ddot{w}\dot{w}] + E[C\dot{w}\dot{w}] + E[Kw\dot{w}] = -E[(M + m)\ddot{w}_g\dot{w}] + E[f(t)\dot{w}] - E[m\ddot{u}\dot{w}], \quad (2-3)$$

where $E[\cdot]$ denotes the expectation, which, under the assumption of ergodicity becomes the time average

$$E[f(t)] = \frac{1}{T} \int_0^T f(t) dt, \quad (2-4)$$

for random input. It simplifies to the time average in one cycle for the case of harmonic excitation. When the steady state response is of concern, the theory of random vibration states that $E[\ddot{w}\dot{w}] = E[\dot{w}w] = 0$, see e.g. Newland³¹ or Parkus³².

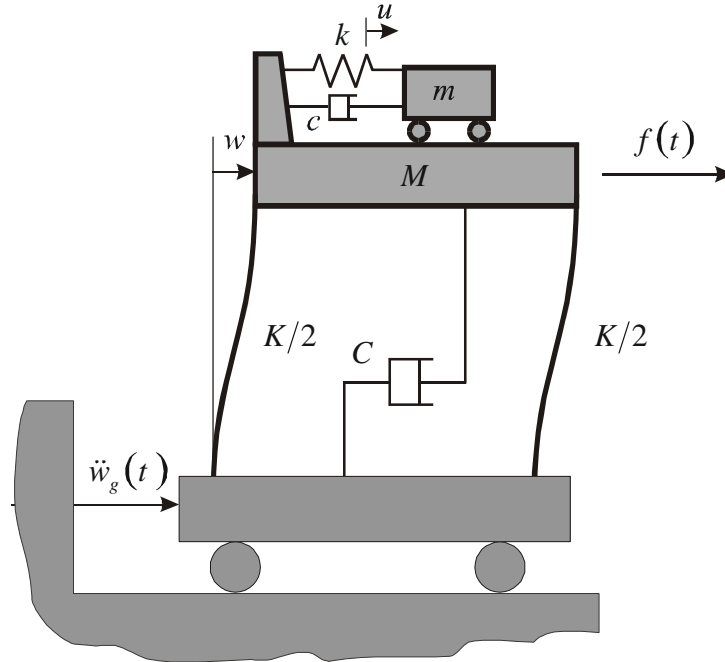


Figure 2-12: Model of a SDOF structure with TMD attached

Eq.(2-3) is thus simplified and reduces to a simple power balance equation

$$C E[\dot{w}^2] = E[(f(t) - (M + m)\ddot{w}_g)\dot{w}] - m E[\ddot{u}\dot{w}], \quad (2-5)$$

in which $C E[\dot{w}^2]$ is the dissipated power due to structural damping, and $E[(f(t) - (M + m)\ddot{w}_g)\dot{w}]$ is the external power input from the excitation source. The remaining term $m E[\ddot{u}\dot{w}]$, describes the power flow from the structural system to the absorber mass, and plays a central role for the application of dynamic absorbers in structures. The basic relation given by Eq.

(2-5) is, that the larger the power flow, the smaller the mean square velocity response of the host structure. Apparently the power flow becomes a maximum, if \ddot{u} and \dot{w} are in phase, which is equivalent to a relative absorber displacement phase lag of $\pi/2$ when compared to the main structure. As the application of a TMD can increase the energy dissipation capability

of a structural system, it is convenient to define a total equivalent effective damping C_{eq} , and an effective damping ratio $\zeta_{eq} = \zeta + \Delta\zeta$ where

$$C_{eq} = C + \Delta C, \quad \Delta C = m \frac{E[\ddot{u} \dot{w}]}{E[\dot{w}^2]} \quad (2-6)$$

It is worth noting, that an incompetent choice of absorber parameter, can also inverse the desired effect of increasing the energy dissipation capabilities. Furthermore, the amount of input energy from the external source can change depending on the TMD efficiency. However, this variation is small when compared to the power flow, and can even decrease for a properly tuned absorber. The definition of the equivalent damping C_{eq} shows clearly that it is not a constant value, but strongly depends on the excitation frequency, as will be shown in the next section, where DenHartog's approach, see DenHartog²⁸, for finding the optimal absorber parameter is presented.

2.6.2. DenHartog's solution for optimal absorber parameter

In order to obtain more general results, it is advisable to normalise Eq.(2-1), with respect to the acceleration terms,

$$(1 + \mu) \ddot{w} + \mu \ddot{u} + 2\zeta_s \Omega_s \dot{w} + \Omega_s^2 w = -(1 + \mu) \ddot{w}_g + \frac{f(t)}{M}. \quad (2-7)$$

$$(\ddot{u} + \ddot{w}) + 2\zeta_A \omega_A \dot{u} + \omega_A^2 u = -\ddot{w}_g, \quad (2-8)$$

$$\Omega_s = \sqrt{\frac{K}{M}}, \omega_A = \sqrt{\frac{k}{m}}, \zeta_s = \frac{C}{2\Omega_s M}, \zeta_A = \frac{c}{2\omega_A m}, \mu = \frac{m}{M},$$

where $\Omega_s, \omega_A, \zeta_s, \zeta_A$ denote the fundamental frequency of the SDOF-structure and the attached absorber, as well as the corresponding damping ratios, respectively, μ is the absorber to building mass ratio. Having introduced the ratio of the natural frequencies $\delta = \omega_A / \Omega_s$, DenHartog solved Eqs.(2-7) and (2-8) for a time harmonic force excitation $f(t) = f_0 e^{i\nu t}$ with forcing frequency ν assigned. Under steady state conditions the system's response will also be a harmonic with the excitation frequency ν and the complex displacement amplitudes $W(\nu)$ and $U(\nu)$. The dynamic effect of a TMD is measured in

comparison with the static deflection produced by the maximum force f_0 when applied statically to the structure. This static displacement is $W_{st} = f_0/K$, while the dynamic amplification factor $|W(\nu)|/W_{st}$ is given by

$$A_d(\gamma) = \frac{W}{W_{st}} = \sqrt{\frac{(2\zeta_A \gamma \delta)^2 + (\gamma^2 - \delta^2)^2}{(2\zeta_A \gamma \delta)^2 (1 - \gamma^2(1 + \mu))^2 + (\mu \gamma^2 \delta^2 + (1 - \gamma^2)(\gamma^2 - \delta^2))^2}}. \quad (2-9)$$

DenHartog's approach assumes negligibly small structural damping, $\zeta_s \approx 0$, and when keeping the mass ratio μ arbitrary, but constant, the frequency ratio δ and the damping coefficient ζ_A become the free parameter for the optimisation. This assumption of negligible structural damping is realistic as vibration problems mainly occur in lightly damped structures. Figure 2-13 shows a typical plot of the amplitude amplification $A_d(\gamma)$, Eq.(2-9), as a function of the nondimensional excitation frequency γ for $\delta = 1$ (tuned case), a mass ratio of $\mu = 0.05$, and several damping ratios ζ_A .

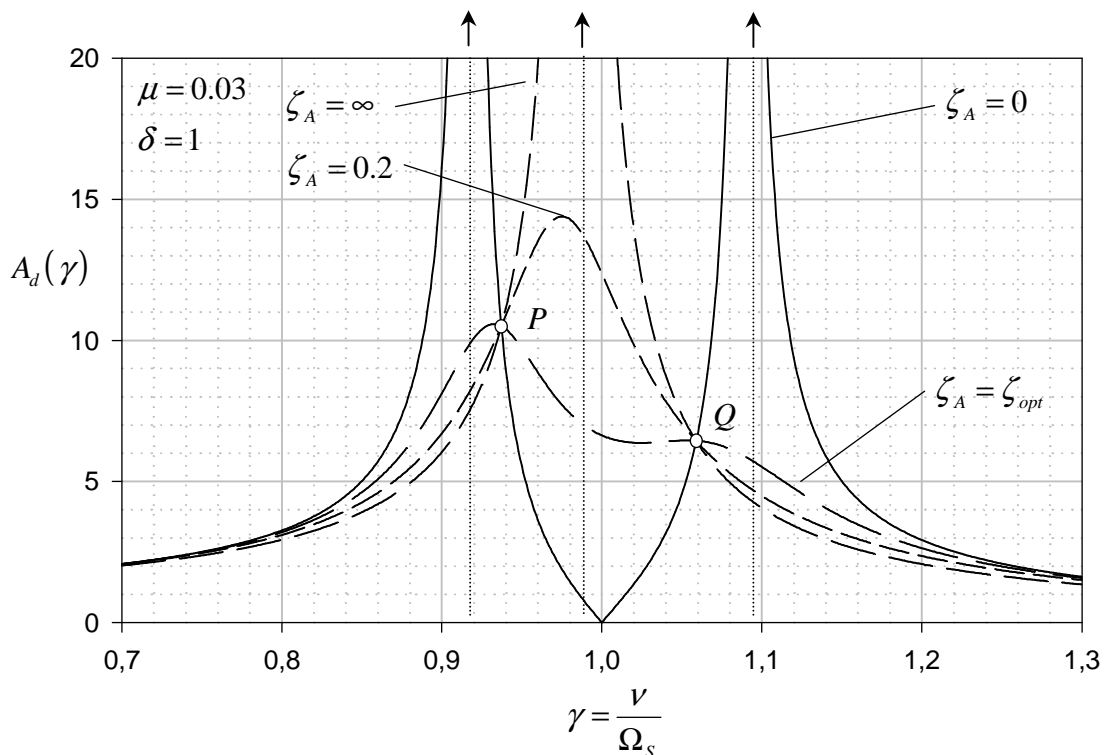


Figure 2-13: Amplification factor as a function of γ and ζ_A

It is important to note the influence of the TMD damping, without absorber damping ($\zeta_A = 0$) the response amplitude of the combined system is infinite at two new resonant frequencies on either side of the tuning frequency. However, exactly at the tuning frequency, the amplitude response vanishes, which is the ideal situation for narrow band, or single frequency excitation at stationary motion. If the TMD damping is infinite, the two masses are virtually fixed together, forming a new single-degree-of-freedom system with an increased mass $M(1 + \mu)$ and a slightly decreased resonant frequency. Therefore, somewhere between these extremes there must be an optimal value of ζ_A for which the peak response becomes a minimum for broad band excitation. The main objective in designing the TMD is to reduce the peaks of $A_d(\nu)$ over a broad band of the excitation frequency.

Figure 2-13 also shows an important phenomenon which occurs in case of an undamped structure: independent of the absorber damping ratio ζ_A there exist two invariant points P and Q where all response curves possess the same amplification factor, see again DenHartog²⁸. The objective of minimal structural response is accomplished by demanding that the invariant points P and Q have equal heights, e.g. equal response amplification factors. This is achieved by the correct choice of δ and subsequently ζ_A can be employed to adjust the response curve to pass horizontally through either of P or Q in Figure 2-13. Following this procedure, DenHartog has given the optimum frequency ratio δ as

$$\delta = \frac{\omega_A}{\Omega_s} = \frac{1}{1 + \mu}, \quad (2-10)$$

which gives the minimum response amplitude at P and Q :

$$A_{PQ} = \sqrt{1 + \frac{2}{\mu}}. \quad (2-11)$$

The determination of the optimal absorber damping ratio ζ_A is more involved, and after a long and tedious derivation, the optimal damping ratio turns out to be dependent on whether the response curve passes horizontally through P or Q . The corresponding optimal values of ζ_A are found to be, see DenHartog²⁸,

$$\zeta_{opt}^P = \frac{\mu \left(3 - \sqrt{\frac{\mu}{\mu+2}} \right)}{8(1+\mu)^3}, \quad \zeta_{opt}^Q = \frac{\mu \left(3 + \sqrt{\frac{\mu}{\mu+2}} \right)}{8(1+\mu)^3} \quad (2-12)$$

The arithmetic mean is a useful alternative value for the broad band optimisation:

$$\zeta_{opt} = \frac{3 \mu}{8(1+\mu)^3} \quad (2-13)$$

From Eq.(2-11) it is obvious, that an increase in TMD mass will always reduce the maximum amplification factor, for an optimally designed TMD. The response amplification for an optimally designed absorber has been calculated, and is illustrated in Figure 2-14: The invariant points possess the same amplification factor.

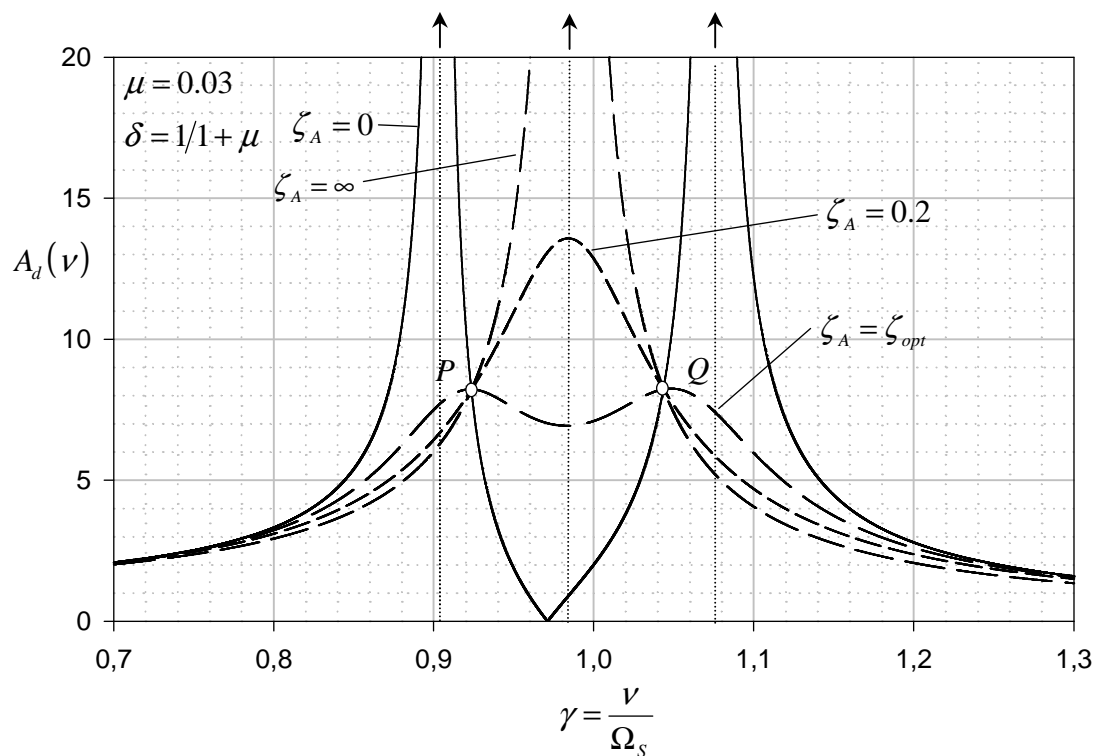


Figure 2-14: Optimally Tuned TMD for broad band excitation, see also DenHartog²⁸

Once the TMD is designed, it might be interesting, to study the influence on the overall structural damping. Hence it is convenient to express the equivalent damping factor of Eq.

(2-6) in terms of the equivalent nondimensional damping ratio ζ_{eq} ,

$$\zeta_{eq} = \zeta_s + \Delta\zeta_s = \frac{C}{2M\Omega_s} + \frac{\Delta C}{2M\Omega_s}. \quad (2-14)$$

Apparently, the equivalent damping ratio cannot be decreased, as, in average, there is no energy transfer from the TMD to the structure. In Figure 2-15 the increase in the equivalent damping ratio $\Delta\zeta_s$ is plotted against the nondimensional excitation frequency γ . For small values of ζ_A (light TMD damping) very high effective structural damping can be achieved in a narrow frequency band, which is ideal for single frequency excitation. Increasing ζ_A further, increases $\Delta\zeta_s$ on a broad frequency band, before this desired effect starts to disappear for highly damped TMDs. From Figure 2-15, it is apparent, that for a given ζ_A , the effective damping ratio varies with the excitation frequency. Therefore it is misleading to calculate an equivalent damping ratio from the complex eigenvalues of the 2-DOF system.

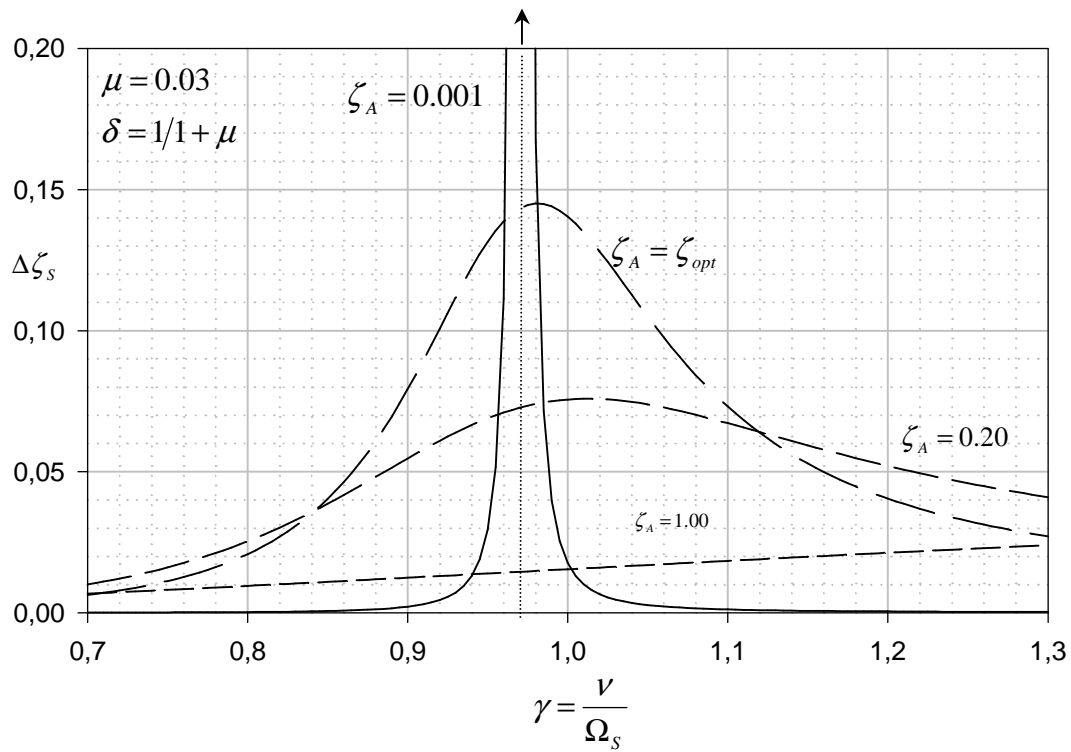


Figure 2-15: Change in Equivalent Damping Ratio $\Delta\zeta_s$, see Eq.

(2-6), due to TMD

Since the assumption of undamped host structures does not hold in reality, a numerical optimisation of Eq. (2-9) must be performed to find the optimal values of γ and ζ_A . A

detailed analysis was carried out by Warburton³³, who has determined optimal parameters for both, harmonic and stationary random excitations. Comparison has revealed that even for moderately damped structures the DenHartog formulas guarantee an excellent optimisation, at least for civil engineering purpose in the elastic range, especially when taking into account uncertainties in stiffness and mass distribution of the real structure. In Figure 2-16 the amplitude response curves are shown for an exact and approximated optimisation of a TMD system where a structural damping of $\zeta_s = 5\%$ is assumed. Although the amplification response curve is no longer symmetric, the response of the optimal designed system, does not differ significantly for broad band excitation.

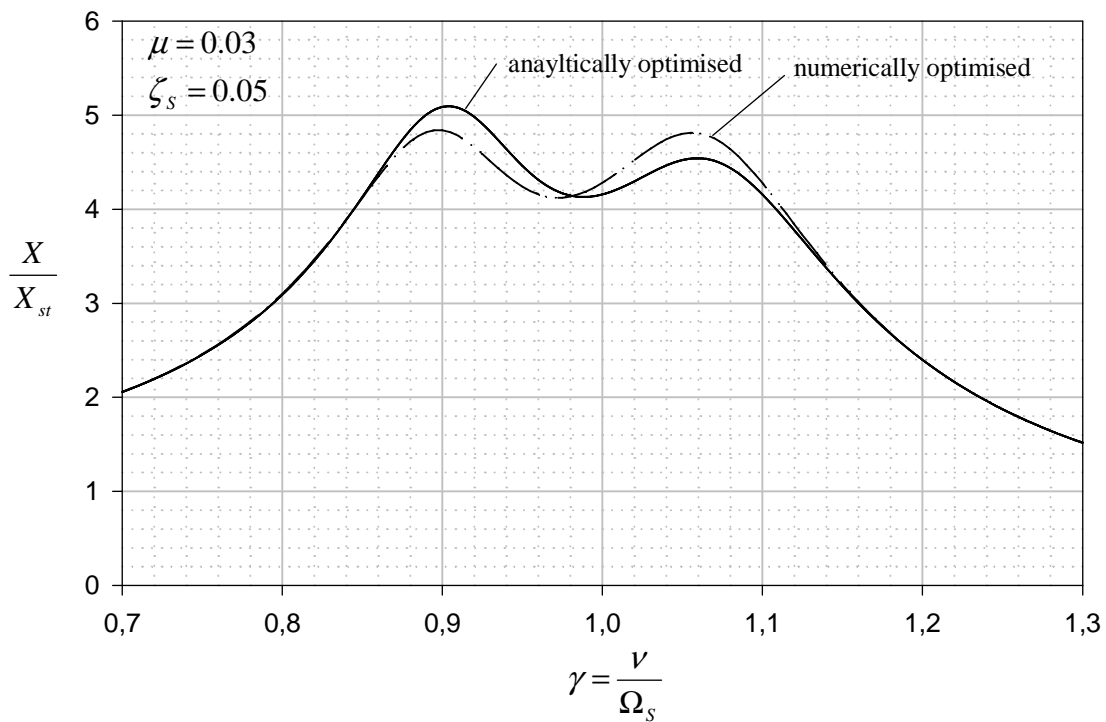


Figure 2-16: Comparison of analytical and numerical TMD design

The reduction of the maximum response amplification due to an external force (wind load), was the optimisation goal for the formulas derived above. However, several other optimisation criteria have been proposed in literature, some of which are summarised in Table 2-1, see Constantinou³⁴:

Excitation		Optimised response		Optimised absorber parameters	
Type	Applied to	Parameter optimised	$\frac{w}{w_{stat}}$	δ_{opt}	$\zeta_{A,opt}$
Force $f_0 \sin(\nu t)$	Structure	$\frac{w}{f_0/K}$	$\sqrt{1 + \frac{2}{\mu}}$	$\frac{1}{1 + \mu}$	$\sqrt{\frac{3\mu}{8(1 + \mu)}}$
Force $f_0 \sin(\nu t)$	Structure	$\frac{\ddot{w}}{f_0/M}$	$\sqrt{\frac{2}{\mu(1 + \mu)}}$	$\frac{1}{\sqrt{1 + \mu}}$	$\sqrt{\frac{3\mu}{8(1 + \mu/2)}}$
Acceleration $\nu^2 w_g \sin(\nu t)$	Base	$\frac{\ddot{w}}{\nu^2 w_g}$	$\sqrt{\frac{2}{\mu}}(1 + \mu)$	$\frac{\sqrt{1 - \mu/2}}{1 + \mu}$	$\sqrt{\frac{3\mu}{8(1 + \mu)(1 - \mu/2)}}$
Acceleration $\nu^2 w_g \sin(\nu t)$	Base	$\frac{\ddot{w}_g + \ddot{w}}{\ddot{w}_g}$	$\sqrt{\left(1 + \frac{2}{\mu}\right)}$	$\frac{1}{1 + \mu}$	$\sqrt{\frac{3\mu}{8(1 + \mu)}}$
stat. Random Force	Structure	$\frac{E[w^2]K^2}{2\pi S_0 \Omega_s}$	$\sqrt{\frac{1 + 3\mu/4}{\mu(1 + \mu)}}$	$\sqrt{\frac{1 + \mu/2}{(1 + \mu)^2}}$	$\sqrt{\frac{\mu(1 + 3\mu/4)}{4(1 + \mu)(1 + \mu/2)}}$
stat. Random Acceleration	Base	$\frac{E[w^2]\Omega_s^3}{2\pi S_0}$	$\left((1 + \mu)^3 \left(\frac{\mu}{4} - \frac{1}{4}\right)\right)^{\frac{1}{2}}$	$\sqrt{\frac{1 - \mu/2}{(1 + \mu)^2}}$	$\sqrt{\frac{\mu(1 - \mu/4)}{4(1 + \mu)(1 - \mu/2)}}$
Note: $E[w^2]$ is the mean square value of $w(t)$. S_0 is the force intensity or acceleration intensity, $\mathcal{F}\{f(t)\} = S_0$, or $\mathcal{F}\{\ddot{w}_g(t)\} = S_0$					

Table 2-1: Optimal TMD parameters for various excitations and response parameters of a SDOF-system

Several other criteria, including absorber, and mixed absorber-structure measures, have been proposed, and an excellent overview of the results published can be found again in Soong³⁵.

2.6.3. Structural implementations

A number of practical considerations must be observed in the engineering design of a TMD system. First and foremost is the amount of added mass that can be practically placed on the top of the building, modelled as SDOF-structure. Secondly, the TMD travel relative to the

building is another important design parameter. Large movements often need to be accommodated for reasonable response reduction of the building. Another major engineering technique associated with a sliding mass arrangement is to provide a low friction bearing surface (often hydrostatic pressure bearings) so that the mass can respond to the building movement at low levels of excitation. To compensate for friction losses the installation of an active force system is required, causing the need for complex electronics and an operation triggering system. Nevertheless a number of TMD systems have been installed in tall buildings, bridges and towers for response control of primarily wind induced external loads, see Holmes³⁶ and EERC³⁷ for a list of world-wide installations. Kwok et al.³⁸ report the successful installation of TMD in several tall buildings in great detail. The first structure in which a TMD was installed in 1973, appears to be the CN-Tower, Toronto, Canada. In USA the Citicorp Center (1978) in New York and the John Hancock Tower (1977) in Boston are equipped with TMDs. In Japan, several towers, building and cable stayed bridges have been equipped, and countermeasures against traffic induced vibrations were carried out by means of TMD. Furthermore installations are reported from Saudi Arabia, United Arab Emirates, Germany, Belgium, Pakistan, Australia, see again Holmes³⁶ and EECR³⁷.

2.7. Smart Materials

Passive energy dissipation is only one approach to structural control. In recent years research and development efforts have been focused towards the utilisation of active systems, with the main difference that those applications need a reliable large external energy source. Between those well established control technologies is the relatively new field of innovative or smart materials for sensing and control purposes. Being incorporated into structural members or system components those materials are capable of quickly modifying their own behaviour and thus, the structural behaviour according to external parameters. The most famous materials that have been examined for structural implementations in recent years are shape memory alloys, piezoelectric elements, electro-rheological and magneto-rheological fluids. Most of the successful applications of such materials are reported in the field of aerospace structures and mechanical systems, weapon systems and robotics, as well as other high precision devices. Their application potential to civil engineering structures remains to be assessed from the point of view of cost as well as technical feasibility.

2.7.1. Shape memory alloys

The shape memory effect (SME) of an alloy is generally referred to its ability to undergo reversible and diffusionless transformation between austenite, the high temperature phase ($T > T_A$ where T_A is the transition temperature to the austenite state) and martensite, the low temperature crystalline phase ($T < T_M$ where T_M is the temperature below which the microstructure is martensitic). In-between there is a third phase, the stress induced martensite, which is formed in the austenite phase if sufficient stress is applied. For cyclic loading in the martensite phase the schematic stress strain diagram is similar to that for conventional steel. The same is true for the high temperature austenite phase. However, if the ambient temperature is slightly higher than T_A then a superelastic behaviour can be observed, shown in Figure 2-17a, see McKelvey³⁹.

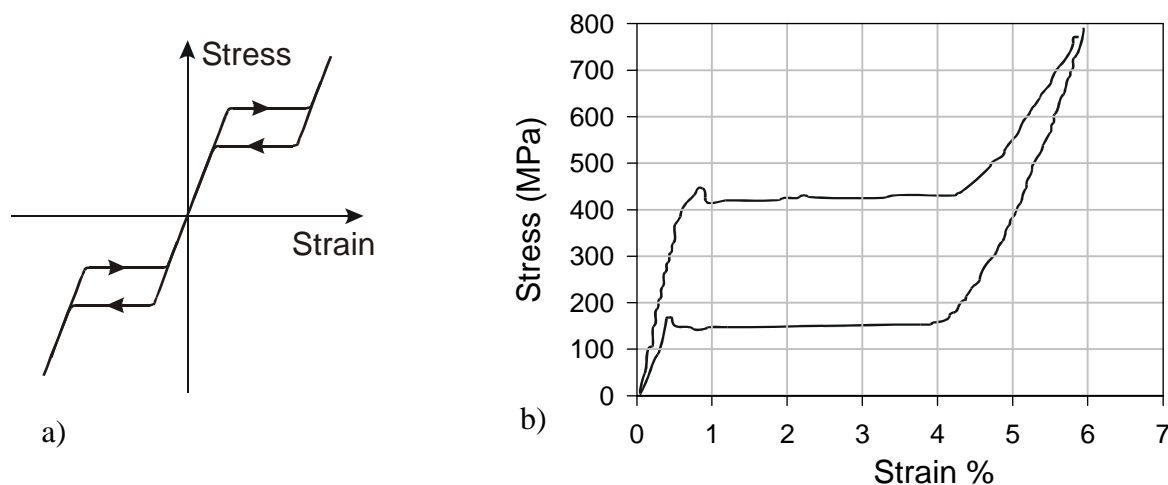


Figure 2-17: Superelasticity of Shape Memory Alloys a) Schematic stress strain b) measured hysteresis for tensile cycle of NiTi material, see McKelvey³⁹

This superelastic SMA behaviour results from the elastic loading of a stable austenitic parent phase up to a threshold stress above which a stress induced transformation from austenite to martensite takes place. This transformation occurs at a significantly reduced modulus, thus giving the appearance of a yield point. As deformation proceeds, the volume of martensite increases, and the path of the stress strain curve forms a stress plateau. If the microstructure is fully martensitic, further straining will cause the martensite to be loaded elastically at a modulus lower than that of initial austenite. Since the martensite is stable only due to the applied stress, a reverse transformation takes place during unloading, but at a lower stress

level. Ideally, after a full loading cycle the material returns to its original geometry with zero residual strains and therefore the term “superelasticity” applies. At much higher temperatures this effect disappears, leading to linear elastic behaviour again.

This material property of SMAs are of interest for structural applications. An additional advantage is the inherent self centring mechanism even for hysteretic behaviour. Today it is possible to create different SMA some of which show low temperature sensitivity and excellent corrosion behaviour. At present, SMAs are well established for medical purposes (stents for clogged arteries), and mechanical engineering (clamps, actuators), where the shape memory effect is used, and recently and increased research effort in SMA has been noted, see e.g. Graesser et al.⁴⁰, Casciati et al.⁴¹, Dolce et al.⁴², Wilde⁴³. Two structural applications of SMA have been reported in Italy, where church towers (one is the famous church of Francesco d’Assisi) have been equipped with energy dissipating SMA-devices. A major problem is still the heat generated during dissipation, which is the reason that most SMA devices work with a bunch of thin wire filaments to absorb mechanical energy, see Figure 2-18 where a passive device, based on SMA is illustrated.

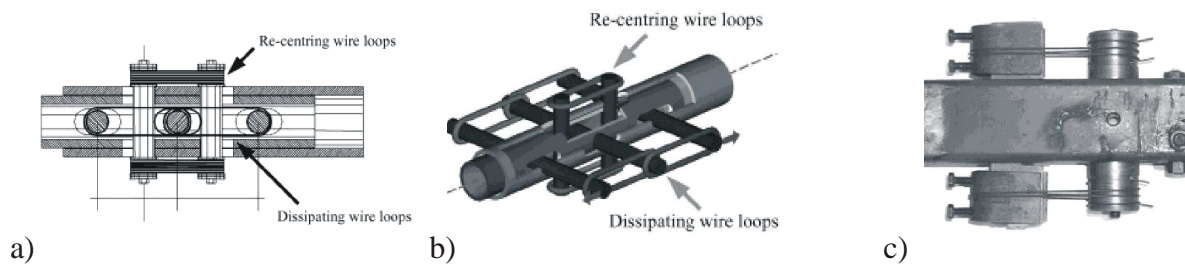


Figure 2-18: SMA dissipating device: a) plan view b) schematic 3D-view with wire filaments c) actual implementation, see Dolce et al.⁴²

2.7.2. Piezoelectric materials

The piezoelectric effect was first discovered at the end of the 19th century, when it was shown that a stress field applied to certain crystalline materials produce an electrical charge on the material surface. This phenomenon is called the direct piezoelectric effect. It was subsequently demonstrated that the converse effect is also true: when an electric field is applied to a piezoelectric material it changes its shape and size, see Cady⁴⁴. This observation resulted in their use as an actuator in many applications, but piezoelectric materials can also be used as sensors, or combined as a self sensing actuator. Piezoelectric materials can produce large forces or induce high voltages which lead to the invention of novel devices applied to

vibration sensing and control of aerospace structures, robotics, micro-mechanical systems and recently structural elements, see Soong³⁵. Compactness, light weight, simplicity, reliability and effectiveness over a wide frequency range makes piezoelectric devices superior to many other actuators and sensors. The conversion of mechanical energy into its electrical equivalent and vice versa leads also to interesting applications in passive structural control. If a piezoelectric material, fixed to a structural member, is connected to a resonant electrical network, the vibration reducing characteristics of a TMD can be obtained, see e.g. von Flotow⁴⁵. Furthermore, piezoelectric material can be used to actively influence the dynamic behaviour of structural elements, see e.g. Hagenauer et al.⁴⁶, Irschik et al.^{47,48}, Pichler et al.⁴⁹ or Krommer et al.⁵⁰

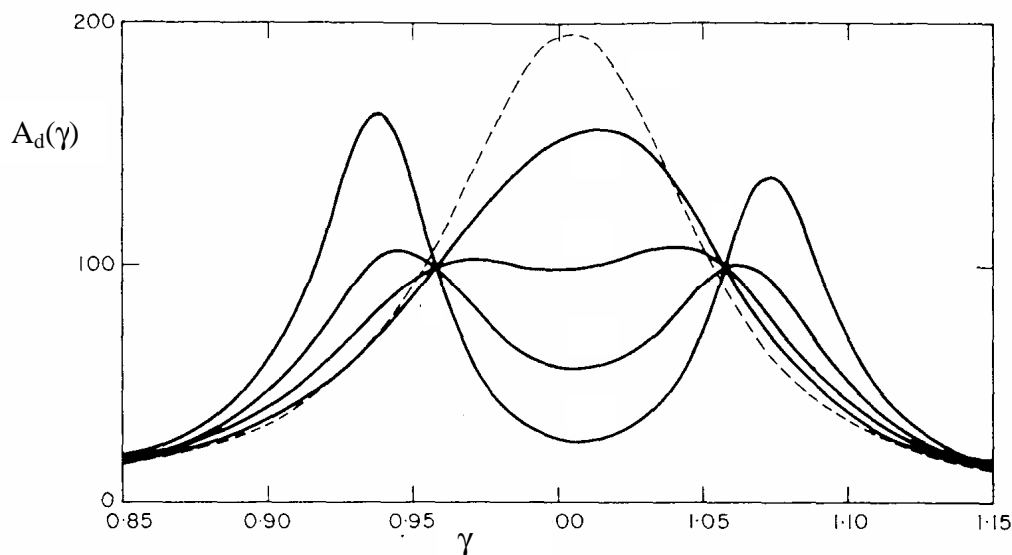


Figure 2-19: Frequency response curves of a SDOF system containing a piezoelectric element connected to a passive resonant electrical network Flotow⁴⁵

Although considerable progress has been made in research and applications of piezoelectric control technology, its implementation to large-scale civil engineering structures remains to be examined. A major problem is caused by the high voltage required to generate an effective control action which can be in the range of up to several thousand volts.

2.7.3. Electrorheological fluid

Electrorheological (ER) fluids are suspensions of highly polarised fine particles dispersed in an insulating oil. When an electric field is applied to the ER fluid the particles form chains which lead to changes in viscosity of the medium in the range of several orders of magnitude, as well as alterations of elasticity. The potential of ER fluids in applications as control devices

was early recognised, but only the discovery of new ER materials in the late 1980s lead to an increased development of ER devices, including clutches, engine mounts, shock absorbers, robotic devices and structural vibration dampers. A typical device, see e.g. Burton et al.⁵¹, is shown in Figure 2-20, and consists of a main cylinder and a piston rod that pushes an ER through an annular duct, where the varying electric field is applied.

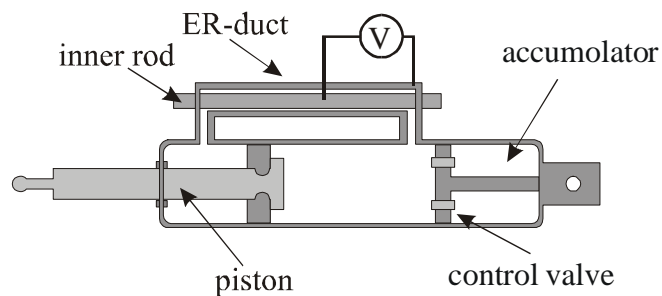


Figure 2-20: ER damper with annular duct, see Burton et al.⁵¹

2.7.4. Magnetorheological fluid

Magnetorheological (MR) fluids, are the magnetic counterpart of ER fluids, where the reversible change in viscosity is based on magnetically polarisable particles. This resistance to flow can be used in a similar manner as indicated for ER fluids. Additional to all these similarities, MR fluids show further attractive features like low viscosity and a stable hysteretic behaviour over a broader temperature range. Spencer et al.⁵² have investigated the possible application of magnetorheological dampers for semi-active control.

2.8. References

- ¹ Wen, Y.K., *Methods of random vibration for inelastic structures*, Applied Mechanics Reviews, vol.42(2), 1989
- ² Skinner, R.I., Tyler, R.G., Heine, A.J., Robinson, W.H., *Hysteretic Dampers for the Protection of Structures from Earthquakes*, Bulletin New Zealand Society of Earthquake Engineering, vol.13(1), pp.22-36, 1980
- ³ Chiampi, V., *Use of Energy Dissipation Devices, based on yielding of steel, for earthquake protection of structures*, Proceedings of International Meeting on Earthquake Protection of Buildings, pp.14/D-58/D, 1991
- ⁴ Perry, C.L., Fierro, E.A., Sedarat, H., Scholl, R.E., *Seismic Upgrade in San Francisco Using Energy Dissipation Devices*, Earthquake Spectra, vol.9(3), pp.559-579, 1993
- ⁵ Martinez-Romero, E., *Experiences on the Use of Supplemental Energy Dissipators on Building Structures*, Earthquake Spectra, vol.9(3), pp.581-625, 1993

- ⁶ Pall, A.S., Pall, R., *Friction-dampers for seismic control of buildings "A Canadian Experience"*, 11th world conference on earthquake engineering, paper no.497, Acapulco, Mexico 1996
- ⁷ Lei, Y., *Sure and Random Vibrations of Simple Dissipative Civil Engineering Steel Structures*, dissertation and report, Technical University of Vienna, 1994
- ⁸ Lei, Y., Ziegler, F., *Random Response of Friction Damped Braced Frames under Severe Earthquake Excitation*, Fifth U.S. Nat. Conference on Earthquake Engineering, Chicago, Illinois, July 10-14, 1994, pp.683-692, Earthquake Research Institute, ISBN 0-943198-46-1
- ⁹ Samali, B., Kwok, K.C.S., *Use of viscoelastic dampers in reducing wind- and earthquake-induced motion of building structures*, Engineering Structures, vol.17(9), pp.639-654, 1995
- ¹⁰ Zhang, R., Soong, T.T., Mahmoodi, P., *Seismic Response of Steel Frame Structures with Added Viscoelastic Dampers*, Earthquake Engineering and Structural Dynamics, vol.18, pp. 389-296, 1989
- ¹¹ Tsai, C.S., Lee, H.H., *Applications of Viscoelastic Dampers to High-Rise Buildings*, Journal of Structural Engineering, vol.119(4), pp.1222-1233, 1993
- ¹² Makris N., Constantinou, M.C., *Fractional-Derivative Maxwell Model for Viscous Dampers*, Journal of Structural Engineering, vol.117(9), pp.2708-2724, 1991
- ¹³ Taylor, D.P., Constantinou, M.C., *Development and Testing of an Improved Fluid Damper Configuration for Structures having High Rigidity*, WWW-publication, Taylor Devices, Inc., www.taylordevices.com
- ¹⁴ Yeung, N., Pan, A.D.E., *The effectiveness of viscous-damping walls for controlling wind vibrations in multi-story buildings*, Journal of Wind Engineering and Industrial Aerodynamics, vol.77&78, pp.337-348, 1998
- ¹⁵ Housner G.W., Bergman, L.A., Caughey, T.K., Chassiakos, A.G., Claus, R.O., Masri, S.F., Skelton, R.E., Soong, T.T., Spencer, B.F., Yao, J.T.P., *Structural Control: Past, Present, and Future*, Journal of Engineering Mechanics, vol.123(9), pp.897-971
- ¹⁶ Bauer, H.F., *Oscillations of Immiscible Liquids in Rectangular Container: A New Damper for Excited Structures*, Journal of Sound and Vibration, 1984, vol.92(1),117-133
- ¹⁷ Rammerstorfer, F.G., Scharf, K., Fischer, F.D., *Storage tanks under earthquake loading*, Applied Mechanics Reviews, vol.43(11), pp.261-282, 1990
- ¹⁸ Heuer, R., *Dynamische Wirkung eines Dach-Schwimmbeckens*, (in German), Master Thesis, TU-Vienna, 1984
- ¹⁹ Haßlinger, L., Heuer, R., Ziegler, F., *Dynamische Wirkung eines Dachschwimmbeckens auf einen harmonisch erregten Stockwerkrahmen (mit Modellversuchen)*, ÖIAZ, vol.130, 1985
- ²⁰ Hayek, H., *Räumliche Bebenerrregte Schwingungen eines Hochbehälters, rechnerische und experimentelle Untersuchungen*, (in German), Master Thesis, TU-Vienna, 1985
- ²¹ Modi, V.J., Welt, F., Seto, M.L., *Control of wind-induced instabilities through application of nutation dampers: a brief overview*, Engineering Structures, vol.17(9), pp.626-638, 1995
- ²² Tamura, Y., Fujii, K., Ohtsuki, T., Wakahara, T., Koshaka, R., *Effectiveness of Tuned Liquid Column Dampers in Tower-like Structures*, Engineering Structures, 1995, 17(9), 609-621
- ²³ Naeim, F., Kelly, J.M., *Design of Seismic Isolated Structures*, J Wiley, 1999
- ²⁴ Chopra, A.K., *Dynamics of structures*, Prentice Hall, 1995

- ²⁵ Clark, P., *Response of Base Isolated Buildings*, WWW-publication, National Information Service for Earthquake Engineering, sponsored by the National Science Foundation and the University of California, Berkeley, 1997, WWW-address: <http://www.nd.edu/~quake/>
- ²⁶ Kelly, J.M., *Base Isolation: Origins and Development*, WWW-publication, National Information Service for Earthquake Engineering, sponsored by the National Science Foundation and the University of California, Berkeley, 1998
- ²⁷ Frahm, H. *Device for Damped Vibrations of Bodies*, U.S. Patent No. 989958, 1909
- ²⁸ DenHartog, J.P., *Mechanical Vibrations*, reprint of 4th ed. McGrawHill 1956
- ²⁹ Roberson, R.E., Synthesis of a Non-linear Dynamic Vibration Absorber, J. Franklin Inst., vol.254, pp.205-220, 1952
- ³⁰ Snowdown, J.C., Dynamic Vibration Absorbers that have Increased Effectiveness, J. Eng. for Ind., ASME, Paper No.74-DE-J, pp.940-945, 1960
- ³¹ Newland, D.E., *Random Vibrations, Spectral and Wavelet Analysis*, Longman 1993
- ³² Parkus, H., *Random Processes in Mechanical Sciences*, CISM Courses and Lectures, Springer Verlag, 1969
- ³³ Warburton G.B., *Optimum Absorber Parameter for Simple Systems*, Earthquake Engineering and Structural Dynamics, vol.8, pp.197-217, 1980
- ³⁴ Constantinou, M.C., Soong, T.T., Dargush, G.F., *Passive Energy Dissipation Systems for Structural Design and Retrofit*, Multidisciplinary Center for Earthquake Engineering Research, Monograph Series, 1998
- ³⁵ Soong, T.T., Dargush, G.F., *Passive Energy Dissipation Systems in Structural Engineering*, Wiley, 1997
- ³⁶ Holmes, J.D., *Listing of installations, Engineering Structures*, vol.17(9), pp.676-678, 1995
- ³⁷ EERC (Earthquake Engineering Research Centre), *Worldwide Applications of Tuned Mass Dampers*, WWW-publication, National Information Service for Earthquake Engineering, Berkeley, 1995
- ³⁸ Kwock, K.C.S., Samali, B., *Performance of tuned mass dampers under wind loads*, Engineering Structures, vol.17(9), pp.655-667, 1995
- ³⁹ McKelvey, A.L., Ritchie, R.O., *Fatigue-crack propagation in Nitinol, a shape-memory and superelastic endovascular stent material*, Journal of Biomedical Materials Research, vol.47(3), pp.301-308, 1999
- ⁴⁰ Graesser, E.J.; Cozzarelli, F.A., *Shape-memory alloys as new materials for aseismic isolation*, Journal of Engineering Mechanics, vol.117(11), p.2590-2608, 1991
- ⁴¹ Casciati, F.; Faravelli, L., *Coupling SMA and steel in seismic control devices*, book article in: Analysis multiechelle et systemes physiques couples, Presses de l'Ecole nationale des ponts et chaussees, Paris, 1997
- ⁴² Dolce, M., Cardone, D., Marnetto, R., *Implementation and testing of passive control devices based on shape memory alloys*, Earthquake Engineering and Structural Dynamics, vol.29(7), p.945-968, 2000
- ⁴³ Wilde, K., *Base isolation system with shape memory alloy device for elevated highway bridges*, Engineering Structures, vol.22(3), p.222-229, 2000
- ⁴⁴ Cady, W.G., *Piezoelectricity*, McGraw-Hill, New York, 1946
- ⁴⁵ Flotow, von A., *Damping of Structural Vibrations with Piezoelectric Materials and Passive Electrical Networks*, Journal of Sound and Vibration, 1991, 146(2), 243-268,

- ⁴⁶ Hagenauer, K., Irschik, H., Ziegler, F., *An Exact Solution for Structural Shape Control by Piezoelectric Actuation*, VDI-Fortschrittberichte: Smart Mechanical Systems - Adaptronics, Reihe 11, vol.244, pp.93-98, VDI Verlag 1997
- ⁴⁷ Irschik, H., Krommer, M., *Piezothermoelastic Behaviour of Shear Deformable Composite Shallow Shells*, Proc. of the Euromech 373 Colloquium Modelling and Control of Adaptive Mechanical Structures, Magdeburg, VDI-Fortschrittberichte, Reihe 11, vol.268, pp.229-238, VDI Verlag 1998
- ⁴⁸ Irschik, H., Krommer, M., Pichler, U., *Shaping Distributed Piezoelectric Self-Sensing Layers for Static Shape Control of Smart Structures*, Journal of Structural Control, vol.7, pp.173-189, 2000
- ⁴⁹ Pichler, U., Irschik, H., Krommer, M., Hagenauer, K., *Experimental Verification of a new Piezoelectric Sensor for Beam Deflections*, Proc. of the 15th Symposium "Danubia-Adria" on Experimental Methods in Solid Mechanics, Bertinoro 1998 (R.Beer, ed.), pp. 173-174
- ⁵⁰ Krommer, M., Irschik, H., *An Eletromechanically Coupled Theory for Piezoelastic Beams Taking into account the Charge Equation of Electrostatics*, Acta Mechanica, accepted for publication, 2001
- ⁵¹ Burton, S.A., Markis, N., Konstantopoulos, I., Antsaklis, P.J., Modeling the response of ER damper: phenomenology and emulation, Journal of Engineering Mechanics, Sept. 1996, pp.897-906
- ⁵² Spencer, B.F., Dyke, S.J., Sain, M.K., Carlson, J.D., *Phenomenological Model for Magnetorheological Dampers*, Journal of Engineering Mechanics, vol.123(3), pp.230-238, 1997

3. State of the art review on Tuned Liquid Column Damper

Tuned liquid column dampers (TLCD) are a relatively new development in vibration control, and became of civil engineering interest in 1989 when Sakai¹ has shown their effectiveness in reducing the vibrations of civil engineering structures. However, to the author's best knowledge, the first implementation of tuned liquid dampers date back to the beginning of the 20th century, when the German shipbuilder Frahm, see e.g. DenHartog², introduced anti-rolling tanks in ships, see Figure 3-1, to stabilise these vessels.

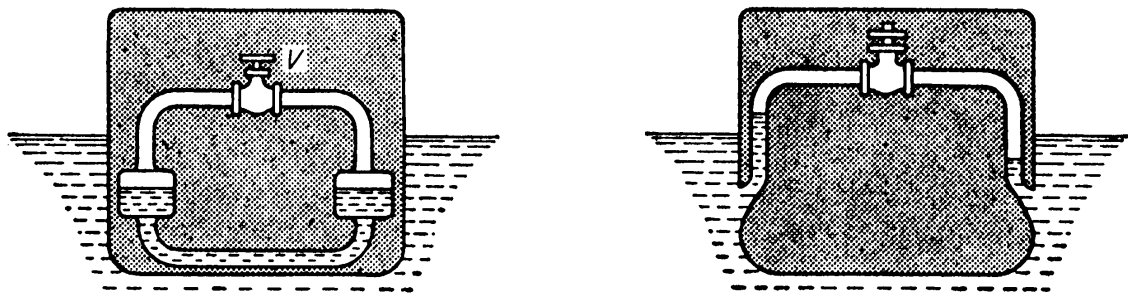


Figure 3-1: Anti-rolling tanks, developed by Frahm in 1902, see DenHartog²

Since the early works of Frahm, no major contribution has been made until the development of another type of liquid damper, the sloshing motion damper, or tuned liquid damper (TLD). It is well known that this highly nonlinear device suffers from a lack of energy dissipating capabilities, but nevertheless, a lot of research has been undertaken, see e.g. Bauer³, Tamura⁴, Sun et al.⁵, Lou et al.⁶, Yu et al.⁷, Reed et al.⁸, Fujino et al.⁹, Sun et al.¹⁰, Banerji et al.¹¹, Chang et al.¹². An extensive review on recent advances on liquid sloshing dynamics is given in Ibrahim et al.¹³.

Due to the controlled liquid flow in TLCD they are superior to TLDs, and an increased research interest in the last decade has resulted in a number of publications, some of which are discussed in the remainder of this chapter.

Abé et al.¹⁴ (*Control laws for semi-active tuned liquid column damper with variable orifice openings*) proposed two different semi-active control laws to adjust the TLCD's orifice opening based on the perturbation solution of a single U-shaped TLCD attached onto a SDOF structure, the control strategies assume the orifice opening to be adjustable during the zero

crossing of the liquid velocity. The first strategy is to keep the equivalent damping ratio constant by adjusting the orifice opening to eliminate the velocity dependence. The other strategy is to excite the second, highly damped vibration mode by taking advantage of the dependence of the mode shape on the head loss coefficient. Numerical simulation, which use parameter of the Higashi Kobe Bridge, (where passive TLCD were installed to reduce vibrations during construction) confirm the improvement of the proposed device, especially for the second control strategy.

Haroun et al.¹⁵ (*Suppression of environmentally-induced vibrations in tall buildings by hybrid liquid column dampers*) have developed a very interesting hybrid liquid column damper, where an adaptation to active control was done. The U-shaped device has a compressor unit added which allows supplemental energisation by pressurising the air filled pipe section. In addition, an orifice control system has been added for semi-active control. Based on instantaneous optimal control algorithms, see e.g. Yang et al.^{16,17,18,19,20}, an optimal control force is determined which can be applied to the system by either changing the orifice opening, if the energy must be dissipated, or by active pressurisation of the air chamber, if energy input is required. Numerical results are given for two structures, including a SDOF and a MDOF building mode, showing that the active orifice control does not improve the dynamic response when compared to constant orifice opening. The activation of the compressor unit can improve the dynamic results of the SDOF system: about 7% for peak and 20% for RMS responses. The author believes, that those results can be improved significantly, if a better control law is applied.

Based on the work of Hruska²¹ and Kofler²², experimental investigations on small laboratory models have been published by Adam et al.²³ (*Elastic Structures with tuned liquid column dampers*), where the influence of U-shaped TLCD with constant cross sectional area on the structural response of SDOF shear frame structures is investigated. The length of the liquid column is varied for free vibration experiments, and, in another experimental series, forced harmonic vibrations are explored. For the virtually undamped main structure (0.15% structural damping), and an absorber-structure mass ratio between 5.1% and 7.6%, a maximum main-structure acceleration reduction of 84% is achieved. Similarly, the decay time for the free vibration experiments is reduced to about 12% for the perfectly tuned TLCD and the same host structure.

The effectiveness for TLCD to mitigate wind induced vibrations was shown by Balendra et al.²⁴ (*Effectiveness of tuned liquid column dampers for vibration control of towers*). They use

the linearised equations of motion to obtain the stochastic response of the tower due to wind turbulence. A SDOF tower model is equipped with a single TLCD and the response reduction is calculated for various tower models. Interestingly, the amount of response reduction was found to be almost the same for any tower of practical interest. Thorough investigations about the influence of the opening ratio of the orifice plate are performed, including the error due to equivalent linearisation, the dependence of the liquid displacement and the reduction in structural acceleration or displacement. It is suggested that the natural frequencies of the TLCD and the tower are identical for best performance, but even if the TLCD is not tuned optimally adjustments of the opening ratio of the orifice plate can be used to obtain acceptable results. Furthermore, the characteristics of a real U-shaped TLCD is reported to be determined experimentally. In another work Balendra et al.²⁵ (*Vibration Control of tapered buildings using TLCD*) applied U-shaped TLCD to linearly tapered structures, subjected to wind loading. Both, shear and flexural behaviour are considered by modelling the structure by shear-flexural beams. A continuum formulation is adopted to overcome the drawbacks of a lumped mass formulation, and the non-linearity resulting from the turbulent damping term in the TLCD equation of motion was linearised for the analysis. A discretisation of the coupled partial differential equation of motion using Ritz-approximations allows to calculate the response reduction in terms of acceleration and displacement variances. A tapered structure (Transamerica building in San Francisco, USA), is studied in detail, and the effect of several TLCDs as well as the effect of damper mass and damper position variations are reported. It is concluded that flexural buildings experienced greater response reductions than shear buildings, an effect which decreases with the degree of taper. In a later publication Balendra et al.²⁶ (*Effectiveness of TLCD on various structural systems*) presented further numerical simulations using the same continuum formulation. U-shaped TLCD were installed in four non-uniform buildings, and the acceleration reduction for wind excitation in a typical city centre was calculated. Firstly, a single TLCD tuned to the fundamental frequency is utilised, but if the response variations also contained higher mode contributions, a second TLCD is installed and tuned to this higher frequency mode. Extended parameter studies have also been performed, Balendra et al.²⁷ (*Vibration control of various types of building using TLCD*), where in addition to the already mentioned investigation the relation between optimal damping ratio and the structural period, the structural damping ratio, and the damper position, respectively, is analysed.

In a recent publication Balendra et al.²⁸ (*Control of wind-excited towers by active tuned liquid column damper*) have proposed an active TLCD. Contrary to the system proposed in this thesis, the active power input is obtained from a movement of the TLCD housing, which is placed on an active tuned mass damper, see Chapter 8. The authors are still using U-shaped TLCD for vibration absorption, and the wind-excited towers are modelled by SDOF-systems. The frequency domain feedback control law supposed is strongly dependent on the type of sensor used, and contains only two design parameter, which are optimised with respect to the RMS response under the actual wind load. Surprisingly the ATLCD performs better than the corresponding solid mass system, which is due to different control laws applied.

Chang et al.²⁹ (*Control performance of liquid column vibration absorbers*) have investigated the LCVA, a liquid column vibration absorber, which is a U-shaped TLCD with variable cross sections. An equivalent linearisation of the head loss factor is performed on a stochastic basis, and the optimal head loss coefficient is derived explicitly under the condition that the natural frequencies of the LCVA and the host structure are identical. Parameter studies are presented for the optimal damping and head loss factor, and the influence of cross sectional variations is investigated numerically. From numerical examples it is concluded that the performance of LCVA deteriorates with varying loading conditions and is slightly inferior to that of the TMD. Under broad band white noise excitation a set of formulas for optimal design is given by Chang³⁰ (*Mass dampers and their optimal designs for building vibration control*) for TMD, TLCD and the LCVA. Closed forms for wind and earthquake excitation are given for SDOF systems equipped with one single absorber. Assuming a constant linearised damping ratio, a comparison between the different absorber types is performed and presented through extensive parameter studies. Without establishing an TLCD-TMD analogy, the optimal design quantities were found for minimal displacement variances of the host structure, even for the LCVA, by rather cumbersome mathematical derivations. An efficiency index is defined, showing that the LVCA can perform better than a TLCD with constant cross section, but always less than the TMD. Unified design formulas are also established in Chang et al.³¹, where five different passive absorber systems are considered: TMD, TLCD, LCVA, Circular TLD and Rectangular TLD. For wind induced vibrations of tall buildings analytical results are given for minimum variance design, and a numerical example ranks the performance of the absorbers as: TMD, LCVA, TLCD, Rectangular TLD, Circular TLD, in descending order. In another work Chang et al.³² (*Control of buildings using single and multiple tuned liquid column dampers*) study the behaviour of buildings using single and

multiple TLCD and show again, that the performance of TLCD is inferior to TMD because not the entire liquid mass interacts with the building. A modal decomposition of multiple story buildings is used to obtain SDOF where the TLCDs are installed. In case of multiple TLCD (MTLCD) the design guidelines are given for an odd number of TLCDs which have identical properties, except the liquid column length which is chosen to obtain TLCD natural frequencies which are evenly spaced and symmetrical with respect to the host structures fundamental frequency. The main results demonstrate that the application of MTLCD can mitigate the loading sensitivity of the optimal design parameter, thus MTLCD can perform more robust.

In a recent publication Chen et al.³³ (*Optimal damping ratio of TLCDs*) have studied the optimal damping ratio of U-shaped TLCDs attached to SDOF structures. Under conditions of negligible structural damping, and based on DenHartog's² work, the optimal absorber frequency and damping ratio has been determined. A pendulum type experimental structure is presented, and the effectiveness in reducing free and forced vibrations is shown for this very lightly damped model. A more efficient active TLCD is discussed, where two impellers are inserted into the liquid path, to pump the water actively through the piping system.

Gao et al.³⁴ (*Optimization of tuned liquid column dampers*) investigate TLCDs to control structural vibrations. The influence of the cross sectional area on the liquid column length is pointed out, and the V-shaped TLCD, is found to be appropriate for reducing stronger vibrations because it allows larger TLCD displacement amplitudes. For a SDOF structure a comprehensive parametric study is performed including variations in the load intensity, the cross sectional area ratio, the absorber-structure mass ratio and the structural damping ratio. The outcome of this study are optimal damping and frequency ratios obtained from numerical integration of the equation of motion. One main result is that the nonlinear effects on the system response are weak, with the exception of the head loss coefficient, which is inversely proportional to the excitation intensity. All parametric studies are repeated for the V-shaped TLCD, taking into account another nonlinearity: the nonlinear coupling force resulting from the proposed V-shaped TLCD geometry. It is concluded that the V-shaped TLCD has higher capacity for suppressing stronger vibrations with nearly the same efficiency level as a U-shaped TLCD. An extension to MTLCD is given in Gao et al.³⁵ (*Characteristics of multiple tuned liquid column dampers in suppressing structural vibration*), where the effects of the MTLCD frequency range, head loss coefficients, number of TLCDs and central frequency on the structural performance are studied numerically by time-integration of given excitation

loads. The MTLCD configuration consists of an odd number of TLCD which have equal head loss coefficients and constantly spaced natural frequencies. It is found, the number of TLCDs used in the MTLCD array, enhances the robustness to frequency changes while leading to an increased head-loss-coefficient-sensitivity and to higher TLCD's peak responses, raising the need for V-shaped MTLCDs, see Figure 3-2

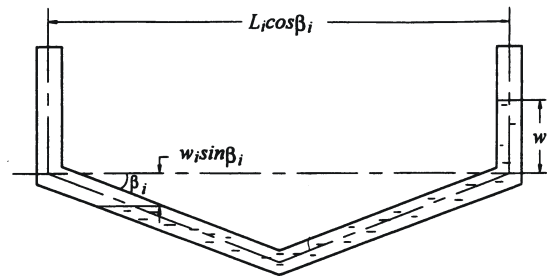


Figure 3-2: Single V-shaped TLCD as part of a MTLCD, see Gao et al.³⁵

The main outcome of this research is that MTLCDs can be more efficient than a single TLCD, but rising the number of TLCDs above five does not increase the efficiency significantly. The research confirmed that the sensitivity to the frequency ratio is less for MTLCD when compared to an optimised single TLCD, and an increased robustness is also achieved in the sense that similar performance can be obtained by a wider range for suitable MTLCD frequencies and damping coefficients.

The effects of geometrical configurations on the U-shaped TLCD's natural frequency and damping ratio are investigated experimentally by Hitchcock et al.³⁶ (*Characteristics of liquid column vibration (LCVA)-I*). Reasonable agreement is observed between theoretical predictions and experimental data, but for varying cross sections the error increases up to 5% probably due to flow separation at the corners. The nonlinear relation between damping forces and liquid velocity is confirmed in experimental investigations which have also shown a viscous damping ratio of about 2%. Therefore an orifice plate must be installed to further increase the energy dissipation. In addition, the liquid viscosity was varied by mixing fresh water and methylated spirit. All experiments indicate that the damping ratio is dependent on three nondimensional parameter: Reynolds number, area ratio and orifice opening. In part two of this study, see Hitchcock et al.³⁷ (*Characteristics of liquid column vibration (LCVA)-II*), the unidirectional TLCD is extended to a bi-directional TLCD. The bi-directional TLCD consists of two very broad TLCD, positioned perpendicular with respect to each other, to be able to share the horizontal pipe section, and therefore the horizontal liquid mass is available for both TLCD, see Figure 3-3.

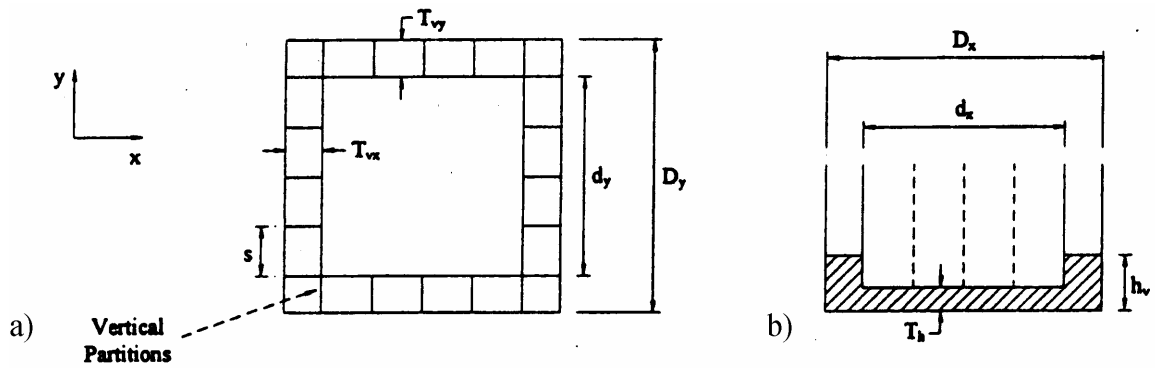


Figure 3-3: Bi-directional Tuned Liquid Column Damper: a) plan view b) front view, see Hitchcock et al.³⁷

In a first approximation the TLCD is modelled as solid mass vibration absorber (SMVA) to derive simple analytical results, and to compare them to experimental data. Bi-directional free vibration and frequency sweep experiments are carried out showing the effectiveness of the proposed device for vibration absorption, and the same dependencies of natural frequency and damping ratio on the geometry and excitation level as for the conventional TLCD. Again there is a need for the inclusion of an appropriate orifice in the liquid path, and an empirical factor in the theoretical liquid column length is proposed to achieve better accordance between theory and experiments. Fine tuning, however, is more difficult, as adding water to one TLCD also increases the liquid column length of the other TLCD and it must be done by changing the length of the horizontal pipe section.

The dynamics of shear frames with TLCD is investigated analytically and numerically by Hochrainer et al.³⁸ (*Dynamics of shear frames with tuned liquid column dampers*), where DenHartog's approach is adapted and applied to the linearised TLCD equations of motion. For well separated natural frequencies a modal decomposition is performed and for both, the optimal natural frequency and the optimal damping ratio of the TLCD analytical formulas are derived. Numerical investigations, taking the nonlinear damping term into account confirm the TLCD design guidelines. Further TLCD design aspects are discussed in Hochrainer³⁹ (*Dynamisches Verhalten von Bauwerken mit Flüssigkeitstilgern*), where multiple story buildings equipped with multiple TLCDs are investigated. For each TLCD, placed arbitrarily in the structure of interest, the optimal design is determined by a numerical optimisation with a performance index, taking into account the different importance of the individual floor and TLCD responses. An entirely new TLCD design is proposed by Hochrainer et al.⁴⁰

(*Application of tuned liquid column dampers for passive structural control*), where a ring-shaped TLCD is presented to mitigate torsional vibrations of structures. This novel geometry does not influence the bending motion of the host building, and can be applied to alleviate the coupled flexural-torsional vibration problems. Most work published so far does neglect coupled flexural-torsional vibration problems and other complex vibration phenomena, like mode jumping, which can now be dealt with. As a result of the relatively bad performance of TLCD during the transient vibration regime during ground excitation, Hochrainer⁴¹ (*Dynamisches Verhalten von Bauwerken mit aktiven und passiven Flüssigkeitstilgern*) has improved the TLCD, by developing an active air spring element which enables the TLCD to perform similar to an ATMD. Thus it is possible to mitigate the peak responses during the transient response until the energy absorption of the passive device is fully developed. The proposed system is still independent of external energy supply since a high pressure air container delivers the necessary energy. A simple and efficient switching control strategy is proposed and successfully applied to a complex building where the story modal displacements are reduced significantly. Further aspects of active control are discussed in Hochrainer⁴² (*Investigation of active and passive tuned liquid column damper for structural control*), where wind induced vibration problems are investigated, and a comparison between active and passive TLCD can be found for a complex model of a high rise office tower.

A very interesting paper has been published by Kagawa et al.⁴³ (*Semi-active and Passive Vibration Control of Structure by Fluid System*), where the authors carry out model tests and vibration experiments in building and ship structures using U-shaped TLCD. The air space in the TLCD is used as a pneumatic spring to adjust the natural frequency – a technique which allows much higher frequencies than the conventional hardware setup. A SDOF test model was built and for a 12kg TLCD water mass, and frequencies up to 27Hz were achieved by proper pressure variation, see Figure 3-4.

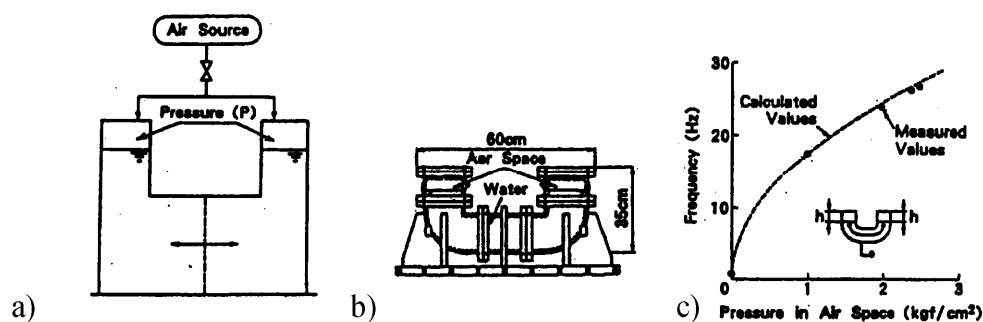


Figure 3-4: Semi-active TLCD: a) schematic view b) experimental model c) Frequency measurements and comparison with theory, Kagawa et al.⁴³

Experiments have been conducted and indicate an efficient response reduction. Furthermore the fabrication and installation of a full scale TLCD is reported in a 9-story steel structure building. The mass ratio was about 1% and the optimum vibration factor was found to be 6.4%. With a total liquid length of 5m and an air pressure of maximal 1bar, the frequency adjustment range of the device was 0.6-1.5Hz. The importance of an easy to tune absorber was shown as the natural frequencies of the building changed by approximately 3% over the first 9 month after completion. Vibration monitoring has proven the effectiveness of the TLCD, with maximum response reductions of up to 75%. Furthermore a typhoon attacked the building in 1991 and the vibration felt beyond the reference level for living comfortability was decreased to about 1/5 when compared to a situation where the TLCD was not in operation. Another TLCD was fabricated and installed on a ship, where the application is particularly promising, as the natural frequency changes with water, freight loading and engine conditions. An automatic frequency follow-up system is installed, and all tests are very promising. The frequency range of the 6tons TLCD is between 1.7 and 12Hz for air pressures up to 7bar.

A comprehensive deterministic analysis using 72 ground motion earthquake records was carried out by Sadek et al.⁴⁴ (*Single and multiple-tuned liquid column dampers for seismic applications*), with the aim of determining optimal design parameter for U-shaped TLCDs for seismic applications. For single TLCDs the frequency tuning, the damping ratio and the liquid column to tube width ratios were determined whereas for multiple TLCDs the central tuning ratio, the tuning bandwidth and number of TLCD are found through a deterministic response analysis. The results are used to compute the response of several SDOF (including a simple single span, box girder, concrete bridge) and MDOF structures for different earthquake excitations. Response reductions of up to 47% for both, displacements and accelerations are reported, showing that single TLCD are not inferior to MTLCD, but the latter are more robust with respect to errors in the approximated structural parameter. When comparing TLCD to TMD similar response reducing capabilities are reported.

In 1996 Teramura et al.⁴⁵ (*Development of vibration control system using U-shaped water tank*) have reported a structural implementation of a bi-directional vibration control system called the tuned liquid column damper with period adjustment equipment (LCD-PA) which can provide vibration reduction of high-rise buildings excited by strong winds or earthquakes. The LCD-PA is based on an U-shaped TLCD, but the air-chambers are connected to a period adjustment equipment. This is essentially a liquid filled U-shaped valve where the water

displacement loads a physical spring which is connected to a pendulum. The stiffness of the spring can be used to adjust the natural frequency of the absorber, see Figure 3-5.

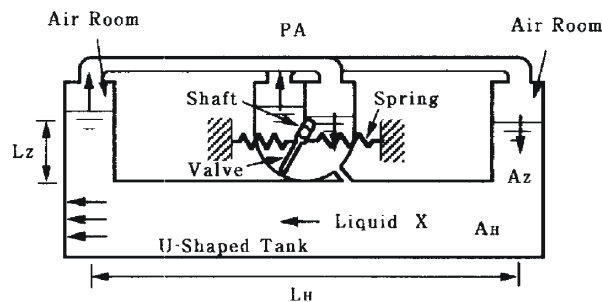


Figure 3-5: LCD-PA with period adjustment equipment (Teramura et al.⁴⁵)

This absorber has been installed in a 106m high 26 story hotel in Japan. The bi-directional configuration with a total mass of 58 tons (mass ratio $\mu = 1.26\%$) is installed on the top floor to reduce the vibrations during strong winds and earthquakes of small and medium strength. A compact LCD-PA setup (6x6x3.4m) allowed maximum water movements of 0.8m and a maximum velocity of 0.25 m/s, see Figure 3-6.

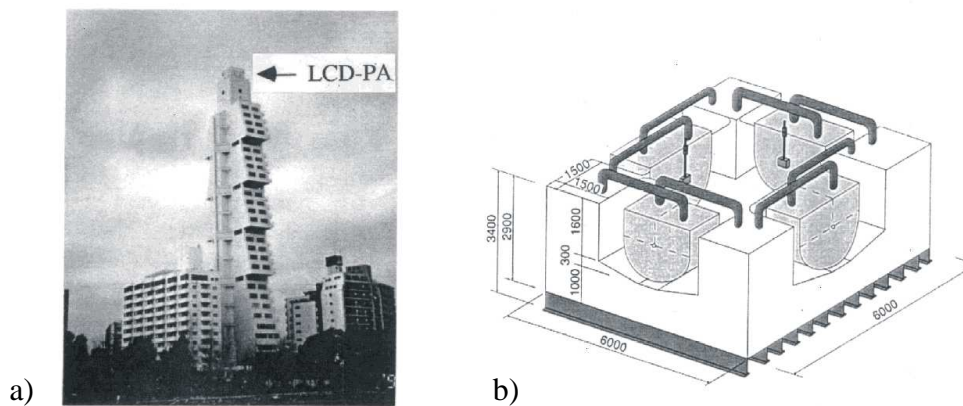


Figure 3-6: LCD-PA: a) view of real building b) schematic view of bi-directional LCD-PA (Teramura et al.⁴⁵)

Variations in the period adjustment unit allowed natural frequencies between 0.45Hz and 0.55Hz . The first two natural frequencies of the actual building were 0.48Hz and 1.69Hz in NS-direction, as well as 0.50Hz and 1.69Hz in the EW-direction, respectively. The building's damping ratio was about 0.5% in both directions, and the application of the absorber unit increased the damping by a factor of 10! The maximum frequency response amplitude was

reduced by a factor of 5, and wind observation results (top floor wind speed 21.6 m/s) indicated a maximum acceleration reduction of 60% and a 40% reduction for the RMS acceleration, when compared to simulated results of the building without TLCD. About the same performance was reported for an earthquake, which hit the hotel in 1994.

The seismic performance of U-shaped TLCD is evaluated by Won et al.^{46,47} (*Performance assessment of tuned liquid column dampers under seismic loading, Stochastic seismic performance evaluation of tuned liquid column dampers*), using time-domain random vibration analysis. A parametric study is conducted to evaluate the sensitivity of the mass ratio, the head loss coefficient, the tuning ratio, the structural damping, and the loading intensity. Optimal values for the head loss coefficient as well as the tuning ratio are found for a given mass ratio, but both depend on the intensity, duration and frequency contents of the loading. Random vibration analysis is applied to compute response variances and their derivatives with respect to the design parameter. Numerical optimisation algorithms are used to determine the optimal TLCD design parameter for a given structure and loading condition. The drawback of U-shaped TLCD to accommodate to large absorber displacements is pointed out, as it becomes apparent when working with strong motion ground excitation. Illustrative examples given include non-stationary ground motion inputs as well as long- and short-duration loading. However, it is remarked that the traditional U-shaped design is not suitable for short period structures and the results suggest that the use of active control can increase the TLCD performance.

Yalla et al.⁴⁸ (*Optimum Absorber Parameter for Tuned Liquid Column Dampers*) have also used a statistical approach to find the optimal TLCD parameter. Again a simple U-shaped TLCD is investigated, equivalent linearisation is applied to the head loss coefficient, and the same optimisation method is employed as used by Chang³⁰. Analytical expressions for minimum response variances are given for a SDOF host structure and single TLCD under white noise excitation. In addition first and second order filtering equations are added to adapt the spectrum characteristics of the excitation, and the results of numerical optimisation of the response variances are given in tabular form. The application of MTLCD on a SDOF system has been studied and confirms the results of Gao³⁵. The MTLCD consists of an array of TLCDs, where the central TLCD is tuned to the host structure's natural frequency, and the other TLCDs have constantly separated natural frequencies, and equal damping ratios. The study includes the effect of the number of the TLCDs, the effect of the damping ratio, and the effect of the frequency range on the structural response.

An interesting research on the efficiency of TLCD to suppress pitching motions of structures was carried out by Xue et al.⁴⁹ (*Tuned liquid column damper for suppressing pitching motion of structures*), who have shown that the conventional U-shaped TLCD can also be used to suppress the pitching vibration on, e.g., long span bridges, see Figure 3-7.

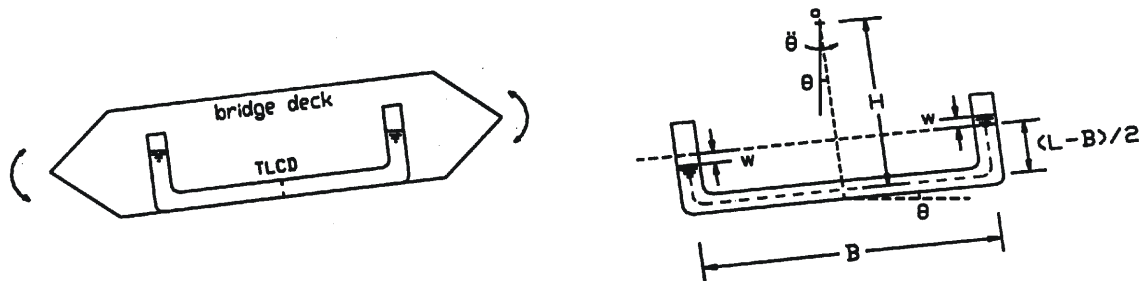


Figure 3-7: Pitching vibration and TLCD installed in long span bridge decks (Xue et al.⁴⁹)

The linear governing equations are established for a SDOF structural model, and experimental results are presented for the application of the TLCD on a bridge deck. Free and forced harmonic vibration experimental data are presented, which compare well with simulations. The vibration reduction achieved in most cases was around 50%, making the TLCD appropriate for applications on long span bridge decks under gust winds or even earthquakes. In an early work, Xu et al.⁵⁰ (*Control of Along-Wind Response of Structures by Mass and Liquid Dampers*) have investigated and compared the along wind response of high-rise structures equipped with TMD, TLCD, and the tuned liquid column-mass damper. The latter consists of a standard TMD onto which a TLCD is attached, thus two degrees-of-freedom are added to the system. This design operates properly unless the natural frequencies of TMD and TLCD are identical. In such a situation the TLCD attenuates the desired damping motion of the TMD. A matrix transfer formulation for non-periodic structures is developed showing in two numerical examples, a 370m high TV-tower and a 306m tall concrete building, that the tuned liquid column damper systems can achieve performance comparable to the TMD, while keeping the competitive practical advantages of TLCDs.

3.1. References

¹ Sakai, F., Takaeda, S., Tamaki, T., *Tuned liquid column damper – new type device for suppression of building vibrations*, Proceedings International Conference on Highrise Buildings, Nanjing, China, pp.926-931, 1989

² DenHartog, J.P., *Mechanical Vibrations*, reprint, 4th ed., Dover Publications, 1985

- ³ Bauer, H.F., *Oscillations of Immiscible Liquids in Rectangular Container: A New Damper for Excited Structures*, Journal of Sound and Vibration, 1984, 92(1),117-133
- ⁴ Tamura, Y., Fujii, K., Ohtsuki, T., Wakahara, T., Koshaka, R., *Effectiveness of Tuned Liquid Column Dampers in Tower-like Structures*, Engineering Structures, 1995, 17(9), 609-621
- ⁵ Sun, L.M., Fujino, Y., Koga, K., *A model of tuned liquid damper for suppressing pitching motions of structures*, Earthquake Engineering and Structural Dynamics, vol.24, pp.625-636, 1995
- ⁶ Lou, J.Y.K., Lutes, L.D., Li, J.J., *Active tuned liquid damper for structural control*, 1st World Conference on Structural Control, 3-5 August 1994, Los Angeles, California, USA, pp.TP1.70-TP1.79, 1994
- ⁷ Yu, J., Sakahara, T., Reed, D., *A non-linear numerical model of the tuned liquid damper*, Earthquake Engineering and Structural Dynamics, vol.28, pp.671-686, 1999
- ⁸ Reed, D., Yu, J., Harry, Y., Gardarsson, S., *Investigation of Tuned Liquid Dampers under Large Amplitude Excitation*, ASCE Journal of Engineering Mechanics, vol.124(4), pp.405-413, 1998
- ⁹ Fujino, Y., Sun, L.M., *Vibration Control by Multiple Tuned Liquid Dampers (MTLDs)*, Journal of Structural Engineering, vol.112(12), pp.3482-3502, 1993
- ¹⁰ Sun, L.M., Fujino, Y., Chaiseri, P., Pacheco, B.M., *The Properties of Tuned Liquid Dampers using a TMD Analogy*, Earthquake Engineering and Structural Dynamics, vol.24, pp. 967-976, 1995
- ¹¹ Banerji, P., Murudi, M., Shah, A.H., Popplewell, N., *Tuned liquid dampers for controlling earthquake response of structures*, Earthquake Engineering and Structural Dynamics, vol.29, pp. 587-602, 2000
- ¹² Chang, C.C., Gu, M., *Suppression of vortex-excited vibration of tall buildings using tuned liquid dampers*, Journal of Wind Engineering and Industrial Aerodynamics, vol.83, pp.225-237, 1999
- ¹³ Ibrahim R.A., Pilipchuk, V.N., *Recent advances in liquid sloshing dynamics*, Applied Mechanics Reviews, vol.54(2), 2001
- ¹⁴ Abé, M., Kimura, S., Fujino, Y., *Control laws for semi-active tuned liquid column damper with variable orifice openings*, 2nd International Workshop on Structural Control, 18-21 December 1996, Kong Kong, pp.5-10, 1996
- ¹⁵ Haroun, M.A., Pires, J.A., Won, A.Y.J., *Suppression of environmentally-induced vibrations in tall buildings by hybrid liquid column dampers*, The structural Design of Tall Buildings, vol.5, pp.45-54, 1996
- ¹⁶ Yang, J.N., Akbarpour, A., Ghaemmaghami, P., *Instantaneous optimal control laws for tall buildings under seismic excitation*, Technical Report, NCEER-87-00007, State University of New York, Buffalo, 1987
- ¹⁷ Yang, J.N., Akbarpour, A., Ghaemmaghami, P., *New Optimal Control Algorithms for Structural Control*, ASCE Journal of Engineering Mechanics, vol.113(9), pp.1369-1386, 1987
- ¹⁸ Yang, J.N., Li, Z., Liu, S.C., *Stable Controllers for Instantaneous Optimal Control*, ASCE Journal of Engineering Mechanics, vol.118(7), pp.1612-1630, 1992
- ¹⁹ Yang, J.N., Li, Z., Danielians, A., Liu, S.C., *Aseismic Hybrid Control of Nonlinear and Hysteretic Structures I*, ASCE Journal of Engineering Mechanics, vol.118(8), pp.1423-1440, 1992
- ²⁰ Yang, J.N., Li, Z., Danielians, A., Liu, S.C., *Aseismic Hybrid Control of Nonlinear and Hysteretic Structures II*, ASCE Journal of Engineering Mechanics, vol.118(8), pp.1441-1456, 1992
- ²¹ Hruska, A., *Elastische Rahmentragwerke mit U-rohrförmigen Flüssigkeitsdämpfern – eine computergesteuerte Modelluntersuchung* (in German), Master Thesis, Technical University of Vienna, Austria, 1999

- ²² Kofler, M., Master Thesis, *Eine experimentelle und numerische Modelluntersuchung von ebenen Rahmentragwerken mit U-rohrförmigen Flüssigkeitsdämpfern*, Technical University of Vienna, Austria, 2000
- ²³ Adam, C., Hruska, A., Kofler, M., *Elastic Structures with tuned liquid column dampers*, XVI IMEKO World Congress, Vienna, Austria, September 25-28, 2000
- ²⁴ Balendra, T., Wang, C.M., Cheong, H.F., *Effectiveness of tuned liquid column dampers for vibration control of towers*, Engineering Structures, vol.17(9), pp.668-675, 1995
- ²⁵ Balendra, T., Wang, C.M., Rakesh, G., *Vibration Control of tapered buildings using TLCD*, Journal of Wind Engineering and Industrial Aerodynamics, 77&78, pp.245-257, 1998
- ²⁶ Balendra, T., Wang, C.M., Rakesh, G., *Effectiveness of TLCD on various structural systems*, Engineering Structures, vol.21, pp.291-305, 1999
- ²⁷ Balendra, T., Wang, C.M., Rakesh, G., *Vibration control of various types of building using TLCD*, Journal of wind engineering and industrial aerodynamics, vol.83, pp.197-208, 1999
- ²⁸ Balendra, T., Wang, C.M., Yan, N., *Control of wind-excited towers by active tuned liquid column damper*, Engineering Structures vol.23, pp.1054-1067, 2001
- ²⁹ Chang, C.C., Hsu, C.T., *Control performance of liquid column vibration absorbers*, Engineering Structures, vol.20(7), pp.580-586, 1998
- ³⁰ Chang, C.C., *Mass dampers and their optimal designs for building vibration control*, Engineering Structures, vol.21, pp.454-463, 1999
- ³¹ Chang, C.C., Qu, W.L., *Unified dynamic absorber design formulas for wind-induced vibration control of tall buildings*, The Structural Design of Tall Buildings, vol.7, pp.147-166, 1998
- ³² Chang, C.C., Hsu, C.T., Swei, S.M., *Control of buildings using single and multiple tuned liquid column dampers*, Structural Engineering and Mechanics, vol.6(1), pp.77-93, 1998
- ³³ Chen, Y.H., Chao, C.C., *Optimal damping ratio of TLCDs*, Structural Engineering and Mechanics, vol.9(3), p.227-240, 2000
- ³⁴ Gao, H., Kwok, K.C.S., Samali, B., *Optimization of tuned liquid column dampers*, Engineering Structures, vol.19(6), pp.476-486, 1007
- ³⁵ Gao, H., Kwok, K.S.C., Samali, B., *Characteristics of multiple tuned liquid column dampers in suppressing structural vibration*, Engineering Structures, vol.21, pp.316-331, 1999
- ³⁶ Hitchcock, P.A., Kwok, K.C.S., Watkins, R.D., Samali, B., *Characteristics of liquid column vibration (LCVA)-I*, Engineering Structures, vol.19(2), pp.126-134, 1997
- ³⁷ Hitchcock, P.A., Kwok, K.C.S., Watkins, R.D., Samali, B., *Characteristics of liquid column vibration (LCVA)-II*, Engineering Structures, vol.19(2), pp.135-144, 1997
- ³⁸ Hochrainer, M.J., Adam, C., *Dynamics of shear frames with tuned liquid column dampers*, ZAMM vol.80 supplement 2, pp.283-284, 2000
- ³⁹ Hochrainer, M.J., *Dynamisches Verhalten von Bauwerken mit Flüssigkeitstilgern*, ZAMM vol.81, supplement 2, pp.191-192, Göttingen Germany, 2000
- ⁴⁰ Hochrainer, M.J., Adam, C., Ziegler, F., *Application of tuned liquid column dampers for passive structural control*, Proc. 7th International Congress on Sound and Vibration, 4.July-7.July 2000, Garmisch-Partenkirchen,

Germany, 2000, CD-Rom paper, also available at: Inst. f. Allgemeine Mechanik (E201), TU-Wien, Wiedner Hauptstr. 8-10/E201, 1040 Wien, Austria.

⁴¹ Hochrainer, M.J., *Dynamisches Verhalten von Bauwerken mit aktiven und passiven Flüssigkeitstilgern*, Jahrestagung GAMM 2001, CD-Rom paper, Zürich, available at: Inst. f. Allgemeine Mechanik (E201), TU-Wien, Wiedner Hauptstr. 8-10/E201, 1040 Wien, Austria.

⁴² Hochrainer, M.J., *Investigation of active and passive tuned liquid column damper for structural control*, 8th International Congress on Sound and Vibration, 2.-6. July 2001, Hong Kong, China, 2001, also available at: Inst. f. Allgemeine Mechanik (E201), TU-Wien, Wiedner Hauptstr. 8-10/E201, 1040 Wien, Austria.

⁴³ Kagawa, K., Yoshimura, Y., Fujita, K., Yamasaki, Y., Ayabe, S., *Semi-active and Passive Vibration Control of Structure by Fluid System*, PVP-Vol.289, Active and Passive Control of Mechanical Vibration, pp.41-48, ASME, New York, 1994

⁴⁴ Sadek, F., Mohraz, B., Lew, H.S., *Single and multiple-tuned liquid column dampers for seismic applications*, Earthquake Engineering and Structural Dynamics, vol.27, pp.439-463, 1998

⁴⁵ Teramura, A., Yoshida, O., *Development of vibration control system using U-shaped water tank*, Elsevier Science Ltd. 11th World Conference on Earthquake Engineering (edited by Sociedad Mexicana de Ingenieria Sismica, A.C.), paper no. 1343, 1996,

⁴⁶ Won, A.Y.J, Pires, J.A., Haroun, M.A., *Performance assessment of tuned liquid column dampers under seismic loading*, Int. J. of Non-Linear Mechanics, vol.32(4),pp.745-758, 1997

⁴⁷ Won, A.J., Pires, J.A., Haroun, M.A., *Stochastic seismic performance evaluation of tuned liquid column dampers*, Earthquake Engineering and Structural Dynamics, vol.25, pp.1259-1274, 1996

⁴⁸ Yalla, S.K., Kareem, A., *Optimum Absorber Parameter for Tuned Liquid Column Dampers*, Journal of Structural Engineering, pp.906-915, August 2000

⁴⁹ Xue, S.D., Ko, J.M., Xu, Y.L., *Tuned liquid column damper for suppressing pitching motion of structures*, Engineering Structures, vol.23, pp.1538-1551, 2000

⁵⁰ Xu, Y.L., Samali, B., Kwok, K.C.S., *Control of Along-Wind Response of Structures by Mass and Liquid Dampers*, ASCE Journal of Engineering Mechanics, vol.118(1), 1992

4. Mathematical description and discussion of the general shaped TLCD

Subsequently to the above discussion of different absorber types, a review of the research done in the field of TLCD, and a phenomenological description of various damping concepts, TLCDs are analysed and characterised mathematically.

Important performance aspects are highlighted, and it is shown, that TLCDs are simple and easy to construct devices which can operate from very low frequencies up to several Hertz, if the air-spring effect is utilised. The derivations of the equation of motion for the base excited plane TLCD are followed by the determination of the interaction forces and important geometry factors. Their influence on the vibration damping effectiveness is pointed out before the advantages of TLCD are considered and compared to the popular TMD. In addition to the plane TLCD, which can mitigate flexural vibrations, a torsional tuned liquid column damper (TTLCD) is developed to alleviate torsional or coupled flexural-torsional motions.

4.1. Equations of motion for plane TLCD

Several different TLCD-geometries have been proposed in the literature, see Chapter 3 for a survey. The most popular amongst these designs is a U-shaped container consisting of one horizontal and two vertical water filled pipe sections. A more flexible device is the symmetric V shaped TLCD with a horizontal element of variable length, and arbitrary inclined pipe sections (opening angle β), as shown in Figure 4-1. Sectionwise constant cross section areas allow to model numerous geometries, including the U-shaped TLCD as special case for $\beta = \pi/2$. It is assumed that the bending radius of the transition from the horizontal to the vertical sections is small compared to the overall dimensions, but a minimal radius of curvature is necessary to provide a smooth change in the flow direction thereby minimising turbulence and energy losses. If the inherent fluid damping is not sufficient, turbulent losses are desirable and can be introduced by the application of a hydraulic resistance (orifice plate) inserted into the liquid path, see again Figure 4-1. Although the described geometry allows for large fluid displacements, the limit of the operating range is reached if the free liquid surface enters the horizontal pipe section. In such a situation the liquid column can separate, and dynamic behaviour is difficult to predict and beyond the limitations of the applied streamline theory. For that reason, a situation where the assumption of a compact liquid entity, with

known dimensions and velocities is no longer true, must be avoided by increasing the length of the inclined pipe sections.

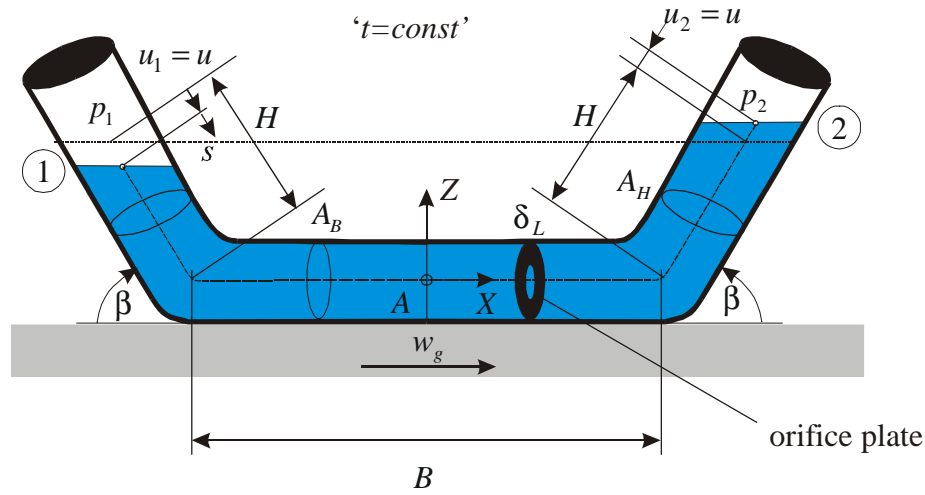


Figure 4-1: TLCD of general shape with a relative streamline from 1-2.
For a short hand notation absolute floor displacement is denoted w_g

The TLCD considered, sketched in Figure 4-1, is attached to a supporting floor, with its motion characterised by the horizontal ground or floor acceleration \ddot{w}_g . Let ρ , H , B , denote the liquid density, $\rho = 1000 \text{ kg/m}^3$ for water, the length of the liquid column in the inclined pipe sections at rest, and the horizontal length of the liquid column, respectively. Furthermore A_H , A_B and β denote the inclined and horizontal cross-sectional areas of the liquid column and the opening angle of the inclined pipe section, respectively. The relative motion of the liquid inside the container is described by the free surface displacement u along the liquid path. It is important to emphasise that u is a relative displacement of the liquid with respect to the moving container. As the ends of the piping system might be closed and filled with gas, an internal gas pressure can build up on either side of the liquid path, denoted p_1 and p_2 . Because the actual velocity distribution is unknown and strongly depends on the cross sectional area, a mean velocity \dot{u}_m is introduced to characterise the mass flow rate \dot{m} . This assumption can be justified by the fact that for high Reynolds numbers the velocity profile in a pipe is constant, apart from a thin boundary layer, see e.g. Idelchick¹ or Richter². At this point, the equations of motion of such a TLCD can be derived by either applying Lagrange's equation of motion or by using the modified Bernoulli equation for moving frames. Both methods, presented in the following sections, yield identical results.

4.1.1. Derivation of the equation of motion using the Lagrange equations of motion

As the entire liquid mass is considered when deriving the equations of motion, it is not necessary to apply a control volume concept, and, as a result, the application of Lagrange's principle is straightforward. Neglecting the compressibility of the fluid, the law of mass conservation reduces to the principle of constant mass flow rate through all cross sectional areas along the streamline, and thus

$$\dot{m} = \rho A(s) \dot{u}(s) = \text{const} , \quad (4-1)$$

where \dot{u} denotes the relative mean velocity at the cross sectional areas $A(s)$. Consequently the mean velocity in the horizontal pipe element is $\dot{u}_B = \dot{u} A_H / A_B$, and the absolute kinetic energy of the entire moving liquid is given by

$$E_{kin} = \frac{1}{2} \left(2 \rho A_H H \left| \begin{pmatrix} \dot{u} \cos \beta + \dot{w}_g \\ \dot{u} \sin \beta \end{pmatrix} \right|^2 + \rho A_B B \left| \begin{pmatrix} \dot{u} \frac{A_H}{A_B} + \dot{w}_g \\ 0 \end{pmatrix} \right|^2 \right), \quad (4-2)$$

an expression which can be simplified to

$$E_{kin} = \frac{1}{2} \left(\rho A_H 2 H \left(\dot{u}^2 + 2 \dot{w}_g \dot{u} \cos \beta + \dot{w}_g^2 \right) + \rho A_B B \left(\dot{u} \frac{A_H}{A_B} + \dot{w}_g \right)^2 \right). \quad (4-3)$$

Due to the pressure difference $\Delta p = p_2 - p_1$ and gravity forces acting on the liquid, restoring forces are present which can be regarded as potential energy E_{pot} ,

$$E_{pot} = \rho g A_H \left(H + u \right) \frac{H + u}{2} \sin \beta + \rho g A_H \left(H - u \right) \frac{H - u}{2} \sin \beta + \Delta p A_H u . \quad (4-4)$$

In a compact form Eq.(4-4) becomes

$$E_{pot} = \rho g A_H \left(H^2 + u^2 \right) \sin \beta + \Delta p A_H u , \quad (4-5)$$

thereby assuming that the level of zero potential energy coincides with the horizontal pipe section. Energy dissipation is caused by viscous and turbulent damping, which is described by the generalised damping force Q_u , given by

$$Q_u = -\Delta p_L A_H, \quad (4-6)$$

$$\Delta p_L = \frac{\rho |\dot{u}| \dot{u}}{2} \lambda(\text{Re}), \quad (4-7)$$

where Δp_L denote the pressure loss along the streamline. Δp_L is the product of the stagnation pressure $\frac{\rho |\dot{u}| \dot{u}}{2}$ (signum function included) and the loss factor $\lambda(\text{Re})$, which is a function of the Reynolds number $\text{Re} = 2R\dot{u}/\nu$. R is a characteristic cross sectional dimension, and ν denotes the kinematic viscosity. The loss factor λ depends on the type of flow and for $\text{Re} > 5000$ the flow is turbulent, and the loss factor λ becomes independent of the Reynolds number, see e.g. Ziegler⁵. For a circular cross sectional piping system with $R = 0.5\text{m}$ and $\nu_{\text{water}} = 1 \cdot 10^{-6} \text{m}^2/\text{s}$, the Reynolds number becomes $\text{Re} = 10^6 \dot{u}$, thus turbulent flow must be assumed for a large portion of the period. The turbulent losses can be increased by inserting an orifice plate into the liquid path. A comprehensive selection of loss factors for industrial relevant pipe elements and cross sections is given in Idelchick¹, Fried et al.³ and Blevins⁴. The application of the Lagrange equations of motion $\frac{d}{dt} \left(\frac{\partial E_{\text{kin}}}{\partial \dot{u}} \right) - \frac{\partial E_{\text{kin}}}{\partial u} + \frac{\partial E_{\text{pot}}}{\partial u} = Q_u$, renders a second order differential equation for the relative water level displacement u ,

$$\ddot{u} + \frac{1}{2L_{\text{eff}}} |\dot{u}| \dot{u} \lambda + \frac{\Delta p}{\rho L_{\text{eff}}} + \omega_A^2 u = -\kappa \ddot{w}_g, \quad (4-8)$$

$$\kappa = \frac{2H \cos \beta + B}{L_{\text{eff}}}, L_{\text{eff}} = 2H + \frac{A_H}{A_B} B, \quad (4-9)$$

$$\omega_A = \sqrt{\frac{2g \sin \beta}{L_{\text{eff}}}}, \Delta p = p_2 - p_1. \quad (4-10)$$

The effective length L_{eff} can be regarded as equivalent length of a TLCD with constant cross sectional area A_H , having the same kinetic energy. ω_A and κ are the natural frequency of the undamped TLCD and a geometry dependent coupling factor linking the floor acceleration and

the TLCD excitation. A high coupling factor κ is necessary to provide sufficient energy transfer from the structure to the absorber. In TLCD literature the loss factor is commonly replaced by the head loss coefficient $\delta_L = \frac{\lambda}{2 L_{eff}} [1/m]$ and the quadratic turbulent damping term in Eq.(4-8) becomes $\delta_L |\dot{u}| \dot{u}$. The method of equivalent linearisation is commonly used to approximate the nonlinear loss term by an equivalent linear one: Demanding that the dissipated energy during one cycle must be equal for turbulent and viscous damping the equivalent viscous damping ζ_A is given by $\zeta_A = 4U_0 \delta_L / 3\pi$, see Appendix A, where U_0 denotes the relative vibration displacement amplitude. Insertion of ζ_A into Eq.(4-8) renders its linearised form

$$\ddot{u} + 2\zeta_A \omega_A \dot{u} + \frac{\Delta p}{\rho L_{eff}} + \omega_A^2 u = -\kappa \ddot{w}_g, \quad (4-11)$$

$$\zeta_A = 4U_0 \delta_L / 3\pi,$$

where ζ_A denotes the effective viscous damping of the TLCD. Generally, the equivalent viscous damping is a parameter which is optimised during the TLCD design (normally done for a linear TLCD model). Thus, δ_L has to be determined from the optimised ζ_A , which can be achieved by $\delta_L = \zeta_A 3\pi / 4U_0$. For the transient TLCD response is recommended to replace the vibration amplitude U_0 by the maximum vibration amplitude U_{max} found from simulations of the linear system. A comparison given in Chapter 9 reveals that this method works satisfactorily, in fact the behaviour of the TLCD with turbulent damping included is slightly superior to a TLCD with viscous damping.

4.1.2. Bernoulli's equation for moving coordinate systems

Alternatively to the application of Lagrange's principle, the Bernoulli equation can be used to derive the TLCD's equations of motion. As the TLCD housing performs a relative motion with respect to an inertial frame, the standard form of the instationary Bernoulli equation is not applicable and it has to be extended, see e.g. Ziegler⁵. A detailed derivation of its instationary formulation for a relative streamline, e.g. with respect to an arbitrary moving reference system is given, before the special cases of a translational and a plane motion will

be investigated in Sections 4.1.3 and 4.5.2. The relationship of pressure and (subsonic) velocity in inviscid flow is of crucial importance and can be given by considering the vector equation of motion in the absence of any shear stresses

$$\rho \mathbf{a} = \mathbf{k} - \text{grad } p, \quad (4-12)$$

where \mathbf{k} , p denote the force density and the pressure acting on a liquid particle. A projection of Eq.(4-12) in the relative streamline's tangential direction \mathbf{e}_t' and integrating along this streamline, while keeping the time constant, see Figure 4-2, renders

$$\int_{s_1}^{s_2} \mathbf{a} \cdot \mathbf{e}_t' ds = \int_{s_1}^{s_2} \frac{1}{\rho} \mathbf{k}_t ds - \int_{s_1}^{s_2} \frac{1}{\rho} \frac{\partial p}{\partial s} ds, \quad (4-13)$$

where $\mathbf{k}_t = \mathbf{k} \cdot \mathbf{e}_t'$ denotes the tangential direction of the body force, and the projection of the pressure gradient becomes $\text{grad}(p) \cdot \mathbf{e}_t' = \partial p / \partial s$. If the body force is due to gravity, a parallel force field is assumed, $\mathbf{k} = -\rho g \mathbf{e}_z$, thus the integration yields the difference of the potential energy per unit of mass according to the difference in the geodesic height of the two mass points of the relative streamline with respect to a common reference plane,

$$\int_{s_1}^{s_2} \frac{1}{\rho} \mathbf{k}_t ds = -g (z_2 - z_1). \quad (4-14)$$

Assuming a steady pressure distribution along the streamline, the second integral on the left hand side of Eq.(4-13) renders for the incompressible flow,

$$-\int_{s_1}^{s_2} \frac{1}{\rho} \frac{\partial p}{\partial s} ds = -\frac{1}{\rho} (p_2 - p_1), \quad (4-15)$$

and Eq.(4-13) simplifies to

$$\int_{s_1}^{s_2} \mathbf{a} \cdot \mathbf{e}_t' ds = -g (z_2 - z_1) - \frac{1}{\rho} (p_2 - p_1). \quad (4-16)$$

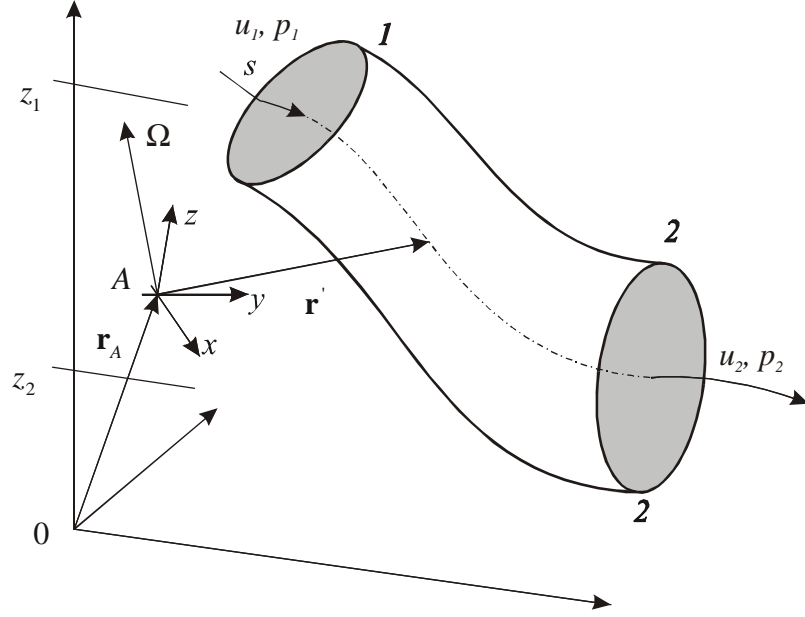


Figure 4-2: Streamline of an instationary flow at constant time, with respect to a moving reference frame A

The absolute acceleration \mathbf{a} of a liquid particle can be split by considering the kinematics of the relative motion. Let the position of a liquid particle with respect to the inertial system 0 be described by $\mathbf{r} = \mathbf{r}_A + \mathbf{r}'$, where \mathbf{r}' denotes the relative motion with respect to the origin A of the moving frame, whose position with respect to the inertial system is given by \mathbf{r}_A . The velocity \mathbf{v} can be derived straightforwardly by differentiating \mathbf{r} with respect to time,

$$\mathbf{v} = \frac{d\mathbf{r}_A}{dt} + \frac{d\mathbf{r}'}{dt} = \mathbf{v}_A + \boldsymbol{\Omega} \times \mathbf{r}' + \frac{d'\mathbf{r}'}{dt} = \mathbf{v}_g + \dot{\mathbf{u}}, \quad (4-17)$$

where $\dot{\mathbf{u}} = \frac{d'\mathbf{r}'}{dt} = \dot{u}_i \mathbf{e}_i'$ denotes the relative velocity of the point with respect to the moving reference frame, rotating with the angular velocity $\boldsymbol{\Omega}$, and the local time derivative is defined by $\frac{d'\mathbf{x}}{dt} = \dot{x} \mathbf{e}_x + \dot{y} \mathbf{e}_y + \dot{z} \mathbf{e}_z$. $\mathbf{v}_g = \mathbf{v}_A + \boldsymbol{\Omega} \times \mathbf{r}'$ denotes the guiding velocity. A second derivation with respect to time renders an expression for the absolute acceleration,

$$\mathbf{a} = \frac{d\mathbf{v}}{dt} = \mathbf{a}_A + \frac{d\boldsymbol{\Omega}}{dt} \times \mathbf{r}' + \boldsymbol{\Omega} \times (\boldsymbol{\Omega} \times \mathbf{r}') + 2\boldsymbol{\Omega} \times \dot{\mathbf{u}} + \frac{d'\dot{\mathbf{u}}}{dt}, \quad (4-18)$$

with the guiding acceleration $\mathbf{a}_g = \mathbf{a}_A + \dot{\mathbf{\Omega}} \times \mathbf{r}' + \mathbf{\Omega} \times (\mathbf{\Omega} \times \mathbf{r}')$, and the Coriolis acceleration $\mathbf{a}_c = 2\mathbf{\Omega} \times \dot{\mathbf{u}}$, which is perpendicular to the relative velocity $\dot{\mathbf{u}} = \dot{u} \cdot \mathbf{e}_t'$. The relative acceleration with respect to the moving reference frame, $\mathbf{a}' = \frac{d'\dot{\mathbf{u}}}{dt}$, can be expressed as $\mathbf{a}' = \partial \dot{\mathbf{u}} / \partial t + (\dot{\mathbf{u}} \cdot \nabla) \cdot \dot{\mathbf{u}}$, or equivalently in Weber's form

$$\mathbf{a}' = \partial \dot{\mathbf{u}} / \partial t + \text{grad} \left(\dot{u}^2 / 2 \right) - \dot{\mathbf{u}} \times \text{curl} (\dot{\mathbf{u}}). \quad (4-19)$$

Projecting the absolute acceleration, Eq.(4-18), along the relative streamline tangent \mathbf{e}_t' yields

$$\mathbf{a} \cdot \mathbf{e}_t' = \mathbf{a}_g \cdot \mathbf{e}_t' + \frac{\partial \dot{u}}{\partial t} + \frac{\partial}{\partial s} \left(\frac{\dot{u}^2}{2} \right) \quad (4-20)$$

where $\text{grad} \left(\frac{\dot{u}^2}{2} \right) \cdot \mathbf{e}_t' = \frac{\partial}{\partial s} \left(\frac{\dot{u}^2}{2} \right)$, and the components of the Coriolis acceleration and of the term $\dot{\mathbf{u}} \times \text{curl} (\dot{\mathbf{u}})$ vanish, since both vectors are perpendicular to \mathbf{e}_t' . Insertion of Eq.(4-20) into Bernoulli's equation, Eq(4-16), renders

$$\int_{s_1}^{s_2} \frac{\partial \dot{u}}{\partial t} ds + \frac{1}{2} (\dot{u}_2^2 - \dot{u}_1^2) = -g (z_2 - z_1) - \frac{1}{\rho} (p_2 - p_1) - \int_{s_1}^{s_2} \mathbf{a}_g \cdot \mathbf{e}_t' ds \quad (4-21)$$

where $\int_{s_1}^{s_2} \frac{\partial}{\partial s} \left(\dot{u}^2 / 2 \right) ds = \frac{1}{2} (\dot{u}_2^2 - \dot{u}_1^2)$. The only difference between Eq.(4-21) and the standard

Bernoulli's equation for nonstationary flow is the integral expression $\int_{s_1}^{s_2} \mathbf{a}_g \cdot \mathbf{e}_t' ds$, which

accounts for the moving reference frame. Applying the rules for the vectorial triple product, the guiding acceleration can be expressed as

$$\mathbf{a}_g = \mathbf{a}_A + \dot{\mathbf{\Omega}} \times \mathbf{r}' + \mathbf{\Omega}^2 \mathbf{n}_p, \quad (4-22)$$

$$\mathbf{n}_p = \frac{1}{\Omega^2} (\mathbf{\Omega} \cdot \mathbf{r}') \cdot \mathbf{\Omega} - \mathbf{r}'$$

which allows further simplification in case of a pure translation or a plane motion of the moving reference system.

4.1.3. Derivation of the equation of motion applying the generalised Bernoulli equation

If the uniaxial floor or ground acceleration is given by $\mathbf{a}_A = \ddot{w}_g \mathbf{e}_x$, then the additional integral term accounting for the moving frame becomes $\int_{s_1}^{s_2} \ddot{w}_g \mathbf{e}_x \cdot \mathbf{e}_t'(s) ds$, where \mathbf{e}_x denote the unit vector in X-direction, in accordance with Figure 4-1. Insertion into the generalised Bernoulli's equation, Eq.(4-21), renders

$$\int_0^{L(t)} \frac{\partial \dot{u}}{\partial t} ds = -g(z_2 - z_1) - \frac{1}{\rho}(p_2 - p_1) - \frac{1}{\rho} \Delta p_L - \int_0^{L(t)} \ddot{w}_g \mathbf{e}_x \cdot \mathbf{e}_t'(s) ds, \quad (4-23)$$

where \dot{u} , p , z , g , $L(t)$ denote the relative fluid velocity, the absolute pressure, the geodesic height, the constant of gravity, and the liquid column length $L(t) = 2H + B$, which remains constant, for the special symmetric case of equal cross sectional areas in the inclined pipe sections. As the entire liquid is considered, the indices 1 and 2 refer to the left and right free surface of the liquid volume, see Figure 4-1, where $u_1 = u_2 = u$. Energy dissipation due to viscous and turbulent damping is described by additional pressure losses Δp_L . Analytical expression of the pressure loss Δp_L can be found e.g. in Ziegler⁵. Performing the integration along the relative streamline, and rearranging terms in Eq. (4-23) directly yields the equation of motion,

$$\ddot{u} + \frac{\Delta p_L}{\rho L_{eff}} + \frac{\Delta p}{\rho L_{eff}} + \omega_A^2 u = -\kappa \ddot{w}_g \quad (4-24)$$

$$\kappa = \frac{2H \cos \beta + B}{L_{eff}}, \quad L_{eff} = 2H + \frac{A_H}{A_B} B,$$

$$\omega_A = \sqrt{\frac{2g \sin \beta}{L_{eff}}}, \quad \Delta p = p_2 - p_1, \quad \Delta p_L = \frac{\rho |\dot{u}| \dot{u}}{2} \lambda(\text{Re})$$

Replacing the generally nonlinear damping term $\frac{\Delta p_L}{\rho L_{eff}}$ by its viscous equivalent $2\zeta_A \omega_A \dot{u}$, see again Appendix A, Eqs. (4-11) and (4-24) become identical. If the liquid container is not sealed, then the air pressure at the free surfaces is approximately equal to the ambient pressure $p_1 = p_2 = p_0$ and the pressure difference Δp vanishes. If, however, the piping system is closed and there is no gas exchange between the container and its surroundings, then the pressure cannot be assumed to be constant, and it will have a considerable influence on the dynamic behaviour, as it acts as a nonlinear spring, whose force displacement relation is determined in section 4.3.

4.2. Reaction forces and moments for the plane TLCD

Having found the equation of motion for a ground or floor excited TLCD, the interaction forces between TLCD and the moving supporting floor are still to be determined for dynamic analysis. Assuming that the dead weight of a rigid container is added to the corresponding floor mass, only the interaction forces between the massless, rigid, liquid filled piping system and the supporting floor are considered. Principally, the control volume concept for moving frames would be adequate to calculate these interaction forces, but this approach becomes complicated, if the pressure p_1 or p_2 differ from the ambient pressure p_0 . Thus the entire piping system is considered, and the basic law of conservation of momentum for a material volume, applied to the virtual, massless container renders the resultant of the external forces \mathbf{F} acting on the piping system

$$\frac{d\mathbf{I}}{dt} = \mathbf{F}, \quad (4-25)$$

$$\mathbf{I} = \int_{m_f} (\dot{\mathbf{u}} + \dot{\mathbf{w}}_g) dm, \quad \dot{\mathbf{w}}_g = \dot{w}_g \mathbf{e}_x \quad (4-26)$$

where \mathbf{I} denotes the linear momentum of the entire piping system with the liquid mass included. Equation (4-25) is a vector equation and thus reaction forces in the horizontal X-direction and the vertical Z-direction are expected. Similarly, the resultant of the acting moments can be calculated by applying the law of conservation of angular momentum. If A is a moving reference point, see e.g. Ziegler⁵,

$$\frac{d \mathbf{H}'_A}{dt} + m_f \mathbf{r}'_g \times \mathbf{a}_A = \mathbf{M}_A, \quad \mathbf{a}_A = \ddot{w}_g \mathbf{e}_x \quad (4-27)$$

$$\mathbf{H}'_A = \int_{m_f} \mathbf{r}' \times \dot{\mathbf{u}} dm$$

where \mathbf{H}'_A , m_f , \mathbf{r}'_g , \mathbf{a}_A are the relative moment of momentum, the liquid mass, the relative position vector to the liquid's centre of gravity and the absolute acceleration of the reference point A , respectively. It is pointed out that in Eqs.(4-25) - (4-27) the resultant forces are acting on the container. Insertion of the relative liquid velocity distribution into Eq.(4-25) and (4-26), thereby neglecting the mass of the air inside the piping system, renders an analytic expression for the momentum of the fluid mass

$$\begin{aligned} \mathbf{I} = \int_{m_f} (\dot{\mathbf{u}} + \dot{\mathbf{w}}_g) dm = \rho A_H \left((H - u) \begin{pmatrix} \dot{w}_g + \dot{u} \cos \beta \\ 0 \\ -\dot{u} \sin \beta \end{pmatrix} + (H + u) \begin{pmatrix} \dot{w}_g + \dot{u} \cos \beta \\ 0 \\ +\dot{u} \sin \beta \end{pmatrix} \right) \\ + \rho A_B B \begin{pmatrix} \dot{w}_g + \frac{A_H}{A_B} \dot{u} \\ 0 \\ 0 \end{pmatrix} = \rho A_H \begin{pmatrix} 2H(\dot{w}_g + \dot{u} \cos \beta) + \dot{u} B + \frac{A_B}{A_H} B \dot{w}_g \\ 0 \\ 2u \dot{u} \sin \beta \end{pmatrix} \end{aligned} \quad (4-28)$$

Taking the total time derivative ($\Omega = 0$), and applying the reaction principle, straightforwardly generates an expression for the reaction forces acting on the supporting floor, where it must be mentioned, that static dead weight loading of the fluid mass is not included in the vertical reaction force component f_z ,

$$f_x = -m_f (\ddot{w}_g + \bar{\kappa} \ddot{u}), \quad (4-29)$$

$$f_z = -m_f \bar{\kappa} (u \ddot{u} + \dot{u}^2), \quad (4-30)$$

$$\bar{\kappa} = \kappa \left(1 + \frac{A_H}{A_B} \frac{B}{2H} \right) \bigg/ \left(1 + \frac{A_B}{A_H} \frac{B}{2H} \right) = \frac{\rho A_H B + 2\rho A_H H \cos \beta}{m_f}, \quad (4-31)$$

$$\bar{\bar{\kappa}} = \frac{2\rho A_H \sin \beta}{m_f}, \quad (4-32)$$

where $m_f = \rho A_H (2H + B A_B / A_H)$ denotes the total fluid mass and $\bar{\kappa}$ defines a geometry factor such that the ‘active’, horizontally moving mass, and the ‘passive’, vertically moving liquid mass are given by $m_B = \bar{\kappa} m_f$ and $m_H = m_f (1 - \bar{\kappa})$. To be able to calculate the resultant moment, the reference point A must be selected. For simplicity, A is located at the centre of the horizontal pipe section moving with the floor, as indicated in Figure 4-1, and hence only the inclined pipe sections contribute to H'_A . According to Eq.(4-27), the relative angular momentum becomes

$$\begin{aligned} \mathbf{H}'_A = \int_{m_f} \mathbf{r}'_A \times \dot{\mathbf{u}} dm = \rho A_H \int_0^{H-u} \begin{pmatrix} -\frac{B}{2} - s \cos(\beta) \\ 0 \\ s \sin(\beta) \end{pmatrix} \times \begin{pmatrix} \dot{u} \cos(\beta) \\ 0 \\ -\dot{u} \sin(\beta) \end{pmatrix} ds \\ + \rho A_H \int_0^{H+u} \begin{pmatrix} \frac{B}{2} + s \cos(\beta) \\ 0 \\ s \sin(\beta) \end{pmatrix} \times \begin{pmatrix} \dot{u} \cos(\beta) \\ 0 \\ \dot{u} \sin(\beta) \end{pmatrix} ds = -\rho A_H B H \dot{u} \sin \beta \mathbf{e}_y \end{aligned} \quad (4-33)$$

\mathbf{e}_y is a unit vector pointing out of the X-Z plane. Inserting into Eq.(4-27), directly yields the resulting moment \mathbf{M}_A acting on the piping system. Again $\mathbf{\Omega} = \mathbf{0}$ is considered in the time derivatives

$$\mathbf{M}_A = \frac{d \mathbf{H}'_A}{dt} + m_f \mathbf{r}'_g \times \mathbf{a}_A = -\frac{m_f \bar{\bar{\kappa}}}{2} \left(B H \ddot{u} - (H^2 + u^2) \ddot{w}_g \right) \mathbf{e}_y, \quad (4-34)$$

where the vertical component of the position vector of the centre of gravity with respect to A is given by $\rho A_H (H^2 + u^2) \sin \beta / m_f \mathbf{e}_z$. The undesired moment \mathbf{M}_A is the sum of the TLCD-floor interaction moment \mathbf{M}_{TLCD} and a second contribution resulting from gravity forces acting at the (displaced) centre of mass. However, it is common practice to neglect the

influence of the undesired moments which also exist for the TMD, since the centre of mass of the floor and the absorber do not coincide, and thus \mathbf{r}_m does not vanish, as shown in Figure 4-3.

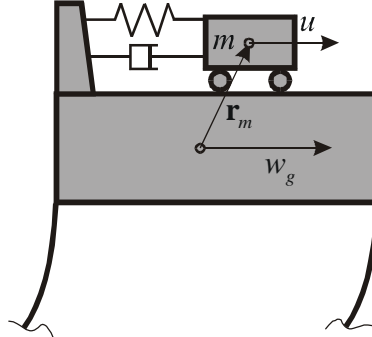


Figure 4-3: Classical TMD setup

However, when working with framed structures, those moments and the vertical force components are generally both found negligible. By setting $\beta = \pi/2$ in Eq.(4-31) and Eq.(4-32) the reaction forces, Eqs.(4-29) and (4-30), for the classical U-shaped TLCD are generated, see e.g. Balendra et al⁶, Chang et al⁷, Gao et al⁸ and Hitchcock et al⁹.

4.3. Determination of the air spring effect

As already mentioned, in case of a closed piping system, the air contained in the piping system is compressed or released, depending on the water level displacement level. Therefore an additional restoring force is created, whose influence on the dynamic behaviour is described in this section. From the gas dynamic point of view, the operating range of TLCD is limited to low frequencies only, and therefore a quasi-static approach seems adequate to compute the pressure difference $\Delta p = p_2 - p_1$. Starting from the polytropic material law for gases,

$$\frac{p}{p_0} = \left(\frac{\rho}{\rho_0} \right)^n, \quad 1 \leq n \leq \kappa_a = c_p/c_v, \quad (4-35)$$

or equivalently in its incremental form

$$dp = K_t \frac{d\rho}{\rho}, \quad K_t = n p \quad (4-36)$$

where K_t denotes the tangent modulus, the actual pressure p can be obtained from the initial pressure p_0 and the initial mass density ρ_0 , where n denotes the polytropic index, which is determined by the type of state change of the gas. For an adiabatic process of any two atomic gas, $\kappa_a = 1.4$, whereas for an isothermal (slow) process, $n = 1$. Any other process is in-between those two extreme situations. If the water column is moving along a constant cross sectional area A_H , the ratio of mass densities ρ/ρ_0 is given by $V_0/(V_0 \pm A_H u)$, where V_0 denotes the gas volume in static equilibrium. Consequently, the pressure difference $\Delta p = p_2 - p_1$ is found to be

$$\Delta p(u) = p_0 \left[\left(\frac{V_0}{V_0 - A_H u} \right)^n - \left(\frac{V_0}{V_0 + A_H u} \right)^n \right]. \quad (4-37)$$

A Taylor series expansion of Eq.(4-37) renders the pressure difference, which fully determines the air spring effect by the stiffness K_n . If the higher order terms are neglected, e.g., linearisation is performed,

$$\Delta p(u) = \frac{2n p_0 A_H}{V_0} u + O(u^3) \approx \frac{2n p_0}{h_{eff}} u = 2 K_n u / h_{eff}, \quad (4-38)$$

$$h_{eff} = V_0 / A_H, \quad K_n = n p_0.$$

h_{eff} denotes the effective height of the air spring, an important design variable, as it will directly influence the TLCD's natural frequency. Because all terms of even order vanish in the Taylor series expansion, the linearised expression is accurate for relatively large displacements which is shown graphically by introducing the nondimensional displacement $\chi = u/h_{eff}$, and comparing the exact and the approximated solution, see Figure 4-4

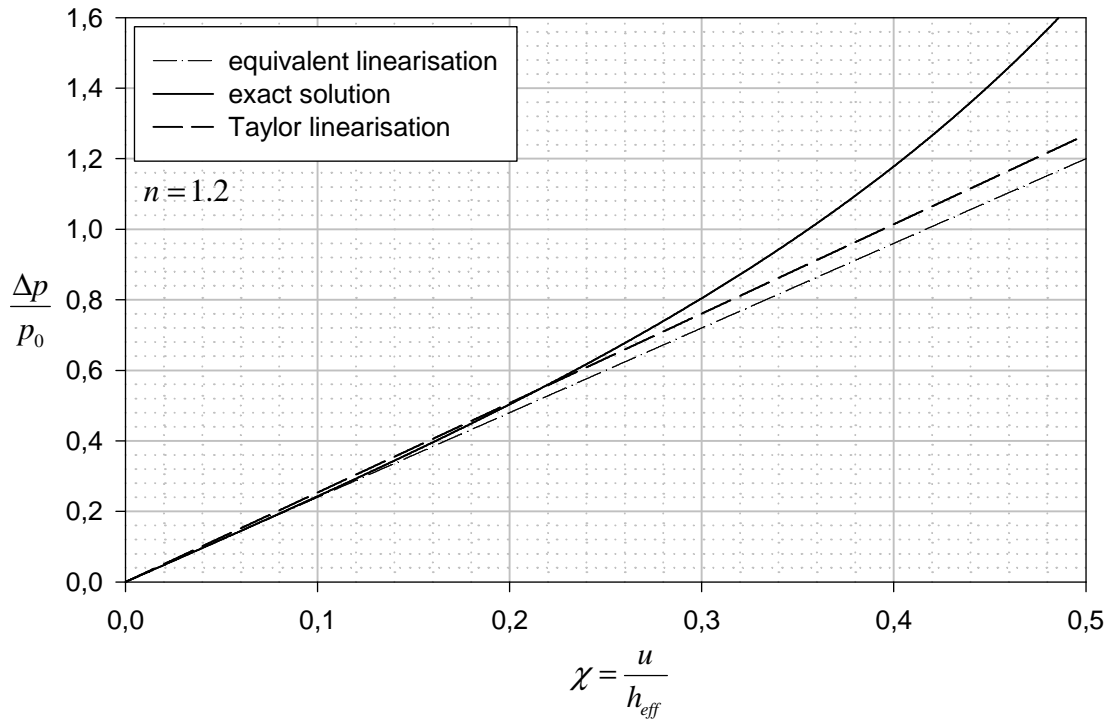


Figure 4-4: Comparison of linearised and exact tangent modulus

Visual inspection shows that for $\chi < 0.25$, the linear approximation is sufficiently accurate for engineering purposes, with an error smaller than 10.2% in the pressure difference. For larger displacements the air spring stiffness is underestimated. A better way of linearisation is to demand that the potential energy stored in a linear elastic spring (stiffness K_{eq}) and the nonlinear air spring is equivalent at a certain amplitude U_0 , thus

$$K_{eq} = \frac{\int_0^{U_0} p(u) du}{\frac{1}{2} U_0^2}. \quad (4-39)$$

For $U_0 = 0.25 h_{eff}$, the result is given graphically in Figure 4-4. When compared to the linear Taylor approximation, the method of harmonic balance performs slightly better. Inserting the linearised pressure difference Δp from Eq.(4-38) into Eq.(4-24) yields a linear equation of motion,

$$\ddot{u} + 2\zeta_A \omega_A \dot{u} + \omega_A^2 u = -\kappa \ddot{w}_g \quad (4-40)$$

$$\kappa = \frac{2H \cos \beta + B}{L_{eff}}, L_{eff} = 2H + \frac{A_H}{A_B} B, \quad \omega_A = \sqrt{\frac{2g \sin \beta}{L_{eff}} + \frac{2K_n}{\rho L_{eff} h_{eff}}}, K_n = n p_0. \quad (4-41)$$

For closed piping systems, the TLCD's natural frequency ω_A is not only dependent on the geometry (angle β and effective liquid column length L_{eff}), but also on the air spring stiffness K_n . Without the air spring effect the natural frequencies are very low, as the only restoring forces are provided by gravity. Table 4-1 lists the natural frequencies of a TLCD for various effective lengths L_{eff} and opening angles β . Obviously a realistic implementation is possible for structures with natural frequencies lower than 0.3 Hz. This fact reduces the possible applications to the fundamental vibration mode of towers and high-rise buildings of about 150m or more in height, and to large vertical cylindrical tanks, see Rammerstorfer et al.¹⁰.

no air spring	$\beta = 30^\circ$	$\beta = 45^\circ$	$\beta = 60^\circ$	$\beta = 90^\circ$
$L_{eff} = 1m$	0.50 Hz	0.59 Hz	0.65 Hz	0.71 Hz
$L_{eff} = 5m$	0.22 Hz	0.26 Hz	0.29 Hz	0.32 Hz
$L_{eff} = 10m$	0.15 Hz	0.19 Hz	0.21 Hz	0.22 Hz
$L_{eff} = 20m$	0.11 Hz	0.13 Hz	0.15 Hz	0.16 Hz
$L_{eff} = 40m$	0.078 Hz	0.094 Hz	0.10 Hz	0.11 Hz

Table 4-1: Natural frequencies of TLCD without air spring effect

To obtain higher frequencies, the angle of inclination β , should approach 90° , which, on the other hand, either decreases the active liquid mass, or cuts down the maximum TLCD liquid displacement radically. Thus, from a performance point of view β must be kept as small as possible, thereby restricting the application to low frequency problems. Nevertheless, the

introduction of the air spring overcomes this low frequency problem, see Table 4-2, where the natural frequencies of a TLCD for varying effective lengths L_{eff} and opening angles β are listed for two effective heights $h_{eff} = A_H/V_0$. For simplicity it is assumed that p_0 equals the atmospheric pressure, so that no pressure supply has to be provided for the TLCD. The liquid is assumed to be water, $\rho = 1000 \text{ kg/m}^3$, and the polytropic process is assumed to be described by $n = 1.2$, which is the arithmetic mean of an adiabatic ($n = 1.4$) and the isothermal process.

air spring	$h_{eff} = 10m, p_0 = 10^5 Pa$		$h_{eff} = 1m, p_0 = 10^5 Pa$	
	$\beta = 45^\circ$	$\beta = 60^\circ$	$\beta = 45^\circ$	$\beta = 60^\circ$
$L_{eff} = 1m$	0.98 Hz	1.01 Hz	2.52 Hz	2.56 Hz
$L_{eff} = 5m$	0.44 Hz	0.46 Hz	1.13 Hz	1.15 Hz
$L_{eff} = 10m$	0.31 Hz	0.32 Hz	0.80 Hz	0.81 Hz
$L_{eff} = 20m$	0.22 Hz	0.23 Hz	0.56 Hz	0.57 Hz
$L_{eff} = 40m$	0.15 Hz	0.16 Hz	0.40 Hz	0.41 Hz

Table 4-2: Natural frequencies of TLCD with air-spring effect

Apparently, the air spring can increase the natural frequencies substantially, and as for higher frequencies the expected amplitudes become smaller it is also possible to reduce h_{eff} thereby increasing the possible tuning frequencies even further. If, besides the reduction of h_{eff} , the air spring stiffness is too small, the gas filled volume V_0 has to be pressurised.

From Table 4-2 and Eq.(4-40) it is apparent that the influence of gravity on the fundamental frequency is almost negligible and consequently β should be chosen as small as possible while still meeting all physical implementation requirements, e.g. a continuous flow of the liquid mass m_f .

4.4. General discussion of the TLCD's design and its advantages

4.4.1. Influence of geometry

The passive air-spring allows to overcome the limited TLCD frequency range, but the effectiveness of TLCDs in reducing structural vibrations mainly depends on the geometry parameters κ and $\bar{\kappa}$. The former is given by

$$\kappa = \frac{2H \cos \beta + B}{2H + B A_H / A_B}, \quad (4-42)$$

and acts as an excitation factor for the TLCD, see Eq.(4-9). To reduce the TLCD vibration amplitudes it should be chosen as small as possible. This must be achieved by increasing the denominator in Eq.(4-42), because reducing the numerator will also reduce the second geometry factor $\bar{\kappa}$, and thus the active moving mass $m_B = \bar{\kappa} m$ where $\bar{\kappa}$ is defined by Eq.(4-31),

$$\bar{\kappa} = \kappa \left(1 + \frac{A_H}{A_B} \frac{B}{2H} \right) / \left(1 + \frac{A_B}{A_H} \frac{B}{2H} \right), \quad (4-43)$$

and determines the interaction forces between TLCD and the host structure. Therefore it must be chosen as large as possible. Obviously, one has to compromise between κ and $\bar{\kappa}$, because increasing κ lessens $\bar{\kappa}$ and vice versa. For absorbers with constant cross sectional area, κ and $\bar{\kappa}$ are identical, however, for structural implementations, a variation of the cross sectional area can help to reduce the TLCD vibration amplitude, if $A_H > A_B$ is selected.

If a V-shaped TLCD is chosen, the possible vibration amplitudes can reach a maximum one half of the liquid column length, if there is no horizontal pipe element. Thus, the possible vibration amplitudes are extremely large when compared to classical TMD, whose stroke is normally limited to about one meter. However, allowing large amplitudes also implies providing sufficient space for the piping system. If this is not possible, then a decrease in amplitude comes at the price of a performance reduction.

4.4.2. Installation and maintenance

Another advantage of TLCDs is their simplicity in design and maintenance. For traditional TMD damping systems a lot of technical equipment is used to ensure a low-friction sliding movement, and normally active hydraulic systems are utilised to compensate friction losses. For liquid column dampers this problem does not exist as the liquid acts as bearing and mass at the same time, minimising all maintenance requirements. Basically, only a sealed piping system is necessary, and the passive absorber is absolutely independent of external energy supply, electronic equipment and measuring devices. Turbulent flow provides the necessary damping, and no other energy dissipating mechanisms are needed. Many liquids can be used for the absorber since at the end, most dissipated energy is converted into heat. Normal water however, seems most suited as it is everywhere available, cheap, easy with respect to environmental considerations, and enormous amounts of water are already stored in high-rise buildings to ensure the water supply and provide water for fire fighting. Thus simply re-shaping the already existing water container according to the TLCD guidelines can decrease the vibration proneness of a structure. It has been shown, that the vibration characteristics of TLCD is limited to low frequencies. Therefore they are not particularly suitable to mitigate high frequency vibrations, but best qualified to reduce low frequency vibration problems in structures. Frequencies as low as 0.1Hz can be handled by TLCDs, an operating range which causes serious problems with traditional TMDs. A salient feature of TLCD is the simple implementation into civil engineering: only a properly designed and water proof piping system must be installed. Fine tuning can be achieved by altering the amount of water, thus changing the effective liquid column length. Disadvantages, on the other side are the restriction that the liquid mass can only be used to reduce vibration in one direction and the low mass density of water when compared to iron or concrete, results in physically large absorber systems. The first drawback can be partially overcome by using a so called bi-directional TLCD, see Hitchcock¹¹, at the price of a reduced maximum vibration amplitude and increased implementation requirements, as well as tuning difficulties. The latter problem cannot be overcome, because the application of liquids other than water is not realistic, thus only a smooth integration of the piping system into walls, floors, and along other structural members is advised.

4.4.3. In situ testing of structures

Of outstanding importance is the easy adaptation of the TLCD for in-situ testing of a structure. In Chapter 8 it is discussed in detail how to extend the passive TLCD to an active TLCD which is able to induce a liquid motion by pressurising the gas (air) volume at either side of the liquid column. The resulting forces, given by Eqs.(4-29) and (4-30), can be used to excite the host structure and perform in-situ measurements. This method will be most effective if the energy dissipation via the TLCD is minimised, thus the orifice plate should be removed. Using a periodic pressure input the steady state structural response will have vibration amplitudes high enough to obtain reliable acceleration measurement for the identification of the structural system.

4.5. *Torsional Tuned Liquid Column Damper (TTLCD)*

4.5.1. Introduction

The plane TLCD configuration discussed in Sections 4.1 and 4.2 is suitable to mitigate translational motions. However, torsional vibration do also occur in high-rise structures, normally as coupled flexural torsional vibrations. The torsional tuned liquid column damper (TTLCD) is designed to mitigate torsional motions in buildings. Like the plane TLCD, it consists of a liquid filled piping system, whose geometry is given in Figure 4-5a. In plan view, the piping system encloses the arbitrarily shaped floor area A_p . To minimise horizontal interaction forces, it is crucial that the projection of the liquid path onto the floor is a closed curve, see Figure 4-5b.

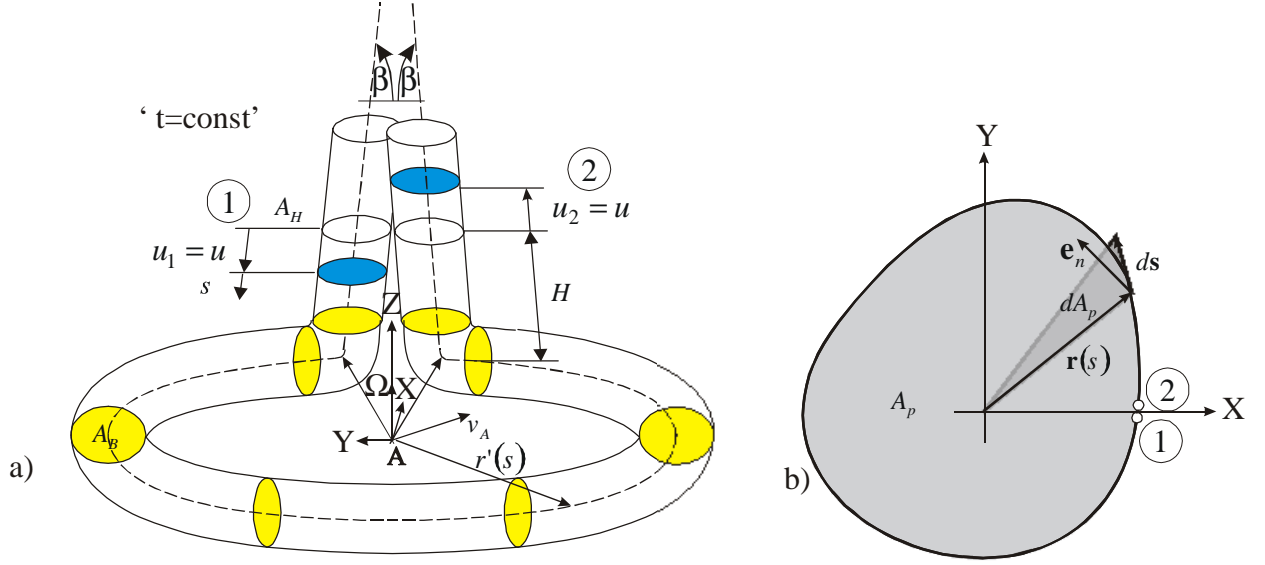


Figure 4-5: a) schematic of torsional TLCD, relative streamline from 1 to 2 considered
b) projection of relative streamline onto supporting floor

4.5.2. Equation of motion

As shown in Section 4.1.2, the instationary Bernoulli equation generalised for a relative streamline in a moving reference system takes the form,

$$\int_0^{L(t)} \frac{\partial \dot{u}}{\partial t} ds = -g(z_2 - z_1) - \frac{1}{\rho}(p_2 - p_1) - \frac{1}{\rho} \Delta p_L - \int_0^{L(t)} \mathbf{a}_g \cdot \mathbf{e}_t'(s) ds, \quad (4-44)$$

where \dot{u} , p , z , g , $L(t)$ again denote the relative liquid velocity, the absolute pressure, the geodesic height, the constant of gravity and the length of the liquid column, which is given by $L(t) = 2H + B$, where B denotes the length of the plane pipe section. As the entire liquid is considered, the indices 1 and 2 refer to the left and right free surface of the liquid volume, see Figure 4-5, where $u_1 = u_2 = u$. Again, energy dissipation due to viscous and turbulent

damping is described by additional pressure losses Δp_L . The integral term $\int_0^{2H+B} \mathbf{a}_g \cdot \mathbf{e}_t'(s) ds$

has to be evaluated at constant time, where the guidance acceleration of the moving frame \mathbf{a}_g

is defined by Eq.(4-22), $\mathbf{a}_g = \mathbf{a}_A + \dot{\boldsymbol{\Omega}} \times \mathbf{r}' + \boldsymbol{\Omega}^2 \mathbf{n}_p$. For a plane motion, the integral

$$\int_0^{2H+B} \mathbf{a}_A \cdot \mathbf{e}_t' ds = \mathbf{a}_A \cdot \oint_s ds = a_{A,x} \oint_s dx + a_{A,y} \oint_s dy + 0 \int_{z_1}^{z_2} dz = 0$$

vanishes, since $ds = [dx, dy, dz]^T$ and \mathbf{a}_A has no vertical component. Now Bernoulli's equation with respect to the relative streamline becomes

$$\ddot{u} \left(2H + \frac{A_H}{A_B} B \right) = -2 g u \sin \beta - \frac{1}{\rho} (p_2 - p_1) - \frac{1}{\rho} \Delta p_L \quad (4-45)$$

$$- \int_0^{2H+B} (\dot{\boldsymbol{\Omega}} \times \mathbf{r}') \cdot \mathbf{e}_t' ds - \Omega^2 \int_0^{2H+B} \mathbf{n}_p \cdot \mathbf{e}_t' ds .$$

Let \mathbf{r}' , ds , $\boldsymbol{\Omega}$ and \mathbf{n}_p be given by $\mathbf{r}' = [x, y, z]^T$, $ds = \mathbf{e}_t ds = [dx, dy, dz]^T$, $\boldsymbol{\Omega} = [0, 0, \omega_z]^T$ and $\mathbf{n}_p = \frac{1}{\Omega^2} (\boldsymbol{\Omega} \cdot \mathbf{r}') \cdot \boldsymbol{\Omega} - \mathbf{r}'$ respectively, then \mathbf{n}_p simplifies to $\mathbf{n}_p = [-x, -y, 0]^T$ and the path

integral $\Omega^2 \int_0^{2H+B} \mathbf{n}_p \cdot \mathbf{e}_t' ds$ vanishes, since

$$\oint x dx + \oint y dy + \int_{z_1}^{z_2} 0 dz = 0 . \quad (4-46)$$

The path integration remaining in Eq.(4-45), $\int_0^{2H+B} (\dot{\boldsymbol{\Omega}} \times \mathbf{r}') \cdot \mathbf{e}_t' ds$, is performed by integrating separately over the horizontal part of the relative streamline and its vertical projection. Thus

$$- \oint_B (\dot{\boldsymbol{\Omega}} \times \mathbf{r}'_{xy}) \cdot \mathbf{e}_t' ds - \int_0^{2H+B} \underbrace{\dot{\boldsymbol{\Omega}} \times \mathbf{r}'_z}_0 \cdot \mathbf{e}_t' ds = -\dot{\omega}_z \oint_B \underbrace{\mathbf{e}_z \times \mathbf{r}'_{xy}}_{r(s) \mathbf{e}_n} \cdot \mathbf{e}_t' ds = -2 A_p \dot{\omega}_z , \quad (4-47)$$

$$\mathbf{r}'_{xy} = [x, y, 0]^T, \quad \mathbf{r}'_z = [0, 0, z]^T,$$

where $r(s)$, A_p denote the length of the relative position vector and the floor area of the horizontal projection of the streamline, see Figure 4-5. Finally, insertion into Eq.(4-45), and the introduction of an equivalent viscous damping ratio ζ_A renders the linearised (with respect to turbulent damping) second order equation of motion,

$$\ddot{u} + 2\zeta_A \omega_A \dot{u} + \omega_A^2 u + \frac{\Delta p}{\rho L_{eff}} = -\frac{2 A_p \dot{\omega}_z}{\rho L_{eff}}, \quad (4-48)$$

$$L_{eff} = \int_0^{2H+B} \frac{A_H}{A(s)} ds, \quad \omega_A = \sqrt{\frac{2g \sin \beta}{L_{eff}}}.$$

Similar to the plane TLCD, the pressure difference $\Delta p = p_2 - p_1$ describes the air spring effect. In a first approximation, the increased stiffness results in a higher natural frequency

$$\omega_A = \sqrt{\frac{2g \sin \beta}{L_{eff}} + \frac{2 K_n}{\rho L_{eff} h_{eff}}}, \quad (4-49)$$

$$K_n = \frac{2n p_0}{h_{eff}}, \quad h_{eff} = \frac{V_0}{A_H},$$

where K_n , $1 \leq n \leq \kappa_a = 1.4$, p_0 , h_{eff} , V_0 denote the linearised air-spring stiffness, the polytropic index, the initial pressure, the effective height, and the air volume at rest, respectively. For details on these parameters, see section 4.3

4.5.3. Forces and Moments

To couple absorber and structure it is important to know the interface reactions. Forces and moments can be obtained by applying the linear momentum and moment of momentum equations for moving frames, see Eqs.(4-26) and (4-27)

$$\frac{d}{dt} \mathbf{I} = \mathbf{F}, \quad \frac{d\mathbf{I}}{dt} = \frac{d'\mathbf{I}'}{dt} + \boldsymbol{\Omega} \times \mathbf{I} \quad (4-50)$$

$$\mathbf{I} = \int_{m_f} (\mathbf{v}_A + \mathbf{v}') dm \quad (4-51)$$

$$\frac{d}{dt} \mathbf{H}'_A + m_f \mathbf{r}'_g \times \mathbf{a}_A = \mathbf{M}_A, \quad \frac{d\mathbf{H}'_A}{dt} = \frac{d'\mathbf{H}'_A}{dt} + \boldsymbol{\Omega} \times \mathbf{H}'_A \quad (4-52)$$

$$\mathbf{H}'_A = \int_{m_f} \mathbf{r}' \times \mathbf{v}' dm,$$

where m_f , \mathbf{H}'_A , $\mathbf{v}' = \frac{d\mathbf{r}'}{dt}$, \mathbf{r}'_g denote the liquid mass, the relative moment of momentum with respect to an arbitrary moving reference point A , the relative velocity with respect to the moving reference point A , and the relative position vector of the instantaneous centre of the fluid mass with respect to A , respectively. For the subsequent derivation the reference point A is selected such, that \mathbf{r}'_g is fixed in the moving frame and given by $\mathbf{r}'_g = r'_g \mathbf{e}_z$. Inserting $\mathbf{v}' = \boldsymbol{\Omega} \times \mathbf{r}' + \dot{\mathbf{u}}$, into Eq.(4-50), and subsequent integration yields $\mathbf{I} = \int_{m_f} \mathbf{v}_A dm + m_f (\boldsymbol{\Omega} \times \mathbf{r}_g) + \int_{m_f} \dot{\mathbf{u}} dm$. Since $\boldsymbol{\Omega} = \omega_z \mathbf{e}_z$ and $\mathbf{r}'_g = r'_g \mathbf{e}_z$, the second term, $m_f (\boldsymbol{\Omega} \times \mathbf{r}_g)$, vanishes and the momentum simplifies to $\mathbf{I} = m_f \mathbf{v}_A + \int_{m_f} \dot{\mathbf{u}} dm$. Since $\int_{m_f} \dot{\mathbf{u}} dm = \int_s \rho A(s) \dot{u}(s) \mathbf{e}_t ds = \dot{m} \int_s ds$, where $ds = \mathbf{e}_t ds$ and $\dot{m} = \rho A(s) \dot{u}(s) = \text{const.}$ As the horizontal projection of the TTLCD is a closed loop, see Figure 4-5, the momentum of the fluid mass can be expressed as

$$\mathbf{I} = m_f \mathbf{v}_A + \dot{m} \int_{z_1}^{z_2} dz \mathbf{e}_z = m_f \mathbf{v}_A + 2 \rho A_H \dot{u} u \sin \beta \mathbf{e}_z,$$

where the integration limits $z_1 = (H - u(t)) \sin \beta$ and $z_2 = (H + u(t)) \sin \beta$ are considered. Now the application of the reaction principle directly yields the interaction forces $(-\mathbf{F})$ acting on the structure, by taking the time derivative

$$-\mathbf{F} = m_f \left(\mathbf{a}_A + \frac{2 \rho A_H}{m_f} \sin \beta (\dot{u}^2 + u \ddot{u}) \mathbf{e}_z \right), \quad (4-53)$$

The horizontal components of the resulting force only depend on the acceleration of the reference point, and the TLCD acts like dead weight loading. There is, however, an undesired resultant vertical force from the liquid motion which is negligible for small displacements u or can be kept small by small angles of inclination β .

Consequently, splitting the relative velocity vector and the relative position vector \mathbf{r}' again into their horizontal and vertical components, $\mathbf{r}' = \mathbf{r}'_{xy} + \mathbf{r}'_z$, $\mathbf{v}' = \mathbf{v}'_{xy} + \mathbf{v}'_z$, and substituting into Eq.(4-52) renders the relative momentum of the liquid mass m_f .

$$\begin{aligned}
\mathbf{H}'_A &= \int_{m_f} (\mathbf{r}'_{xy} + \mathbf{r}'_z) \times (\mathbf{v}'_{xy} + \mathbf{v}'_z) dm = \int_{m_f} \mathbf{r}'_{xy} \times \mathbf{v}'_{xy} dm + \int_{m_f} \mathbf{r}'_{xy} \times \mathbf{v}'_z dm \\
&+ \int_{m_f} \mathbf{r}'_z \times \mathbf{v}'_{xy} dm + \int_{m_f} \underbrace{\mathbf{r}'_z \times \mathbf{v}'_z}_0 dm = \int_{m_f} \mathbf{r}'_{xy} \times \mathbf{v}'_{xy} dm + \mathbf{H}'_{res} \\
\mathbf{H}'_{res} &= \int_{m_f} [(\mathbf{r}'_{xy} \times \mathbf{v}'_z) + (\mathbf{r}'_z \times \mathbf{v}'_{xy})] dm,
\end{aligned} \tag{4-54}$$

As the TLCD setup is not symmetric about the Y-Z-plane it is useful to install a second TLCD of same geometry in a mirrored position, such that symmetry is achieved. This will force the unwanted 'residual' components \mathbf{H}'_{res} to vanish, which is of great interest as it reduces undesired reaction moments. Since the relative velocity with respect to the reference point A , \mathbf{v}' , can be expressed as $\mathbf{v}' = \boldsymbol{\Omega} \times \mathbf{r}' + \dot{\mathbf{u}}$, its horizontal projection \mathbf{v}'_{xy} becomes

$$\mathbf{v}'_{xy} = \omega_z \mathbf{e}_z \times \mathbf{r}'_{xy} + \dot{\mathbf{u}}_{xy}. \tag{4-55}$$

Therefore Eq.(4-54) takes on its final form

$$\begin{aligned}
\mathbf{H}'_A &= \omega_z \mathbf{e}_z \int_{m_f} |\mathbf{r}'_{xy}|^2 dm + \int_0^{2H+B} \rho A(s) \mathbf{r}'_{xy} \times \dot{\mathbf{u}}_{xy} ds \\
&= \omega_z \mathbf{e}_z \int_{m_f} |\mathbf{r}'_{xy}|^2 dm + \dot{m} \int_0^{2H+B} \underbrace{\mathbf{r}'_{xy} \times \mathbf{e}_t}_{2dA_p \mathbf{e}_z} ds, \\
\mathbf{H}'_A &= (\omega_z I_z + 2\dot{u} \rho A_H A_p) \mathbf{e}_z = m_f (\omega_z r_f^2 + \dot{u} \bar{r}_f) \mathbf{e}_z \\
I_z &= \int_{m_f} |\mathbf{r}'_{xy}|^2 dm, \quad \bar{r}_f = \frac{2\rho A_p A_H}{m_f}, \quad r_f^2 = \frac{I_z}{m_f}
\end{aligned} \tag{4-56}$$

where I_z , r_f denote the axial moment of inertia of the fluid mass, and radius of inertia for the fluid mass, and A_p , \bar{r}_f denote the area of the horizontal TLCD projection and an equivalent mass radius, respectively. Since the centre of gravity of the liquid mass, \mathbf{r}'_g in Eq.(4-52), is given by

$$\mathbf{r}_g' = [\rho A_H \sin(\beta)(H^2 + u^2)/m_f] \mathbf{e}_z, \quad (4-57)$$

the expression for the interaction moments acting on the supporting floor of the symmetrical arrangement of two TLCDs, takes on the form

$$\mathbf{M}_{TLCD} = -m_f (r_f^2 \dot{\omega}_z + \bar{r}_f \ddot{u}) \mathbf{e}_z - \rho A_H \sin \beta (H^2 + u^2) \mathbf{e}_z \times \mathbf{a}_A, \quad (4-58)$$

where the reaction principle is applied ($\mathbf{M}_{TLCD} = -\mathbf{M}_A$). Since the centre of gravity is only moving vertically, the horizontal components of \mathbf{r}_g' vanish, and thus there is no resulting moment due to gravity forces acting on the fluid mass. Again, the TLCD construction exhibits undesired axial moments about the X-Y-axes which are due to the fact that the vertical component of the centre of gravity varies with u . For small vibrations, or small angles $\beta \ll 1$, those terms are neglected, yielding a linear system behaviour. Neglecting the nonlinear terms, the interaction moment has two contributions: the first, $-m_f r_f^2 \dot{\omega}_z \mathbf{e}_z$, corresponds to a rigid body motion of the fluid mass rotating with the rigid floor, whereas the second, $-m_f \bar{r}_f \ddot{u} \mathbf{e}_z$, describes reaction of the liquid moving with respect to the piping system. Apparently high interaction moments can be expected for high values of \bar{r}_f , corresponding to a large area A_p .

4.6. References

- ¹ Idelchick; I.E., *Handbook of hydraulic resistance*, Hemisphere Publishing Corporation, 1986
- ² Richter, H., *Rohrhydraulik*, Springer, Berlin 1934
- ³ Fried, E., Idelchik, I., *Flow Resistance: a Design Guide for Engineers*, Hemisphere, 1989
- ⁴ Blevins, R.D., *Applied Fluid Dynamics Handbook*, reprint, Kireger Publ., 1992
- ⁵ Ziegler, F., *Mechanics of Solids and Fluids*, 2nd reprint of second edition, Springer, New York, Vienna, 1998
- ⁶ Balendra, T., Wang, C.M., Cheong, H.F., *Effectiveness of tuned liquid column dampers for vibration control of towers*, Engineering Structures, vol.17(9), pp.668-675, 1995
- ⁷ Chang, C.C., Hsu, C.T., *Control performance of liquid column vibration absorbers*, Engineering Structures, vol.20(7), pp.580-586, 1998
- ⁸ Gao, H., Kwok, K.C.S., Samali, B., *Optimization of tuned liquid column dampers*, Engineering Structures, vol.19(6), pp.476-486, 1997

⁹ Hitchcock, P.A., Kwok, K.C.S., Watkins, R.D., Samali, B., *Characteristics of liquid column vibration (LCVA)-I, Engineering Structures*, vol.19(2), pp.126-134, 1997

¹⁰ Rammerstorfer, F.G., Scharf, K., Fischer, F.D., *Storage tanks under earthquake loading*, Applied Mechanics Reviews, vol.43(11), pp.261-282, 1990

¹¹ Hitchcock, P.A., Glanville, M.J., Kwok, K.C.S., Watkins, R.D., Samali, B., *Damping properties and wind-induced response of a steel frame tower fitted with liquid column vibration absorbers*, Journal of wind engineering and industrial aerodynamics, 83, pp.183-196, 1999

5. Optimal design of TLCDs attached to host structures

Having found a suitable mathematical description of tuned liquid column dampers of various shapes, see Chapter 4, ideal design parameter must be determined to achieve a desired level of vibration absorption. This is normally achieved by minimising the dynamic response with respect to a carefully selected excitation signal, and therefore the coupled TLCD-main structure equations of motion must be solved in the time or frequency domain. Theoretically, all design strategies developed for dynamic vibration absorbers, see Section 2.5, can be applied to TLCD, especially the methods from TMD optimisation see Section 2.6. However, due to the TLCD geometry factors κ and $\bar{\kappa}$, Eqs.(4-9) and (4-33), analytical approaches become rather difficult and tedious. Instead of deriving optimal tuning parameter, this chapter presents an analogy between TMD and generally shaped TLCD, allowing to utilise both, analytical and numerical results available from TMD design.

5.1. Analogy between TMD and TLCD for SDOF host structure

Comparing the equations of motion of TMD and TLCD, it becomes apparent that there is a close relationship between both dynamic absorber types. A strong indication is the fact that the TMD behaviour can be derived from the corresponding TLCD by setting $\kappa = \bar{\kappa} = 1$, in Eq.(4-11) and Eq.(4-43). Even though the TLCD is the more involved absorber, it is possible to find a TMD-TLCD analogy. The first step is to define the equations of motion for a coupled system consisting of a SDOF host structure and a TLCD under the wind load, $f(t)$, and the ground excitation \ddot{w}_g , which are given by Eq.(1-2), (4-11) and (4-43),

$$\ddot{w} + 2\zeta_s \Omega_s \dot{w} + \Omega_s^2 w = -\ddot{w}_g + \frac{1}{M} f(t) + \frac{1}{M} f_x, \quad (5-1)$$

$$\ddot{u} + 2\zeta_A \Omega_A \dot{u} + \Omega_A^2 u = -\kappa (\ddot{w} + \ddot{w}_g),$$

$$f_x = -m_f (\ddot{w} + \ddot{w}_g + \bar{\kappa} \ddot{u}).$$

Inserting the coupling force f_x , Eq.(4-31), into Eq.(5-1) renders the coupled equations of motion, in matrix notation,

$$\begin{pmatrix} 1+\mu & \mu \bar{\kappa} \\ \kappa & 1 \end{pmatrix} \begin{pmatrix} \ddot{w} \\ \ddot{u} \end{pmatrix} + \begin{pmatrix} 2\zeta_s \Omega_s & 0 \\ 0 & 2\zeta_A \omega_A \end{pmatrix} \begin{pmatrix} \dot{w} \\ \dot{u} \end{pmatrix} + \begin{pmatrix} \Omega_s^2 & 0 \\ 0 & \omega_A^2 \end{pmatrix} \begin{pmatrix} w \\ u \end{pmatrix} = - \begin{pmatrix} 1+\mu \\ \kappa \end{pmatrix} \ddot{w}_g + \begin{pmatrix} 1/M \\ 0 \end{pmatrix} f, \quad (5-2)$$

where the absorber-structure mass ratio is determined by

$$\mu = m_f / M, \quad (5-3)$$

Introduction of the newly scaled displacement coordinate $u^* = u/\kappa$ of the free liquid surface, allows us to rewrite Eq.(5-2) in terms of u^* .

$$\begin{pmatrix} 1+\mu & \mu \bar{\kappa} \kappa \\ \kappa & \kappa \end{pmatrix} \begin{pmatrix} \ddot{w} \\ \ddot{u}^* \end{pmatrix} + \begin{pmatrix} 2\zeta_s \Omega_s & 0 \\ 0 & 2\kappa \zeta_A \omega_A \end{pmatrix} \begin{pmatrix} \dot{w} \\ \dot{u}^* \end{pmatrix} + \begin{pmatrix} \Omega_s^2 & 0 \\ 0 & \kappa \omega_A^2 \end{pmatrix} \begin{pmatrix} w \\ u^* \end{pmatrix} = - \begin{pmatrix} 1+\mu \\ \kappa \end{pmatrix} \ddot{w}_g + \begin{pmatrix} 1/M \\ 0 \end{pmatrix} f \quad (5-4)$$

Multiplication of Eq.(5-4) with $\text{diag} (1/(1+\mu(1-\kappa\bar{\kappa})), 1/\kappa)$ yields

$$\begin{pmatrix} 1+\mu^* & \mu^* \\ 1 & 1 \end{pmatrix} \begin{pmatrix} \ddot{w} \\ \ddot{u}^* \end{pmatrix} + \begin{pmatrix} 2\zeta_s^* \Omega_s^* & 0 \\ 0 & 2\zeta_A^* \omega_A^* \end{pmatrix} \begin{pmatrix} \dot{w} \\ \dot{u}^* \end{pmatrix} + \begin{pmatrix} \Omega_s^{*2} & 0 \\ 0 & \omega_A^* \end{pmatrix} \begin{pmatrix} w \\ u^* \end{pmatrix} = - \begin{pmatrix} 1+\mu^* \\ 1 \end{pmatrix} \ddot{w}_g + \begin{pmatrix} 1/M^* \\ 0 \end{pmatrix} f \quad (5-5)$$

where

$$\begin{aligned} \mu^* &= \frac{m^*}{M^*} = \frac{\kappa \bar{\kappa} \mu}{1 + \mu(1 - \kappa \bar{\kappa})}, & \Omega_s^* &= \Omega_s \frac{1}{\sqrt{1 + \mu(1 - \kappa \bar{\kappa})}}, \\ \zeta_s^* &= \zeta_s \frac{1}{\sqrt{1 + \mu(1 - \kappa \bar{\kappa})}}, & \omega_A^* &= \omega_A, \\ \zeta_A^* &= \zeta_A, & M^* &= M(1 + \mu(1 - \kappa \bar{\kappa})), \\ m^* &= m_f \kappa \bar{\kappa}. \end{aligned} \quad (5-6)$$

μ^* , ζ_s^* , Ω_s^* , ζ_A^* , ω_A^* , M^* , m^* denote the equivalent mass ratio, the structural damping ratio, the structure's fundamental frequency, the absorber damping ratio, the absorber's natural

frequency, the host structure's mass (including the dead weight of TLCD, $m_f (1 - \kappa \bar{\kappa})$) and the active mass of the TMD of the conjugate system (indicated by the superscript *), respectively. Since the geometry factors κ , $\bar{\kappa}$ have been eliminated, Eqs.(5-5) are identical to those of a simple TMD attached to a SDOF host structure, see Eqs.(2-7) and (2-8). Hence, it is possible to find the optimal absorber tuning δ^* and damping ratio ζ_A^* of the conjugate TMD problem from the literature, and transform the results back to obtain the desired TLCD design parameter. The TLCD frequency ratio is thus related as

$$\delta^* = \frac{\omega_A^*}{\Omega_S^*} = \frac{\omega_A}{\Omega_S} \sqrt{1 + \mu (1 - \kappa \bar{\kappa})} = \delta \sqrt{1 + \mu (1 - \kappa \bar{\kappa})}, \quad (5-7)$$

and explicitly given by

$$\delta = \frac{\delta^*}{\sqrt{1 + \mu (1 - \kappa \bar{\kappa})}}. \quad (5-8)$$

The optimal damping remains unaffected,

$$\zeta_A = \zeta_A^*. \quad (5-9)$$

In Eqs.(5-7) and (5-9) δ^* and ζ_A^* denote the design parameter for the analogue TMD problem. It is important to emphasise that the proposed transformation is also applicable to solutions for TMD systems with a damped or even nonlinear main structure, which allows a straightforward design of TLCDs even for complex problems whenever a solution exists for the classical TMD. The interpretation of the proposed transformation is certainly important, and becomes much clearer when inspecting the definition of the mass ratio of the conjugate system μ^* , see Eq. (5-6),

$$\mu^* = \frac{m^*}{M^*} = \frac{\kappa \bar{\kappa} \mu}{1 + \mu (1 - \kappa \bar{\kappa})} = \frac{m_f}{M} \cdot \frac{\kappa \bar{\kappa}}{1 + \mu (1 - \kappa \bar{\kappa})}. \quad (5-10)$$

As μ^* is always smaller than $\mu = m_f / M$, every TLCD setup behaves like a TMD system with m^* acting as active mass. The remaining fluid mass $m_f - m^*$ provides the restoring forces and must be regarded as dead weight loading of the main structure, see Figure 5-1.

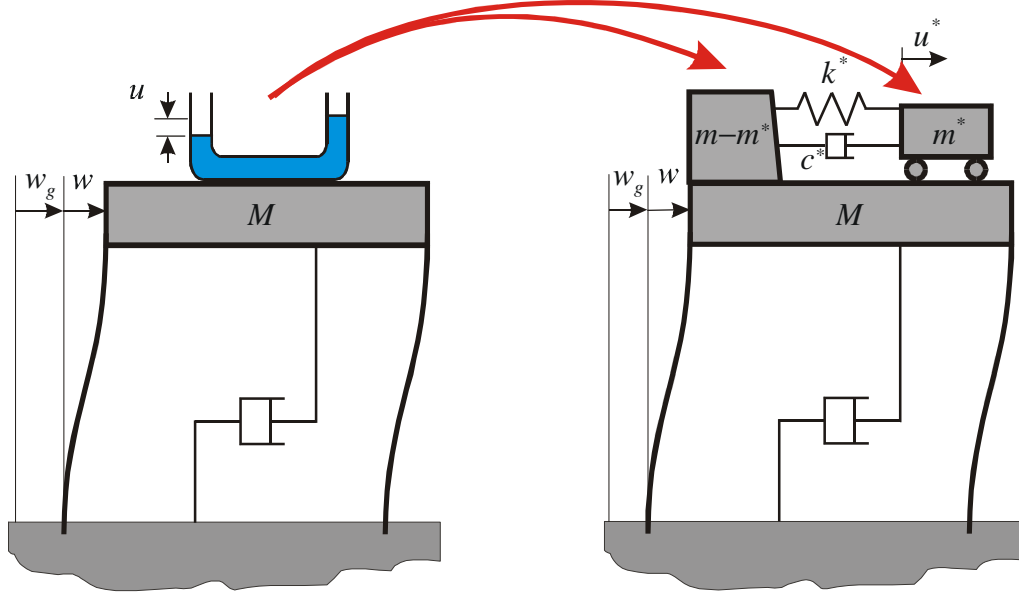


Figure 5-1: Frequency response of optimally designed TLCD, interpretation in terms of a conjugate TMD

This transformation of the original SDOF-TLCD into the conjugate TMD allows simple physical interpretations, because the only difference between the conjugate TMD system and a real physical TMD is the difference in the vibration amplitude u^* . Due to the transformation $u^* = u/\kappa$ the actual amplitude differs from the conjugate TMD, which must be taken into account during any optimisation which includes both, structural and absorber response quantities. Figure 5-1 clearly indicates that the active mass m^* must be maximised for best vibration attenuation. From this interpretation it is obvious that one has to maximise the amount of water moving horizontally and thus to choose β as small as possible.

5.4.1. Application of TMD-TLCD analogy to SDOF host structure with TLCD attached

The effectiveness of the proposed transformation is given by the determination of the optimal TLCD absorber parameter for a force excited SDOF structural model. The optimisation criterion is a minimisation of the maximal interstory drift. In case of an undamped host structure equipped with a single TMD this problem has been solved analytically, and simple expressions for the optimal TMD design parameters have been published, (see Table2-1, and the references given there),

$$\delta_{opt}^* = \frac{1}{1 + \mu^*}, \quad (5-11)$$

$$\zeta_{opt}^* = \sqrt{\frac{3\mu^*}{8(1+\mu^*)}}.$$

Substituting the conjugate mass ratio, $\mu^* = \frac{\kappa \bar{\kappa} \mu}{1 + \mu(1 - \kappa \bar{\kappa})}$, into Eq.(5-8) and (5-9), the optimal TLCD parameter are obtained explicitly

$$\delta_{opt} = \frac{\delta_{opt}^*}{\sqrt{1 + \mu - \kappa \bar{\kappa} \mu}} = \frac{\sqrt{1 + \mu(1 - \kappa \bar{\kappa})}}{1 + \mu}, \quad (5-12)$$

$$\zeta_{opt} = \zeta_{opt}^* = \sqrt{\frac{3\kappa \bar{\kappa} \mu}{8(1 + \mu)}} \quad (5-13)$$

The correctness of the solution can be checked by plotting the amplification response curves as shown in Figure 5-2. For comparison's sake several other response curves with the same optimal frequency tuning and various other damping ratios are given. From visual inspection it is apparent that Eq.(5-12) renders the desired optimal result.

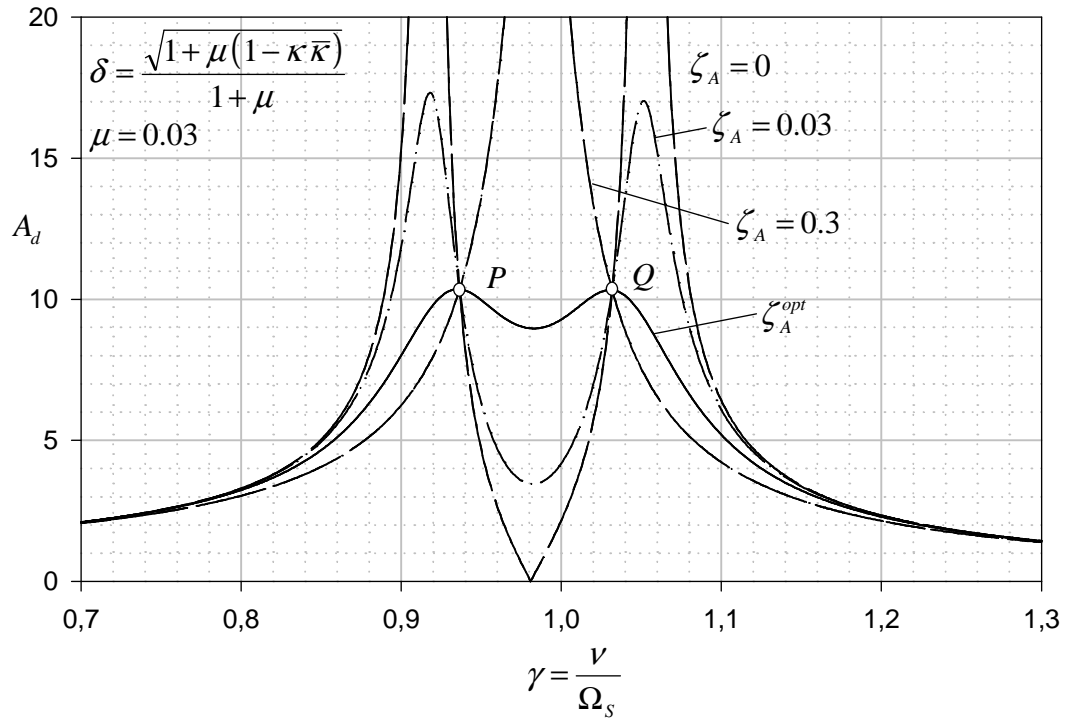


Figure 5-2: Frequency response curve of base excited SDOF-TLCD system ($\mu = 0.03$, $\zeta_s = 0$, $\kappa = 0.9$, $\bar{\kappa} = 0.7$). Conjugate TMD considered.

Arriving at Eq.(5-12) using DenHartog's approach, see DenHartog¹, is a rather tedious and lengthy operation, and almost impossible without computer algebra programs, even for this simple problem. The transformation, in the contrary, is straightforward, and opens the entire literature on TMDs to TLCDs. Thus a huge amount of knowledge and a large variety of solutions is available for TLCD design. A schematic overview of how to find the optimal TLCD parameter is given in Figure 5-3.

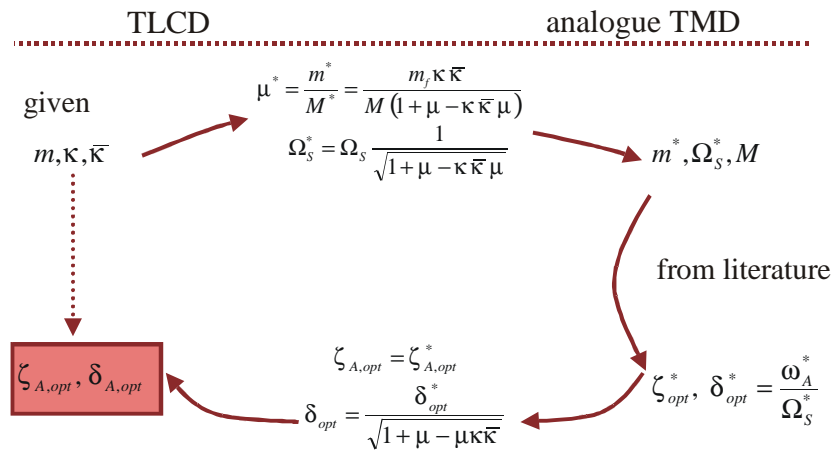


Figure 5-3: Schematic overview of the transformations to find optimal TLCD parameter

From the example given, it can be seen that the proposed transformation is a very simple and powerful method for quick and efficient TLCD design. However, the vibration reduction largely depends on the chosen TMD design parameter. The choice of minimising the relative structural displacement is just one simple performance measure amongst several others, e.g.:

- Minimum shear force in main structural members or minimum base shear
- Minimum acceleration/velocity of main structure
- Mixed criteria, involving both, the main structure and the absorber motion
- Maximum effective damping of combined structure

It becomes clear that some of those criteria overlap and it might be necessary to evaluate several possible combinations of design parameter for a given problem. For a given loading, numerical simulations will help to find the best absorber tuning, but it has turned out that most

optimisation strategies arrive at similar TLCD parameter, consequently the minimisation of base shear, will e.g. also result in small floor displacements and accelerations.

5.2. Control of MDOF host structures by TLCD

The analytical optimisations presented in Section 5.1 has been based on a single degree of freedom structural model. Real structures, however, are commonly modelled as multiple degree of freedom systems and the aim of this section is to give approximate analytical TLCD design guidelines for systems where the dynamic behaviour is dominated by a few well separated natural frequencies and the corresponding mode shapes should be controlled by the application of TLCDs. The TLCD can be placed anywhere in the building. Nevertheless, a strong position dependence of the TLCD effectiveness in vibration reduction will be found. If a single TLCD is installed in an N -DOF shear frame building the structural motion, solely containing absolute floor displacements, can be given by, see Eq.(1-35)

$$\mathbf{M} \ddot{\mathbf{w}} + \mathbf{C} \dot{\mathbf{w}} + \mathbf{K} \mathbf{w} = -\mathbf{M} \mathbf{r}_s \ddot{w}_g + \mathbf{f} + \mathbf{s} f_x \quad (5-14)$$

$$\ddot{u} + 2\zeta_A \omega_A \dot{u} + \omega_A^2 u = -\kappa (\ddot{w}_g + \mathbf{s}^T \ddot{\mathbf{w}}) \quad (5-15)$$

$$f_x = -m_f (\ddot{w}_g + \mathbf{s}^T \ddot{\mathbf{w}} + \bar{\kappa} \ddot{u}), \mathbf{s} = [0, \dots, \underset{i}{1}, \dots, 0]^T \quad (5-16)$$

where f_x denotes the TLCD-structure interaction force, see Eqs.(4-31), and the position vector \mathbf{s} defines the floor level where the TLCD is installed. All elements of \mathbf{s} vanish except a single unit entry in the i -th element, if the TLCD is installed on the i -th floor. Assuming that a minimisation of the modal displacements will also reduce the actual floor displacements substantially, a decomposition into the main structures' mode shapes is performed. If the floor displacements \mathbf{w} are replaced by the modal displacements $\mathbf{w} = \Phi \mathbf{q}$, where Φ denotes the main structure modal matrix $\Phi = [\phi_1, \dots, \phi_N]$, then Eq.(5-14) decouples on the left hand side for all classically damped systems by pre-multiplication with the transposed Φ^T ,

$$\Phi^T \mathbf{M} \Phi \ddot{\mathbf{q}} + \Phi^T \mathbf{C} \Phi \dot{\mathbf{q}} + \Phi^T \mathbf{K} \Phi \mathbf{q} = -\Phi^T \mathbf{M} \mathbf{r}_s \ddot{w}_g + \Phi^T \mathbf{f} + \Phi^T \mathbf{s} f_x \quad (5-17)$$

$$\ddot{u} + 2\zeta_A \omega_A \dot{u} + \omega_A^2 u = -\kappa (\ddot{w}_g + \mathbf{s}^T \Phi \ddot{\mathbf{q}}) \quad (5-18)$$

$$f_x = -m_f (\ddot{w}_g + \mathbf{s}^T \Phi \ddot{\mathbf{q}} + \bar{\kappa} \ddot{u}) \quad (5-19)$$

As only one TLCD is applied, the TLCD design must be focused on the vibration reduction of one resonance frequency ω_j . Warburton² has shown that it is possible to approximate the floor displacements in the vicinity of the j -th natural frequency Ω_s by $\mathbf{w} = \boldsymbol{\varphi}_j q_j$ if the natural frequencies are well separated, e.g. the ratio of two adjacent natural frequencies is larger than 2. Applying this estimate, the right hand side of Eq.(5-17) decouples, and two linear differential equations are obtained to minimise the modal displacement q_j , see Hochrainer et al.³.

$$\begin{pmatrix} 1+\mu & \mu \bar{\kappa}/\varphi_{ji} \\ \varphi_{ji} \kappa & 1 \end{pmatrix} \begin{pmatrix} \ddot{q}_j \\ \ddot{u} \end{pmatrix} + \begin{pmatrix} 2\zeta_s \Omega_s & 0 \\ 0 & 2\zeta_A \omega_A \end{pmatrix} \begin{pmatrix} \dot{q}_j \\ \dot{u} \end{pmatrix} + \begin{pmatrix} \Omega_s^2 & 0 \\ 0 & \omega_A^2 \end{pmatrix} \begin{pmatrix} q_j \\ u \end{pmatrix} = - \begin{pmatrix} \xi_j \\ \kappa \end{pmatrix} \ddot{w}_g + \begin{pmatrix} f_j \\ 0 \end{pmatrix} \quad (5-20)$$

$$\begin{aligned} \xi_j &= \frac{\boldsymbol{\varphi}_j^T \mathbf{M} \mathbf{r}_s + \varphi_{ji} m_f}{\boldsymbol{\varphi}_j^T \mathbf{M} \boldsymbol{\varphi}_j}, & \mu &= \frac{\varphi_{ji}^2 m_f}{\boldsymbol{\varphi}_j^T \mathbf{M} \boldsymbol{\varphi}_j}, & f_j &= \frac{\boldsymbol{\varphi}_j^T \mathbf{f}}{\boldsymbol{\varphi}_j^T \mathbf{M} \boldsymbol{\varphi}_j}, & \Omega_s^2 &= \frac{\boldsymbol{\varphi}_j^T \mathbf{K} \boldsymbol{\varphi}_j}{\boldsymbol{\varphi}_j^T \mathbf{M} \boldsymbol{\varphi}_j}, \\ 2\zeta_s \Omega_s &= \frac{\boldsymbol{\varphi}_j^T \mathbf{C} \boldsymbol{\varphi}_j}{\boldsymbol{\varphi}_j^T \mathbf{M} \boldsymbol{\varphi}_j}. \end{aligned} \quad (5-21)$$

Above φ_{ji} is the i -th component of the j -th mode (at the story where the TLCD is attached). Again, introducing the new liquid displacement coordinate $u^* = u/\kappa\varphi_{ji}$ and multiplying Eq.(5-21) with $\text{diag}\left(1/(1+\mu(1-\kappa\bar{\kappa})), 1/\kappa\varphi_{ji}\right)$ yields

$$\begin{pmatrix} 1+\mu^* & \mu^* \\ 1 & 1 \end{pmatrix} \begin{pmatrix} \ddot{q}_j \\ \ddot{u}^* \end{pmatrix} + \begin{pmatrix} 2\zeta_s^* \Omega_s^* & 0 \\ 0 & 2\zeta_A^* \omega_A^* \end{pmatrix} \begin{pmatrix} \dot{q}_j \\ \dot{u}^* \end{pmatrix} + \begin{pmatrix} \Omega_s^{*2} & 0 \\ 0 & \omega_A^{*2} \end{pmatrix} \begin{pmatrix} q_j \\ u^* \end{pmatrix} = - \begin{pmatrix} \xi_j^* \\ 1/\varphi_{ji} \end{pmatrix} \ddot{w}_g + \begin{pmatrix} f_j^* \\ 0 \end{pmatrix} \quad (5-22)$$

$$\mu^* = \frac{\kappa \bar{\kappa} \mu}{1 + \mu(1 - \kappa \bar{\kappa})}, \quad \Omega_s^* = \Omega_s \frac{1}{\sqrt{1 + \mu(1 - \kappa \bar{\kappa})}}, \quad f_j^* = \frac{\boldsymbol{\varphi}_j^T \mathbf{f}}{M^*} \quad (5-23)$$

$$\zeta_s^* = \zeta_s \frac{1}{\sqrt{1 + \mu(1 - \kappa \bar{\kappa})}}, \quad \omega_A^* = \omega_A, \quad \xi_j^* = \frac{\boldsymbol{\varphi}_j^T \mathbf{M} \mathbf{r}_s + \varphi_{ji} m_f}{M^*} \quad (5-24)$$

$$\zeta_A^* = \zeta_A, \quad M^* = \boldsymbol{\varphi}_j^T \mathbf{M} \boldsymbol{\varphi}_j (1 + \mu - \kappa \bar{\kappa} \mu), \quad (5-25)$$

where μ^* , ζ^* , Ω_s^* , ζ_A^* , ω_A^* , M^* denote the equivalent modally transformed quantities: mass ratio, the structural damping ratio, the structure's fundamental frequency, the absorber damping ratio, the absorber's natural frequency and the conjugate mass, respectively. Note

again, that κ , $\bar{\kappa}$ have been eliminated, and thus Eq.(5-22) describes the dynamics of a structural system with an equivalent TMD installed. Under wind type loading, $\ddot{w}_g = 0$, the effectiveness of an equivalent TMD is exactly the same as in the SDOF system discussed before, thus the optimal solution for SDOF systems can be applied. In case of ground excitation, however, the participation factor ξ_j is different from that in the SDOF case where $\xi_j = 1$, and the SDOF solution cannot be transformed to obtain exact optimal solutions for multiple degree of freedom systems, see e.g. Soong and Dargush⁴. Nevertheless the transformation to an equivalent TMD system is always possible, and having designed the equivalent TMD, the optimal absorber tuning ratio δ^* and the damping ratio ζ_A^* are given by

$$\delta = \delta^* / \sqrt{1 + \mu(1 - \kappa\bar{\kappa})}, \quad (5-26)$$

and the unaffected damping ratio

$$\zeta_A = \zeta_A^*. \quad (5-27)$$

When working with multiple story structures, the floor level at which the absorber is installed must be chosen carefully, since it highly influences the TLCD performance. This relationship is not apparent from Eq.(5-22) because it is hidden in the definition of the modal mass ratio,

given by $\mu = \frac{\boldsymbol{\phi}_{ji}^T \mathbf{m} \boldsymbol{\phi}_{ji}}{\boldsymbol{\phi}_j^T \mathbf{M} \boldsymbol{\phi}_j}$. A large mass ratio is always required for a good TLCD performance

and thus, the floor level must be chosen to maximise $\boldsymbol{\phi}_{ji}$. For a uniform 5-story shear frame building, with constant mass distribution, all mode shape vectors $\boldsymbol{\phi}_j$ contained in the modal matrix $\boldsymbol{\Phi}$ and the corresponding floor displacements $\boldsymbol{\phi}_{ji}$ are illustrated in Figure 5-4. It is quite apparent, that the optimal position of the TLCD varies with each vibration mode. Thus, the position of the TLCD has to be selected carefully for each vibration problem, but as a general rule of thumb it can be noted that the top floor is suitable for low frequencies.

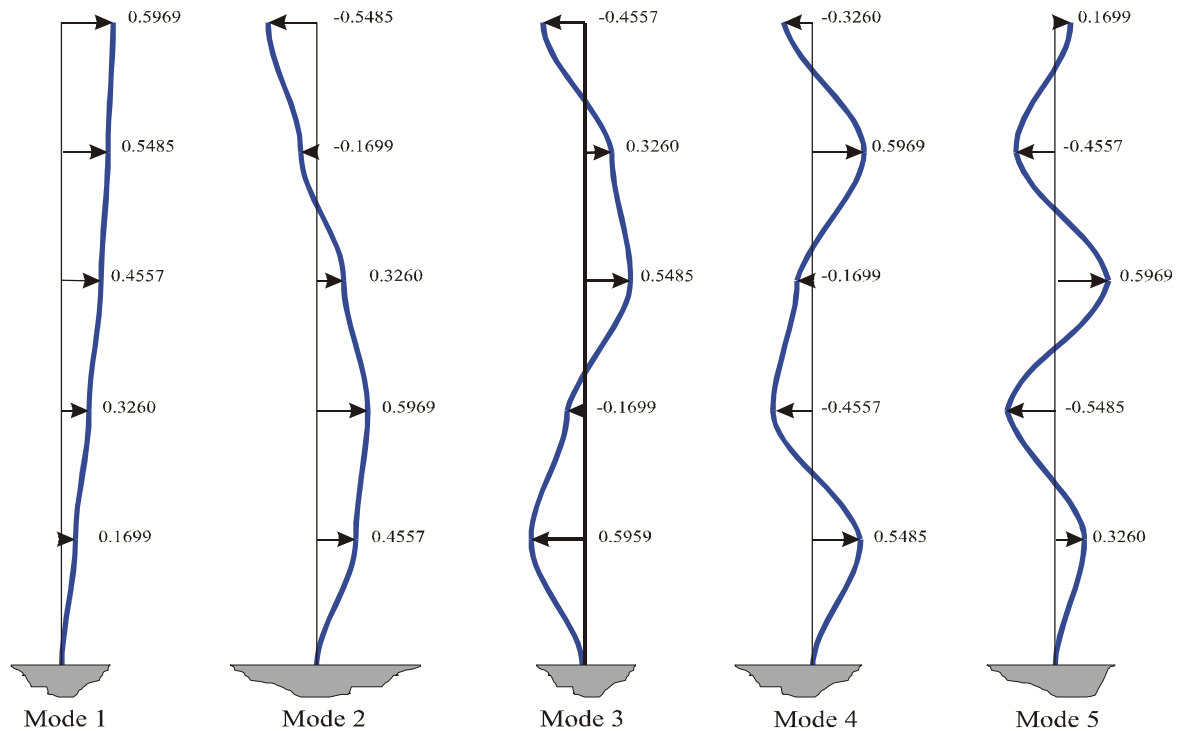


Figure 5-4: Modal displacements of a uniform 5-story building, see Chopra⁵

Ideally, the TLCD should be placed in the floor with the largest modal displacement, because this will maximise the modal mass ratio and thus yield the best absorbing behaviour. When properly positioned it is possible to obtain a modal mass ratio which is significantly higher than the actual absorber to building mass ratio, as shown in Table 5-1: For a total mass ratio of 1% the maximum modal mass ratios for different buildings are summarised. Table 5-1 includes the already mentioned 5 story structure, as well as a 20 and a 76 story benchmark building, for details see Spencer⁶.

Building type:	opt. floor level	mass ratio mode 1	opt. floor level	mass ratio mode 2	opt. floor level	mass ratio mode 3	opt. floor level	mass ratio mode 4	opt. floor level	mass ratio mode 5
5 story	5	0.0178	2	0.0178	1	0.0178	4	0.0178	3	0.0178
20 story	20	0.0498	20	0.0592	20	0.0656	20	0.0590	20	0.0494
76 story	76	0.0403	76	0.0554	76	0.0554	76	0.0507	76	0.0455

Table 5-1: Optimal modal mass ratios for a total mass ratio $\mu = 0.01$

Building type:	floor level	mass ratio mode 1	floor level	mass ratio mode 2	floor level	mass ratio mode 3	floor level	mass ratio mode 4	floor level	mass ratio mode 5
20 story	20	0.0498	7	0.0354	4	0.0342	3	0.0339	2	0.0333
			20	0.0592	13	0.0367	10	0.0356	8	0.0326
					20	0.0656	16	0.0420	13	0.0372
							20	0.0590	17	0.0438
									20	0.0494

Table 5-2: Modal mass ratios for the 20 story building with a total mass ration

$$\mu = 0.01$$

Table 5-2 also shows sub-optimal positions where the TLCD can be installed, if an attachment on the top floor is not possible.

The modal mass ratios in Table 5-1 and Table 5-2 vary as they depend on the modal shapes of the structural system. For a structure approximated by an ideal cantilevered beam the modal mass ratio is four times the actual mass ratio, and in case of the 76-story structure this modal mass to actual mass ratio varies between 4.03 and 5.54, which certainly guarantees excellent steady state performance. Furthermore it is noteworthy, that for the higher modes the TLCD can be installed in lower floors without significantly decreasing the performance, which is important from a practical design point of view, because the TLCD can be distributed over the entire building without decreasing the optimal performance.

5.3. General remarks on TMD-TLCD analogy

In Section 5.1 and Section 5.2, the TMD-TLCD analogy has been applied to host structures, approximated by SDOF systems. If the assumption of a single degree of freedom does not apply it is still possible to apply the TMD-TLCD analogy, even for nonlinear structures, if the TLCD is transformed into the conjugate TMD, see Figure 5-1. Again, the active mass m^* of Eq.(5-6) describes the conjugate TMD mass, and the dead weight loading (liquid mass minus active mass) is added to the floor mass. The conjugate stiffness and damping are determined by

$$k^* = \omega_A^2 m^*, \quad (5-28)$$

$$c^* = 2 \zeta \omega_A m^*, \quad (5-29)$$

and the scaled liquid displacement u^* corresponds to the displacement of the conjugate mass. If the nonlinear turbulent damping term described by the head loss coefficient δ_L is considered, the conjugate damping δ_L^* is given by

$$\delta_L^* = \delta_L \kappa. \quad (5-30)$$

After those transformations any optimisation developed for TMD systems can be applied to the TLCD, independent of the degrees of freedom or the separation of the natural frequencies. Even nonlinear host structures can be investigated, if an optimal design or analysis tool for TMD is available.

5.4. References

- ¹ DenHartog, J.P., *Mechanical Vibrations*, reprint of 4th ed. McGrawHill, 1956
- ² Warburton, G.B., *Optimum Absorber Parameters for minimising vibration response*, Earthquake Engineering and Structural Dynamics, vol.9, pp.251-262, 1981
- ³ Hochrainer, M.J., Adam, C., *Dynamics of shear frames with tuned liquid column dampers*, ZAMM, vol.80 supplement 2, pp.S283-S284, 2000
- ⁴ Soong, T.T., Dargush, G.F., *Passive Energy Dissipation Systems in Structural Engineering*, Wiley, Chichester England, 1997
- ⁵ Chopra, A.K., *Dynamics of Structures*, Prentice Hall, New Jersey, 1995
- ⁶ Spencer, B.F. Jr., Christenson, R. Dyke, S.J., *Next Generation Benchmark Problem*, Proceedings of the Second World Conference on Structural Control, Kyoto, Japan, 1998, also www-publication: <http://www.nd.edu/~quake/>

6. Equations of motion of linear MDOF structures

6.1. Introduction

The reliability of all information gained from structural analysis is directly dependent on the quality of the mathematical model, and therefore it is indispensable to determine equations of motion whose dynamic behaviour is close to reality. As long as SDOF host structures are assumed an analytical absorber design is possible. However, simplified SDOF models often provide a fairly crude description of the real structural behaviour, and therefore more complex structural models have to be considered. Having determined a MDOF structural model, the calculation of the response under arbitrary loading can be accomplished by several different procedures. Nowadays, mainly time integration methods are used, which are provided in numerical simulation packages. Still, the most crucial step in dynamic analysis is the determination of a proper mathematical model, because the validity of the calculated results depends directly on how well the mathematical description can represent the physical system. Therefore some general aspects in modelling real structures are discussed, starting with the generation of the equations of motion and several aspects of model reduction.

6.2. General approach

Modelling the real structure with finite elements and solving for a given problem with an element mesh as fine as possible, will certainly render best results. However, several thousand degrees of freedom are necessary for reliable results, and the amount of response data often impedes deep insight into physical phenomena. A first step in model simplification is to treat structural members like columns or girders as single elements at the price of losing detailed information about the local stress and strain variations. This simplification is justifiable since in a dynamic analysis the nodal displacements, which control the inertial forces, are not sensitive to local field variations, like e.g., the stress distribution. For any linear multiple degree of freedom systems the equation of motion is cast in the form

$$\mathbf{M} \ddot{\mathbf{w}} + \mathbf{C} \dot{\mathbf{w}} + \mathbf{K} \mathbf{w} = -\mathbf{M} \mathbf{r}_s \ddot{w}_g + \mathbf{f}(t), \quad (6-1)$$

where \mathbf{M} , \mathbf{C} , \mathbf{K} , \ddot{w}_g , \mathbf{f} denote the mass, damping and stiffness matrix, as well as single point ground acceleration and the external force loading, respectively. \mathbf{r}_s is the static influence vector, which for an upright building becomes $\mathbf{r}_s = \mathbf{i}$, $\mathbf{i} = [1, 1, \dots, 1]^T$, by inspecting the rigid body motion of foundation and building.

6.3. General approach for framed structures

Any framed structure can be assembled by beams, columns and shear walls, interconnected at nodal points. Often structural members can be assumed massless, with an equivalent lumped mass placed at the corresponding nodes. Each node has generally six degrees of freedom, but based on mechanical assumptions, some of those might be neglected, as shown in Figure 6-1, where the axial deformation of the structural elements is ignored. To determine the stiffness matrix \mathbf{K} of Eq.(6-1), a generalised constant unit displacement is applied to every degree of freedom while keeping the other generalised displacements to zero. The forces required to maintain these displacements are in static equilibrium with the restoring forces of the deflected shape. For a unit displacement at DOF j the stiffness influence coefficient k_{ij} is equal to the force associated with DOF i . For a unit displacement of node 1 and a unit rotation at DOF 4 this “direct method” is illustrated in Figure 6-2.

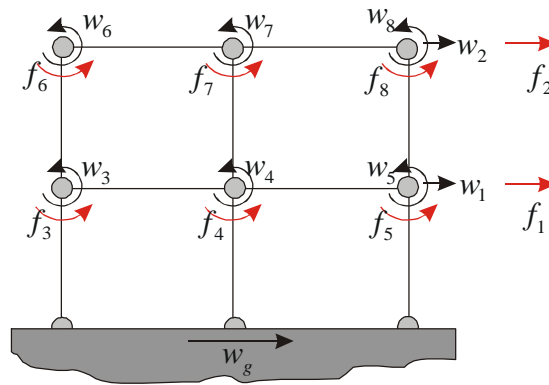


Figure 6-1: Typical plane frame structure without axial deformation of structural elements

For any given deflection \mathbf{u} the external node forces \mathbf{f}_s for static equilibrium can be directly derived from Eq.(6-1) as all time dependent terms vanish:

$$\mathbf{f}_s = \mathbf{K} \mathbf{w} \quad (6-2)$$

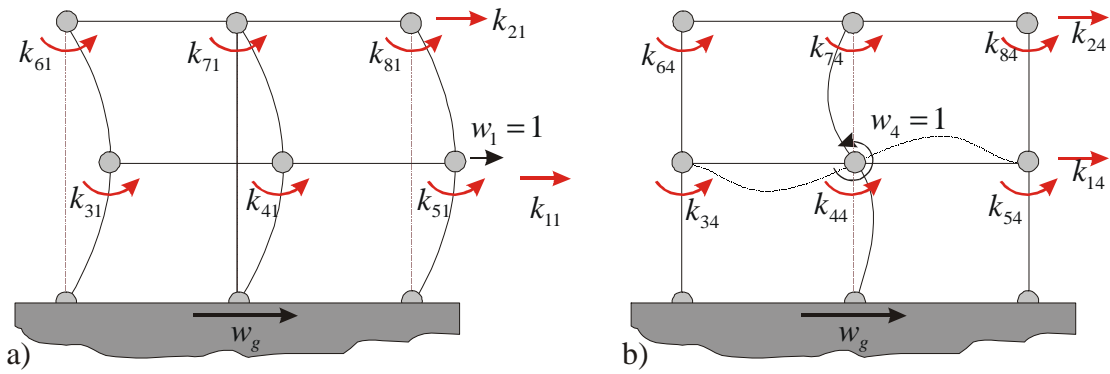


Figure 6-2: “Direct stiffness approach”; Stiffness influence coefficients for a unit displacement at
a) DOF 1 b) DOF 4

Exactly the same methodology can be applied to derive the mass matrix \mathbf{M} . Let a unit acceleration be applied at DOF j at the structure at rest, while all other DOF are kept zero. Then, according to Newton’s law, an external force \mathbf{f} is necessary for the dynamic system equilibrium. The mass influence coefficient m_{ij} is the external force in DOF i due to unit acceleration along DOF. For any given acceleration $\ddot{\mathbf{u}}$ the external node forces \mathbf{f}_D for dynamic equilibrium can be directly derived from Eq.(6-1) by regarding all acceleration terms,

$$\mathbf{f}_D = \mathbf{M} \ddot{\mathbf{w}}. \quad (6-3)$$

Commonly no inertia is assumed in rotational DOF, hence, \mathbf{M} has a special form, affecting only the actual displacements in $\ddot{\mathbf{w}}$.

Damping is responsible for energy dissipation in the structure and it is generally expressed by (equivalent) viscous damping, which relates the node velocities to the damping forces. If a unit velocity is applied along DOF j while all other DOF are kept zero. Due to the node velocity internal damping forces will be generated which oppose the motion. Therefore external forces are necessary to maintain the motion. The damping influence coefficients c_{ij} are equal to the external force in DOF i due to a unit velocity in DOF j . However, unless there are discrete damping devices (e.g. viscous dampers) installed in the structure it is hardly possible to find the damping coefficients c_{ij} because too little information is known about the

distributed damping process. Instead modal damping ratios, based on experience or experimental data are utilised.

Working with larger structural elements, instead of a detailed finite element mesh, reduces the degrees of freedom dramatically, resulting in a system of much smaller order, which of course, is beneficial, but at the price of loosing information about the resulting stress distribution. Nevertheless it can be recalculated by a static analysis using a more refined finite element mesh. Unfortunately tall buildings consist of several thousand structural elements, and further simplification might be necessary. It can be achieved by methods which are described in the following sections.

6.4. Kinematic constraints

The introduction of kinematic constraints, which express the displacements of many degrees of freedom in terms of a much smaller set of primary variables, is an uncomplicated method to decrease the number of degrees of freedom further. Typically, the displacements of a group of individual members, e.g. interstory columns, are constrained by the displacements of floors. One of the most widely used applications of this type is the modelling of multiple-story building frames¹.

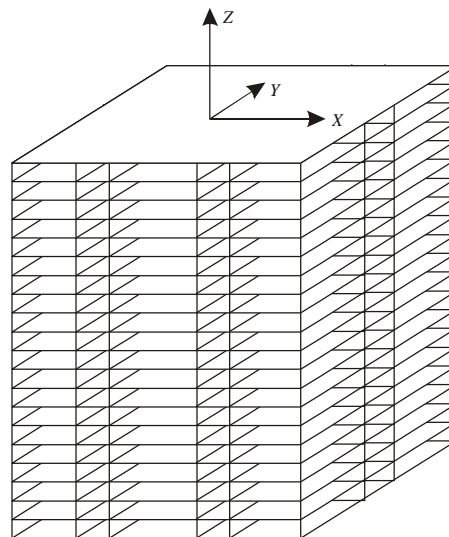


Figure 6-3: Twenty story building frame (2880 DOF)

Figure 6-3 shows a 20-story rectangular building frame with six frames (480 girders) parallel to the X-Z-plane and 4 frames (400 girders) parallel to the Y-Z-plane. The total model

contains 480 columns, thus a total of 1360 one-dimensional elements. The number of nodes interconnecting the elements is the same as the number of columns, yielding 2880 degrees of freedom when allowing for three rotations and three translations per joint.

Taking the constraining effect of the floor slabs into consideration reduces this number substantially, if each floor diaphragm is rigid in its own plane but flexible in the vertical direction. These kinematic constraints reduce the degrees of freedom of each joint from six to three. On top there is a rigid body motion in each floor yielding a total of $2880/2 + 3 \cdot 20 = 1500$ degrees of freedom. Further reduction cannot be accomplished by kinematic constraints, but e.g. the method of static condensation, can decrease the model size further to about 2% of the original model, see e.g. Clough-Penzien¹.

6.5. Static condensation

In contrast to the kinematic constraint idea the concept of static condensation is based on static equilibrium constraints, and for a successful application of this technique the degrees of freedom are divided into two types: those in which no mass or damping participates, denoted by \mathbf{w}_0 and those who can develop inertia or damping forces, called \mathbf{w}_M . Obviously this approach assumes concentrated lumped masses which are found for most elements by simple energy principles. Having recognised the different degrees of freedom, the equations of motion under the effective loading $\mathbf{f}_{eff} = [\mathbf{f}_0 \ \mathbf{f}_M]^T$ can be rearranged using “hypermatrices” as indicated

$$\begin{pmatrix} \mathbf{0} & \mathbf{0} \\ \mathbf{0} & \mathbf{M} \end{pmatrix} \begin{pmatrix} \ddot{\mathbf{w}}_0 \\ \ddot{\mathbf{w}}_M \end{pmatrix} + \begin{pmatrix} \mathbf{0} & \mathbf{0} \\ \mathbf{0} & \mathbf{C} \end{pmatrix} \begin{pmatrix} \dot{\mathbf{w}}_0 \\ \dot{\mathbf{w}}_M \end{pmatrix} + \begin{pmatrix} \mathbf{K}_{11} & \mathbf{K}_{12} \\ \mathbf{K}_{21} & \mathbf{K}_{22} \end{pmatrix} \begin{pmatrix} \mathbf{w}_0 \\ \mathbf{w}_M \end{pmatrix} = \begin{pmatrix} \mathbf{f}_0 \\ \mathbf{f}_M \end{pmatrix}. \quad (6-4)$$

Eq.(6-4) can be solved for $\mathbf{w}_0 = -\mathbf{K}_{11}^{-1}\mathbf{K}_{12}\mathbf{w}_M + \mathbf{K}_{11}^{-1}\mathbf{f}_0$ and back substitution yields the reduced order dynamic system

$$\mathbf{M} \ddot{\mathbf{w}}_M + \mathbf{C} \dot{\mathbf{w}}_M + (\mathbf{K}_{22} - \mathbf{K}_{21}\mathbf{K}_{11}^{-1}\mathbf{K}_{12}) \mathbf{w}_M = \mathbf{f}_M - \mathbf{K}_{21}\mathbf{K}_{11}^{-1}\mathbf{f}_0. \quad (6-5)$$

This static condensation procedure can be used to effectively reduce the degrees of freedom, such as the reduction from 1500 to 60 in the building frame discussed in the previous section, if all masses are lumped onto the floor level. The remaining 60 DOF correspond to the rigid body motion of each floor. Up to this point, there was no major simplification, and all

dynamic systems generated with one method described above yield, independent of their order, similar simulation results. Additional model reduction can only be achieved at the price of a certain change in system dynamics. If, however, dominant degrees of freedom can be located, further reduced models can be a good representation of the original system. Two methods capable of such a simplification are the modal truncation, and a generalised order reduction method appropriate to all linear, stable systems.

6.6. Modal truncation

A commonly used method in structural analysis is to perform dynamic investigations in the modal space, and consequently restrict the research to the dominating mode-shapes. Several well established methods have been developed for finding the mode vectors and solving the vibration eigenproblem, most prominent amongst those are the Rayleigh-Ritz method and the subspace iteration, see Clough-Penzien¹. Instead of taking all modal coordinates and the corresponding mode-shapes into account, only the major degrees of freedom are considered in the investigation.

The main difficulty, however, is to determine the set of coordinates which depicts the dynamic behaviour of the original system with sufficient precision, thus the key question is which modal coordinates must be maintained to avoid significant modal truncation errors. To evaluate the errors resulting from modal truncation, the dynamic response contributions of the individual modes are considered. For an arbitrary mode i the equation of motion is given by

$$\ddot{q}_i + 2\zeta_i\omega_i\dot{q}_i + \omega_i^2q_i = f_{i,eff}, \quad (6-6)$$

where the effective modal load factor is given by $f_{i,eff} = \boldsymbol{\phi}_i^T (-\mathbf{M}\mathbf{r}_s\ddot{w}_g + \mathbf{f}(t)) = \boldsymbol{\phi}_i^T \mathbf{f}_{eff}(t)$, and $\boldsymbol{\phi}_i$ denotes the i -th mode shape vector, normalised with respect to the modal mass, $\boldsymbol{\phi}_i^T \mathbf{M} \boldsymbol{\phi}_j = \delta_{ij}$, see Eq.(1-37). By inspection of Eq.(6-6) it can be concluded, that the relative importance of single mode contributions to the total dynamic response depends on

- The modal load factor which depends on the interaction between mode shape and external load.
- The spectrum of the applied external load.

- The dynamic magnification factor which depends on the ratio of the applied loading frequencies to the modal frequency.

Assuming a time variant but spatially constant load distribution $\mathbf{f}_{eff}(t) = \mathbf{r} f(t)$, a modal participation factor exists, and is defined by $\xi_i = \boldsymbol{\phi}_i^T \mathbf{r}$, for derivations see Chapter 1. For any ground motion of a single point excitation characterised by \ddot{w}_g , $\mathbf{r} = \mathbf{M} \mathbf{r}_s$ and for simple cases of high-rise framed structures with displacement degrees of freedom, \mathbf{r}_s becomes $\mathbf{r}_s = \mathbf{M} [1, \dots, 1]^T$. Figures 6-4 a-c show typical flexural mode shapes of a high rise building, and Figure 6-4d displays its mass distribution. Obviously the vector product $\boldsymbol{\phi}_i^T \mathbf{r}_s$ is relatively large for the fundamental mode and is rapidly decreasing for higher mode shapes. For this reason the participation factor of the first mode is dominant for ground excited structures. If the load is not distributed uniformly, see e.g. Figure 6-4e for a force loading with common time function, then the second mode has a large participation factor whereas the first and the third mode would contribute only little to the overall response.

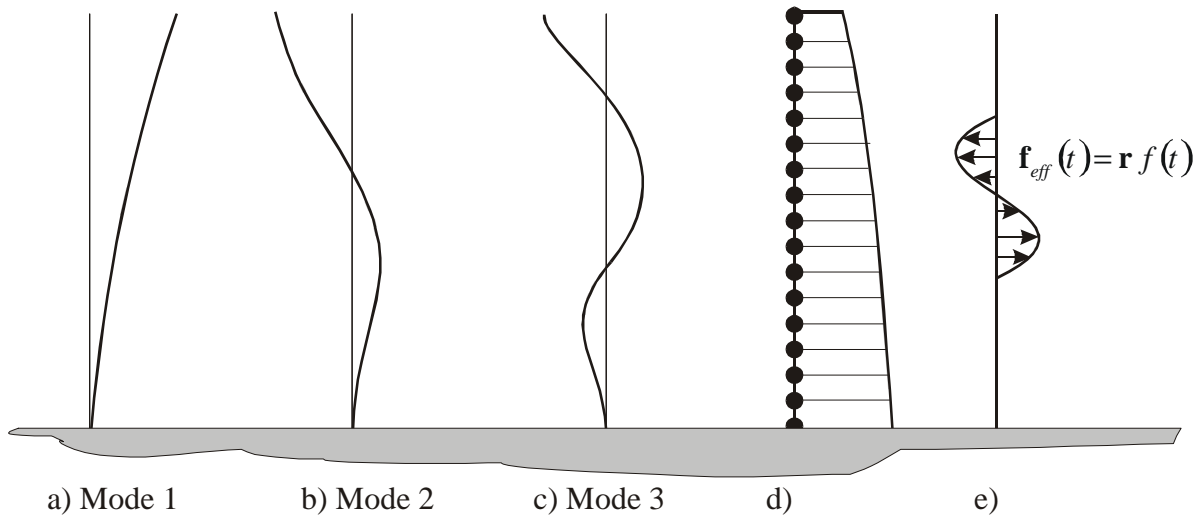


Figure 6-4: a)- c) vibration mode shapes d) mass distribution e) locally distributed force loading with common time function

For a sufficiently long loading time, the dynamic magnification factor largely depends on the excitation spectrum and the damping ratio of the modal equation. If the external loading contains a resonant frequency, the corresponding mode shape is expected to cause important contributions to the entire dynamic response.

Having identified the dominant modal coordinates, the modal truncation can be performed by discarding all other coordinates. Often it is desired to perform this simplification without losing the physical interpretation of the original displacement coordinates. Let n denote the order of the reduced system, then it is possible to describe the reduced order system with n arbitrary elements of the original generalised displacement vector \mathbf{w} . Firstly, the rows of the matrix equation are rearranged by pre-multiplying with a transformation matrix \mathbf{T} , such that the coordinates which are kept are contained in the “observable” vector \mathbf{w}_o , whereas all coordinates discarded form the vector \mathbf{w}_r . This rearrangement allows to give the equations of motion of the structure under effective force loading by

$$\mathbf{M}\ddot{\mathbf{w}} + \mathbf{C}\dot{\mathbf{w}} + \mathbf{K}\mathbf{w} = \mathbf{f}_{eff}, \quad (6-7)$$

$$\mathbf{M} = \mathbf{M}\mathbf{T}, \quad \mathbf{C} = \mathbf{C}\mathbf{T}, \quad \mathbf{K} = \mathbf{K}\mathbf{T},$$

$$\mathbf{w} = \begin{pmatrix} \mathbf{w}_r \\ \mathbf{w}_o \end{pmatrix}, \quad \mathbf{f}_{eff} = \begin{pmatrix} \mathbf{f}_{eff}^r \\ \mathbf{f}_{eff}^o \end{pmatrix}.$$

\mathbf{M} , \mathbf{C} , \mathbf{K} , \mathbf{w} , \mathbf{f}_{eff} denote the rearranged mass matrix, damping matrix, stiffness matrix, displacement vector and excitation load vector, respectively. In modal coordinates Eq.(6-7) can be rewritten as

$$\Phi^T \mathbf{M} \Phi \ddot{\mathbf{q}} + \Phi^T \mathbf{C} \Phi \dot{\mathbf{q}} + \Phi^T \mathbf{K} \Phi \mathbf{q} = \Phi^T \mathbf{f}_{eff} \quad (6-8)$$

where

$$\Phi^T \mathbf{M} \Phi = \begin{pmatrix} \mathbf{M}_{rr} & \mathbf{0} \\ \mathbf{0} & \mathbf{M}_{oo} \end{pmatrix}, \quad \Phi^T \mathbf{C} \Phi = \begin{pmatrix} \mathbf{C}_{rr} & \mathbf{0} \\ \mathbf{0} & \mathbf{C}_{oo} \end{pmatrix}, \quad \Phi^T \mathbf{K} \Phi = \begin{pmatrix} \mathbf{K}_{rr} & \mathbf{0} \\ \mathbf{0} & \mathbf{K}_{oo} \end{pmatrix}, \quad (6-9)$$

$$\Phi = \begin{pmatrix} \Phi_{rr} & \Phi_{ro} \\ \Phi_{or} & \Phi_{oo} \end{pmatrix}, \quad \mathbf{q} = \begin{pmatrix} \mathbf{q}_r \\ \mathbf{q}_o \end{pmatrix} \quad (6-10)$$

$$\mathbf{w} = \begin{pmatrix} \mathbf{w}_r \\ \mathbf{w}_o \end{pmatrix} = \begin{pmatrix} \Phi_{rr} & \Phi_{ro} \\ \Phi_{or} & \Phi_{oo} \end{pmatrix} \begin{pmatrix} \mathbf{q}_r \\ \mathbf{q}_o \end{pmatrix}. \quad (6-11)$$

\mathbf{M}_{oo} , \mathbf{C}_{oo} , \mathbf{K}_{oo} , \mathbf{M}_{rr} , \mathbf{C}_{rr} , \mathbf{K}_{rr} denote the dominant modal mass, the dominant damping, the dominant stiffness, the residual mass, the residual damping and the residual stiffness matrices,

respectively. All matrices are separated according to the dominant and residual modal coordinates. The modal matrix $\underline{\Phi}$ consists of the dominant (observable) mode-shape vectors $\underline{\phi}_i^o$ and the residual mode-shape vectors $\underline{\phi}_i^r$:

$$\underline{\Phi} = [\underline{\phi}_1^r, \dots, \underline{\phi}_n^r, \underline{\phi}_1^o, \dots, \underline{\phi}_{N-n}^o]. \quad (6-12)$$

Through modal truncation the residual modes are neglected, $\mathbf{q}_r = \mathbf{0}$, and Eq.(6-8) simplifies to

$$\underline{\mathbf{M}}_{oo} \ddot{\mathbf{q}}_o + \underline{\mathbf{C}}_{oo} \dot{\mathbf{q}}_o + \underline{\mathbf{K}}_{oo} \mathbf{q}_o = \underline{\Phi}_{oo}^T \mathbf{f}_{eff}^o + \underline{\Phi}_{ro}^T \mathbf{f}_{eff}^r. \quad (6-13)$$

From Eq.(6-11) the relation between the modal coordinates and the displacement vector is given by $\mathbf{w}_o = \underline{\Phi}_{oo} \mathbf{q}_o$. Unless \mathbf{w}_o contains only nodal points of a certain mode shape, the inverse of $\underline{\Phi}_{oo}$ exists, and Eq.(6-13) can be transformed to

$$\underline{\mathbf{M}}_{oo} \underline{\Phi}_{oo}^{-1} \ddot{\mathbf{w}}_o + \underline{\mathbf{C}}_{oo} \underline{\Phi}_{oo}^{-1} \dot{\mathbf{w}}_o + \underline{\mathbf{K}}_{oo} \underline{\Phi}_{oo}^{-1} \mathbf{w}_o = \underline{\Phi}_{oo}^T \mathbf{f}_{eff}^o + \underline{\Phi}_{ro}^T \mathbf{f}_{eff}^r. \quad (6-14)$$

Eq.(6-14) is very convenient because it still consists of a mass, damping and stiffness matrix, and has the structure of a linear equation of motion, thus it can be handled with all tools available for linear systems without any modifications. However, as a result of the order reduction, the stiffness matrix might not be symmetric any more, thus $\underline{\mathbf{K}} \neq \underline{\mathbf{K}}^T$. If one is interested in the discarded states \mathbf{w}_r Eq.(6-11) has to be considered again and renders

$$\mathbf{w}_r = \underline{\Phi}_{ro} \mathbf{q}_o = \underline{\Phi}_{ro} \underline{\Phi}_{oo}^{-1} \mathbf{w}_o. \quad (6-15)$$

The method of strict truncation can be improved by a residualisation, where only dynamics of the residual modes is neglected ($\dot{\mathbf{q}}_r = \mathbf{0}$, $\ddot{\mathbf{q}}_r = \mathbf{0}$), and Eq.(6-8) simplifies to a static relation which can be easily solved for \mathbf{q}_r :

$$\mathbf{q}_r = \underline{\mathbf{K}}_{rr}^{-1} \left(\underline{\Phi}_{or}^T \mathbf{f}_{eff}^o + \underline{\Phi}_{rr}^T \mathbf{f}_{eff}^r \right). \quad (6-16)$$

Inserting Eq.(6-16) into Eq.(6-11) renders a pseudo static component \mathbf{w}_0^{st}

$$\mathbf{w}_0^{st} = \underline{\Phi}_{or} \underline{\mathbf{K}}_{rr}^{-1} \left(\underline{\Phi}_{or}^T \mathbf{f}_{eff}^o + \underline{\Phi}_{rr}^T \mathbf{f}_{eff}^r \right) \quad (6-17)$$

which must be added to the solution of Eq.(6-14) for an improved accuracy.

6.7. Modal reduction

In the previous sections several different possibilities for the reduction of the number of degrees of freedom in the dynamic system have been discussed. Static condensation, e.g. is able to reduce the dynamic behaviour of a structural model to three independent motions per floor. Further model reduction can be achieved by a modal transformation, and a subsequent modal truncation, keeping only those mode-shapes which make major contributions to the desired structural response quantities. Sometimes even the knowledge of participation factors and dynamic magnification factors are insufficient to decide which modes to keep and which to discard, and for this reason it is of importance to alternatively find a quantitative measure reflecting the influence of certain state variables on the structural behaviour. The following summary is based on a landmark paper by Moore², where a state reduction method developed for control engineering is presented. The key idea is to find a state transformation which gives a clear indication which state variables contribute mainly to the structural response. These are consequently dominating the system behaviour and must be kept, whereas all others are of less importance and might be discarded. Such methods are of outmost importance in automatic control since the order of the system model should be minimised for several reasons, e.g. for controller design and implementation and for high sampling rates. It is convenient to use a state space description of a system, Eq.(1-60),

$$\dot{\mathbf{z}} = \mathbf{A} \mathbf{z} + \mathbf{B} \mathbf{u}_a, \quad (6-18)$$

$$\mathbf{y} = \mathbf{C} \mathbf{z}$$

with $\mathbf{z} = [\mathbf{u}, \mathbf{v}, \mathbf{w}, \dot{\mathbf{u}}, \dot{\mathbf{v}}, \dot{\mathbf{w}}]^T$, \mathbf{A} , \mathbf{B} , \mathbf{C} denoting the state space vector, the system matrix, the input and output matrix, respectively. Depending on the excitation, the input term $\mathbf{B} \mathbf{u}_a$ represents either wind or earthquake loading. To be compatible with the nomenclature in control literature, the system input vector is denoted \mathbf{u}_a . No conflict of notation is to be expected with the displacement of the fluid since it is hidden in the state vector \mathbf{z} . The output vector \mathbf{y} describes the mechanical property of interest e.g. interstory drifts. At this point it is necessary to assume that the structural dynamic system described by Eq.(6-18) is controllable and observable in a control engineering sense, see e.g. Müller³. However, this condition is

satisfied for most civil engineering problems. The first step in model reduction is to find the influence of an input signal on the state variables. Among several possible measures, the covariance matrix for an infinite time period

$$\mathbf{Q}_I = \int_0^{\infty} \mathbf{z} \cdot \mathbf{z}^T dt = \int_0^{\infty} \begin{pmatrix} z_1^2 & z_1 z_2 & \cdots & z_1 z_{2n} \\ z_1 z_2 & z_2^2 & \cdots & z_2 z_{2n} \\ \vdots & \vdots & \ddots & \vdots \\ z_{2n} z_1 & z_{2n} z_2 & \cdots & z_{2n}^2 \end{pmatrix} dt, \quad (6-19)$$

can be chosen (it converges for asymptotically stable systems). If it is possible to find a transform $\mathbf{z} = \mathbf{T} \mathbf{z}_B$ such that \mathbf{Q}_I becomes diagonal, then the diagonal elements are the variances of the corresponding state. \mathbf{Q}_I depends on the input signal, and a unit impulse excitation which contains the entire frequency spectrum, seems to be a suitable excitation. The general solution of the dynamic system, Eq.(6-18) is, see Eq.(1-66),

$$\mathbf{z}(t) = e^{\mathbf{A}(t-t_0)} \mathbf{z}(t_0) + \int_{t_0}^t e^{\mathbf{A}(t-\tau)} \mathbf{B} u_a(\tau) d\tau, \quad (6-20)$$

where the matrix exponential is defined by Eq.(1-67). For a unit impulse input $u = \delta(t_0 = 0)$ and homogenous initial conditions, the system response simplifies to the Green's function, $\mathbf{z}(t) = e^{\mathbf{A}t} \mathbf{B}$. Substitution into (6-19) renders an integral expression,

$$\mathbf{Q}_I = \int_0^{\infty} e^{\mathbf{A}t} \mathbf{B} \mathbf{B}^T e^{\mathbf{A}^T t} dt, \quad (6-21)$$

which control engineers refer to as the controllability Gramian, see Moore². If this matrix has full rank, the system is controllable, in other words, any arbitrary state configuration can be achieved by properly choosing the external input. As shown in Appendix B, \mathbf{Q}_I is equivalent to the solution of the Lyapunov equation, see also Müller and Schiehlen^{3,4}

$$\mathbf{A} \mathbf{Q}_I + \mathbf{Q}_I \mathbf{A}^T + \mathbf{B} \mathbf{B}^T = 0. \quad (6-22)$$

Having found a suitable expression describing the influence of a unit impulse on the state variables, the influence of the state variables on the output \mathbf{y} remains to be determined. Similar to a performance index, the term

$$J = \int_0^{\infty} \mathbf{y}^T \mathbf{y} dt = \int_0^{\infty} \mathbf{z}^T \mathbf{C}^T \mathbf{C} \mathbf{z} dt \quad (6-23)$$

characterises the effect of the state variables on the output. For free vibrations with arbitrary initial conditions \mathbf{z}_0 , the properly reduced Eq.(6-20) when substituted into Eq.(6-23) yields

$$J = \mathbf{z}_0^T \int_0^{\infty} e^{\mathbf{A}^T t} \mathbf{C}^T \mathbf{C} e^{\mathbf{A} t} dt \mathbf{z}_0 = \mathbf{z}_0^T \mathbf{P}_I \mathbf{z}_0, \quad (6-24)$$

$$\mathbf{P}_I = \int_0^{\infty} e^{\mathbf{A}^T t} \mathbf{C}^T \mathbf{C} e^{\mathbf{A} t} dt$$

with the corresponding Lyapunov equation, see Appendix B,

$$\mathbf{A}^T \mathbf{P}_I + \mathbf{P}_I \mathbf{A} + \mathbf{C} \mathbf{C}^T = 0. \quad (6-25)$$

In control literature, e.g. Müller^{3,4}, \mathbf{P}_I of Eq.(6-24) is commonly known as observability Gramian. If this matrix has full rank, the system is called observable, which means that any state configuration can be reconstructed only by knowing the external input and output of the dynamic system. Performing any regular state transformation \mathbf{T} , Eq.(6-18) becomes

$$\begin{aligned} \dot{\hat{\mathbf{z}}} &= \hat{\mathbf{A}} \hat{\mathbf{z}} + \hat{\mathbf{B}} \mathbf{u} \\ \mathbf{y} &= \hat{\mathbf{C}} \hat{\mathbf{z}}, \end{aligned} \quad (6-26)$$

where $\hat{\mathbf{A}} = \mathbf{T}^{-1} \mathbf{A} \mathbf{T}$, $\hat{\mathbf{B}} = \mathbf{T}^{-1} \mathbf{B}$, $\hat{\mathbf{C}} = \mathbf{C} \mathbf{T}$. Some little algebra renders the Gramians $\mathbf{Q}(\mathbf{T})$, $\mathbf{P}(\mathbf{T})$ after the transformation \mathbf{T} as a function of the Gramians of the original system \mathbf{Q}_I and \mathbf{P}_I :

$$\mathbf{Q}(\mathbf{T}) = \mathbf{T}^{-1} \int_0^{\infty} e^{\mathbf{A}^T t} \mathbf{B} \mathbf{B}^T e^{\mathbf{A} t} dt (\mathbf{T}^{-1})^T = \int_0^{\infty} e^{\hat{\mathbf{A}}^T t} \hat{\mathbf{B}} \hat{\mathbf{B}}^T e^{\hat{\mathbf{A}} t} dt = \mathbf{T}^{-1} \mathbf{Q}_I (\mathbf{T}^{-1})^T, \quad (6-27)$$

$$\mathbf{P}(\mathbf{T}) = \mathbf{T}^T \int_0^{\infty} e^{\mathbf{A}^T t} \mathbf{C}^T \mathbf{C} e^{\mathbf{A} t} dt \mathbf{T} = \int_0^{\infty} e^{\hat{\mathbf{A}}^T t} \hat{\mathbf{C}}^T \hat{\mathbf{C}} e^{\hat{\mathbf{A}} t} dt = \mathbf{T}^T \mathbf{P}_I \mathbf{T}.$$

If it is possible to find a transformation to generate an often called balanced system, such that $\mathbf{P}(\mathbf{T}) = \mathbf{Q}(\mathbf{T}) = \text{diag}(\sigma_1^2, \dots, \sigma_{2n}^2)$, $\sigma_1 > \sigma_2 > \dots > \sigma_{2n}$, then σ_i^2 describes the effect of a unit impulse on the state as well as the relation of this state on the system response. In other words: if $\sigma_i/\sigma_1 \ll 1$ then this state has little influence on the overall dynamic behaviour and

might be neglected. Moore² has shown, that such a transformation can be found in two steps: Firstly, both symmetric matrices \mathbf{P}_I and \mathbf{Q}_I are decomposed into $\mathbf{P}_I = \mathbf{V}_P \mathbf{\Sigma}_P^2 \mathbf{V}_P^T$ and $\mathbf{P}_I = \mathbf{V}_Q \mathbf{\Sigma}_Q^2 \mathbf{V}_Q^T$ with $\mathbf{V}_Q, \mathbf{V}_P$ denoting unitary matrices ($\mathbf{V}^T = \mathbf{V}^{-1}$) and $\mathbf{\Sigma}_P^2, \mathbf{\Sigma}_Q^2$ represent the diagonal singular value matrices, see e.g. Skogestad⁵. A first state transformation

$$\mathbf{T}_1 = \mathbf{V}_Q \mathbf{\Sigma}_Q, \quad (6-28)$$

can be used to generate an input-normal-system with $\mathbf{Q}(\mathbf{T}_1) = \mathbf{Q}_{T_1} = \mathbf{I}$, where \mathbf{I} denotes the identity matrix, and $\mathbf{P}(\mathbf{T}_1) = \mathbf{P}_{T_1} = \mathbf{\Sigma}_Q^T \mathbf{V}_Q^T \mathbf{P}_I \mathbf{V}_Q \mathbf{\Sigma}_Q$. A subsequent modal decomposition of the transformed system renders a new set of matrices

$$\mathbf{Q}_{T_1} = \mathbf{I}, \quad (6-29)$$

$$\mathbf{P}_{T_1} = \mathbf{V}_{P_{T_1}} \mathbf{\Sigma}_{P_{T_1}}^2 \mathbf{V}_{P_{T_1}}^T$$

From Eq.(6-29), it is quite obvious that there exists a second transformation \mathbf{T}_2 to bring both, \mathbf{P}_{T_1} and \mathbf{Q}_{T_1} to diagonal form. By substitution, it can be proven that for the second state transformation the transformation matrix

$$\mathbf{T}_2 = \mathbf{V}_{P_{T_1}} \mathbf{\Sigma}_{P_{T_1}}^{-1/2}, \quad (6-30)$$

must be applied in order to obtain the balanced state representation where

$$\mathbf{Q}_{bal} = \mathbf{T}_{bal}^{-1} \mathbf{Q}_I (\mathbf{T}_{bal}^{-1})^T = \mathbf{\Sigma}_{bal}, \quad (6-31)$$

$$\mathbf{P}_{bal} = \mathbf{T}_{bal}^T \mathbf{P}_I \mathbf{T}_{bal} = \mathbf{\Sigma}_{bal}, \quad (6-32)$$

$$\mathbf{T}_{bal} = \mathbf{T}_1 \mathbf{T}_2, \quad \mathbf{\Sigma}_{bal} = \sigma(\mathbf{T}_1^T \mathbf{P}_I \mathbf{T}_1). \quad (6-33)$$

$\sigma(\mathbf{T}_1^T \mathbf{P}_I \mathbf{T}_1)$ denotes the diagonal matrix containing the singular values of $\mathbf{T}_1^T \mathbf{P}_I \mathbf{T}_1$. Now, \mathbf{Q}_{bal} and \mathbf{P}_{bal} are two identical diagonal matrices whose diagonal elements σ_i^2 determine significance of the i -th states on the dynamic response. It is important to mention that the individual components σ_i^2 of the balanced system might not differ a lot. In such a situation no system state can be removed without a deterioration of the model's quality. However, if small

values of σ_i^2 exist, then the corresponding state can be neglected and consequently removed by either truncation or residualisation. With appropriate partitioning, the state vector is given by $\hat{\mathbf{z}} = [\hat{\mathbf{z}}_1, \hat{\mathbf{z}}_2]^T$, where $\hat{\mathbf{z}}_1$ should be removed, and Eq.(6-18) can be rewritten as

$$\dot{\hat{\mathbf{z}}}_1 = \hat{\mathbf{A}}_{11}\hat{\mathbf{z}}_1 + \hat{\mathbf{A}}_{12}\hat{\mathbf{z}}_2 + \hat{\mathbf{B}}_1\mathbf{u}_a, \quad (6-34)$$

$$\dot{\hat{\mathbf{z}}}_2 = \hat{\mathbf{A}}_{21}\hat{\mathbf{z}}_1 + \hat{\mathbf{A}}_{22}\hat{\mathbf{z}}_2 + \hat{\mathbf{B}}_2\mathbf{u}_a,$$

$$\mathbf{y} = \hat{\mathbf{C}}_1\hat{\mathbf{z}}_1 + \hat{\mathbf{C}}_2\hat{\mathbf{z}}_2.$$

In truncation the first set of equations in Eqs.(6-34) is simply removed and $\hat{\mathbf{z}}_1 = \mathbf{0}$, as in modal truncation. Residualisation, on the other side is similar to static condensation, where instead of discarding all states associated with $\hat{\mathbf{z}}_1$, the time derivative is simply set to zero $\dot{\hat{\mathbf{z}}}_1 = 0$. One can then solve for $\hat{\mathbf{z}}_1$ in terms of $\hat{\mathbf{z}}_2$ and \mathbf{u} and back substitution gives

$$\dot{\hat{\mathbf{z}}}_2 = (\hat{\mathbf{A}}_{22} - \hat{\mathbf{A}}_{21}\hat{\mathbf{A}}_{11}^{-1}\hat{\mathbf{A}}_{12})\hat{\mathbf{z}}_2 + (\hat{\mathbf{B}}_2 - \hat{\mathbf{A}}_{21}\hat{\mathbf{A}}_{11}^{-1}\hat{\mathbf{B}}_1)\mathbf{u}_a \quad (6-35)$$

$$\mathbf{y} = (\hat{\mathbf{C}}_2 - \hat{\mathbf{C}}_1\hat{\mathbf{A}}_{11}^{-1}\hat{\mathbf{A}}_{12})\hat{\mathbf{z}}_2 - \mathbf{C}_1\hat{\mathbf{A}}_{11}^{-1}\mathbf{B}_1\mathbf{u}_a$$

Furthermore attention has to be drawn to the fact that the successful application of model reduction is largely dependent on the structural response quantities included in the possible output vector \mathbf{y} . A warning example is a simple untuned mass absorber system where the order reduction potential depends on the response one is interested in, e.g., the main mass displacement or the absorber displacement. For exactly the same system the former situation will allow a successful order reduction whereas in the latter case no reduction is feasible. For this reason the elimination of states is generally difficult unless the output quantities have been determined.

6.8. Examples

Several methods discussed within this chapter have been successfully applied to real civil engineering problems, presented in Chapter 9, where high-rise buildings are investigated. Several benchmark structures have been published by Spencer^{6,7} where the reduction of the

degrees of freedom is shown in detail: first the complex structures are discretised by finite elements, usually frames, and a model with several thousand degrees of freedom is obtained. The use of kinematic constraints and static condensation reduce the model to several hundred degrees of freedom. A further reduction can be achieved by modal approximations or balanced realisations. Investigations will show that most buildings have a high reduction potential. Depending on the excitation, the final model can be reduced by a factor of up to 100-1000.

6.9. References

- ¹ Clough, R.W., Penzien, J., *Dynamics of Structures*, McGraw-Hill, Singapore, 2nd edition, 1993
- ² Moore, B.C., *Principal Component Analysis in Linear Systems: Controllability, Observability, and Model Reduction*, IEEE Transaction on Automatic Control, Vol. AC26(1), pp.17-32, 1981
- ³ Müller, P.C., *Stabilität und Matrizen*, Springer-Verlag, 1977
- ⁴ Müller, P.C., Schiehlen, W.O., *Lineare Schwingungen*, Akademische Verlagsgesellschaft, Wiesbaden, 1976
- ⁵ Skogestad, S., Postlethwaite, I., *Multivariable Feedback Control*, John Wiley & Sons, Chichester, GB, 1988
- ⁶ Spencer, B.F. Jr., Dyke, S.J., Doeskar, H.S., *Part I: Active Mass Driver System, Part II: Active Tendon System*, Special issue of Earthquake Engineering and Structural Dynamics, vol.27(11), pp.1127-1148, 1998
- ⁷ Spencer, B.F. Jr., Christenson, R. Dyke, S.J., *Next Generation Benchmark Problem*, Proceedings of the Second World Conference on Structural Control, (ed. Nishitani, A.), Kyoto, Japan, 1998, also www-publication: <http://www.nd.edu/~quake/>

7. Optimisation of multiple TLCDs and MDOF structural systems in the state space domain

Traditionally, dynamic systems have been described by second order differential systems because Newton's law as well as energy principles (e.g. Lagrange equations of motion, Hamilton's principle) render inertia proportional to acceleration. Alternatively, the state space representation can be used to describe dynamic systems, and it turns out that it is particularly suitable for dynamic investigations, since the difference between non-classically and classically damped systems vanish, the design and incorporation of the absorber into the structural model is straightforward, and numerical processing is possible. A structural model with dozens of degrees of freedom can be quite difficult to investigate, and intuitive analytical design schemes must give way to a more systematic approach, which is adaptable for automated processing. Independent of the size of the structural model, any linear structure with N degrees of freedom can be described by, see Eq.(6-1), which is properly generalised to include a number of n TLCDs installed in the building,

$$\mathbf{M} \ddot{\mathbf{w}} + \mathbf{C} \dot{\mathbf{w}} + \mathbf{K} \mathbf{w} = -\mathbf{M} \mathbf{r}_s \ddot{w}_g + \mathbf{f}(t) + \mathbf{L} \mathbf{f}_A \quad (7-1)$$

where \mathbf{f}_A , \mathbf{L} denote the structure-absorber interaction forces and a position matrix, respectively. The TLCD position matrix has the following form:

$$\mathbf{L} = \begin{bmatrix} 0 & 1 & \cdots & 0 \\ \vdots & \vdots & \ddots & \vdots \\ 1 & 0 & \cdots & 0 \end{bmatrix} \quad \begin{array}{l} \leftarrow \text{degree of freedom which is influenced by TLCD} \\ \uparrow \\ \text{number of TLCD} \end{array} \quad (7-2)$$

Obviously \mathbf{L} is a sparse matrix of dimension $[N \times n]$. The components of $\mathbf{f}_A = [f_1, \dots, f_n]^T$ are the individual interaction forces f_i of the TLCDs, given by Eq.(4-31) or Eq.(4-60),

$$f_i = -m_{f,i} [\ddot{w}_{abs,i} + \bar{K} \ddot{u}_i], \quad (7-3)$$

where $m_{f,i}$, $\ddot{w}_{abs,i}$ represents the liquid mass of the i -th TLCD and the absolute acceleration of its supporting floor. The corresponding TLCD equation of motion is, see Eq.(4-11),

$$\ddot{u}_i + 2\zeta_i \omega_i \dot{u}_i + \omega_i^2 u_i = -\kappa_i \ddot{w}_{abs,i}, \quad (7-4)$$

It has to be pointed out that the following derivation is only valid for the case where \mathbf{w} describes the floor displacement with respect to the basement. If the vector \mathbf{w} contains e.g. interstory drifts, a linear transformation $\mathbf{w}_b = \mathbf{T} \mathbf{w}$ to displacement coordinates \mathbf{w}_b (with respect to the base) is inevitable for the calculation of the interaction forces. For convenience, the TLCDs dynamics, given by Eqs.(7-3) and (7-4), can be formulated in matrix notation:

$$\mathbf{f}_A = -\mathbf{M}_A \left[\left(\mathbf{L}^T \mathbf{T} \ddot{\mathbf{w}} + \mathbf{i} \ddot{w}_g \right) + \overline{\mathbf{K}} \ddot{\mathbf{u}} \right], \quad (7-5)$$

$$\ddot{\mathbf{u}} + \mathbf{C}_A \dot{\mathbf{u}} + \mathbf{K}_A \mathbf{u} = -\mathbf{K} \left(\mathbf{L}^T \mathbf{T} \ddot{\mathbf{w}} + \mathbf{i} \ddot{w}_g \right), \quad (7-6)$$

where

$$\mathbf{M}_A = \text{diag}(m_{f,1}, \dots, m_{f,n}), \quad \mathbf{C}_A = \text{diag}(2\zeta_1 \omega_1, \dots, 2\zeta_n \omega_n) \quad (7-7)$$

$$\mathbf{K}_A = \text{diag}(\omega_1^2, \dots, \omega_n^2),$$

$$\mathbf{K} = \text{diag}(\kappa_1, \dots, \kappa_n), \quad \overline{\mathbf{K}} = \text{diag}(\overline{\kappa}_1, \dots, \overline{\kappa}_n)$$

Eliminating the interaction forces in the structural equations by substituting Eq.(7-6) into Eq.(7-1) generates the coupled matrix equations of motion:

$$\begin{pmatrix} \mathbf{M} + \mathbf{L} \mathbf{M}_A \mathbf{L}^T & \mathbf{L} \mathbf{M}_A \overline{\mathbf{K}} \\ \mathbf{K} \mathbf{L}^T & \mathbf{I} \end{pmatrix} \begin{pmatrix} \ddot{\mathbf{w}} \\ \ddot{\mathbf{u}} \end{pmatrix} + \begin{pmatrix} \mathbf{C} & \mathbf{0} \\ \mathbf{0} & \mathbf{C}_A \end{pmatrix} \begin{pmatrix} \dot{\mathbf{w}} \\ \dot{\mathbf{u}} \end{pmatrix} + \begin{pmatrix} \mathbf{K} & \mathbf{0} \\ \mathbf{0} & \mathbf{K}_A \end{pmatrix} \begin{pmatrix} \mathbf{w} \\ \mathbf{u} \end{pmatrix} = - \begin{pmatrix} \mathbf{M} \mathbf{r}_S + \mathbf{L} \mathbf{M}_A \mathbf{i} \\ \mathbf{K} \mathbf{i} \end{pmatrix} \ddot{w}_g + \begin{pmatrix} \mathbf{f}(t) \\ \mathbf{0} \end{pmatrix} \quad (7-8)$$

An explicit expression for the building and absorber accelerations $\ddot{\mathbf{w}}, \ddot{\mathbf{u}}$ can be obtained by firstly defining the regular non-diagonal mass matrix of the combined system

$$\mathbf{M}_S = \begin{pmatrix} \mathbf{M} + \mathbf{L} \mathbf{M}_A \mathbf{L}^T & \mathbf{L} \mathbf{M}_A \overline{\mathbf{K}} \\ \mathbf{K} \mathbf{L}^T & \mathbf{I} \end{pmatrix}, \quad (7-9)$$

and, secondly, pre-multiplying Eq.(7-8) with its inverse

$$\begin{pmatrix} \ddot{\mathbf{w}} \\ \ddot{\mathbf{u}} \end{pmatrix} = -\mathbf{M}_S^{-1} \begin{pmatrix} \mathbf{C} & \mathbf{0} \\ \mathbf{0} & \mathbf{C}_A \end{pmatrix} \begin{pmatrix} \dot{\mathbf{w}} \\ \dot{\mathbf{u}} \end{pmatrix} - \mathbf{M}_S^{-1} \begin{pmatrix} \mathbf{K} & \mathbf{0} \\ \mathbf{0} & \mathbf{K}_A \end{pmatrix} \begin{pmatrix} \mathbf{w} \\ \mathbf{u} \end{pmatrix} - \mathbf{M}_S^{-1} \begin{pmatrix} \mathbf{M} \mathbf{r}_S + \mathbf{L} \mathbf{M}_A \mathbf{i} \\ \overline{\mathbf{K}} \mathbf{i} \end{pmatrix} \ddot{\mathbf{w}}_g + \mathbf{M}_S^{-1} \begin{pmatrix} \mathbf{f}(t) \\ \mathbf{0} \end{pmatrix}. \quad (7-10)$$

This system of second order differential equations can be converted to a first order state space representation by introducing the new state vector $\mathbf{z} = [\mathbf{w}^T \mathbf{u}^T \dot{\mathbf{w}}^T \dot{\mathbf{u}}^T]^T$, and its time derivative

$$\dot{\mathbf{z}} = (\mathbf{A} + \mathbf{B} \mathbf{R}) \mathbf{z} - \mathbf{e}_g \ddot{\mathbf{w}}_g + \mathbf{E}_f \mathbf{f}(t), \quad (7-11)$$

where in a hypermatrix notation

$$\mathbf{A} = \begin{pmatrix} \mathbf{0} & \mathbf{0} & \mathbf{I} & \mathbf{0} \\ \mathbf{0} & \mathbf{0} & \mathbf{0} & \mathbf{I} \\ -\mathbf{M}_S^{-1} \begin{pmatrix} \mathbf{K} & \mathbf{0} \\ \mathbf{0} & \mathbf{0} \end{pmatrix} & -\mathbf{M}_S^{-1} \begin{pmatrix} \mathbf{C} & \mathbf{0} \\ \mathbf{0} & \mathbf{0} \end{pmatrix} \end{pmatrix}, \quad \mathbf{B} = \begin{pmatrix} \mathbf{0} & \mathbf{0} & \mathbf{0} & \mathbf{0} \\ \mathbf{0} & \mathbf{0} & \mathbf{0} & \mathbf{0} \\ -\mathbf{M}_S^{-1} \begin{pmatrix} \mathbf{I} & \mathbf{0} \\ \mathbf{0} & \mathbf{I} \end{pmatrix} & -\mathbf{M}_S^{-1} \begin{pmatrix} \mathbf{I} & \mathbf{0} \\ \mathbf{0} & \mathbf{I} \end{pmatrix} \end{pmatrix}, \quad (7-12)$$

$$\mathbf{R} = \begin{pmatrix} \mathbf{0} & \mathbf{0} & \mathbf{0} & \mathbf{0} \\ \mathbf{0} & \mathbf{K}_A & \mathbf{0} & \mathbf{0} \\ \mathbf{0} & \mathbf{0} & \mathbf{0} & \mathbf{0} \\ \mathbf{0} & \mathbf{0} & \mathbf{0} & \mathbf{C}_A \end{pmatrix}, \quad \mathbf{e}_g = \begin{pmatrix} \mathbf{0} \\ \mathbf{0} \\ \mathbf{M}_S^{-1} \begin{pmatrix} \mathbf{M} \mathbf{r}_S + \mathbf{L} \mathbf{M}_A \mathbf{i} \\ \overline{\mathbf{K}} \mathbf{i} \end{pmatrix} \end{pmatrix}, \quad \mathbf{E}_f = \begin{pmatrix} \mathbf{0} \\ \mathbf{0} \\ \mathbf{M}_S^{-1} \begin{pmatrix} \mathbf{I} \\ \mathbf{0} \end{pmatrix} \end{pmatrix}.$$

A system matrix $\mathbf{A}_r = \mathbf{A} + \mathbf{B} \mathbf{R}$ apparent in Eq.(7-12) can be used, however sometimes the separated two term expression $\mathbf{A} + \mathbf{B} \mathbf{R}$ has the advantage that \mathbf{A} solely contains the given structural dynamics and the second term, $\mathbf{B} \mathbf{R}$ includes the TLCD design parameter, natural frequency and damping ratio.

7.1. Optimisation for free vibration of MDOF structure with several TLCD installed

Having established the set of $2(N+n)$ equations of motion, the dynamic performance of the system has to be determined, often by a performance index, which is a scalar measure of the system behaviour. The choice of a practical performance index is difficult and becomes a critical task where the engineer's knowledge and experience plays a central role. Usually, deep insight into the structural behaviour, and a good understanding of dynamic phenomena are required to be able to describe a complex behaviour by a simple number. A commonly

used technique is to examine the free vibrations of a building with the aim of minimising the time integral of a weighted sum of the quadratic state variables for the infinite time interval $0 \leq t < \infty$. Mathematically this quadratic performance index is described by

$$J = \int_0^{\infty} \mathbf{z}^T(\tau) \mathbf{S} \mathbf{z}(\tau) d\tau, \quad (7-13)$$

with a symmetric, positive semidefinite weighing matrix \mathbf{S} , which defines the relative importance of the states with respect to each other. The performance index given in Eq.(7-13) quantifies the free vibration such, that large displacements and velocities are rated heavily - an important criteria from a practical point of view. However, the initial conditions and the weighing matrix \mathbf{S} must be chosen to account for engineering requirements. Furthermore it is important to know efficient algorithms for the computation of J , as its minimisation is, in general, performed numerically. For given initial conditions $\mathbf{z}(0) = \mathbf{z}_0$ the free vibration is given by $\mathbf{z}(t) = e^{\mathbf{A}_r t} \mathbf{z}_0$. Inserting into (7-13) yields

$$J = \mathbf{z}_0^T \int_0^{\infty} e^{\mathbf{A}_r^T \tau} \mathbf{S} e^{\mathbf{A}_r \tau} d\tau \mathbf{z}_0. \quad (7-14)$$

Integration by parts can solve this integral expression, see Appendix B, and the quadratic performance index for an infinite time interval simplifies to

$$J = \mathbf{z}_0^T \mathbf{P} \mathbf{z}_0, \quad (7-15)$$

$$\mathbf{A}_r^T \mathbf{P} + \mathbf{P} \mathbf{A}_r + \mathbf{S} = 0,$$

where \mathbf{P} is the solution of an algebraic Lyapunov matrix equation. Consequently, the calculation of the quadratic performance index J has been reduced to the computation of the solution \mathbf{P} of a linear matrix equation. For asymptotically stable systems, \mathbf{P} has a unique solution if \mathbf{S} is positive semidefinite, see e.g. Müller¹. Finding the solution of a Lyapunov equation is a standard problem in numerical mathematics, and powerful algorithms are readily available, see e.g. Control Toolbox of Matlab⁵.

After J has been defined, it is possible to compute the free system parameters, as defined by the nonzero diagonal elements of \mathbf{R} , see Eq.(7-12). The latter must be varied in order to optimise the free vibrations according to Eq.(7-14). Optimal parameter are found when J reaches a minimum or equivalently

$$\frac{\partial J}{\partial \mathbf{R}} = 0. \quad (7-16)$$

Unfortunately, an analytical expression for Eq.(7-16) can hardly be found, and some of the parameters can have range limitations ($\zeta_A > 0$, $\omega_{\min} < \omega_A < \omega_{\max}$) so that the optimisation is often performed numerically.

Yet, the choice of the initial condition is still not discussed. Basically, \mathbf{z}_0 can take any value, but the response due to a unit impulse load is meaningful from an engineering perspective. For homogenous initial conditions and ground excitation, this response is given by Eq.(1-66), $\mathbf{z}(t) = e^{\mathbf{A}_r t} \mathbf{e}_g$. Therefore a suitable choice of \mathbf{z}_0 would be $\mathbf{z}_0 = \mathbf{e}_g$. Furthermore, the weighing function \mathbf{S} has to be selected such, that the performance index reflects important physical quantities. If displacements or velocities are contained in J , then \mathbf{S} will be of diagonal shape. Alternatively, the minimisation of the accumulated structural energy would be a meaningful performance index. If the instantaneous structural energy $E_{inst} = (\mathbf{w}^T \mathbf{K} \mathbf{w} + \dot{\mathbf{w}}^T \mathbf{M} \dot{\mathbf{w}})/2$ is defined as the sum of the relative kinetic and strain energy, then

$$E_{inst} = \mathbf{z}^T \mathbf{S} \mathbf{z}, \quad (7-17)$$

$$\mathbf{S} = \begin{pmatrix} \mathbf{K} & \mathbf{0} & \mathbf{0} & \mathbf{0} \\ \mathbf{0} & \mathbf{0} & \mathbf{0} & \mathbf{0} \\ \mathbf{0} & \mathbf{0} & \mathbf{M} & \mathbf{0} \\ \mathbf{0} & \mathbf{0} & \mathbf{0} & \mathbf{0} \end{pmatrix}, \quad \mathbf{z} = \begin{pmatrix} \mathbf{w} \\ \mathbf{u} \\ \dot{\mathbf{w}} \\ \dot{\mathbf{u}} \end{pmatrix},$$

and the performance index represents the accumulated energy, which is minimised for free vibrations.

The optimisation for free vibration guarantees optimal behaviour if there is a certain state disturbance at $t = 0$. As the performance index is solely defined in the time domain, the free vibration optimisation method must be categorised as a time domain method. However, as an impulse load is rarely applied to a building, a more realistic design methodology which attenuates external excitation defined in the frequency domain is discussed next.

7.2. Frequency response optimisation for MDOF structures with several TLCD installed

The frequency response spectrum, in particular the amplitude response curve, is a quantity of major importance for describing the sensitivity to external disturbances in the frequency domain. A typical example of a frequency domain method is the optimisation according to DenHartog, see Section 2.6.2, where the maximal amplitude magnification is reduced to obtain a “disturbance rejecting” behaviour. In structural dynamics, resonance problems are often tackled by the application of dynamic vibration absorbers. Therefore the frequency response shaping should be focused at the critical frequency range, as well as by taking the excitation spectrum into account.

7.2.1. Determination of a performance index in the frequency domain

Since the amplitude response function $A(\nu)$ and the Fourier transformed of the impulse response function $h(\nu)$ are proportional and related by a constant scaling factor \mathcal{X} , $A(\nu) = \mathcal{X}_s h(\nu)$, a mathematical generalisation of the DenHartog performance criterion for SDOF systems can be stated by

$$J = \max_{\nu \in \Omega} \{ |h(\nu)| \} \rightarrow \text{minimum}, \quad \nu_{\min} \leq \Omega \leq \nu_{\max}, \quad (7-18)$$

where Ω denotes the frequency range of interest. For multiple degree of freedom systems many impulse response functions can be defined, e.g. $h_1(\nu), \dots, h_N(\nu)$ which must be minimised simultaneously. In such a situation, Eq.(7-18) can be extended to

$$J = \max_{\nu \in \Omega} \{ s_1 |h_1(\nu)|, \dots, s_N |h_N(\nu)| \} \rightarrow \text{minimum}, \quad \nu_{\min} \leq \Omega \leq \nu_{\max}, \quad (7-19)$$

where the positive weighing factors $s_i > 0$ are introduced to describe the importance of the different states. A generalisation which takes into account frequency dependent weighing factors $s_i(\nu)$ is commonly referred to as H_∞ design, see e.g. Levine², Müller³ and Ludyk⁴.

However, the calculation of the H_∞ norm, defined by $\|h(\nu)\|_\infty = \lim_{k \rightarrow \infty} \sqrt[k]{\int_0^\infty (h(\nu))^k d\nu}$, is based

on an iterative method, and thus quite time consuming. Nevertheless, efficient algorithms are available in numerical toolboxes, e.g. Control Toolbox of MATLAB⁵.

A second method of measuring the disturbance attenuation is to minimise the area below the impulse response curve of a SDOF system,

$$J = \int_{\nu_{\min}}^{\nu_{\max}} |h(\nu)|^2 d\nu \rightarrow \text{minimum}. \quad (7-20)$$

Again, a quadratic description is chosen to penalise high amplifications. If several impulse response functions are of interest, e.g. in case of a MDOF-system, an extension of Eq.(7-20) can be given straightforwardly

$$J = \sum_{i=1}^N \int_{\nu_{\min}}^{\nu_{\max}} s_i(\nu) |h_i(\nu)|^2 d\nu \rightarrow \text{minimum}, \quad (7-21)$$

where s_i is a weighing factor which is introduced to account for the different significance of the state variables. Obviously, dominant resonant peaks increase the performance measure J drastically and as a result the optimisation according to Eq.(7-21) will reduce those peaks noticeably, leading to similar results as an optimisation according to Eq.(7-19). This reduction can be explained by the fact that vibration prone structures have only small damping ratios and the amplitude magnification at the critical resonant frequency causes a major contribution to the performance index.

The first step to evaluate Eq.(7-21) is to substitute the quadratic amplitude magnification by $|h(\nu)|^2 = h^*(\nu) \cdot h(\nu)$ where $*$ denotes the conjugate complex of a number. Then J simplifies to

$$J = \int_{\nu_{\min}}^{\nu_{\max}} \mathbf{h}^H(\nu) \mathbf{S}(\nu) \mathbf{h}(\nu) d\nu, \quad (7-22)$$

where $\mathbf{h}(\nu)$ is given by Eq.(1-68). The superscript H denotes the complex transposed of a matrix, and $\mathbf{S}(\nu)$ is a positive semidefinite, frequency dependent weighing matrix, composed of the weighing factors $s_i(\nu)$. For the special case of an unlimited frequency range $\nu_{\min} = -\infty$, $\nu_{\max} = +\infty$ and a constant weighing matrix \mathbf{S} , Eq.(7-22) can be rewritten as

$$J = \int_{-\infty}^{\infty} \mathbf{h}^H \mathbf{S} \int_{-\infty}^{\infty} \mathbf{h}(t) e^{-i\nu t} dt d\nu, \quad (7-23)$$

where $\mathbf{h}(\nu)$ is replaced by its corresponding inverse Fourier transformed time function $h(t)$. Since, for stable systems the integral expressions converge, it is legitimate to rearrange the integral expressions to obtain

$$J = \int_{-\infty}^{\infty} \int_{-\infty}^{\infty} \mathbf{h}^H(\nu) e^{-i\nu t} d\nu \mathbf{S} \mathbf{h}(t) dt = 2\pi \int_{-\infty}^{\infty} \mathbf{h}^T(t) \mathbf{S} \mathbf{h}(t) dt, \quad (7-24)$$

where the time reversal property of the Fourier transform was used $\mathfrak{F}^{-1}(h^*(-\nu)) = h^*(t)$, see e.g. Levine² and Lüke⁶. The impulse response function vanishes for $t < 0$, the lower integration limit can thus be changed to zero. From the general solution of linear differential equations, see Eq.(1-65) it follows directly that, for homogenous initial conditions, the impulse response function $h(t)$ becomes

$$\mathbf{h}(t) = \int_0^t \mathbf{\Gamma}(t-\tau) \mathbf{e}_g \delta(\tau) d\tau = \mathbf{\Gamma}(t) \mathbf{b} = e^{\mathbf{A}_r t} \mathbf{e}_g, \quad (7-25)$$

assuming homogenous initial conditions. Thus

$$J = 2\pi \mathbf{e}_g^T \int_{-\infty}^{\infty} e^{\mathbf{A}_r^T \tau} \mathbf{S} e^{\mathbf{A}_r \tau} d\tau \mathbf{e}_g, \quad (7-26)$$

where the excitation vector \mathbf{e}_g , Eq.(7-12), is assumed to be constant, and the system matrix \mathbf{A} must be asymptotically stable. Further simplification is possible because the integral expression in Eq.(7-26) is again the solution of the Lyapunov matrix equation, and the frequency dependent optimisation index simplifies to, see e.g. Müller-Schiehlen⁷, p.249,

$$J = 2\pi \mathbf{e}_g^T \mathbf{P} \mathbf{e}_g, \quad (7-27)$$

$$\mathbf{A}_r^T \mathbf{P} + \mathbf{P} \mathbf{A}_r + \mathbf{S} = 0,$$

In fact the optimisation of the quadratic amplitude response function for an unlimited frequency range yields exactly the same result as the optimisation of the free vibration if the initial condition is chosen to be $\mathbf{z}_0 = \sqrt{2\pi} \mathbf{e}_g$, which corresponds to a scaled unit impulse excitation. This result is not surprising and states that under the given conditions both optimisation methods yield the same TLCD tuning parameter, as the spectrum of a unit impulse is considered as a unit intensity white noise signal. If coloured noise excitations are

investigated, the same optimisation idea can be used, but an additional filter function must be included in the dynamic system, for such alternatives, see subsequent Section 7.5

7.3. Stochastic optimisation: Minimum Variance

The optimisation methods presented so far, did not take the random character of wind or earthquake loading into account. Excitation forces generated by a random process cause the dynamic response to be a random process as well. For linear systems and simple random excitation processes it is possible to calculate stochastic response quantities like the state variances. Well written introductions into random vibrations can, e.g. be found in Lin⁸, Newland⁹, Parkus¹⁰, Wirsching¹¹, Yang¹², amongst others. For any continuous ergodic (hence stationary) time process X , characterised by its probability density $p(x)$, the expectation value is given by

$$E[X] = \frac{1}{2T} \int_{-T}^T x(t) dt, \quad (7-28)$$

but for vibrations the expectation value vanishes $E[X] = 0$, and thus the autocorrelation function $R(\tau)$ becomes the most important response quantity. For the stationary process it is defined by

$$R(\tau) = E[x(t)x(t+\tau)], \quad (7-29)$$

and its Fourier transform, $S_x(\omega)$, is called the spectral density function of X . The variance of a function in time domain is given by

$$\sigma^2 = E[x(t)^2] - E[x(t)]^2 = R(0). \quad (7-30)$$

For a single output $y(t)$ of a linear system excited by an external excitation $\ddot{w}_g(t)$, the autocorrelation function is given by

$$R(\tau) = E[y(t)y(t+\tau)] = E\left[\int_{-\infty}^{\infty} h(\tau_1)\ddot{w}_g(t-\tau_1)d\tau_1 \cdot \int_{-\infty}^{\infty} h(\tau_2)\ddot{w}_g(t+\tau-\tau_2)d\tau_2\right], \quad (7-31)$$

where $h(\tau)$ denotes the scalar impulse response function. For a stable system both integral expressions converge, and it is allowed to replace the two separate integrals by a single double integral. Computation of the expectation in Eq.(7-31), and rearrangement of the integrals yields, see e.g. Newland⁹ and Parkus¹⁰

$$\begin{aligned} R(\tau) &= \int_{-\infty}^{\infty} \int_{-\infty}^{\infty} h(\tau_1) h(\tau_2) E[\ddot{w}_g(t + \tau - \tau_2) \ddot{w}_g(t - \tau_1)] d\tau_1 d\tau_2 \\ &= \int_{-\infty}^{\infty} \int_{-\infty}^{\infty} h(\tau_1) h(\tau_2) R_{\ddot{w}_g}(\tau + \tau_1 - \tau_2) d\tau_1 d\tau_2 \end{aligned} \quad (7-32)$$

where $R_{\ddot{w}_g}$ denotes the autocorrelation function for the excitation forces, see Eq.(7-29). This involved expression can be considerably simplified as follows. A Fourier transformation of $R_{\ddot{w}_g}$ into its frequency domain counterpart $S_{\ddot{w}_g}$ and substitution into Eq.(7-32) yields

$$R(\tau) = \frac{1}{2\pi} \int_{-\infty}^{\infty} \int_{-\infty}^{\infty} \int_{-\infty}^{\infty} h(\tau_1) h(\tau_2) e^{j\omega(\tau + \tau_1 - \tau_2)} S_{\ddot{w}_g}(\omega) d\tau_1 d\tau_2 d\omega. \quad (7-33)$$

Rearrangement of the integral expressions, followed by another Fourier transformation renders a simpler and very useful expression for $R(\tau)$:

$$R(\tau) = \frac{1}{2\pi} \int_{-\infty}^{\infty} h^*(\omega) h(\omega) S_{\ddot{w}_g}(\omega) e^{j\omega\tau} d\omega = \frac{1}{2\pi} \int_{-\infty}^{\infty} S_y(\omega) e^{j\omega\tau} d\omega, \quad (7-34)$$

$$S_y(\omega) = h^*(\omega) h(\omega) S_{\ddot{w}_g}(\omega), \quad h^*(\omega) = \int_{-\infty}^{\infty} h(\tau) e^{j\omega\tau} d\tau, \quad h(\omega) = \int_{-\infty}^{\infty} h(\tau) e^{-j\omega\tau} d\tau$$

where the time reversal property of the Fourier transform was applied in the definition of h^* , and $S_y(\omega)$ denotes the power spectral density of the system's response. The calculation of the variance σ_y is a special case of the autocorrelation function and thus obtained by setting $\tau = 0$ in Eq. (7-34), see e.g. Lin⁸, Newland⁹, Parkus¹⁰, Wirschig¹¹, Spanos¹³,

$$\sigma_y^2 = R(0) = \frac{1}{2\pi} \int_{-\infty}^{\infty} h^*(\omega) h(\omega) S_{\ddot{w}_g}(\omega) d\omega. \quad (7-35)$$

For linear systems with G inputs $\ddot{w}_i(t)$ the corresponding expression for Eq.(7-35) can be given by

$$\sigma_y^2 = R(0) = \frac{1}{2\pi} \int_{-\infty}^{\infty} \sum_{r=1}^G \sum_{s=1}^G h_r^*(\omega) h_s(\omega) S_{\ddot{w}_r, \ddot{w}_s}(\omega) d\omega, \quad (7-36)$$

where $h_i(t)$ represents the impulse response function due to an excitation at the i -th input. The cross spectral density $S_{\ddot{w}_r, \ddot{w}_s}$ is defined as the Fourier transform $\mathcal{F}\{R_{\ddot{w}_r, \ddot{w}_s}\}$ of the cross correlation $R_{\ddot{w}_r, \ddot{w}_s}(\tau) = E[\ddot{w}_r(t) \ddot{w}_s(t + \tau)]$. If the system of interest has multiple inputs and outputs the extension of Eq.(7-36) can be given conveniently in matrix notation

$$\Sigma^2 = \frac{1}{2\pi} \int_{-\infty}^{\infty} \mathbf{H}(\omega) \mathbf{S}(\omega) \mathbf{H}^H(\omega) d\omega, \quad (7-37)$$

where \mathbf{S} , \mathbf{H} denote the matrix of spectral densities and the matrix of complex impulse response functions, respectively. For physical white noise broad band excitation, $\mathbf{S} = \text{const}$, Eq.(7-37) can be simplified further by replacing $\mathbf{H}(\omega)$ by its inverse Fourier transformed time function $\mathbf{H}(t)$,

$$\Sigma^2 = \int_{-\infty}^{\infty} \mathbf{H}(t) \mathbf{S} \mathbf{H}^T(t) dt, \quad (7-38)$$

where the time reversal property of the Fourier transform was applied again, $\mathcal{F}^{-1}(h_{ij}^*(-\nu)) = h_{ij}^*(t)$. Since $\mathbf{H}(t) = e^{\mathbf{A}_r t} \mathbf{E}$, where \mathbf{E} denotes the excitation input matrix given by e.g. Eq.(7-12), $\mathbf{E} = \mathbf{E}_f$ or $\mathbf{E} = [\mathbf{e}_{g,1}, \dots, \mathbf{e}_{g,G}]$, Eq.(7-38) simplifies further

$$\Sigma^2 = \int_{-\infty}^{\infty} e^{\mathbf{A}_r t} \mathbf{E} \mathbf{S} \mathbf{E}^T e^{\mathbf{A}_r^T t} dt, \quad (7-39)$$

The integral expression of Eq.(7-39) is the solution of a Lyapunov equation, and thus the variances are given by, see e.g. Müller-Schiehlen⁷, p.269,

$$\mathbf{A}_r \Sigma^2 + \Sigma^2 \mathbf{A}_r^T + \mathbf{E} \mathbf{S} \mathbf{E}^T = \mathbf{0}. \quad (7-40)$$

7.4. Comments on systems with multiple inputs

If one is dealing with a multiple input system the performance index has to be modified. For the statistical variance optimisation an analytical solution can be obtained, which is given by Eq.(7-37). If the excitation inputs are independent variables then the cross spectral densities vanish, and the SRSS (square root of sum of squares) rule for the standard deviation σ_y yields the exact solution, see e.g. Newland⁹

$$\sigma_y^2 = \sum_{s=1}^N \int_{-\infty}^{\infty} H_s^*(\omega) H_s(\omega) S_{f_s}(\omega) d\omega = \sum_{s=1}^N \sigma_{y,s}^2, \quad (7-41)$$

$$\sigma_y = \sqrt{\sum_{s=1}^N \sigma_{y,s}^2},$$

where $\sigma_{y,s}^2$ denotes the variance of output y due to the s -th input force f_s . As the other optimisation methods presented above are more of an intuitive character, there is no direct procedure available to derive a mathematical description for several inputs. From an engineering point of view the SRSS method seems to be most suitable, although other criteria like simple summation or weighted summation of the single source excitation indices are possible.

7.5. Coloured noise input

All optimisation methods presented so far have assumed stationary random, physical white noise excitation X , mathematically defined uncorrelated

$$R_x(\tau) = S_0 \delta(\tau), \quad (7-42)$$

where S_0 and $\delta(\tau)$ denote the white noise intensity and the Dirac delta function of the uncorrelated process. Although any real excitation process can hardly be described by white noise excitation, it helps to overcome several mathematical difficulties, and allows to obtain quite general and simple results. A more practical direct generalisation of the white noise

process is given by the coloured noise process, which is defined as the output of a dynamic shape filter for a white noise input. Figure 7-1 shows the spectral density of a white noise process and the coloured noise output of an arbitrary dynamic filter, which must be chosen to approximate a real measured process, by the output of the filter due to a white noise input signal.

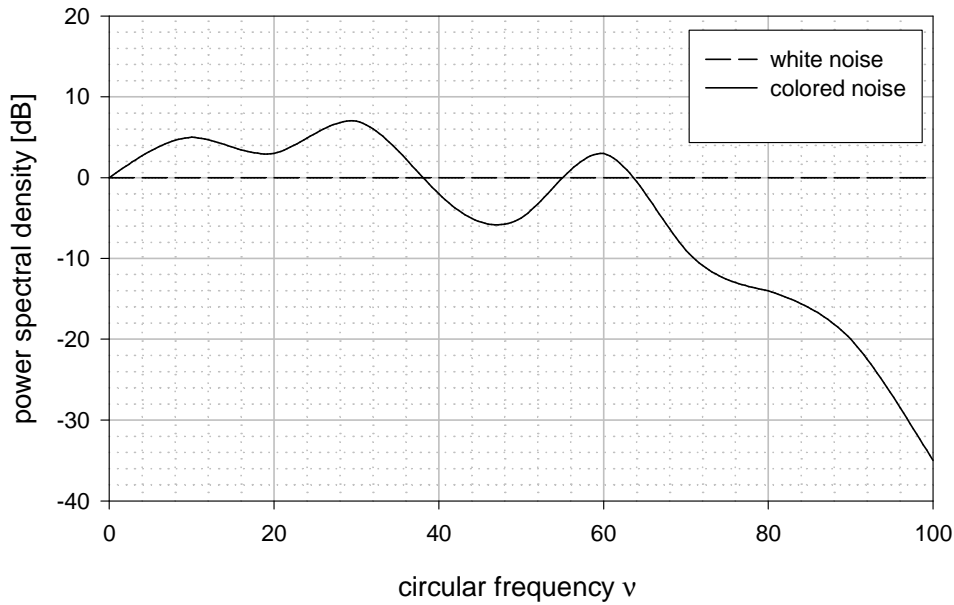


Figure 7-1: Spectral density of white noise input signal and a coloured noise output signal

All linear dynamic filters of order N_ψ can be described in state space formulation as

$$\begin{aligned}\dot{\bar{\Psi}} &= \mathbf{A}_\psi \bar{\Psi} + \mathbf{B}_\psi \xi \\ \Psi &= \mathbf{C}_\psi \bar{\Psi} + \mathbf{D}_\psi \xi\end{aligned}\tag{7-43}$$

where ξ , Ψ are a scalar or vector physical white noise input and the matching scalar or vector coloured noise output, respectively. If the excitation process, the solution of Eq.(7-43), is applied to a structural system of order N , given by Eq.(7-11), then the resulting system dynamics becomes

$$\dot{\bar{\mathbf{z}}} = \bar{\mathbf{A}} \bar{\mathbf{z}} + \bar{\mathbf{B}} \xi, \tag{7-44}$$

$$\bar{\mathbf{A}} = \begin{pmatrix} \mathbf{A} & \mathbf{E} \mathbf{C}_\psi \\ \mathbf{0} & \mathbf{A}_\psi \end{pmatrix}, \quad \bar{\mathbf{B}} = \begin{pmatrix} \mathbf{E} \mathbf{D}_\psi \\ \mathbf{B}_\psi \end{pmatrix}$$

Note that the new system, given by Eq.(7-44), is again a linear system, but with an extended system order of $N + N_\Psi$.

In earthquake engineering only lowpass filter are of interest, and soil amplification is often modelled with the Kanai/Tajimi, a typical second order filtering function, see Clough-Penzien¹⁵ or Shinozuka¹⁴, which is given by

$$\xi_1(\omega) = H_1(\omega)\xi(\omega), \quad H_1(\omega) = \frac{1 + 2i\zeta_{\Psi_1}(\omega/\omega_{\Psi_1})}{(1 - (\omega/\omega_{\Psi_1})^2) + 2i\zeta_{\Psi_1}(\omega/\omega_{\Psi_1})}, \quad (7-45)$$

$$\xi_2(\omega) = H_2(\omega)\xi_1(\omega), \quad H_2(\omega) = \frac{(\omega/\omega_{\Psi_2})^2}{(1 - (\omega/\omega_{\Psi_2})^2) + 2i\zeta_{\Psi_2}(\omega/\omega_{\Psi_2})}. \quad (7-46)$$

Eq.(7-45) defines a low-pass filter function which amplifies the frequency content in the neighbourhood of $\omega = \omega_{\Psi_1}$ and attenuates the frequency content for $\omega > \omega_{\Psi_1}$ with 40dB per decade. The second filter equation, Eq.(7-46), attenuates the frequencies below $\omega < \omega_{\Psi_2}$. The parameters ω_{Ψ_1} and ζ_{Ψ_1} must be adapted to local soil conditions. ω_{Ψ_2} and ζ_{Ψ_2} can be adapted to produce the desired filtering of the very low frequencies. Assuming a physical white noise excitation, and putting the filtering equations in series generates the complete filter dynamics:

$$\xi_2(\omega) = H_1(\omega)H_2(\omega)\xi(\omega), \quad (7-47)$$

The spectral density of ξ_2 is given by

$$S_\Psi(\omega) = \frac{(1 + 4\zeta_{\Psi_1}^2(\omega/\omega_{\Psi_1})^2)(\omega/\omega_{\Psi_2})^2}{\left[(1 - (\omega/\omega_{\Psi_1})^2)^2 - 4\zeta_{\Psi_1}^2(\omega/\omega_{\Psi_1})^2 \right] \left[(1 - (\omega/\omega_{\Psi_2})^2)^2 - 4\zeta_{\Psi_2}^2(\omega/\omega_{\Psi_2})^2 \right]} S_0, \quad (7-48)$$

where S_0 describes the intensity of the physical white noise input. In Clough-Penzien¹⁵ the above given Eqs. (7-45)-(7-48) are applied to generate artificial earthquake ground motions. To account for the limited time of strong motion, the artificially generated physical white noise input is additionally multiplied with an envelope function. For the implementation of box-type or exponential envelope functions see Ziegler¹⁶ or Höllinger¹⁷, where Priestley's formula was adapted for nonstationary random excitation. The power spectral density $\bar{S}_{gg}(\omega) = H_1(\omega) \cdot S_0$ of the ground acceleration in Kanai-Tajimi representation, Eq.(7-45), as

a function of ω , $\omega_{\psi_1} = 20 \text{ rad/s}$, $\zeta_{\psi_1} = 0.8$, $S_0 = 260 \cdot 10^{-4} \text{ m}^2/\text{s}^3$, is given in Figure 7-2, see Hasenzagl et al.¹⁸

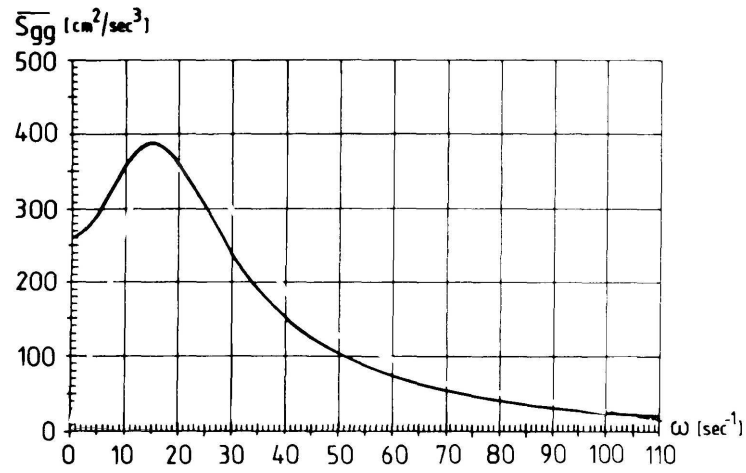


Figure 7-2: Power spectral density $\bar{S}_{gg}(\omega) = H_1(\omega) \cdot S_0$ of the ground acceleration in Kanai-Tajimi representation as a function of ω , $\omega_{\psi_1} = 20 \text{ rad/s}$, $\zeta_{\psi_1} = 0.8$, $S_0 = 260 \cdot 10^{-4} \text{ m}^2/\text{s}^3$, see Hasenzagl et al.¹⁸

7.6. Remarks on the numerical optimisation and choice of initial conditions

A common problem of numerical optimisation is the fact that most algorithms, e.g. all gradient methods, terminate in a local minimum, instead of finding the global minimum. The success of the numerical optimisation sometimes depends on the initial values (good estimates) for the design parameters. Several simulations have shown that the understanding of absorber dynamics helps when choosing the initial TLCD configuration. It is possible to find the global minimum after some trials. As a general rule, every TLCD should be used to reduce one single resonance only, and thus the initial natural TLCD-frequency can coincide with the structural resonant frequency. This rule of thumb is also valid, if several TLCDs are dedicated to a single resonant frequency. The choice of the position in the building is mainly determined by the structural mode shapes. The larger the modal displacements at a certain floor, the better the performance of the absorber, as discussed in Chapter 5. Once the initial configuration is found an optimisation using a gradient method quickly finds an optimal TLCD parameter design. According to the above given rule several other TLCD

configurations can be tested, and the optimal parameters can be quickly determined. For the optimisation itself standard numerical algorithms are applied, e.g. Matlab¹⁹.

7.7. References

- ¹ Müller, P.C., *Stabilität und Matrizen*, Springer Verlag Berlin, 1977
- ² Levine, W.S, (editor), *The Control Handbook*, CRC Press 1995
- ³ Müller, K., *Entwurf robuster Regelungen*, Teubner Stuttgart, 1996
- ⁴ Ludyk, G., *Theoretische Regelungstechnik 2*, Springer Lehrbuch, 1995
- ⁵ MATLAB, *User Guide, Control Toolbox*, MathWorks Inc., Version 5.3.1, 1984-2001
- ⁶ Lüke, H.D., *Signalübertragung*, Springer, 6th edition, 1995
- ⁷ Müller, P.C., Schiehlen, W.O., *Lineare Schwingungen*, Akademische Verlagsgesellschaft, Wiesbaden 1976
- ⁸ Lin, Y.K., Cai, G.Q., *Probabilistic Structural Dynamics*, McGraw-Hill, 1995
- ⁹ Newland, D.E., *An Introduction into Random Vibrations, Spectral & Wavelet Analysis*, 3rd ed., Longman Scientific and Technical, 1993
- ¹⁰ Parkus, H., *Random Processes in Mechanical Sciences*, CISM Courses and Lectures, Springer Verlag, 1969
- ¹¹ Wirsching P.H., Paez, T.L., Orin, K., *Random Vibrations*, John Wiley 1995
- ¹² Yang, C.Y., *Random Vibrations of Structures*, John Wiley 1986
- ¹³ Spanos, P.D., *Random Vibration and Statistical Linearisation*, John Wiley & Sons, 1990
- ¹⁴ Shinozuka, M., Schueller, G.I., *Stochastic Methods in Structural Dynamics*, Martinus Nijhoff Publishers, 1987
- ¹⁵ Clough, R.W., Penzien, J., *Dynamics of Structures*, 2nd ed., McGraw-Hill, New York, 1993
- ¹⁶ Ziegler, F., *Random Vibrations: A spectral method for linear and nonlinear structures*, Probabilistic Eng. Mech., vol.2(2), 1987
- ¹⁷ Höllinger, F., Ziegler, F., *Stationäre Zufallsschwingungen einer elastischen Gewichtsmauer bei beliebig geformtem Becken*, ZAMM, vol.63, pp.49-54, 1983
- ¹⁸ Hasenzagl, R., Irschik, H., Ziegler, F., *Design Charts for Random Vibrations of Elasto-plastic Oscillators Subjected to Kanai-Tajimi Spectra*, Reliability Engineering and System Safety, vol.23, pp.109-126, 1988
- ¹⁹ MATLAB, *User Guide, Optimisation Toolbox*, MathWorks Inc., 1984-2001

8. Active devices for vibration damping

The permanent research and investigation of structural dynamics in the last decades has resulted in the development of active structural control systems, which are a logical advance of passive systems with the innovative idea of injecting energy in the structural system to improve the dynamic response. The well investigated mechanism of passive energy dissipation has been extended by the option of an active energy manipulation. Therefore a central aspect of active control systems is their dependence on external power supply. In addition to a proper absorber design the choice of a suitable control strategy is an important aspect. In feedback control, measured response data are used to activate the control devices and in contrast to passive structural control where any energy dissipating device stabilises a structure, the energy input can have the converse effect of destabilisation, if the active control law is not well suited. Although the idea of feedback control is established in multi-body-mechanics, and important field of engineering mechanics, first applications in structural control were discussed in Leipholz¹, and it gained civil engineering relevance with the first full scale application in 1989, see Kobori², Sakamoto et al.³. Since then a lot of research has been undertaken, mainly to reduce installation and maintenance costs of active systems, to eliminate the dependence on external power supply, to gain acceptance of the non-traditional technology and to find suitable control strategies to increase reliability and system robustness. The need for active structural control arose in recent years as a trend in civil engineering design and construction towards relatively light and flexible structures with a low level of intrinsic damping, i.e. towards new vibration prone structures. A phenomenon which did rarely occur in traditionally designed constructions, as they relied on their strength and ductility, e.g. the ability to dissipate energy under severe dynamic loading. The level of vibration can either exceed safety criteria and cause structural failure, or cause occupant discomfort in case of wind gusts. Both situations create major problems, and the enormous amount of research which has been undertaken in the last decade, see e.g. the review paper by Housner et al.⁴, underlines the central importance of structural control.

Active structural control is commonly divided into semiactive, hybrid and purely active control. All different approaches have in common that there are several control parameters which are dependent on the structural state, which is in contrast to passive structural control.

8.1. Active control

In active structural control a desired system behaviour is obtained by the application of forces acting on the main structure. Several mechanisms have been investigated but amongst the most popular and thoroughly researched are the active mass drivers (AMD), the active tendon systems and the active bracing constructions. The former generates the active forces by the acceleration of an additional mass (inertia forces), whereas the two latter approaches alter the structural stiffness to obtain a desired dynamic behaviour. A schematic view of all three devices is given in Figure 8-1.

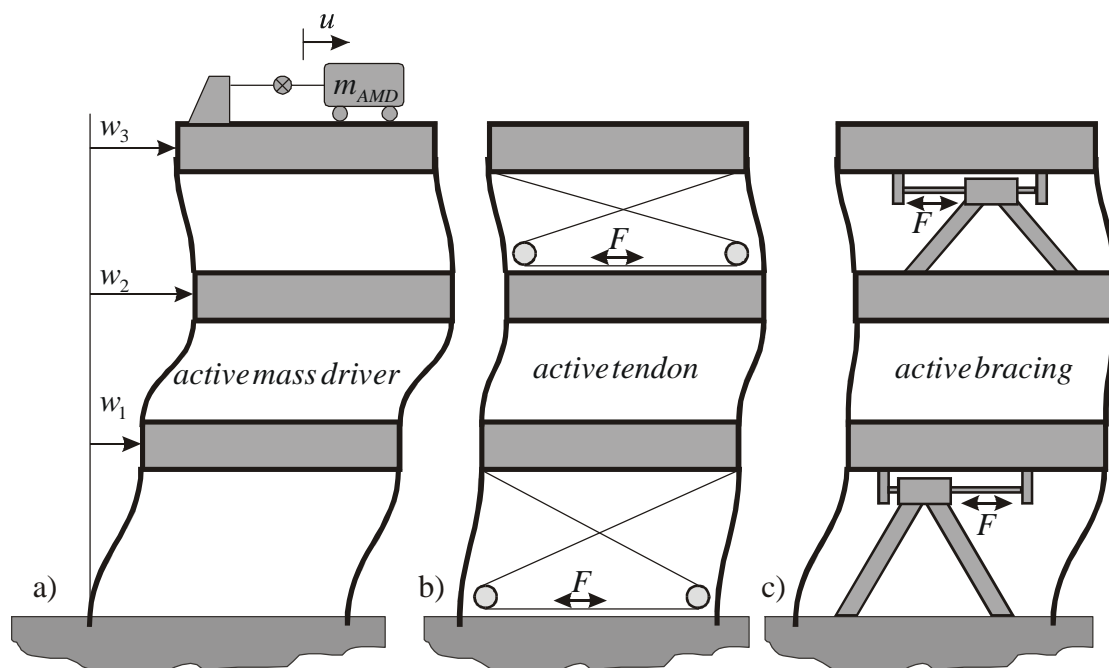


Figure 8-1: Typical active control devices: a) active tuned mass damper (ATMD) b) active tendon system c) active bracing construction

AMD are very popular, and have been used in the first full scale application of active control to a building, which was accomplished in 1989, see Spencer⁵, and again Kobori², Sakamoto et al.³. The Kyobashi Seiwa building, an 11-story structure in Tokyo, Japan, has 2 AMDs installed. The primary mass of 4000kg is designed to reduce bending motion, whereas the secondary mass of 1000kg mitigates torsional motion, see Figure 8-2

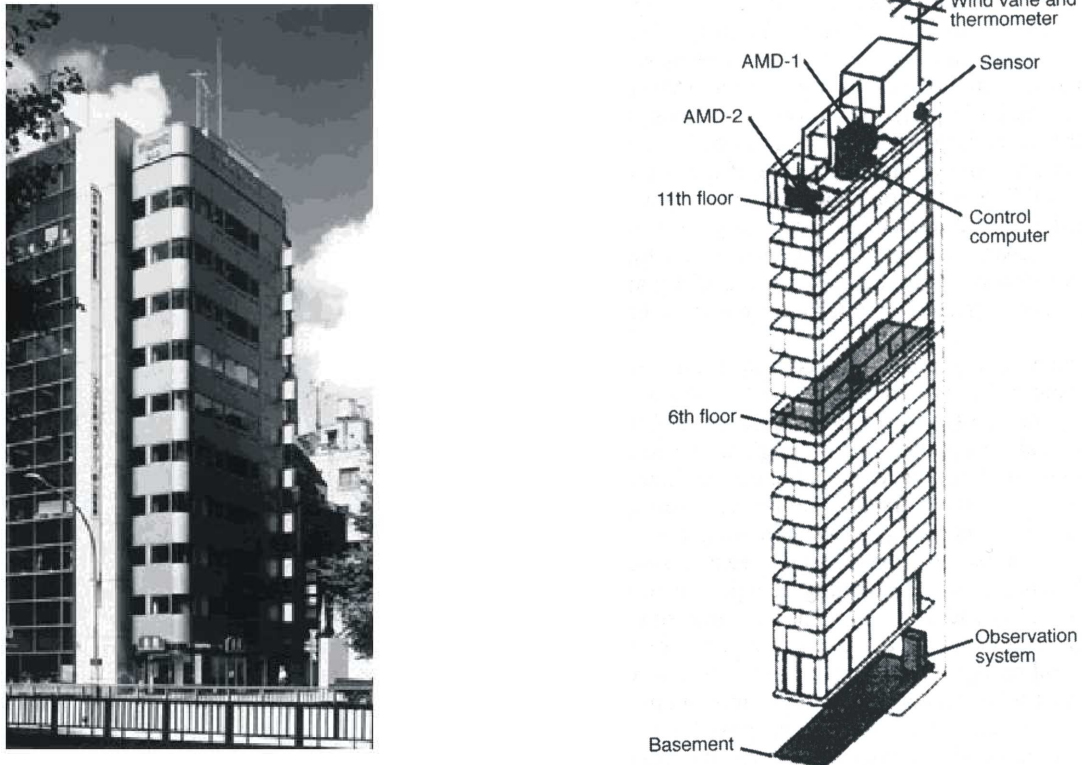


Figure 8-2: 11-story Kyobashi Seiwa building with AMD installation

This active system is designed to reduce vibrations due to strong wind gusts and moderate earthquakes and consequently increases the human comfort of occupants. In Nanjing, China, a 340-meter high television transmission and observation tower was recently constructed, where a 60.000kg ring shaped mass on sliding friction bearings is used as AMD to reduce wind induced vibrations when the human comfort limit is exceeded. The application of H_∞ control for active control devices in engineering structures in seismic zones has been investigated by Chase et al.⁶

8.2. Hybrid Control

If the performance of passive systems can be improved by the application of active elements hybrid control devices are generated. Typically, such a device has the vibration reducing capabilities of an active system while the amount of energy consumption is substantially reduced. Equally, a hybrid system can be obtained from an active system by adding a passive mechanism to decrease the energy requirements, thereby overcoming the limitations of purely passive systems, e.g. the limited frequency range where effective disturbance attenuation can be achieved. Hybrid systems have been applied successfully to buildings and bridges, and

Spencer⁵ reports about 30 structures which employ feedback control strategies, where a vast majority use hybrid control mechanisms. Up to date research has mainly focused on two different systems: hybrid mass dampers (HMD), also entitled active tuned mass damper (ATMD), and hybrid base isolation. An ATMD is obtained by adding together an active actuator to a TMD, see Figure 8-3a. As the main purpose of the ATMD still is energy dissipation, the major vibration reduction is due to the energy dissipating ability of the TMD. Whenever necessary, active forces from the actuator can be added to increase the efficiency or change the overall dynamics temporarily, according to the feedback control scheme. A variation of the ATMD which has also been studied intensively is obtained by adding an AMD on top of a passive TMD, for that DUOX HMD, see Figure 8-3 b.

The working principle of active TMD damper systems is identical to the one of passive systems, however, the reaction force acting on the structure can be actively influenced by the actuator force. ATMD are often referred to as inertia actuators, since the counteracting forces are applied to the absorber mass. The resultant force, acting on the structure can be obtained

by applying Eq.(4-25), $\frac{d\mathbf{I}}{dt} = \mathbf{F}$, where the total impulse is $\mathbf{I} = \int_m \mathbf{v}_{abs} dm = (\dot{u} + \dot{w}_f)m\mathbf{e}_x$, see

Figure 8-3a, and w_f denote the absolute floor displacement. The force acting on the structure becomes

$$\mathbf{F}_{TMD} = -m(\ddot{u} + \ddot{w}_f)\mathbf{e}_x,$$

where the reaction principle is applied, $\mathbf{F}_{TMD} = -\mathbf{F}$. Apparently the influence of the actuator does not explicitly appear in the reaction force, since it is included in the relative absorber mass acceleration \ddot{u} , which certainly differs from the acceleration of a passive TMD.

Several other important contributions have been made to develop practically, easy to install, and compact HMD. They have in common that they must be appropriate for long period vibrations. Koikie et al.⁷ have developed the V-shaped hybrid mass damper, installed in the 227m high 52-story Shinjuku Park Tower, the largest building in Japan in terms of square footage, see Figure 8-3c. A second development which has reached the level of structural implementation is the multi-step pendulum HMD, which has been installed in the 296m high, 70-story Yokohama Landmark Tower, Japan, see Yamazaki⁸, Figure 8-3d.

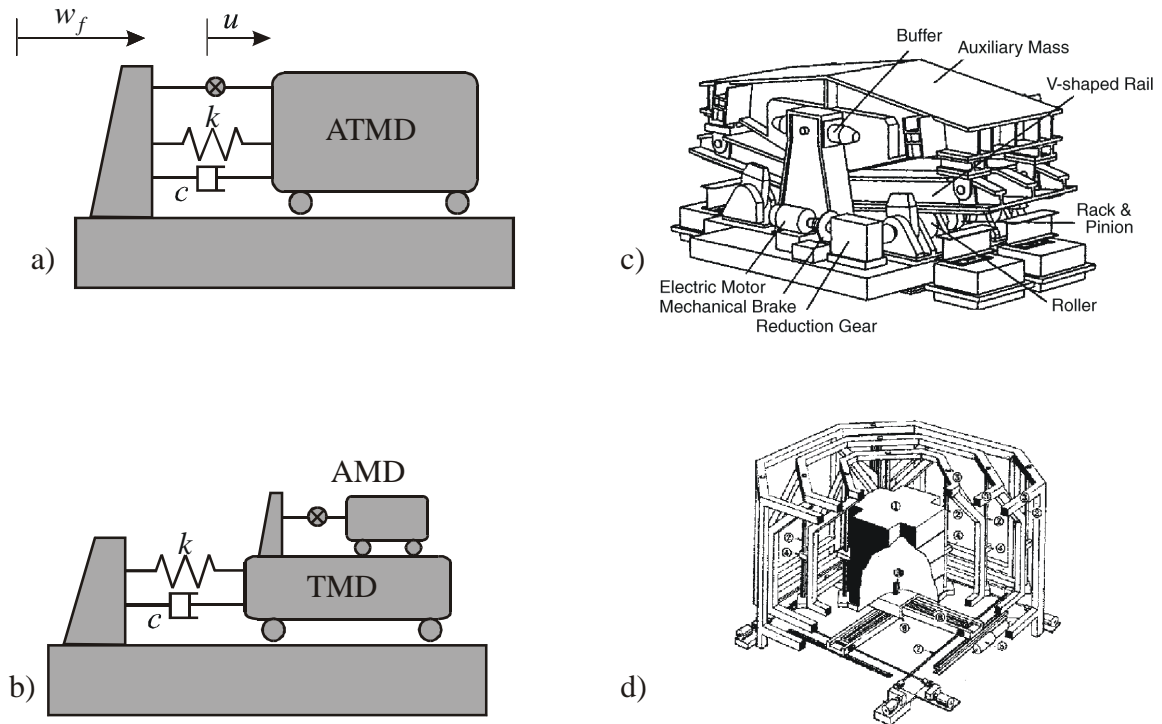


Figure 8-3: Hybrid control devices a) ATMD b) DUOX HMD [7] c) V-shaped Hybrid mass damper d) Multi step pendulum [8]

Hybrid base isolation systems consist of the well established passive base isolation system in parallel with an active control actuator to decrease the structural response further. Without a significant increase in cost, it is possible to add actuators at the base isolation level and reduce the large interstory drifts, as well as the absolute floor accelerations. Small scale experiments have been conducted by Reinhorn and Riley⁹. Schlacher et al.^{10,11,12,13}, Kugi et al.^{14,15} have recently proposed a nonlinear control law, based on feedback linearisation under the assumption of elastic plastic behaviour of the ductile structure, and achieved remarkably good results in disturbance attenuation.

8.3. Semi active control systems

While hybrid control systems still inject energy into the structural system and therefore depend on external power supply, the level of power consumption for semi-active control systems is orders of magnitude less. According to a widely accepted definition, a semi active control device cannot add mechanical energy into the controlled structural system, but has passive energy dissipation properties which can be adjusted to reduce the response of the

system. For that reason it does not have the potential to destabilise a structure. A possible semi-active device can, e.g. alter the damping coefficient of a conventional TMD. Generally, only minor adjustments of passive energy absorbing devices, like the introduction of controllable valves or resistances, are necessary for semi-active devices. Variable stiffness systems can also be categorised as semi-active as long as there is no energy injection into the structural system, see Lei^{16,17} for controlled bracing systems.

A different kind of semi-active device is obtained by adding a variable hydraulic resistance (variable orifice) to viscous fluid dampers and thus changing the dynamic characteristics of the damping device by this means. A similar mechanism can be applied in variable friction systems, which are used for structural bracing mechanisms.

In TLCD a controllable cross sectional area of an orifice plate along the liquid path can influence the turbulent damping, and thus the interaction forces. However, Haroun et al.¹⁸ and Abé¹⁹ have investigated a semi-active TLCD, with the negative result that the reduction of the structural response is rather negligible when compared to a system with constant head loss factor. On the other hand, Dyke et al.²⁰ report the possibility of effective response reduction over a wide range of loading conditions when investigating other types of semi-active damping devices. Another group of vibration dampers use intelligent materials like electrorheological and magnetorheological fluids which have viscous properties depending on an applied electric and magnetic field, respectively. It is therefore straightforward to construct a semi-active device using those materials, see e.g. Gavin^{21,22}, Ribakov et al.²³, Burton et al.²⁴

8.4. Active Tuned Liquid Column Damper (ATLCD)

Since the TLCD considered in the Sections 4-7 is a purely passive device, an active tuned liquid column damper (ATLCD) must be a vibration reducing construction which inherits the ability to dissipate mechanical energy, but is on the other hand able to actively inject energy while reducing the structural response at the same time. Similar to an ATMD, the active behaviour is obtained by forcing the liquid column to move through the piping system. Different working principles are possible, e.g. the application of pumps, but since mechanically moving parts should be avoided, a much more elegant way is to adjust the pressure in the gas (air) chamber at the end of the liquid column using a pressurised reservoir, as shown in Figure 8-4. When releasing the compressed gas from the air chamber there are

reaction forces due to the exhaust stream, which can be neglected since the gas density is small, even for the compressed gas.

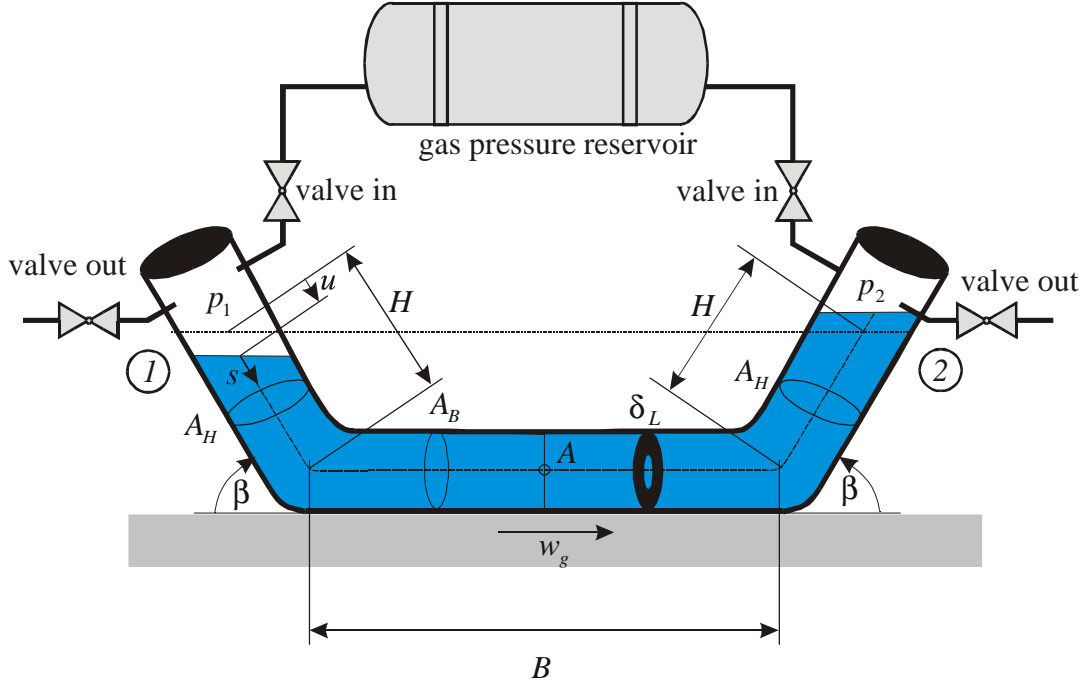


Figure 8-4: ATLCD with pressurised gas supply and input-output valves

Because the working principles of TLCDs and the ATLCDs are identical, the already derived equations of motion for the TLCD can be extended to provide the desired influence on the absorber dynamics. Bernoulli's equation for moving reference frames, see again Ziegler²⁵, p.497, allows deep insight into the TLCD and a direct derivation of the ATLCD's equation of motion thus becomes possible. For inplane motion it is given by, see Eq.(4-23) and Section 4.1.2 for details,

$$\int_0^{2H+B} \frac{\partial u}{\partial t} ds = -g(z_2 - z_1) - \frac{1}{\rho}(p_2 - p_1) - \frac{1}{\rho}\Delta p_L - \int_0^{2H+B} \ddot{w}_g \mathbf{e}_x \cdot \mathbf{e}_t' ds. \quad (8-1)$$

As the operating range is limited to low frequencies only, a quasi-static approach is chosen to compute the pressure difference $\Delta p = p_2 - p_1 = \Delta p_a + \Delta p_p$, where Δp_a represents the actively controlled pressure difference due to gas injection and Δp_p denotes the passive pressure change due to the liquid motion, Eq.(4-40), where it has already been shown that Δp_p is given by, $u_1 = u_2 = u$,

$$\Delta p_p(u) = \frac{2n p_0 A_H}{V_0} u + O(u^3) \approx \frac{2n p_0}{h_{eff}} u = 2K_n u / h_{eff} \quad (8-2)$$

$$h_{eff} = V_0 / A_H, \quad K_n = n p_0.$$

The active pressure change Δp_a can be achieved via the active injection or removal of gas.

Starting from the polytropic material law for gases, with the polytropic index n

$$(p/p_i) = (\rho/\rho_i)^n, \quad (8-3)$$

or equivalently in its incremental form

$$dp = K_t \frac{d\rho}{\rho}, \quad K_t = n p \quad (8-4)$$

where K_t denotes the tangent modulus, an instantaneous change in the gas mass Δm_g will cause a change in the ratio of the mass densities. Assuming a constant gas volume during the instantaneous gas injection/extraction, the mass density ratio is given by $\rho/\rho_i = 1 + \Delta m_g / m_g$ and consequently the pressure change $\Delta p_a = p - p_i$ is found to be

$$\Delta p_a = p_i \left(\left(1 + \Delta m_g / m_g \right)^n - 1 \right), \quad (8-5)$$

where the index i indicates the gas properties just before the mass change. This active pressure modification is possible on either side of the liquid column, and hence any desired pressure can be obtained by a combination of gas injection and removal at both air springs. Since the injection of the gas mass is a continuous process, there is no pressure jump, but a smooth increase in the internal pressure. Inserting Eqs.(8-5) and (8-2) into Eq.(8-1) renders the equation of motion for the base excited TLCD with active instant pressure regulation as, see again Eq.(4-40), for the passive TLCD, note the linearised damping term,

$$\ddot{u} + 2\zeta_A \omega_A \dot{u} + \omega_A^2 u = -\kappa \ddot{w}_f - \Delta p_a^*, \quad (8-6)$$

$$\Delta p_a^* = \frac{\Delta p_a}{\rho L_{eff}}, \quad L_{eff} = \left(2H + \frac{A_H}{A_B} B \right), \quad \omega_A = \sqrt{\frac{2g \sin \beta + 2K_n / (\rho h_{eff})}{L_{eff}}}, \quad 2\zeta_A \omega_A \dot{u} = \frac{\Delta p_L}{\rho L_{eff}},$$

$$\kappa = \frac{2H \cos \beta + B}{L_{eff}}$$

where ω_A , ζ_A and κ are the linear natural circular frequency, the linear equivalent turbulent damping coefficient and the geometry dependent excitation influence factor of the TLCD, respectively. Obviously the pressure adjustment can be regarded as external excitation, used to obtain a desired structure-absorber interaction. The coupling force f between the structure and the ATLCD is obtained by applying the linear momentum equation along the TLCD base orientation and as the influence of the active pressure variation is included in the liquid column acceleration \ddot{u} , see also Section 8.2 for the active TMD, the expression for f is identical with that of the passive TLCD, see Eq.(4-29),

$$f_x = -m_f (\ddot{w}_f + \ddot{u} \bar{\kappa}), \quad (8-7)$$

$$\bar{\kappa} = \kappa \left(1 + \frac{A_H}{A_B} \frac{B}{2H} \right) \left/ \left(1 + \frac{B}{2H} \frac{A_B}{A_H} \right) \right. = \frac{\rho A_H B + 2 \rho A_H H \cos \beta}{m_f}.$$

Again, $m_f = \rho A_H (2H + B A_B / A_H)$ and $\bar{\kappa}$ denote the mass of the moving liquid and a geometry factor, respectively. Exactly the same derivations can be applied to the torsional TLCD, rendering an additional excitation term in the equation of motion which is generalised to, see Eq.(4-50), where A_p is defined in Eq.(4-49) and denotes the area enclosed by the projection of the TLCD onto the rigid floor, see Fig(4-5)b,

$$\ddot{u} + 2 \zeta_A \omega_A \dot{u} + \omega_A^2 u = -2 A_p \dot{\omega}_z - \Delta p_a^*, \quad (8-8)$$

$$\Delta p_a^* = \frac{\Delta p_a}{\rho L_{eff}}, \quad L_{eff} = \int_0^{2H+B} \frac{A_H}{A(s)} ds, \quad \omega_A = \sqrt{\frac{2g \sin \beta + 2 K_n / (\rho h_{eff})}{L_{eff}}}, \quad 2 \zeta_A \omega_A \dot{u} = \frac{\Delta p_L}{\rho L_{eff}},$$

For the symmetric arrangement of two TLCD, discussed in Section 4.4.3, the interaction forces are given by the same expression, however, the actively controlled differential pressure Δp_a^* is included in \ddot{u} ,

$$\mathbf{M}_{TLCD} = -m_f (r_f^2 \ddot{\omega}_z + \bar{r}_f \ddot{u}) \mathbf{e}_z - \rho A_H \sin \beta (H^2 + u^2) \mathbf{e}_z \times \ddot{\mathbf{w}}_g \quad (8-9)$$

8.4.1. State space representation

It has already been shown that the state space representation is a useful description for discretised dynamic systems, and it has been discussed in Chapter 7. We recall that for active TLCD's equation of motion can be generalised to

$$\dot{\mathbf{z}} = \mathbf{A}_r \mathbf{z} + \mathbf{E}_{eff} \mathbf{f}_{eff}(t) + \mathbf{E}_a \Delta \mathbf{p}_a^*, \quad \mathbf{A}_r = \mathbf{A} + \mathbf{B} \mathbf{R} \quad (8-10)$$

$$\mathbf{y} = \mathbf{C}_r \mathbf{z} + \mathbf{D}_{eff} \mathbf{f}_{eff} + \mathbf{D}_a \Delta \mathbf{p}_a^*,$$

$$\mathbf{E}_{eff} \mathbf{f}_{eff}(t) = -\mathbf{e}_g \ddot{\mathbf{w}}_g + \mathbf{E}_f \mathbf{f}, \quad \Delta \mathbf{p}_a^* = [\Delta p_{a,1}^*, \dots, \Delta p_{a,i}^*, \dots, \Delta p_{a,n}^*]$$

$$\mathbf{E}_a = \begin{pmatrix} \mathbf{0} \\ \mathbf{0} \\ -\mathbf{M}_S^{-1} \begin{pmatrix} \mathbf{0} \\ \mathbf{I} \end{pmatrix} \end{pmatrix},$$

where \mathbf{A} , \mathbf{B} , \mathbf{R} , \mathbf{e}_g , \mathbf{E}_f are given by Eq.(7-12), and \mathbf{E}_a , $\Delta \mathbf{p}_a^*$ denote the pressure influence matrix and the vector of active input-pressure changes, respectively. The output matrices \mathbf{D}_a and \mathbf{D}_{eff} depend on the actual output quantity of interest, and both matrices vanish if floor displacements or velocities are calculated. Because $\Delta \mathbf{p}_a^*$, whose components denote the pressure input to the n ATLCD, can be chosen arbitrarily, Eq.(8-10) represents a standard feedback control problem.

The following section will deal with some aspects of feedback control and design, focused on the linear quadratic optimal control. Since it is possible to actively influence the TLCD vibration, a typical hybrid actuator has been created. If the energy supply fails, the ATLCD acts still as the passive damping device. Therefore the passive TLCD design is not influenced by the active pressure input, and follows the guidelines outlined in Chapter 4. For better peak response reduction, particularly in the transient vibration regime, e.g. during (short-time, typically much less than 1 minute) strong motion phases of earthquakes, the active pressure regulation can be used. It is assumed that the optimal passive TLCD-parameter have already been determined (\mathbf{R} is fixed), and only the optimal control law must be found.

8.5. Optimal control

The main task for the active feedback control is to find a suitable instantaneous pressure input $\Delta \mathbf{p}_a^*(t)$, based on measured or estimated system states which guarantees a desired dynamic behaviour. Certainly practical considerations, like limited pressure input or maximum absorber displacements, must also be taken into account. The scientific discipline of control engineering offers a variety of different approaches to obtain suitable feedback control laws, but most approaches are quite involved from a mathematical point of view. However, as long as linear systems are considered, a significant reduction of complexity is possible, and several simple and easy to follow design methodologies are available. An excellent overview over standard control problems can be found in the Control Handbook²⁶, and a highly regarded book about structural control has been recently published by Soong²⁷. If it is possible to define performance criteria which must be minimised, the well researched field of optimal control theory offers powerful and easy to apply design tools. For this reason most of the derivations and considerations are directly related to optimal control theory. Leading publications on optimal control are e.g. Föllinger²⁸, Stengel²⁹, or Lewis³⁰. The classical linear quadratic regulator (LQR) design is a straightforward approach to optimal control. To be compatible with the nomenclature in control literature, the pressure input vector $\Delta \mathbf{p}_a^*(t)$ is substituted by the control vector $\mathbf{u}_a(t)$. No conflict of notation is to be expected with the displacement of the fluid in the TLCD since the latter is hidden in the state vector \mathbf{z} within this section. If a quadratic performance index

$$J = \Phi(\mathbf{z}(T_f)) + \frac{1}{2} \int_0^{T_f} (\mathbf{z}^T \mathbf{Q} \mathbf{z} + \mathbf{u}_a^T \mathbf{S} \mathbf{u}_a) dt. \quad (8-11)$$

is selected as a measure for vibration sensitivity, then an optimal behaviour can be expected if J becomes minimal. Via the positive semidefinite weighing matrices \mathbf{Q} the influence of certain states on the performance index can be regulated whereas the positive definite matrix \mathbf{S} can be used to manipulate the control forces and thus the energy input into the structural system. As there is no fixed final state in structural control, the term $\Phi(\mathbf{z}(T_f))$ can be used to force the free final state to be close to a desired value. However, generally this weighing function is zero in structural applications, and as the final time T_f is chosen arbitrarily,

Eq.(8-11) can be optimised with respect to the input vector \mathbf{u}_a and the “dynamic boundary condition” given by the system dynamics. The equations of motion can be integrated into the performance index using the Lagrange multiplier method,

$$J = \frac{1}{2} \int_0^{T_f} \left[\mathbf{z}^T \mathbf{Q} \mathbf{z} + \mathbf{u}_a^T \mathbf{S} \mathbf{u}_a + 2\boldsymbol{\lambda}^T (\mathbf{A}_r \mathbf{z} + \mathbf{E}_{eff} \mathbf{f}_{eff} + \mathbf{E}_a \mathbf{u}_a - \dot{\mathbf{z}}) \right] dt \quad (8-12)$$

where $\boldsymbol{\lambda}$ denotes the Lagrange multiplier, occasionally denoted as the co-state vector. The Hamiltonian function corresponding to Eq.(8-12) is defined by

$$H = \frac{1}{2} (\mathbf{z}^T \mathbf{Q} \mathbf{z} + \mathbf{u}_a^T \mathbf{S} \mathbf{u}_a) + \boldsymbol{\lambda}^T (\mathbf{A}_r \mathbf{z} + \mathbf{E}_{eff} \mathbf{f}_{eff} + \mathbf{E}_a \mathbf{u}_a). \quad (8-13)$$

Whether the excitation terms are included in Eq. (8-12) and thus in the Hamiltonian function mainly depends on the character of the disturbance. If it is explicitly known, it should be taken into account. If little is known about the excitation, e.g. if it is random in nature, the forcing terms are normally neglected in the Hamiltonian H , and thus, the optimisation is performed for the reduction of free vibrations which ensures good disturbance attenuation as well. Independent of the excitation terms, the necessary conditions for optimality are, see e.g. Lewis³⁰

$$\frac{\partial H}{\partial \mathbf{u}_a} = \mathbf{0}, \quad \frac{\partial H}{\partial \boldsymbol{\lambda}} = \dot{\mathbf{z}}, \quad -\dot{\boldsymbol{\lambda}} = \frac{\partial H}{\partial \mathbf{z}}, \quad \boldsymbol{\lambda}^T(T_f) = 0. \quad (8-14)$$

Carrying out the partial derivatives, setting $\boldsymbol{\lambda} = \mathbf{P} \mathbf{z} + \mathbf{q}$, see e.g. Yang³¹, with an unknown, time dependent matrix \mathbf{P} , and solving for the input vector \mathbf{u}_a yields:

$$\mathbf{u}_a = -\mathbf{S}^{-1} \mathbf{E}_a^T \boldsymbol{\lambda}, \quad (8-15)$$

$$-\dot{\mathbf{P}} = -\mathbf{P} \mathbf{E}_a \mathbf{S}^{-1} \mathbf{E}_a^T \mathbf{P} + \mathbf{P} \mathbf{A}_r + \mathbf{A}_r^T \mathbf{P} + \mathbf{Q}, \quad (8-16)$$

$$\dot{\mathbf{q}} = (\mathbf{P} \mathbf{E}_a \mathbf{S}^{-1} \mathbf{E}_a^T - \mathbf{A}_r^T) \mathbf{q} - \mathbf{P} \mathbf{E}_{eff} \mathbf{f}_{eff}, \quad (8-17)$$

$$\boldsymbol{\lambda}(T_f) = \mathbf{0}. \quad (8-18)$$

Equation (8-16) is known as the Riccati matrix differential equation, and, to be able to solve it, the boundary condition $\lambda(T_f) = \mathbf{0}$ must hold. Thus it must be solved backwards in time and consequently the entire load history must be known (including future loads), to perform optimal control. This non-causal demand is the reason why random excitation terms are neglected in basic optimal control, and thus Eq.(8-17) vanishes. When solving Eq.(8-16), it becomes apparent, that $\mathbf{P}(t)$ establishes a stationary state in a very short period of time starting from T_f backwards. Thus the time derivative vanishes for sufficiently long observation periods and the matrix differential Eq.(8-16) can be approximated by the algebraic Riccati matrix equation

$$-\mathbf{P}\mathbf{E}_a\mathbf{S}^{-1}\mathbf{E}_a^T\mathbf{P} + \mathbf{P}\mathbf{A}_r + \mathbf{A}_r^T\mathbf{P} + \mathbf{Q} = \mathbf{0}, \quad (8-19)$$

and further, the optimal feedback control law becomes a linear state feedback given by substituting $\lambda = \mathbf{P}\mathbf{z}$ into Eq.(8-15)

$$\mathbf{u}_a = -\mathbf{S}^{-1}\mathbf{E}_a^T\mathbf{P}\mathbf{z}. \quad (8-20)$$

It must be emphasised, that the optimal closed-loop control requires the feedback measurements of the full state vector $\mathbf{z}(t)$, but such a complete measurement is hardly possible for large buildings. One possibility to circumvent this difficulty is to utilise state estimating filters, which reconstruct the full state vector from scarce measured inputs. In control literature such filters are denoted Luenberger estimators, or Kalman filters, see e.g. Levine²⁶.

For optimal control, based on a performance index J it is important to select the weighing matrices \mathbf{Q} and \mathbf{S} such that J represents physical quantities to be minimised. Displacements, velocities or accelerations can be calculated by linear combination of the states. Similarly, the relative instantaneous energy stored in the structure of interest can be given by, see Eq.(1-49) and (1-51), $E = E_k + E_s = \frac{1}{2}(\dot{\mathbf{w}}^T\mathbf{M}\dot{\mathbf{w}} + \mathbf{w}^T\mathbf{K}\mathbf{w})$ and thus the weighing matrix \mathbf{Q} , given in hyper matrix notation

$$\mathbf{Q} = \begin{pmatrix} \mathbf{K} & \mathbf{0} & \mathbf{0} & \mathbf{0} \\ \mathbf{0} & \mathbf{0} & \mathbf{0} & \mathbf{0} \\ \mathbf{0} & \mathbf{0} & \mathbf{M} & \mathbf{0} \\ \mathbf{0} & \mathbf{0} & \mathbf{0} & \mathbf{0} \end{pmatrix}, \quad (8-21)$$

will be appropriate to minimise the overall structural energy. Certainly it is useful to include the TLCD's state in the performance index, to avoid large liquid displacements or velocities. The pressure applied to the TLCD can be influenced directly by means of the input-weighting matrix \mathbf{S} or indirectly by the contributions of the TLCD's state to the performance index. For the choice of the weighing matrices there are no strict rules, and the performance of the control law obtained by optimal control must always be checked by simulations. Normally several iterations (trial and error) are necessary to achieve best performance.

An alternative method for optimal control without state estimation is output feedback control. Let the measurable quantities during free vibrations, $\mathbf{f}_{eff} = \mathbf{0}$, are described by the output equation

$$\mathbf{y} = \mathbf{C}_r \mathbf{z} + \mathbf{D}_a \mathbf{u}_a, \quad (8-22)$$

and the performance index is given by

$$J = \frac{1}{2} \int_0^{\infty} (\mathbf{z}^T \mathbf{Q} \mathbf{z} + \mathbf{u}_a^T \mathbf{S} \mathbf{u}_a) dt. \quad (8-23)$$

Assuming the linear output feedback control law,

$$\mathbf{u}_a = -\mathbf{K} \mathbf{y}, \quad (8-24)$$

then the new system dynamics is given by

$$\dot{\mathbf{z}} = (\mathbf{A}_r - \mathbf{E}_a (\mathbf{I} + \mathbf{K} \mathbf{D}_a)^{-1} \mathbf{K} \mathbf{C}_r) \mathbf{z} = \bar{\mathbf{A}} \mathbf{z}, \quad (8-25)$$

insertion of Eqs.(8-22) and (8-24) into Eq.(8-23) renders

$$J = \frac{1}{2} \int_0^{\infty} \left[\mathbf{z}^T \left(\mathbf{Q} + \mathbf{C}_r^T \mathbf{K}^T (\mathbf{I} + \mathbf{K} \mathbf{D}_a)^{-1} \mathbf{S} (\mathbf{I} + \mathbf{K} \mathbf{D}_a)^{-1} \mathbf{K} \mathbf{C}_r \right) \mathbf{z} \right] dt. \quad (8-26)$$

Comparison with Eq.(7-14) directly yields

$$J = \mathbf{z}_0^T \mathbf{P} \mathbf{z}_0 \quad (8-27)$$

where

$$\bar{\mathbf{A}}^T \mathbf{P} + \mathbf{P} \bar{\mathbf{A}} + \left(\mathbf{Q} + \mathbf{C}_r^T \mathbf{K}^T (\mathbf{I} + \mathbf{K} \mathbf{D}_a)^{-1^T} \mathbf{S} (\mathbf{I} + \mathbf{K} \mathbf{D}_a)^{-1} \mathbf{K} \mathbf{C}_r \right) = \mathbf{0}. \quad (8-28)$$

A numerical optimisation algorithm can now be applied, to minimise J . The initial value problem, \mathbf{z}_0 must be known to calculate J , can be circumvented if the expectation value of the performance index is minimised, see Lewis³⁰,

$$J = E \left[\frac{1}{2} \int_0^\infty \left(\mathbf{z}^T \mathbf{Q} \mathbf{z} + \mathbf{u}_a^T \mathbf{S} \mathbf{u}_a \right) dt \right] = \frac{1}{2} E \left[\mathbf{z}_0^T \mathbf{P} \mathbf{z}_0 \right] = \frac{1}{2} \text{trace}(\mathbf{P} \mathbf{Z}), \quad (8-29)$$

$$\mathbf{Z} = E \left[\mathbf{z}_0 \mathbf{z}_0^T \right],$$

where \mathbf{Z} denote the initial autocorrelation of the state. Lewis also derives a set of optimal gain equations, which define \mathbf{K} for the special case of $\mathbf{D}_a = 0$, thus $\mathbf{y} = \mathbf{C}_r \mathbf{z}$,

$$\bar{\mathbf{A}}^T \mathbf{P} + \mathbf{P} \bar{\mathbf{A}} + \mathbf{C}_r^T \mathbf{K}^T \mathbf{S} \mathbf{K} \mathbf{C}_r + \mathbf{Q} = \mathbf{0}, \quad (8-30)$$

$$\bar{\mathbf{A}} \mathbf{L} + \mathbf{L} \bar{\mathbf{A}}^T + \mathbf{Z} = \mathbf{0},$$

$$\mathbf{K} = \mathbf{S}^{-1} \mathbf{E}_a^T \mathbf{P} \mathbf{L} \mathbf{C}_r^T (\mathbf{C}_r \mathbf{L} \mathbf{C}_r^T)^{-1}.$$

Solving Eq.(8-30) is still cumbersome as there are no closed form solutions, but for stable systems simple iterative solution algorithms exist, see Lewis³⁰.

8.6. Modal control

If a state or output feedback controller has been designed, the pressure input is chosen to minimise the overall response, independent of the individual contributions of the vibration modes on the total structural response. Commonly, for the forcing taken into account here, the first few modal contributions dominate the MDOF-system response, and it seems reasonable to dedicate each ATLCD to a vibration mode shape and its corresponding natural frequency,

similar to the passive TLCD design. The advantage of such an assignment is that absorbers tuned to low frequencies do not have to respond to high frequency excitation, and vice versa. This reduces the gas consumption of the active system, and saves a lot of energy, because due to different liquid column displacements the volume V_0 for long-period-TLCD is much larger than for short-period-TLCD. Although perfect modal control is not possible because of the mode-coupling effect of the ATLCD, the spillover (excitation from modal coupling) is often negligible when compared to the external excitation. Modal control has turned out to be very efficient in the reduction of interstory displacements, even if it is only activated above a certain vibrational response level but combined with a switching control law. Details about this control strategy are given in the next section.

8.7. Polynomial and switching control laws

Sufficiently small vibration amplitudes do not influence human comfort and structural safety in civil engineering structures. Therefore structural control must aim at effective peak response reduction. Although linear quadratic optimal control reduces peak responses, a modified performance index, which is not only a function of quadratic states but also includes cubic or even higher order functions of the state, can achieve better maximum response reduction. Wu et al.³² have used a forth order performance index and Agrawal et al.³³ have applied performance indices of arbitrary order to structural control problems. The forth order performance index is a generalisation of Eq.(8-11), $\Phi = 0$,

$$J = \frac{1}{2} \int_0^{T_f} \left[\mathbf{z}^T \mathbf{Q} \mathbf{z} (1 + \alpha \mathbf{z}^T \mathbf{P} \mathbf{z}) + (\alpha \mathbf{z}^T \mathbf{P} \mathbf{z}) \mathbf{z}^T \mathbf{P} \mathbf{E}_a \mathbf{S}^{-1} \mathbf{E}_a^T \mathbf{P} \mathbf{z} (1 + \alpha \mathbf{z}^T \mathbf{P} \mathbf{z}) + \mathbf{u}_a^T \mathbf{S} \mathbf{u}_a \right] dt, \quad (8-31)$$

in which \mathbf{S} and \mathbf{Q} are the same matrices as in optimal quadratic control, α is a positive, nonlinear feedback weighing factor, and \mathbf{P} is an unknown positive definite symmetric matrix, similar to the quadratic optimal control. The Hamiltonian can be constructed analogously to Eq.(8-13) and the necessary conditions of Eqs.(8-14) do still hold. Minimising Eq.(8-31) for long observation intervals, and solving for the control forces renders

$$\mathbf{u}_a = -\left(1 + \alpha \mathbf{z}^T \mathbf{P} \mathbf{z}\right) \mathbf{S}^{-1} \mathbf{E}_a^T \mathbf{P} \mathbf{z}, \quad (8-32)$$

where \mathbf{P} is the solution of the standard Riccati equation

$$\mathbf{A}_r^T \mathbf{P} + \mathbf{P} \mathbf{A}_r - \mathbf{P} \mathbf{E}_a \mathbf{S}^{-1} \mathbf{E}_a^T \mathbf{P} + \mathbf{Q} = \mathbf{0}, \quad (8-33)$$

Apparently the equations for the standard linear quadratic control law are obtained if $\alpha = 0$. It should be emphasised, that the only difference between the linear and the nonlinear control law lies in the feedback gain factor $(1 + \alpha \mathbf{z}^T \mathbf{P} \mathbf{z})$. Clearly, the feedback force is increased according to the quadratic state function $\alpha \mathbf{z}^T \mathbf{P} \mathbf{z}$. As Eq.(8-32) guarantees optimality for all values of $\alpha > 0$ a simple bang-bang control strategy can be chosen to control a single actuator application,

$$u_a = \begin{cases} +u_{a,\max} & \text{if } \mathbf{S}^{-1} \mathbf{E}_a^T \mathbf{P} \mathbf{z} < 0 \\ -u_{a,\max} & \text{if } \mathbf{S}^{-1} \mathbf{E}_a^T \mathbf{P} \mathbf{z} > 0 \end{cases}, \quad (8-34)$$

Such a control law is particularly useful when it is combined with modal control, because at resonance, the switching frequency is in the range of the natural frequency.

The active air spring concept introduced in this Chapter is an extension of the passive control scheme and it acts as supplement to the passive TLCD. Thus it should help to dissipate structural energy when the passive conventional TLCD is not operating properly. Therefore the activation of the active pressure control should be limited to situations where the structural energy exceeds a certain limit and the TLCD's energy dissipation is low, which corresponds to low flow velocities. If the TLCD has high flow velocities, a lot of energy is dissipated via turbulent damping, and no active enhancement is necessary. This control strategy, illustrated in Figure 8-5, where the instantaneous, relative energy density is shown for a transient ground excitation, has proven to work satisfactorily for displacement reductions during the strong motion phase of earthquakes, but the activation limits have to be chosen carefully in order to minimise the energy consumption. The only drawback of modal control is the determination of the modal coordinates, enhancing the need for the application of state estimating filters, which is complicating the control devices over those needed for output feedback. Positively we note the possibility of the application of the simple bang-bang control law, working independently of the available pressure and guaranteeing stability as long as the sign of the applied pressure is correct. Thus it is extremely robust with respect to pressure variations.

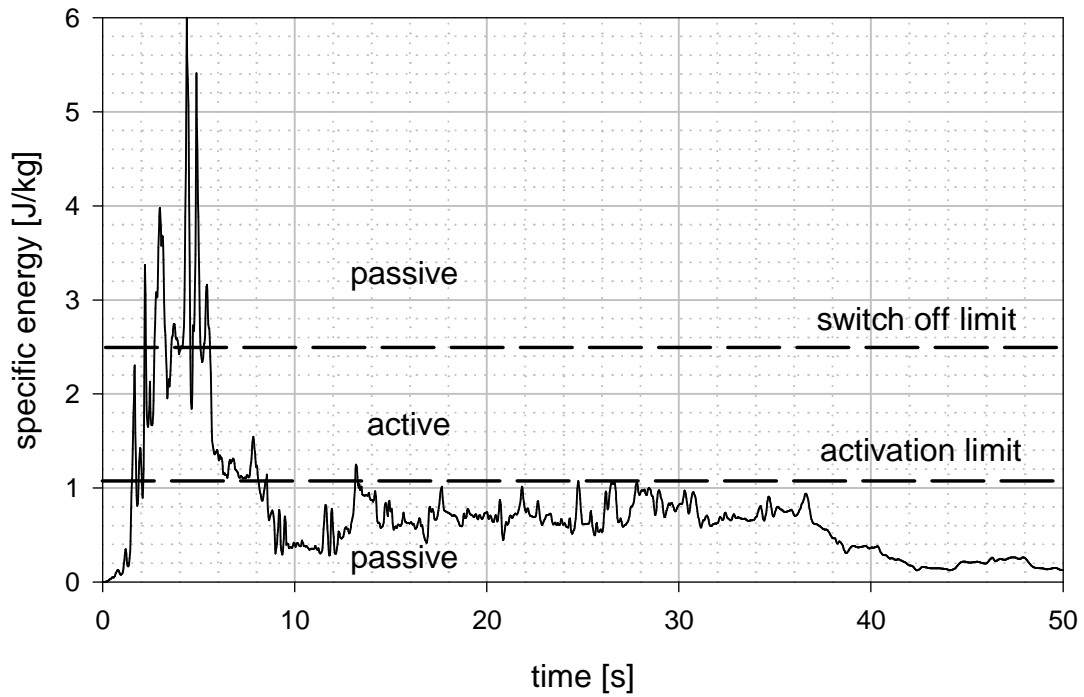


Figure 8-5: Activation and switch off levels of ATLCD

When working in the context of variable structure control theory, see e.g. DeCarlo et al.³⁴, a generalisation of the control law proposed in Eq.(8-32) to multiple ATLCD is possible. The idea of variable structure control is to apply a switching control law to guarantee that the state of a system slides along a predefined trajectory, thus this type of control is also called sliding mode control. It is well known, that sliding mode control is very robust with respect to parameter variations and can perform much better than linear control laws. Assuming that the control input is given by

$$\mathbf{u}_a = -\mathbf{U}_{\max} \text{sign}(\mathbf{s}), \quad (8-35)$$

$$\mathbf{s} = \mathbf{E}_a^T \mathbf{P} \mathbf{z}, \quad \mathbf{U}_{\max} = \text{diag}(u_{\max,1}, \dots, u_{\max,n})$$

with the yet unknown matrix \mathbf{P} , and the positive definite diagonal matrix \mathbf{U}_{\max} , which contains the maximal possible input pressure differences. Under the assumption of negligible external excitation, $\mathbf{f}_{\text{eff}} = 0$, Lyapunov's direct method is applied to show stability of the switching control law given by Eq.(8-35). Let the positive definite Lyapunov function V and its time derivative be given by

$$V = \mathbf{z}^T \mathbf{P} \mathbf{z}, \quad (8-36)$$

$$\dot{V} = \dot{\mathbf{z}}^T \mathbf{P} \mathbf{z} + \mathbf{z}^T \mathbf{P} \dot{\mathbf{z}}. \quad (8-37)$$

Inserting $\dot{\mathbf{z}}$ from Eq.(8-10) into Eq.(8-36) yields

$$\dot{V} = \mathbf{z}^T (\mathbf{A}_r^T \mathbf{P} + \mathbf{P} \mathbf{A}_r) \mathbf{z} + \mathbf{z}^T \mathbf{P} \mathbf{E}_a \mathbf{u}_a + \mathbf{u}_a^T \mathbf{E}_a^T \mathbf{P} \mathbf{z}, \quad (8-38)$$

Selecting \mathbf{P} such, that it is the solution of the Lyapunov equation $\mathbf{A}_r^T \mathbf{P} + \mathbf{P} \mathbf{A}_r + \mathbf{Q} = 0$, with an arbitrary positive definite matrix \mathbf{Q} , and taking the transposed of the scalar quantity $\mathbf{u}_a^T \mathbf{E}_a^T \mathbf{P} \mathbf{z} = (\mathbf{u}_a^T \mathbf{E}_a^T \mathbf{P} \mathbf{z})^T$, Eq.(8-38) can be rewritten as

$$\dot{V} = -\mathbf{z}^T \mathbf{Q} \mathbf{z} - 2 \mathbf{z}^T \mathbf{P} \mathbf{E}_a \mathbf{U}_{\max} \text{sign}(\mathbf{E}_a^T \mathbf{P} \mathbf{z}). \quad (8-39)$$

Setting $\mathbf{s} = \mathbf{E}_a^T \mathbf{P} \mathbf{z}$, the second term of Eq.(8-39) can be expressed as $\mathbf{s}^T \mathbf{U}_{\max} \text{sign}(\mathbf{s}) > 0$. It is always positive since \mathbf{U}_{\max} is a positive definite diagonal shaped matrix and $\mathbf{s}^T \text{sign}(\mathbf{s}) > 0$. Consequently $\dot{V} < 0$, and Lyapunov's stability criteria is fulfilled. In a recent work Cai et al.³⁵ applied such a control scheme to seismically excited structures, and showed that it is superior to standard LQR control. To get rid of the sharp input transitions, the *sign* function is replaced by

$$\text{sign}(x) \approx \tanh(ax), \quad (8-40)$$

where a is a positive number. Using this approximation a smooth transitions between the maximum input quantities is obtained. Previously, Yang et al.^{36, 37} Wu et al.³⁸ and Adhikari et al.³⁹ have also applied sliding mode control to civil engineering structures, mainly with active bracing, active mass drivers and active tendon systems. In contrast to ATLCD, where high switching frequencies must be avoided to minimise air consumption, the bang-bang type of control does not waste energy when applied to conventional damping devices.

8.8. References

¹ Leipholz, H.H.E.(ed.), *The Proceedings of the IUTAM Symposium on Structural Control*, Waterloo, Ontario, Canada, 4-7 June 1979), North-Holland Publishing Company, Amsterdam-New York-Oxford, 1980.

- ² Kobori, T., *Future Direction on Research and Development of Seismic-Response-Controlled Structure*, Proc. 1st World Conf. on Struct. Control, Los Angeles, California, USA, Panel 19-31, August 1994
- ³ Sakamoto, M, Kobori, T., Yamada, T, Takahashi, M., *Practical Applications of Active and Hybrid Response control Systems and their Verifications by Earthquake and Strong Wind Observations*, 1st World Conf. on Struct. Control, Los Angeles, California, USA, pp.WP2:90-99, Los Angeles, published by International Association for Structural Control, August 1994
- ⁴ Housner G.W., Bergman, L.A., Caughey, T.K., Chassiakos, A.G., Claus, R.O., Masri, S.F., Skelton, R.E., Soong, T.T., Spencer, B.F., Yao, J.T.P., *Structural Control: Past, Present, and Future*, Journal of Engineering Mechanics, vol.123(9), pp.897-971
- ⁵ Spencer, B.F. Jr., Sain, M.K., *Controlling Buildings: A New Frontier in Feedback*, Special Issue of the IEEE Control Systems Magazine on Emerging Technology, vol. 17 (6), pp.19-35, 1997
- ⁶ Chase, G.J., Smith, A.H., *H_∞ -Control for Vibration Control of Civil Structures in Seismic Zones*, Report No. 116, The J. Blume Earthquake Engineering Center, Stanford University, September 1995
- ⁷ Koike, Y., Murata, T., Tanida, K., Kobori, T., Ishii, K., Takenaka, Y., *Development of V-Shaped Hybrid Mass Damper and its Application to High Rise Buildings*, Proc. 1st World Conference on Structural Control, Los Angeles, California, pp.FA2:3-12, August 1994
- ⁸ Yamazaki, S., Nagata, N., Abiru, H., *Tuned Active Dampers installed in the Miratu Minai (MM) 21 Landmark Tower in Yokohama*, J. Wind Engineering and Indust. Aerodyn., vol 43, pp.1937-1948, 1992
- ⁹ Yang, J.N., Wu, J.C., Reinhorn, A.M., Riley, M., *Control of Sliding Isolated Buildings Using Sliding-Mode Control*, J. of Struct. Engrg., ASCE, vol. 122 (2) pp.179-186, 1996
- ¹⁰ Schlacher, K., Irschik, H., Kugi, A., *Aktiver Erdbebenschutz für mehrstöckige Gebäude*, e&i - ÖVE Verbandszeitschrift Elektrotechnik und Informationstechnik, 114.Jg. pp.85-91, 1997
- ¹¹ Schlacher, K., Kugi, A., Irschik, H., *Nonlinear control of earthquake excited high raised buildings by appropriate disturbance decoupling*, Acta Mechanica 125, pp.49-62, 1997
- ¹² Schlacher, K., Kugi, A., Irschik, H., *Control of earthquake excited nonlinear shear-wall-type structures using input-output linearization*, 10th European Conference on Earthquake Engineering, Duma(ed), 1995, Balkema, Rotterdam, ISBN 90 5410 528 3
- ¹³ Schlacher, K., Kugi, A., Irschik, H., *Control of Earthquake Excited Nonlinear Structures Using a Differentialgeometric Approach*, Computers and Structures, vol.67, pp.83-90, 1998
- ¹⁴ Kugi, A., Schlacher, K., Irschik, H., *Nonlinear H_∞ -control of Earthquake Excited High Raised Buildings*, Third International Conference on Motion and Vibration Control, pp36-41, Chiba, Sept. 1-6, 1996
- ¹⁵ Kugi, A., Schlacher, K. Irschik, *H_∞ control of Random Structural Vibrations with Piezoelectric Actuators*, Computers and Structures, vol.67, pp.137-145, 1997
- ¹⁶ Lei, Y., *Sure and Random Vibrations of Simple Dissipative Civil Engineering Steel Structures*, Dissertation and Report, Institute of Rational Mechanics, Technical University of Vienna, Austria, 1994
- ¹⁷ Lei, Y., Ziegler, F., *Random Response of Friction Damped Braced Frames under Severe Earthquake Excitation*, Proceedings of 5th U.S. National Conference on Earthquake Engineering, p.683-692, Chicago, Illinois, July 10-14, 1994

- ¹⁸ Haroun, M.A., Pires, J.A., Won, A.Y.J., *Suppression of environmentally-induced vibrations in tall buildings by hybrid liquid column dampers*, The structural Design of Tall Buildings, vol.5, pp.45-54, 1996
- ¹⁹ Abé, M., Kimura, S., Fujino, Y., *Control laws for semi-active tuned liquid column damper with variable orifice openings*, 2nd International Workshop on Structural Control, 18-21 December 1996, Hong Kong, pp.5-10, 1996
- ²⁰ Dyke, S.J., Spencer, B.F.Jr., Sain, M.K., Carlson, J.D., *Experimental verification of Semi-active Structural Control Strategies Using Acceleration Feedback*, Proc. 3rd Int. Conference on Motion and Vibration Control, Chiba, Japan, vol. III, pp- 291-296,1996
- ²¹ Gavin, H.P. Hanson, R.D., Filisko, F.E. *Electrorheological Dampers, Part I: Analysis and Design*, J. Appl. Mech., ASME vol. 63 (3), pp.669-675, 1996
- ²² Gavin, H.P. Hanson, R.D., Filisko, F.E. *Electrorheological Dampers, Part II: Testing and Modeling*, J. Appl. Mech., ASME vol. 63 (3), pp.676-682, 1996
- ²³ Ribakov, Y., Gluck, J., *Active Control of MDOF Structures with Supplemental Electrorheological Fluid Dampers*, Earthquake Engineering and Structural Dynamics, vol.28, pp.143-156, 1999
- ²⁴ Burton, A.B., Makris, N., Konstantopoulos, I., Antsaklis, P.J., *Modeling the Response of ER Damper: Phenomenology and Emulation*, Journal of Engineering Mechanics, vol.122(9), pp. 897-906, 1996
- ²⁵ Ziegler, F., *Mechanics of Solids and Fluids*, 2nd reprint of second edition, Springer, New York, Vienna, 1998.
- ²⁶ Levine, W.S. ed., *The Control Handbook*, CRC Press, IEEE Press, 1996
- ²⁷ Soong, T.T., *Active Structural Control – Theory and Practice*, Longman Scientific&Technical, 1990
- ²⁸ Föllinger, O., *Optimale Regelung und Steuerung*, 3rd edition, Oldenbourg Verlag, 1994
- ²⁹ Stengel, R.F., *Optimal Control and Estimation*, Dover Publications, New York 1993
- ³⁰ Lewis, F.L., Syrmos, V.L., *Optimal Control*, John Wiley&Sons, 1995
- ³¹ Yang, J.N., Akbarpour, A., Ghaemmaghami, P., *Instantaneous Optimal Control Algorithms for Tall Buildings under Seismic Excitations*, Multidisciplinary Center for Earthquake Engineering Research, Buffalo, N.Y., USA, NCEER-87-0007, 1987
- ³² Wu, Z., Soong, T.T., Gattulli, V., Lin, R.C., *Nonlinear Control Algorithms for Peak Response Reduction*, Technical Report NCEER-95-0004, NCEER Buffalo, USA
- ³³ Agrawal, A.K., Yang, J.N., Wu, J.C., *Application of optimal polynomial control to a benchmark problem*, Earthquake Engng. Struct. Dyn. 27, 1291-1302, 1998
- ³⁴ DeCarlo, R.A., Zak, S.H., Mathews, G.P., *Variable Structure Control of Nonlinear Multivariable Systems: A Tutorial*, Proceedings of the IEEE, vol76(3), p.212-232, 1988
- ³⁵ Cai, G., Huang, J., Sun, F., Wang, C., *Modified sliding-mode bang-bang control for seismically excited linear structures*, Earthquake Engineering and Structural Dynamics, vol.29, p.1647-1657, 2000
- ³⁶ Yang, J.N., Wu, J.C., Agrawal, A.K., *Sliding Mode Control for Seismically Excited Linear Structures*, Journal of Engineering Mechanics, vol.121(12), pp.1386-1390, 1995
- ³⁷ Yang, J.N., Wu, J.C., Agrawal, A.K., HSU, S.Y., *Sliding Mode Control with Compensator for Wind and Seismic Response Control*, Earthquake Engineering and Structural Dynamics, vol.26, pp. 1137-1156, 1997
- ³⁸ Wu, J.C., Yang, J.N., Agrawal, A.K., *Applications of Sliding Mode Control to Benchmark Problems*, Earthquake Engineering and Structural Dynamicx, vol27(11), pp.1247-1266, 1998

- ³⁹ Adhikari, R., Yamaguchi, H., Yamazaki, T., *Modal Space Sliding-Mode Control of Structures*, Earthquake Engineering and Structural Dynamics, vol27(**11**), pp.1303-1314, 1998

9. Application to real structures and numerical studies

The aim of this section is to investigate the influence of TLCD on the dynamic behaviour of various structures by numerical simulations. Five different structures are investigated under wind and earthquake excitation, and both, passive and active TLCD are applied to reduce the vibration response. Three numerical studies are based on benchmark problems available in literature, see Spencer et al.¹, see Yang et al.², Ohtori et al.³, and the building data for the study of the 47-floor wind excited tall building was obtained from Prof. T.T. Soong during a short term research visit at the State University of New York at Buffalo in the summer 2000. All structures mentioned are analysed in a plane configuration, and thus the critical loading in one direction is investigated. To be able to prove the working principle of the torsional TLCD, a simple three dimensional structural model is investigated in the first subsection.

9.1. *3D-building with translational and torsional passive TLCD*

Although many structures possess a definite axis of symmetry within their model, the idealising assumption of perfect regularity is never correct. Consequently, flexural and torsional vibration modes are coupled in an imperfect real structure, and although only excited in horizontal direction, a building's torsional vibration mode might start to oscillate. This certainly happens if the centre of gravity and the centre of stiffness at a certain floor level do not coincide and then even the free vibrations are a combination of translational and rotational oscillations. Such a situation is investigated in the following numerical study of a single story structure which is equipped with plane and torsional TLCDs to mitigate both, flexural and coupled flexural-torsional vibrations. The single-storey building, see Figure 9-1, has a rectangular (length/width=2) base and is subject to earthquake loading. It consists of a homogenous rigid floor of mass m , supported by four symmetrically arranged columns, three of which have the same unisotropic stiffness k_x and k_y in X- and Y-directions, respectively. The remaining column has twice these stiffness, since it represents e.g. a staircase, which causes the asymmetry. It is assumed that the torsional rigidity of the supporting columns is negligible, and that the vibration takes place within the elastic range of

the structure. Apparently the structural model has three degrees-of-freedom which can also be interpreted as modal coordinates of a more complex structure. Such an approximation becomes applicable, see Section 6.6, if only the first three mode shapes dominate the vibration response.

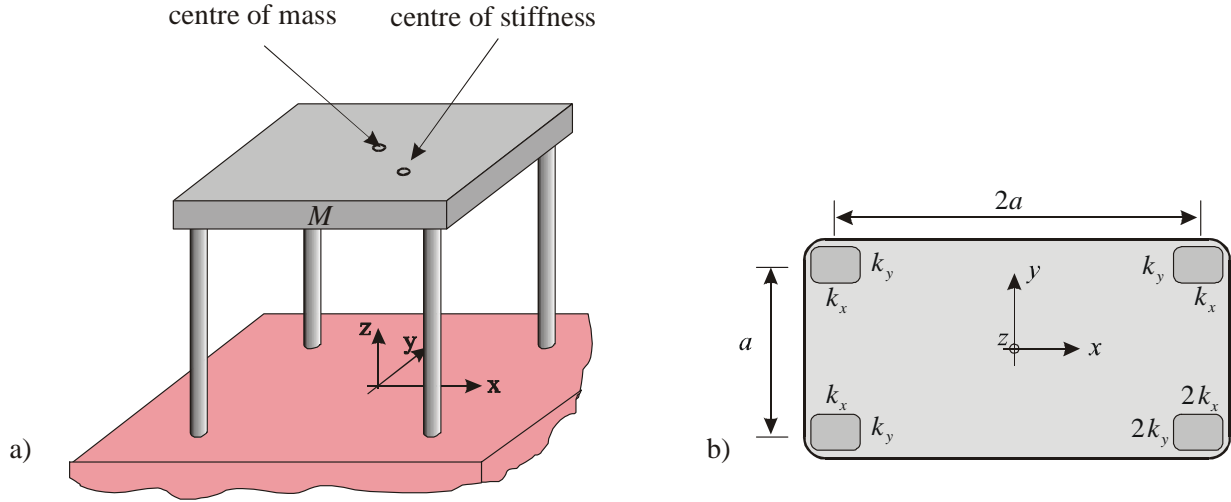


Figure 9-1: 3D single story building a) schematics b) plane view with floor dimensions and column stiffness

The linear equation of motion can be given in standard matrix notation, however, the ground acceleration input $\ddot{\mathbf{w}}_g$ is no longer a scalar quantity, since the horizontal input acceleration can have components in both, X- and Y-directions. The vertical component is neglected throughout this dissertation, and thus

$$\mathbf{M} \begin{pmatrix} \ddot{w}_x \\ \ddot{w}_y \\ \ddot{w}_{xy} \end{pmatrix} + \mathbf{C} \begin{pmatrix} \dot{w}_x \\ \dot{w}_y \\ \dot{w}_{xy} \end{pmatrix} + \mathbf{K} \begin{pmatrix} w_x \\ w_y \\ w_{xy} \end{pmatrix} = \mathbf{M} \mathbf{R}_S \ddot{\mathbf{w}}_g + \mathbf{f} + \mathbf{f}_{TLCD}, \quad (9-1)$$

where $w_{xy} = \alpha a$, and α denotes the angle of rotation of the floor about the Z-axis, and the static

influence matrix is given by $\mathbf{R}_S = \begin{pmatrix} 1 & 0 & 0 \\ 0 & 1 & 0 \end{pmatrix}^T$. A possible wind force loading $\mathbf{f} = [f_x, f_y, 0]^T$ is

assumed to have components in both horizontal directions. The mass and stiffness matrices are given by

(9-2)

$$\mathbf{K} = \begin{pmatrix} 5k_x & 0 & k_x/2 \\ 0 & 5k_y & k_y \\ k_x/2 & k_y & 5k_x/4 + 5k_y \end{pmatrix}, \quad \mathbf{M} = \begin{pmatrix} M & 0 & 0 \\ 0 & M & 0 \\ 0 & 0 & M r_z^2/a^2 \end{pmatrix},$$

where the mass moment of inertia about the vertical Z-axis is given $I = \int_m (x^2 + y^2) dm = M r_z^2$

and r_z denotes the radius of inertia about the centre of mass. The influence of the TLCDs can be incorporated into the equations of motion by means of main structure-TLCD interaction forces \mathbf{f}_A , which are given by Eqs.(4-29) and (4-58). Since little is known about the structural damping characteristics, modal damping coefficients are all assumed to be 1% of the critical damping. Thus the source of coupling due to hysteretic material damping is neglected at all. A transformation of Eq.(9-1) to modal coordinates reveals the coupling between translations and rotations. The mode shapes are given schematically in Figure 9-2, where it is seen that only one vibration mode shape consists of a pure translation, whereas the others describe a complex plane motion of the rigid floor, corresponding to coupled bending torsional vibrations.

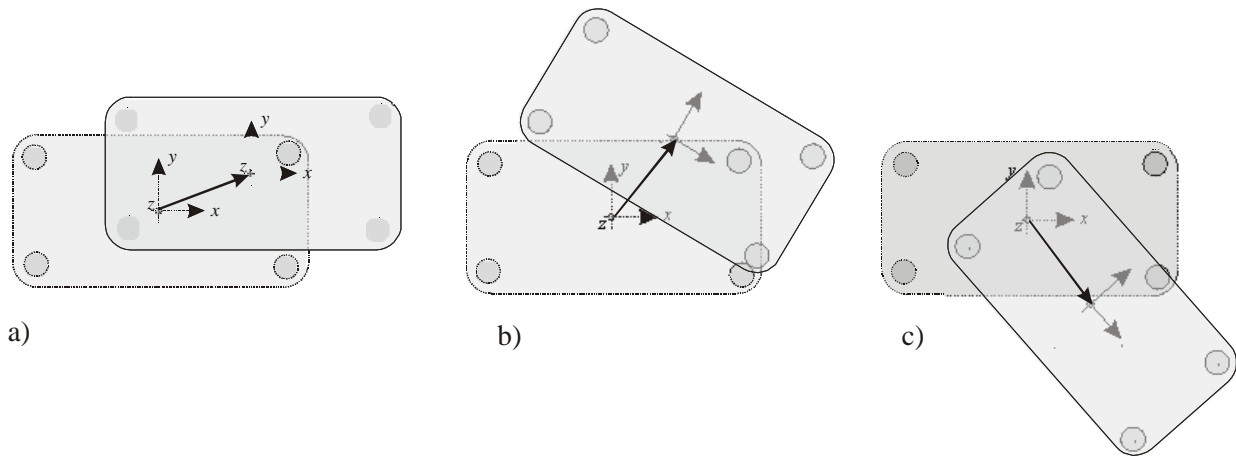


Figure 9-2: Graphical representation of modal displacements in plan view for single floor structure with asymmetric column stiffness, ordered by increasing natural frequencies, 0.79, 1.09, 1.87 Hz

The building is equipped with three TLCDs, one torsional (consisting of two symmetrically arranged TTLCDs) and two plane TLCDs which are installed at the centre of the rigid floor along the X- and Y-axis, see Figure 9-3.

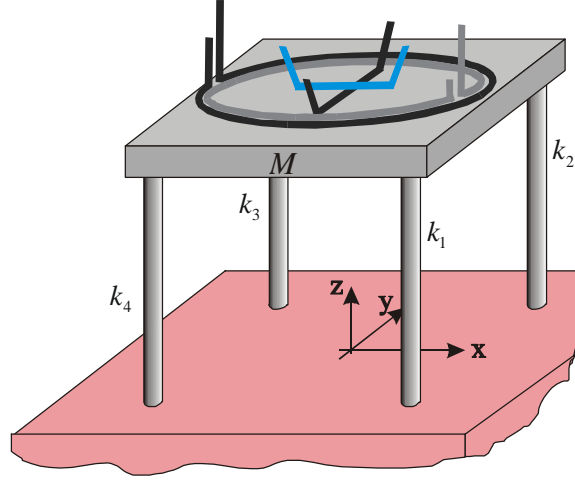


Figure 9-3: 3D single story building with two translational TLCDs and set of two asymmetrically arranged torsional TLCDs

The size of the rectangular rigid floor is given by $10m \times 20m$, its mass is $M = 1 \cdot 10^6 kg$, the column stiffness are chosen consistently with a proper static design, $k_x = 10 \cdot 10^6 [N/m]$ and $k_y = 5 \cdot 10^6 [N/m]$, the natural frequencies are found to be 0.79, 1.09, 1.87 Hz. Each passive TLCD has a constant cross sectional area and a mass ratio as well as a geometry factor of $\mu = 0.01$, $\kappa = 0.9$, $\bar{\kappa} = 0.9$, respectively, see Eqs.(4-9). Furthermore the circular torsional TLCD has a radius of $3m$. Having designed all TLCDs the equations of motion of the structural model, Eq.(9-1), and the TLCDs (Eqs. (4-11) and (4-38)), are combined which results in a dynamic system with 6 DOF. Subsequently it is transformed to a state space representation of order 12 by applying the hypermatrix manipulations given in Chapter 7, Eq.(7-12). The absorber tuning is accomplished by minimising the performance index J , see Eq.(7-21), Section 7.2.1,

$$J = \sum_{i=1}^N \int_{\nu_{\min}}^{\nu_{\max}} s_i |h_i(\nu)|^2 d\nu \rightarrow \text{minimum}, \quad (9-3)$$

with respect to the six free parameters (tuning frequency and damping ratio for each TLCD). For the sake of simplicity, an infinite frequency range $-\infty \leq \nu \leq \infty$ is considered. If the reduction of the floor displacements or velocities is desired, the performance index must contain these quantities and Eq.(9-3) can be rewritten as

$$J = \int_{-\infty}^{\infty} \mathbf{z}_S^T(\nu) \mathbf{S} \mathbf{z}_S(\nu) d\nu, \quad (9-4)$$

where h_i is replaced by the corresponding state variable, and the constant weighting factors s_i are grouped in the diagonal matrix $\mathbf{S} = \text{diag}(1, 1, 10, 0, 0, 0)$. \mathbf{z}_S represents the host structures' state vector given by $\mathbf{z}_S(\nu) = [w_x(\nu), w_y(\nu), w_{xy}(\nu), \dot{w}_x(\nu), \dot{w}_y(\nu), \dot{w}_{xy}(\nu)]^T$. It has to be mentioned that Eq.(9-4) can be evaluated for ground excitation in both, X-direction and Y-direction. Consequently two performance criteria, J_x and J_y are calculated which are combined to the final performance index $J_{tot} = \sqrt{J_x^2 + J_y^2}$ using the SRSS (Square Root of Sum of Squares) approach.

The minimisation of J_{tot} is performed numerically by calling the function *fminsearch* of the Matlab Optimisation Toolbox⁴. *fminsearch* finds the minimum of the scalar function J of several variables, $\mathbf{x} = [\omega_1, \omega_2, \omega_3, \zeta_1, \zeta_2, \zeta_3]$, starting at an initial estimate \mathbf{x}_0 . This is generally referred to as unconstrained nonlinear optimisation. *fminsearch* can also handle discontinuity, particularly if it does not occur near the solution, but it may only give local solutions and it minimises over real numbers only, thus complex functions must be split into two parts. *fminsearch* uses the simplex search method of Lagarias⁵, which is a direct search method that does not use numerical or analytic gradients. A typical function call takes the form $x = \text{fminsearch}(J_calc, x_0)$, starts at the point x_0 and finds a local minimum x of the function described in J_calc . x_0 can be a scalar, vector, or matrix. The user defined function J_calc , calculates the performance index by solving a Lyapunov equation, see Chapter 7. Attention has to be paid to the fact that Eq.(9-4) only converges for stable systems. Thus the damping ratios must remain positive, and J_calc returns an infinite value as soon as the input of x would cause the system to be unstable. The initial frequency ratios for the TLCDs were chosen to coincide with the natural frequencies of the structural model, and all damping ratios were selected 10%. After calling *fminsearch* twice, the optimal circular tuning frequencies and damping ratios are found to be $\omega_1 = 4.83 \text{ rad/s}$, $\omega_2 = 6.63 \text{ rad/s}$, $\omega_3 = 11.69 \text{ rad/s}$, and $\zeta_1 = 7.73\%$, $\zeta_2 = 7.60\%$, $\zeta_3 = 2.34\%$, respectively, where the indices 1, 2 and 3 refer to the TLCDs installed along the X- and Y-direction, and the torsional TLCD, respectively. ζ_3 is smaller than ζ_1 or ζ_2 because the effective mass ratio for the torsional TLCD

is given by the absorber-structure moment of inertia ratio, $\mu_3^{eff} = \frac{r_f^2 m_f}{r_z^2 M}$ which is smaller than

$\mu_1 = \mu_2 = \mu_3 = \frac{m_f}{M}$. The outcome of the optimisation is illustrated in Figure 9-4, which shows the

frequency response of the weighted sum $\sum_{i=1}^6 s_i |z_i(\nu)|$ of the building's states for the original and

the optimised system, in the logarithmic decibel scale, defined by $x[dB] = 20 \log x$. It is obvious that the parameter optimisation reduces the vibration amplitude at the resonant peaks tremendously.

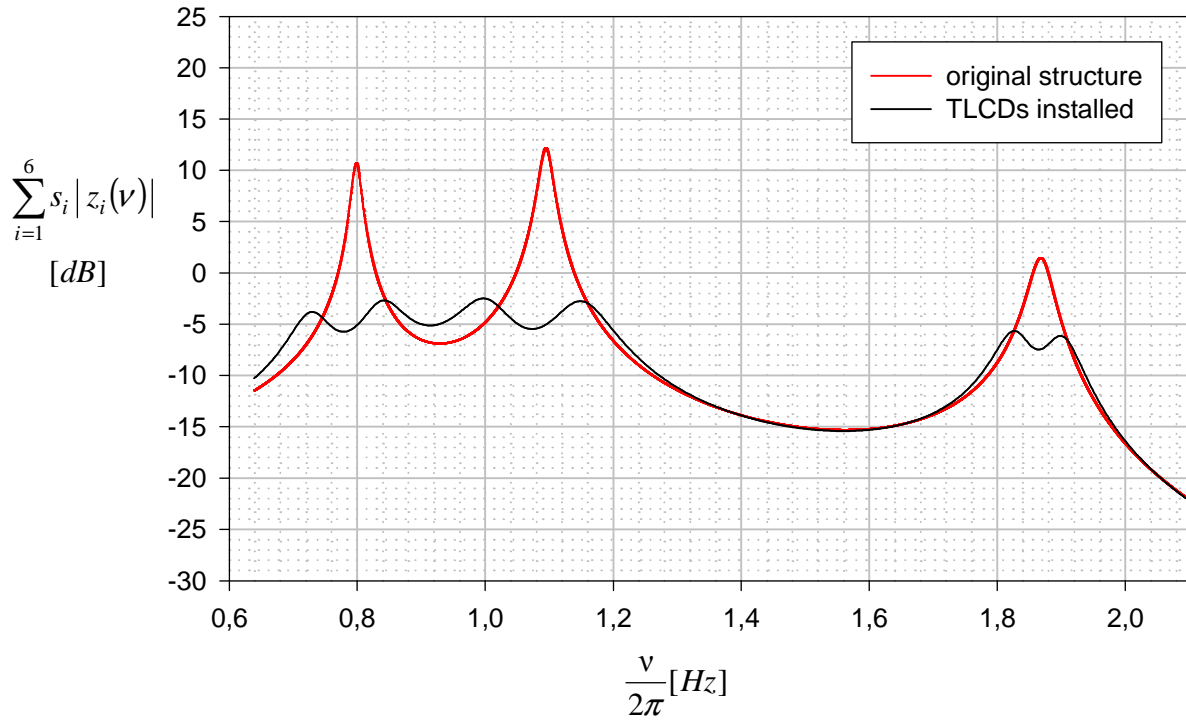


Figure 9-4: Weighted sum of amplitude response functions for the 3DOF structure with three and without the TLCDs

To obtain further, detailed information, an actual earthquake ground excitation is applied to the structure. The historical 1940 El Centro earthquake N-S acceleration, whose strong motion part is given in Figure 9-5, is applied to the basement. The scaled digital El Centro accelerogram with a sampling time of $\Delta t = 0.02s$, and a maximum ground acceleration of $\ddot{w}_{g,\max} = 3.417 \frac{m}{s^2} = 0.35g$, was made available by Spencer et al.¹¹, and can be downloaded from the WebPages of the Structural Dynamics and Control - Earthquake Engineering Laboratory at the University of Notre Dame, Notre Dame, Indiana 46556, USA, <http://www.nd.edu/~quake/>.

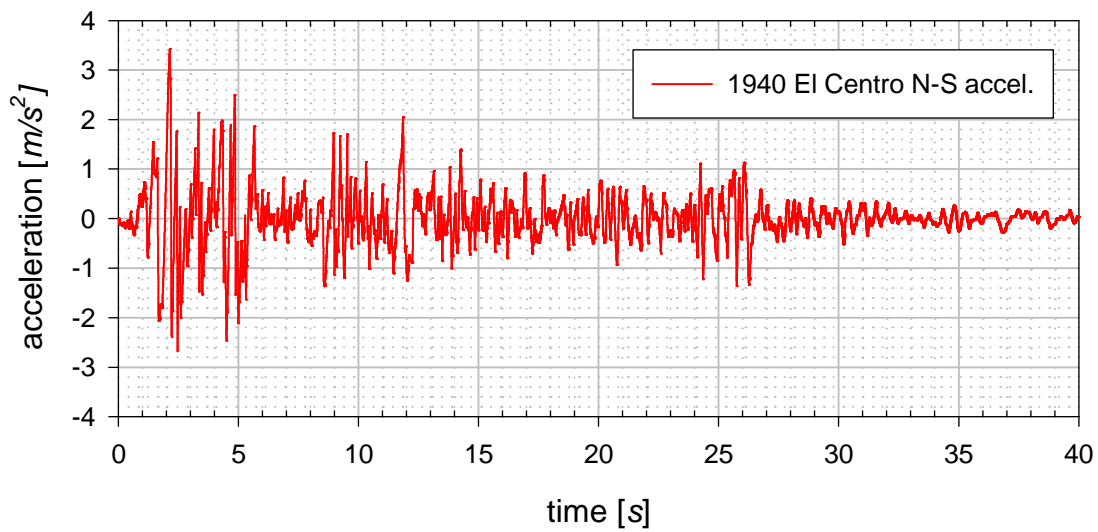


Figure 9-5: 1940 El Centro N-S ground acceleration record, sampling time $\Delta t = 0.02s$

Since a digital representation of the E-W accelerogram is not available and a three dimensional structure is investigated, the N-S acceleration record is applied with an angle of incidence of 45° , exciting the building horizontally in two directions. The calculation of the structural response for the linearised system is straightforward, once a dynamic description in the state space, see Eq.(7-11) , is available. Numerical simulation packages like Matlab provide efficient time integration subroutines like *lsim*, which simulates the (time) response of continuous linear time invariant systems to arbitrary (multiple) inputs. In continuous time, the time sampling Δt of the excitation signal is used to discretise the continuous model in the time domain. However, automatic resampling is performed if Δt is too large (undersampling) and may give rise to hidden oscillations. The discretisation is performed using the *c2d* command of the Matlab Control Toolbox⁶, applying either the zero order hold (zoh) or first order hold (foh) discretising method ('foh' is used for smooth input signals and 'zoh' for discontinuous). For further details see the Matlab Control Toolbox reference book⁶ or Franklin et al.⁷

The structural response is displayed from Figure 9-6 to Figure 9-11, where the relative floor displacements with respect to the basement and the absolute floor accelerations are displayed. It is noted that all TLCDs need several vibration cycles before they start to mitigate the structural vibrations. Thus the RMS vibrations are reduced substantially, whereas the peak responses are hardly affected by the application of passive TLCD.

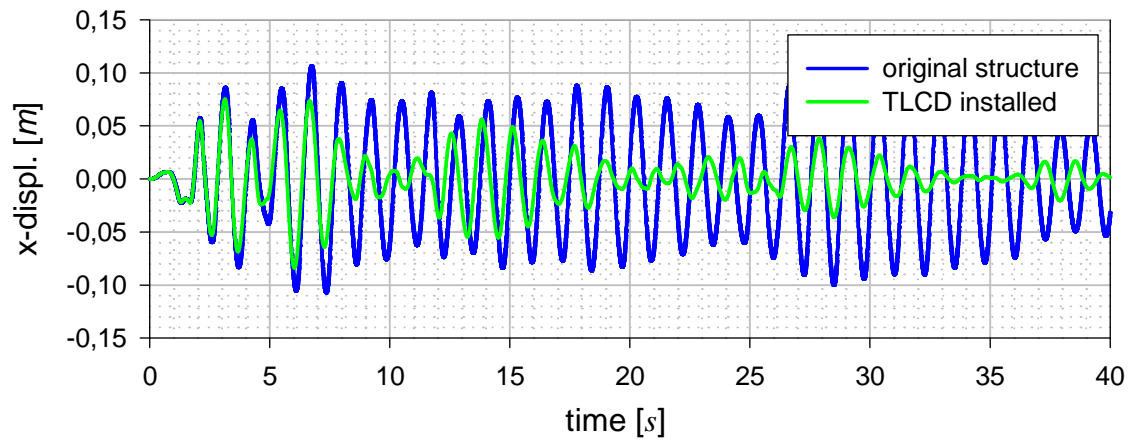


Figure 9-6: Relative floor displacement response in X-direction under the 1940 El Centro earthquake, angle of incidence: 45° (horizontal)

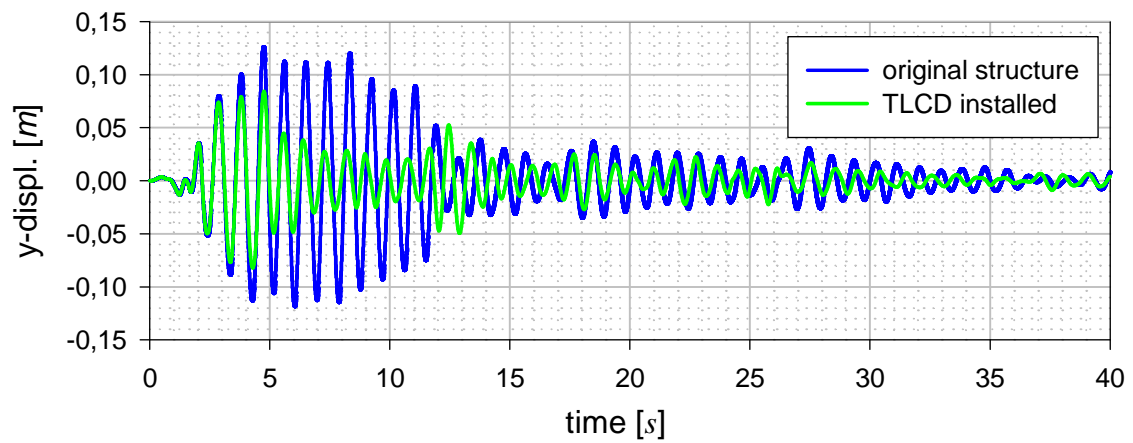


Figure 9-7: Relative floor displacement response in Y-direction under the 1940 El Centro earthquake, angle of incidence: 45° (horizontal)

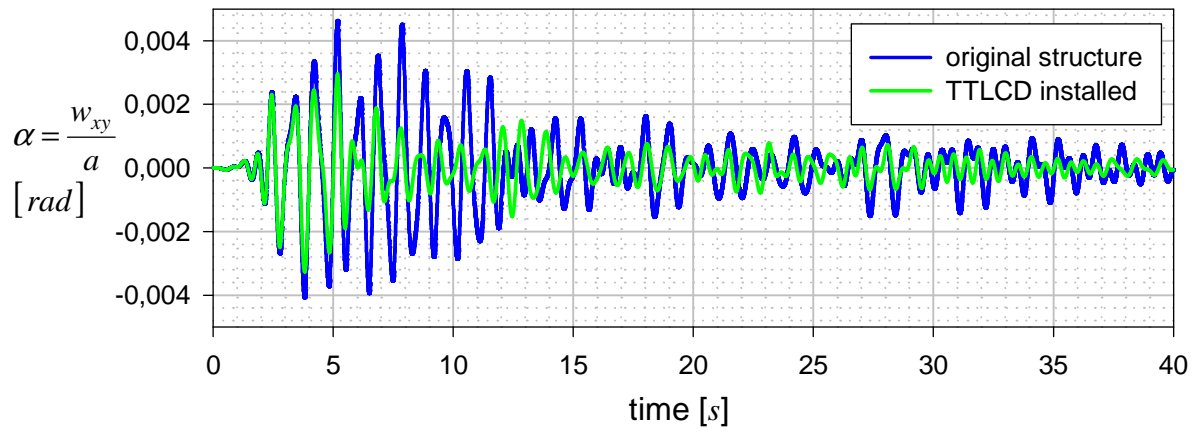


Figure 9-8: Relative floor rotation about Z-axis under the 1940 El Centro earthquake, angle of incidence: 45° (horizontal)

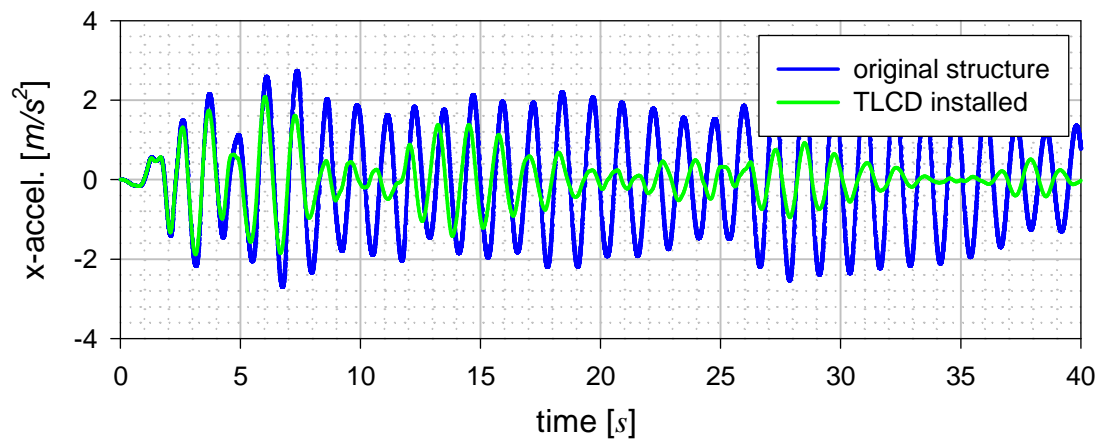


Figure 9-9: Absolute acceleration of 3D-structure in X-direction under the 1940 El Centro earthquake, angle of incidence: 45° (horizontal)

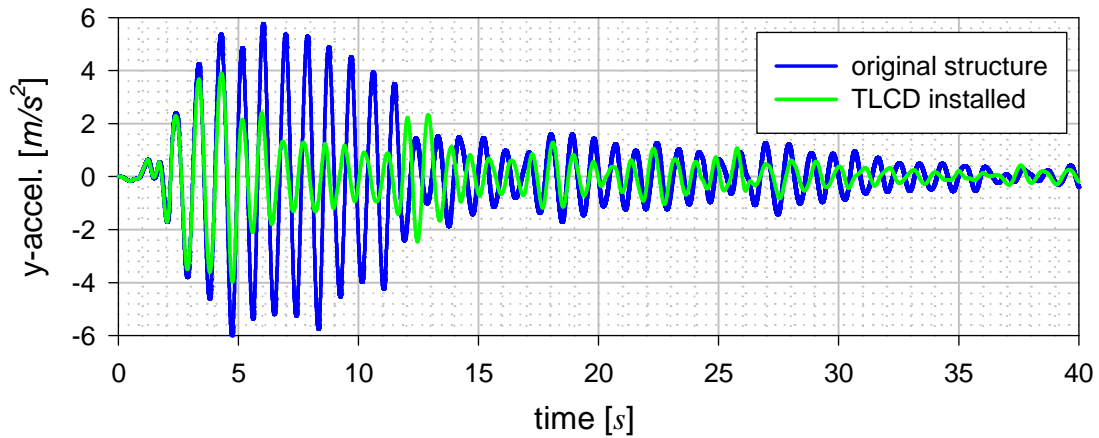


Figure 9-10: Absolute acceleration of 3D-structure in Y-direction under the 1940 El Centro earthquake, angle of incidence: 45° (horizontal)

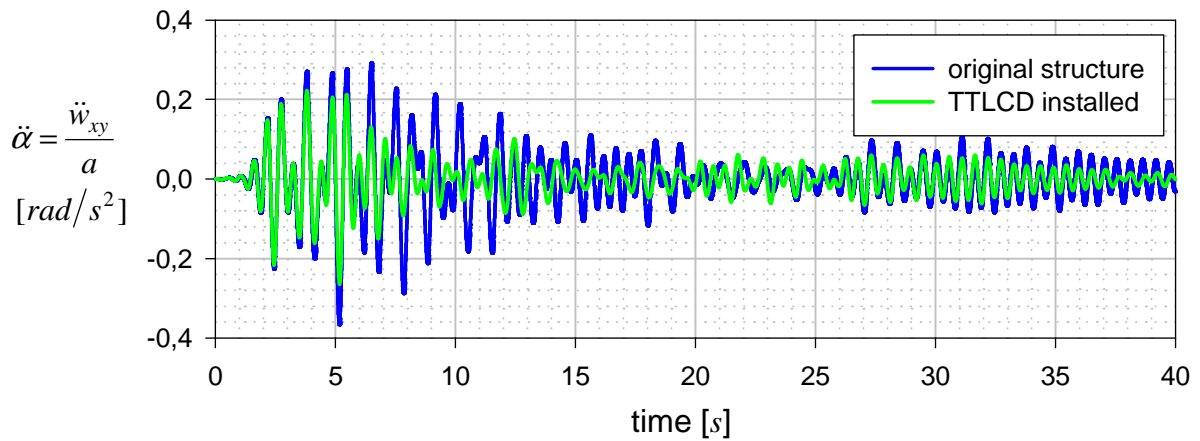


Figure 9-11: Absolute acceleration of 3D-structure about the Z-axis under the 1940 El Centro earthquake, angle of incidence: 45° (horizontal)

In a second numerical simulation an artificially created wind load is applied to the structure under an angle of incidence of 45°. The wind load was generated by filtering an artificially generated white noise through a second order low-pass filter with a cut-off frequency of 3Hz. The mean wind velocity is 25 m/s, corresponding to a classification of wind by Beaufort of 10. The pressure coefficients for the 20m high building can be found in Sockel⁸, p.176, and are given by $c_{py} = 1.1$ and $c_{px} = 0.8$, resulting in peak wind forces of 206.2kN and 566.9kN in X-and Y-directions,

respectively. The pressure gust factors, see Liu¹⁰, p.49, for both directions are given by $p_G = 1.5$, and the corresponding 40 second time segment of the wind load is shown in Figure 9-12.

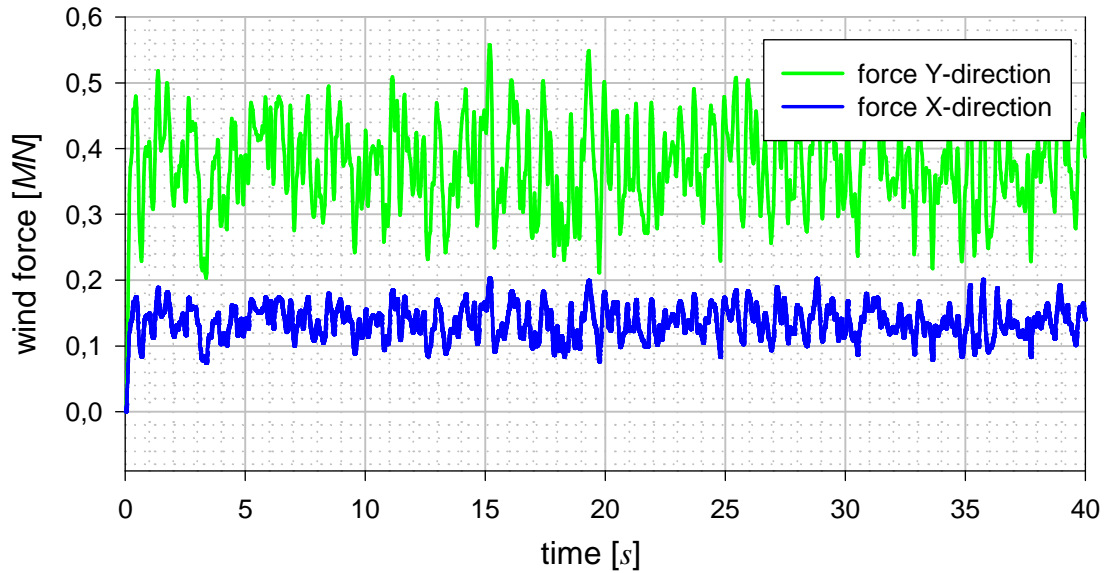


Figure 9-12: Resulting force from a 40 second time segment of an artificially wind load (angle of incidence 45°), with an average wind speed of 25 m/s and a pressure gust factor of $p_G = 1.5$

The structural response due to the wind-force loading is displayed from Figure 9-13 to Figure 9-18. It demonstrates the excellent vibration reduction of the passive device in a situation where resonant vibrations can build up. Apparently it is not necessary to implement an active TLCD since the passive devices operate satisfactorily and reduce both, displacements and acceleration which increases both, the structural safety and the human comfort.

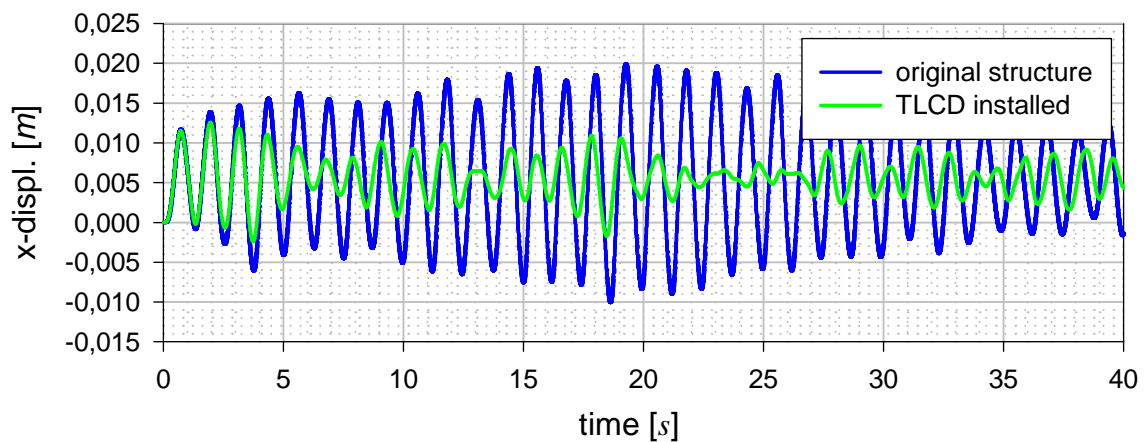


Figure 9-13: Relative floor displacement response in X-direction during the artificially created 40s wind segment, angle of incidence: 45° (horizontal)

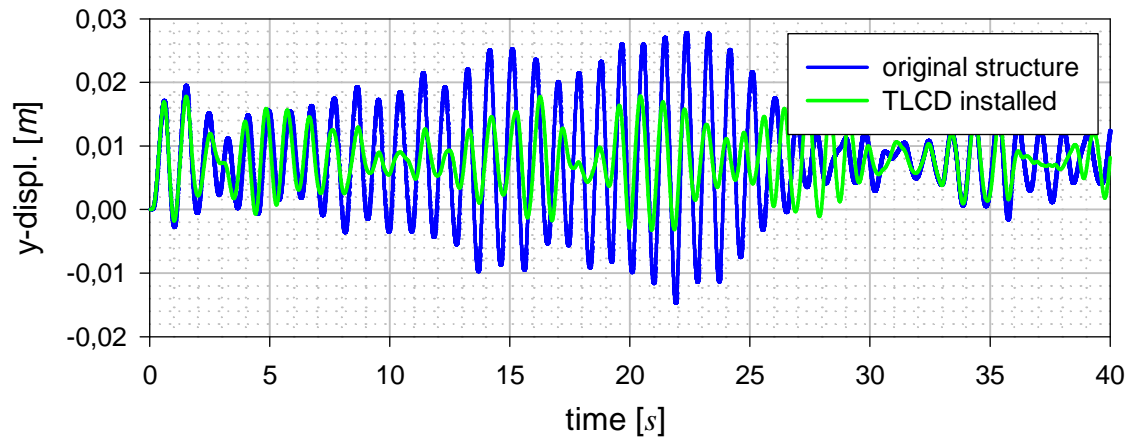


Figure 9-14: Relative floor displacement response in Y-direction during the artificially created 40s wind segment, angle of incidence: 45° (horizontal)

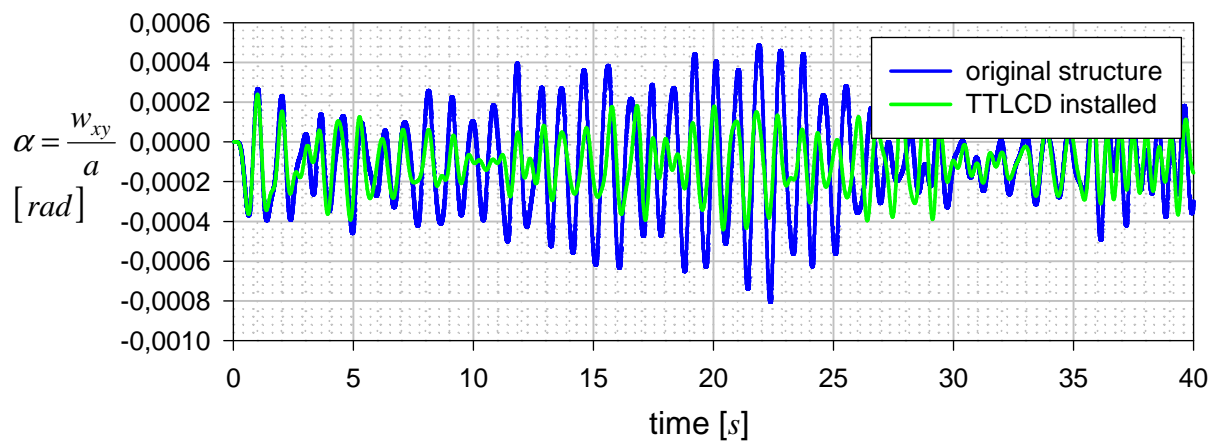


Figure 9-15: Relative floor rotation about Z-axis during the artificially created 40s wind segment, angle of incidence: 45° (horizontal)

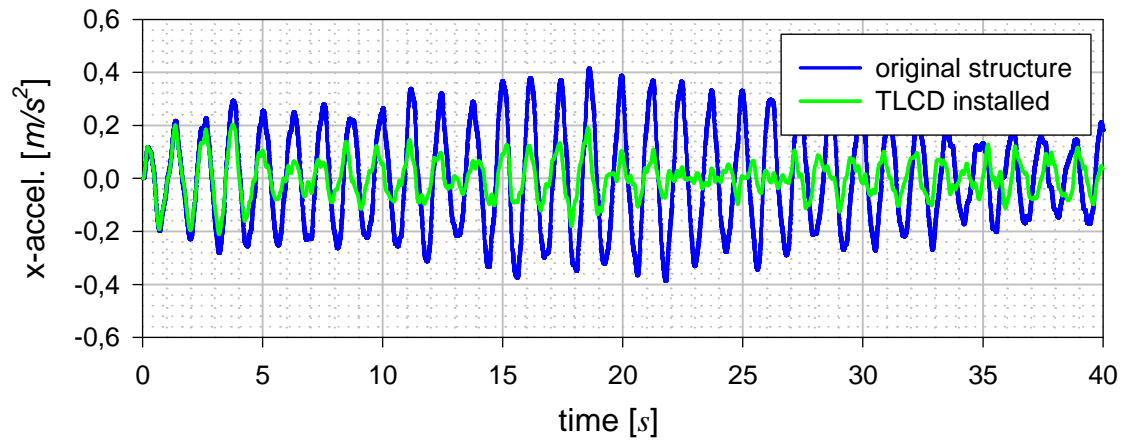


Figure 9-16: Absolute acceleration of 3D-structure in X-direction during the artificially created 40s wind segment, angle of incidence: 45° (horizontal)

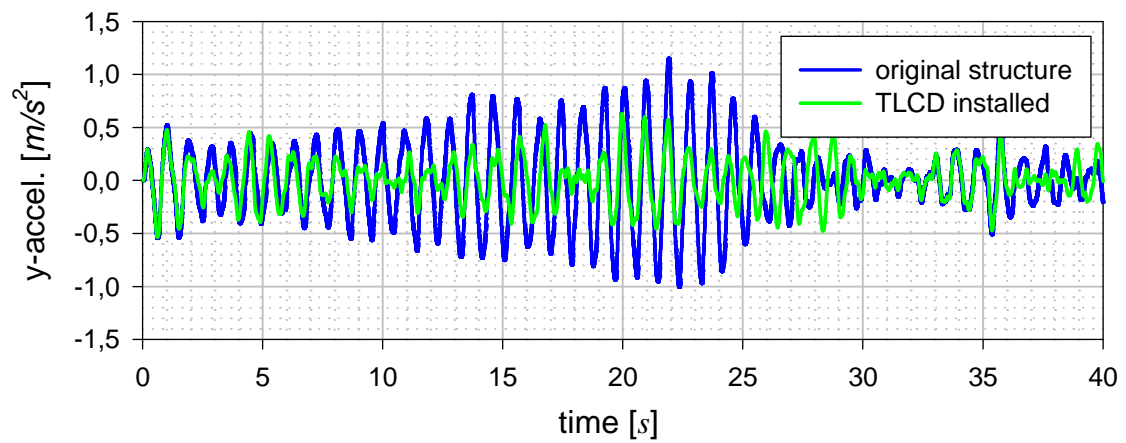


Figure 9-17: Absolute acceleration of 3D-structure in Y-direction during the artificially created 40s wind segment, angle of incidence: 45° (horizontal)

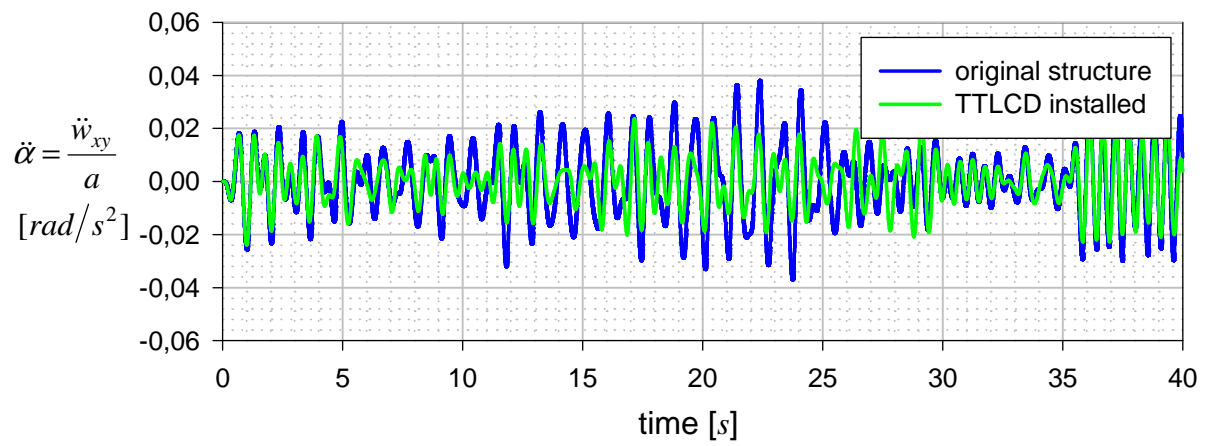


Figure 9-18: Absolute acceleration of 3D-structure about the Z-axis during the artificially created 40s wind segment, angle of incidence: 45° (horizontal)

9.2. *Wind excited 47-story tall building*

Based on a case study by Reinhorn and Soong⁹, the installation of a TMD and a TLCD on an existing tall flexible skeletal steel building is investigated and compared. The building's response criteria optimised are the maximum top-floor displacements and accelerations under a 100-year recurrence wind, according to the basic wind speed map of ANSI Standard A58.1, see e.g.¹⁰. The wind has an hourly mean wind speed of 46 m/s , corresponding to Beaufort number 12, and is thus classified as a hurricane, which causes large scale damage. Both vibration absorbing systems are optimised with respect to their damping characteristics under practical constraints, and the effect on the building's response characteristic is studied. The building considered has 47 floors, a total height of 199 m , and a quadratic cross section, with 65 m side length. However, space limitations on the top floor restrict the available space to 47 m without being able to use the quadratic centre part of the building, because it is occupied by a penthouse flat. Since the dead weights and most of the loads are sustained by the floors, the floor masses are assumed to be lumped at the floor levels. A total building weight of 41.788 metric tons is distributed as follows: floors 2-24 have a mass of 924 tons each, floors 25-39 and 40-47 have 866 and 837 tons, respectively. The building has less than 25% structural steel (10.153 tons), the remaining 75% being cladding, ceiling, and floor dead weights as well as mechanical systems. According to Reinhorn and Soong⁹, the dynamic properties of the structure for the first three modes are natural frequencies of 0.0996 Hz , 0.2247 Hz and 0.3629 Hz , respectively, all modes are symmetric with respect to an X-Y coordinate system and only lightly damped, with just 1% of critical damping. An initially performed five mode analysis (see Soong and Reinhorn⁹) has revealed that the first mode contribution is responsible for more than 99% of the total response. Therefore only the first mode is considered in all subsequent analyses. The building's equivalent modal weight, stiffness and damping is given by of $M = 9.84 \cdot 10^6\text{ kg}$, $3.84 \cdot 10^6\text{ N/m}$, and $\zeta_s = 1\%$, respectively. Due to symmetry the given quantities apply to both, X-direction and Y-direction. The wind pressure distribution for several wind directions was determined in a wind tunnel study for a 100 year storm. The wind tunnel experiments included the rigid building model as well as all neighbouring buildings, and the most critical measured wind data, which causes maximum response amplitudes, are used for analysis purposes. The total modal wind force $\mathbf{f}(t)$ is given by

$$\mathbf{f}(t) = S_m \begin{pmatrix} \underline{m}_x(t) \\ \underline{m}_y(t) \end{pmatrix} \quad (9-5)$$

where the constant normalised loading multiplier is determined by the building's geometry and size and found to be $S_m = 11.31 \cdot 10^6 [N]$. For details on experimental techniques, similarity laws, wind channels, wind load factors for a wide variety of buildings, the interested reader is referred to the excellent book about aerodynamics of structures by Sockel⁸. The loading is described by the time varying load coefficients \underline{m}_x and \underline{m}_y which are displayed in Figure 9-19, for the most critical load segment.

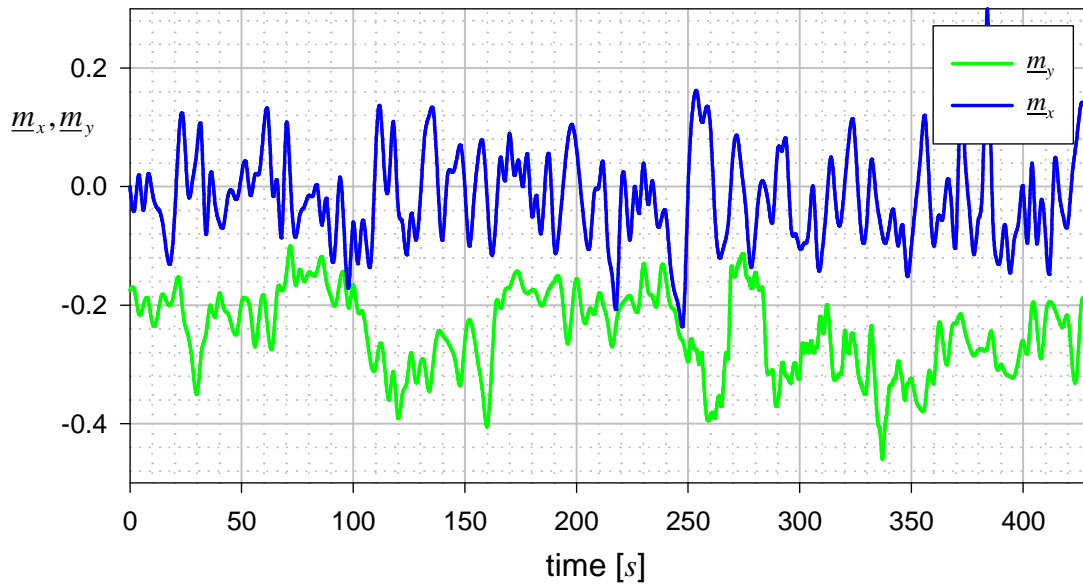


Figure 9-19: Load Coefficients for critical wind direction, see Reinhorn and Soong⁹, manually digitised to a time resolution of 1 second

The building response of the original structure is calculated for the simplified single degree of freedom oscillator (with the structural damping of $\zeta_s = 1\%$ incorporated) by time integration using the *lsim* function of Matlab's Control System Toolbox⁶. *lsim* simulates the time response of linear time invariant models of arbitrary order for arbitrary inputs. The structural response is listed in Table 9-1, and it is apparent, that large displacements, which are not within the acceptable limits, can be expected.

RMS response				peak response			
<i>X-direction</i>		<i>Y-direction</i>		<i>X-direction</i>		<i>Y-direction</i>	
displ. [m]	accel. [m/s ²]	displ. [m]	accel. [m/s ²]	displ. [m]	accel. [m/s ²]	displ. [m]	accel. [m/s ²]
1.62	0.63	1.07	0.30	5.27	1.97	3.17	0.83

Table 9-1: Maximum building response due to critical wind load

Peak top floor displacements of 5.27m and 3.17m in the X- and Y-directions, respectively, as well as peak accelerations of 1.97m/s² and 0.83m/s² are about twice the acceptable limits. In order to keep the displacements around 2.5m, and reduce the peak acceleration by a factor of two, the application of TLCDs and TMDs is investigated and compared in the next subsections.

9.2.1. Optimal TMD design

It has to be mentioned, that for the numerical simulation the building is modelled as a perfectly symmetric structure without a torsional vibration mode. In a practical implementation, however, it might also be necessary to provide a small torsional absorber, as proposed in Section 9.1. Since there is no information about the torsional behaviour of the structure, coupled flexural-torsional vibration problems are neglected. The TMD design starts with the determination of the absorber-building mass ratio $\mu = m/M$. Large values of μ will result in small displacement and acceleration responses but there is a physical limit for the size and the weight of the absorber mass. In addition, other response quantities like the overturning moment and base shear do not always decrease with an increasing μ . A mass of 180 metric tons in X-direction and mass of 363 metric tons in Y-direction have shown to be most efficient, see Soong and Reinhorn⁹ for details. However, since only one TMD-mass is to be used for both X- and Y-directions, a 363t mass is considered optimal. Since the TMD is installed at the top of the building, this mass corresponds to 4% of modal weight and only about 1% of the total structural mass, which is well within the commonly acceptable limits. Analytically optimised TMD parameters can be given for a stationary random white noise force excitation, see e.g. Table 2-1,

$$\delta = \frac{\sqrt{1 + \mu/2}}{1 + \mu} = 0.97, \quad (9-6)$$

$$\zeta_A = \sqrt{\frac{\mu(1 + 3\mu/4)}{4(1 + \mu)(1 + \mu/2)}} = 9.85\% \quad (9-7)$$

These optimal tuning parameter are based on a stationary white noise excitation, but since realistic wind tunnel data are available, it is practical to use simulations to optimise the TMD further: Table 9-2 and Table 9-3 summarise peak and RMS responses for a varying damping coefficient ζ_A , and a fixed tuning ratio of $\delta = 0.97$, as given by Eq.(9-6). Again, the numerical simulation is performed calling Matlab's *lsim* function for varying absorber damping ratios ζ_A , still using the single degree-of-freedom structural model.

	RMS response				peak response			
	<i>Structure</i>		<i>Absorber</i>		<i>Structure</i>		<i>Absorber</i>	
	displ. [m]	accel. [m/s ²]	displ. [m]	accel. [m/s ²]	displ. [m]	accel. [m/s ²]	displ. [m]	accel. [m/s ²]
$\zeta_A = 3\%$	0.49	0.18	2.97	1.13	1.71	0.59	6.83	2.81
$\zeta_A = 5\%$	0.50	0.18	2.71	1.03	1.83	0.64	6.67	2.73
$\zeta_A = 7\%$	0.52	0.19	2.52	0.96	1.94	0.68	6.38	2.61
$\zeta_A = 9\%$	0.56	0.20	2.37	0.90	2.03	0.71	6.06	2.47
$\zeta_A = 11\%$	0.61	0.22	2.25	0.85	2.11	0.75	5.75	2.37

Table 9-2: TMD parameters and structural response with respect to the X-direction due to critical wind load, evaluated for the single DOF damped structural model with 363t TMD attached

	RMS response				peak response			
	<i>Structure</i>		<i>Absorber</i>		<i>Structure</i>		<i>Absorber</i>	
	displ. [m]	accel. [m/s ²]	displ. [m]	accel. [m/s ²]	displ. [m]	accel. [m/s ²]	displ. [m]	accel. [m/s ²]
$\zeta_A = 3\%$	0.82	0.14	1.75	0.72	2.11	0.41	6.03	2.33
$\zeta_A = 5\%$	0.81	0.12	1.40	0.57	2.09	0.41	4.91	1.89
$\zeta_A = 7\%$	0.80	0.11	1.20	0.48	2.11	0.42	4.23	1.62
$\zeta_A = 9\%$	0.80	0.11	1.07	0.43	2.13	0.42	3.76	1.43
$\zeta_A = 11\%$	0.80	0.11	0.97	0.39	2.16	0.43	3.41	1.30
$\zeta_A = 13\%$	0.80	0.11	0.90	0.36	2.18	0.44	3.14	1.19

Table 9-3: TMD parameters and structural response with respect to the Y-direction due to critical wind load, evaluated for the single DOF damped structural model with 363t TMD attached

In contrast to the statistical optimisation, minimal structural response is obtained for damping ratios of less than 5%. Nevertheless, the simulated response listed in Table 9-2 and Table 9-3 reveal that the system is not sensitive to variations in ζ_A , and the differences in the structural response remains small. When compared to the original structure, substantial reduction in the

structural response can be achieved in both, X-and Y-direction. Unfortunately, the extremely large TMD-absorber displacements in X-direction are beyond practical limits, especially if only one single ring-shaped mass serves as absorber for both directions. The maximum absorber stroke can exceed $6m$ and does not meet implementation constraints of about $3m$. In the Y-direction the selected TMD parameters result in absorber displacements of $3.14m$ for $\zeta_A = 13\%$, which is just within the acceptable range. In order to decrease the TMD displacements one has to either increase the TMD mass, or the damping ratio ζ_A . Since the absorber mass is limited, the only alternative is increasing the absorber damping, which will certainly reduce the absorber stroke at the price of higher structural responses. Consequently, further studies with damping coefficients in the range of 10-60% of critical damping are performed, see Table 9-4. It is evident that one has to compromise between good structural vibration attenuation and high absorber displacements. Increasing the damping ratio ζ_A up to 40% or even 60% yields TMD displacements which meet the implementation requirements. Thus ζ_A is increased to 50% to keep the TMD-mass displacement smaller than $3.5m$, reducing the structural displacement about 31% from $5.27m$ to $3.62m$.

	RMS response				peak response			
	<i>Structure</i>		<i>Absorber</i>		<i>Structure</i>		<i>Absorber</i>	
	displ. [m]	accel. [m/s ²]	displ. [m]	accel. [m/s ²]	displ. [m]	accel. [m/s ²]	displ. [m]	accel. [m/s ²]
$\zeta_A = 10\%$	0.58	0.21	2.31	0.87	2.07	0.73	5.90	2.42
$\zeta_A = 20\%$	0.80	0.29	1.85	0.70	2.47	0.88	4.89	2.00
$\zeta_A = 30\%$	0.97	0.36	1.55	0.59	2.95	1.05	4.19	1.69
$\zeta_A = 40\%$	1.10	0.41	1.34	0.50	3.32	1.19	3.65	1.46
$\zeta_A = 50\%$	1.21	0.44	1.18	0.44	3.62	1.30	3.23	1.28
$\zeta_A = 60\%$	1.28	0.47	1.05	0.39	3.86	1.39	2.89	1.14

Table 9-4: TMD parameters and structural response for increase absorber damping ratio ζ_A due to critical wind load in X-direction; evaluated for the single DOF damped structural model with 363t TMD attached

9.2.2. TLCD design

For the tall building studied, the application of TLCDs seems very promising, since the adaptation to large absorber displacements is one of the salient features of TLCD. Other are its simplicity and cheap implementation, little installation and maintenance costs, easy and adjustable frequency

tuning (ageing building), and no moving parts, friction or wear. Similar to the TMD, the TLCD will be installed on top of the building. Because it is impossible to construct a huge bi-directional vibration absorber without using the occupied central area of the top floor, two TLCD must be installed, and, for the sake of a comparative study, the total liquid mass is limited to $363t$, being split into two masses, $220t$ in the X-direction and $143t$ in the Y-direction. Following the TMD-TLCD analogy outlined in Chapter 5, an analytical solution for the optimal tuning and damping ratio can be found. Equations (9-6) and (9-7) give the optimal parameter for the corresponding TMD. Applying the transformation given in Section 5.1, the optimal TLCD parameter can be given straightforwardly,

$$\delta = \frac{\sqrt{1 + \mu(1 - \kappa\bar{\kappa}/2)}}{1 + \mu}, \quad (9-8)$$

$$\zeta_A = \sqrt{\frac{\mu\kappa\bar{\kappa}(1 + \mu(1 - \kappa\bar{\kappa}/4))}{4(1 + \mu)(1 + \mu(1 - \kappa\bar{\kappa}/2))}}. \quad (9-9)$$

Assuming $\kappa\bar{\kappa} \approx 0.8$, estimations for the tuning and damping ratio can be given by $\delta = 0.986$ and $\zeta_A = 6.90\%$, in X-direction, and $\delta = 0.990$, $\zeta_A = 5.56\%$ in Y-direction, respectively. The determination of the optimal damping ratio is again performed by simulations, which confirm the analytical results, see Table 9-5, where the RMS and peak responses of the main structure and the vibration absorber in Y-direction for several damping ratios are displayed. Again, the system is not sensitive to the absorber damping ζ_A , and hence it can be chosen $\zeta_A = 9\%$, thereby decreasing the maximum top floor displacement to $2.44m$, and causing a maximum absorber displacement of $4.93m$.

	RMS response				peak response			
	<i>Structure</i>		<i>Absorber</i>		<i>Structure</i>		<i>Absorber</i>	
	y-displ. [m]	y-accel. [m/s ²]	displ. [m]	accel. [m/s ²]	y-displ. [m]	y-accel. [m/s ²]	displ. [m]	accel. [m/s ²]
$\zeta_A = 5\%$	0.82	0.14	2.18	0.87	2.29	0.49	6.16	2.46
$\zeta_A = 7\%$	0.83	0.14	1.90	0.76	2.37	0.52	5.48	2.18
$\zeta_A = 9\%$	0.84	0.15	1.70	0.67	2.44	0.54	4.93	1.95
$\zeta_A = 11\%$	0.85	0.16	1.53	0.61	2.49	0.57	4.50	1.76
$\zeta_A = 13\%$	0.86	0.17	1.40	0.55	2.54	0.59	4.13	1.60

Table 9-5: Response in Y-direction for $143t$ TLCD installed on top floor, critical wind load segment applied, evaluated for the single DOF damped structural model

From the TMD design it is known, that extremely large vibration amplitudes are expected in X-direction. Therefore it is of interest to investigate the influence of varying cross sectional areas on the vibration response. Table 9-6 summarises the system response for different cross sectional areas, and for this study, the absorber damping ζ_A is chosen such that the maximum structural displacement in the X-direction is approximately $2.5m$.

		$\beta=20^\circ$	$\beta=30^\circ$	$\beta=45^\circ$	$\beta=60^\circ$	$\beta=90^\circ$
$A_H/A_B = 1$	$L_{eff} [m]$	17.01	24.87	35.17	43.08	49.79
	κ	0.94	0.91	0.866	0.814	0.679
	$\bar{\kappa}$	0.94	0.91	0.866	0.814	0.679
	struct.displ. [m]	2.56	2.53	2.52	2.54	2.82
	absorb. displ [m]	7.83	8.07	8.34	8.70	9.44
$A_H/A_B = 2$	$L_{eff} [m]$	17.01 H=5,B=3.5	24.87 H=5,B=7.43	35.17 H=5,B=12.6	43.08 H=5,B=15.5	49.79 H=5,B=19.9
	κ	0.76	0.64	0.56	0.41	0.40
	$\bar{\kappa}$	1.09	1.17	1.20	0.98	1.00
	struct.displ. [m]	2.53	2.53	2.52	2.58	2.58
	absorb. displ [m]	6.53	6.18	5.92	6.84	6.70
$A_H/A_B = 3$	$L_{eff} [m]$	17.01 H=4,B=3.0	24.87 H=4,B=5.62	35.17 H=4,B=9.05	43.08 H=4,B=11.7	49.79 H=4,B=13.9
	κ	0.62	0.50	0.42	0.36	0.28
	$\bar{\kappa}$	1.17	1.27	1.33	1.32	1.10
	struct.displ. [m]	2.55	2.57	2.56	2.58	3.00
	absorb. displ [m]	6.10	5.44	5.14	5.05	5.70

Table 9-6: Response data for 220t TLCD with varying cross sectional areas, varying opening angles β , and optimal damping ratio in X-direction; single DOF structure subject to critical wind load

From Table 9-6 it follows that $A_H/A_B = 3$ is the most suitable area ratio to minimise both, structural and absorber displacements. Choosing the opening angle $\beta = 30^\circ$ causes a maximum absorber displacement of $u_{\max} = 5.44m$ when $\zeta_A = 8\%$, and still keeps the total TLCD height below $6m$. At the same time, the maximum structural displacement in X-direction is reduced to

$w_{x,\max} = 2.57m$. For this TLCD configuration further response quantities are summarised in Table 9-7.

	RMS response				peak response			
	<i>Structure</i>		<i>Absorber</i>		<i>Structure</i>		<i>Absorber</i>	
	displ. [m]	accel. [m/s ²]	displ. [m]	accel. [m/s ²]	displ. [m]	accel. [m/s ²]	displ. [m]	accel. [m/s ²]
$\zeta_A = 8\%$	0,87	0,32	2.34	0,88	2,57	0.92	5,44	2,18

Table 9-7: Response in X-direction for the 220t TLCD installed on top floor, $\beta = 30^\circ$, $A_H/A_B = 3$, evaluated for the SDOF structural model under critical wind load

When comparing the structural response in X- and Y-direction, similar displacements for the main structure and the TLCDs are obtained which is desirable from a practical point of view. Figure 9-20 and Figure 9-21 display the top floor displacement response of the structure with and without the passive devices installed. For the TLCD the vibration reduction is around 50% in both, X- and Y-directions. It has to be mentioned that the quasi-static displacement in Y-direction which results from a nonzero mean wind load, cannot be compensated by a dynamic vibration absorber. When compared to the TMD the TLCD performs excellent, since TMD implementation constraints reduce the vibration attenuation in X-direction dramatically. In the Y-direction, however, the TMD performs excellent, with a vibration reduction better than the TLCD, since its mass ratio is much larger.

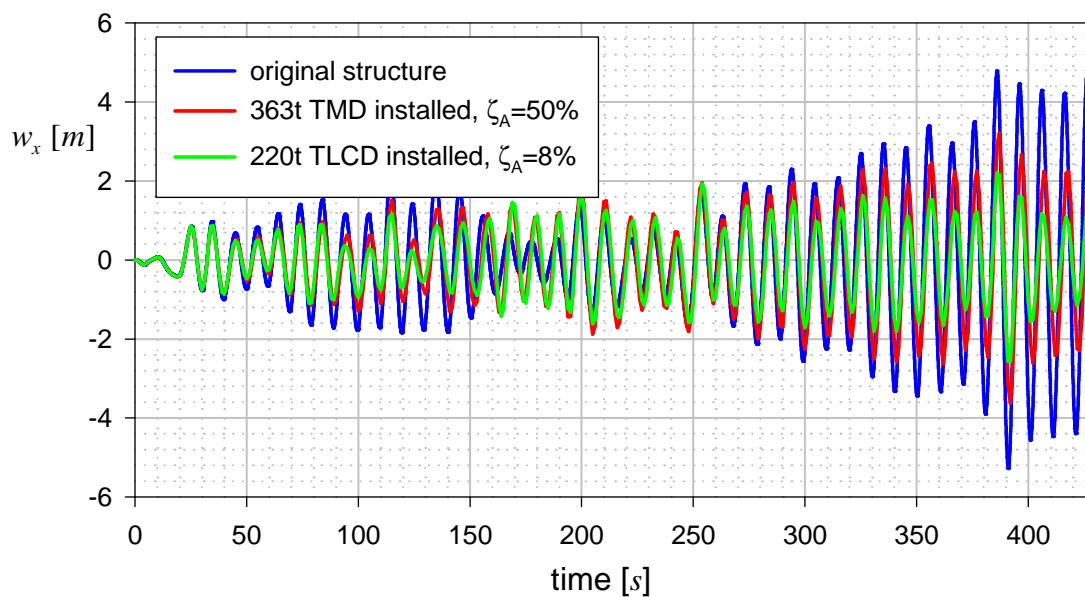


Figure 9-20: Top floor displacement in X-direction with and without TMD and TLCD

installed, single DOF structural model,
numerical integration with *lsim* (Matlab Control Toolbox⁶)

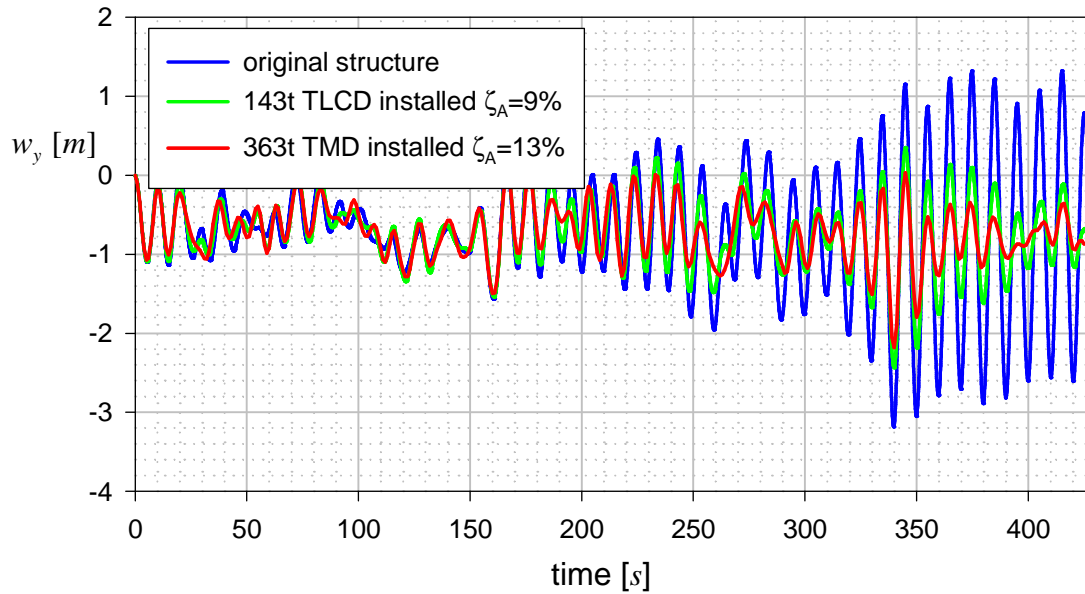


Figure 9-21: Top floor displacement in Y-direction with and without TMD and TLCD installed, single DOF structural model, numerical integration with *lsim* (Matlab Control Toolbox⁶)

9.2.3. Simulation of turbulent damping

Up to now the numerical study is based on a linear system with viscous damping. However, the insertion of an orifice causes turbulent damping, which might change the system behaviour. For comparison, the SDOF building model is equipped with a TLCD described by the nonlinear TLCD equation of motion, Eq.(4-8). The conversion of the equivalent damping factor $\zeta_A = 0.08$ to the head loss factor δ_L is obtained by applying Eq.(A-8), see Appendix A, $\delta_L = \frac{3\pi\zeta_A}{4U_{\max}}$. With

a maximum vibration amplitude of $U_{\max} = 5.44m$ the head loss factor becomes $\delta_L = 0.0346m^{-1}$.

The simulations of the nonlinear system have been performed using Simulink¹⁸, a powerful tool allowing graphical programming, system analysis and simulation, which is smoothly integrated into the Matlab scientific computing environment. Simulink calculates the response of nonlinear systems by time integration. The block diagram of the Simulink model is shown in Figure 9-22.

The time integration was performed using the ode45 (Dormand-Prince) integration with variable time steps and a relative tolerance of 1e-8 and a absolute tolerance of 1e-7.

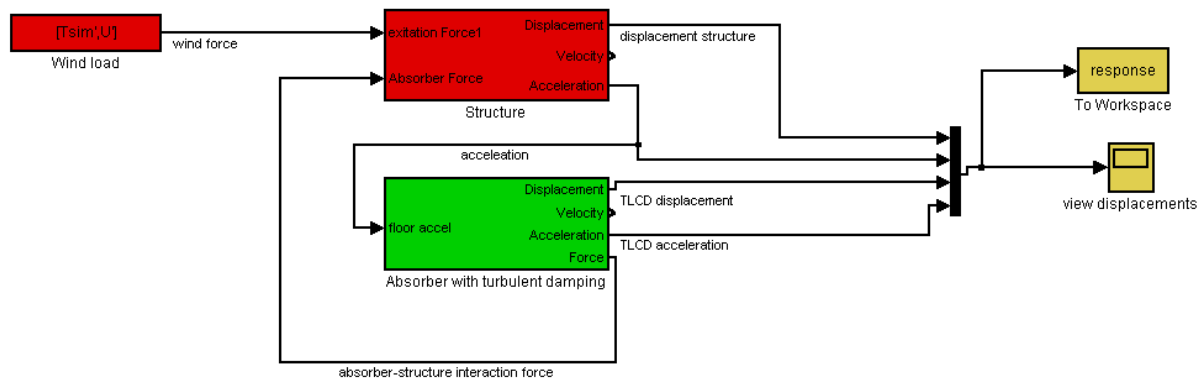


Figure 9-22: Simulink¹⁸ block diagram of SDOF structural model with nonlinear TLCD attached

The simulations have revealed, that the nonlinear system performs even better than the linear one: for small structural vibrations the TLCD is lightly damped thus it starts to oscillates with a fairly large vibration amplitude, thereby absorbing energy and keeping the structural displacements small. When coming to the peak structural vibrations, the turbulent damping prevents excessive TLCD amplitudes. The system response is summarised in Table 9-8

	RMS response				peak response			
	Structure		Absorber		Structure		Absorber	
	displ. [m]	accel. [m/s ²]	displ. [m]	accel. [m/s ²]	displ. [m]	accel. [m/s ²]	displ. [m]	accel. [m/s ²]
$\delta_L = 0.0346m^{-1}$	0,81	0,29	2,65	0,99	2,43	0,87	5,18	2,14

Table 9-8: Response in X-direction for the 220t TLCD installed on top floor, $\beta = 30^\circ$, $A_H/A_B = 3$, evaluated for the SDOF structural model under critical wind load, turbulent TLCD damping included.

9.2.4. Device configuration and concluding remarks

To avoid any unwanted torsional vibrations, both absorber types must be installed symmetrically, see Figure 9-23, where a plan view of the top floor is shown. Basically, the TMD consists of a doughnut shaped mass, see Figure 9-23a) which is sliding on pneumatic bearings and suspended

by linear springs. The TLCD setup, given in Figure 9-23b) consists of two pairs of TLCD, one for each direction. To avoid very large cross sectional areas, each individual TLCD can be subdivided further, to avoid a piping system with huge cross sectional areas. For simple installation it is suggested to install a piping system with rectangular cross section.

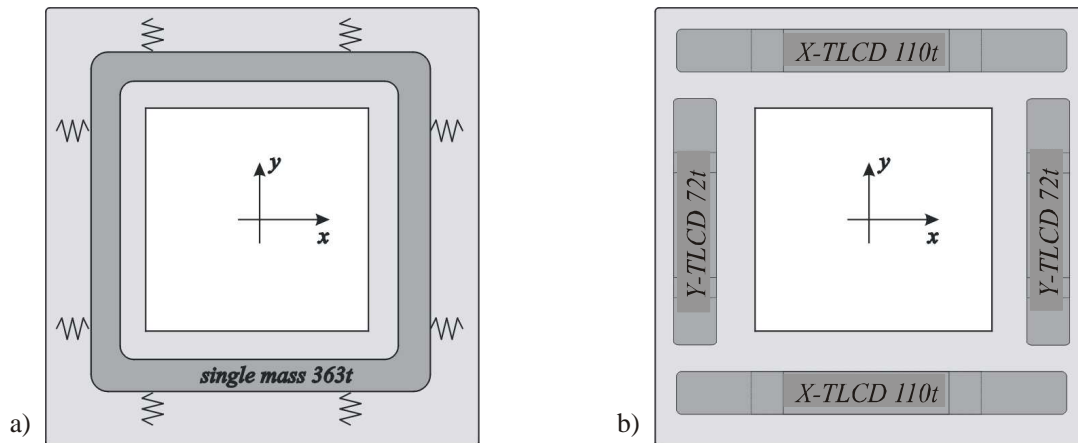


Figure 9-23: Top floor arrangements of dynamic vibration absorber a) bi-directional TMD
b) 4 symmetrically arranged single TLCD

Although there are experiments and concepts on bi-directional TLCD, see Chapter 3, the space restrictions already mentioned do not allow such an implementation. Furthermore, the expected large absorber displacements would reduce the efficiency of the bi-directional TLCD setup, which justifies the decision to install two independent TLCD-systems. Contrary to the TLCD, the passive TMD requires further components, some of which are technically demanding:

1. 2 Linear springs, $k = 71580 \text{ N/m}$, with a maximum force of $F_{\max} = 250000 \text{ N}$ in X-direction
2. 2 Linear springs, $k = 71580 \text{ N/m}$, with a maximum force of $F_{\max} = 250000 \text{ N}$ in Y-direction
3. Viscose dampers to provide the necessary energy dissipation
4. Two small hydraulic actuators with LVDT to compensate for friction losses
5. 12 hydraulic and pneumatic bearings
6. Reaction abutments
7. Control room

Especially the bearings and the hydraulic actuators require regular maintenance and are power dependent. Therefore, additional precautions must be considered to guarantee operation even during power losses. The proposed TLCD, however, is a purely passive system and completely independent of any external power, and even maintenance. There are no friction problems as the design has no moving parts and all the energy dissipation is achieved by an hydraulic resistance, which can be integrated smoothly, as shown in Figure 9-24. The main advantage of this new orifice design is the fact that it allows for even larger liquid displacements since the inclined pipe section is lengthened. The water container has to be constructed sufficiently rigid to withstand the absorbing forces and in case the water is used for normal water supply it is necessary to meet the hygienic standards for water containers, which do not impose mayor restrictions on design and costs. Overall the TLCD seems to be very competitive when compared to the passive TMD setup. Its physical dimensions are slightly larger, but its peak performance is better, and all other salient features (e.g. its simplicity and uncomplicated installation, etc.) make it superior to the TMD for the building studied.

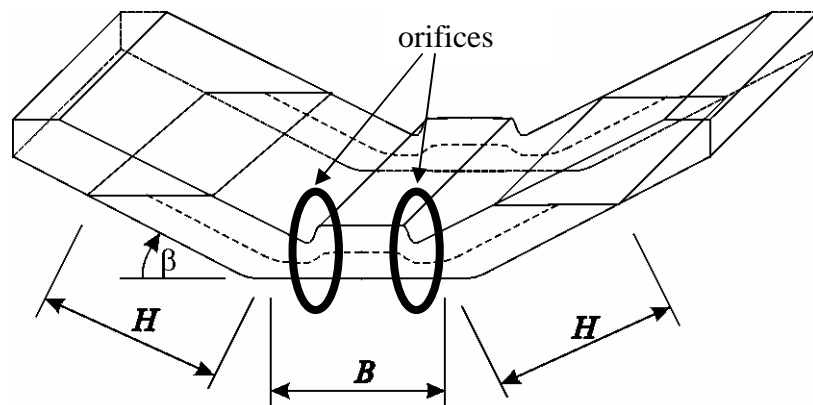


Figure 9-24: Proposed TLCD container with integrated orifice plate

9.3. 3-DOF benchmark structure

9.3.1. Introduction

The effectiveness of TLCDs in vibration reduction is now demonstrated for a three degree-of-freedom test structure under earthquake loading. Based upon the benchmark definition paper, see Spencer et al.¹¹, a structure considered by Chung et al.¹², is equipped with passive and active TLCD. A model of the scaled test structure (originally designed for active tendon control) was built at the National Center for Earthquake Engineering Research (NECCER) at Buffalo, see in Figure 9-25a). It has a total mass of 2.943kg, distributed evenly among the three floors, and is 2.54m in height. A 3-DOF numerical evaluation model, which is based on this real structure is used for the numerical study.

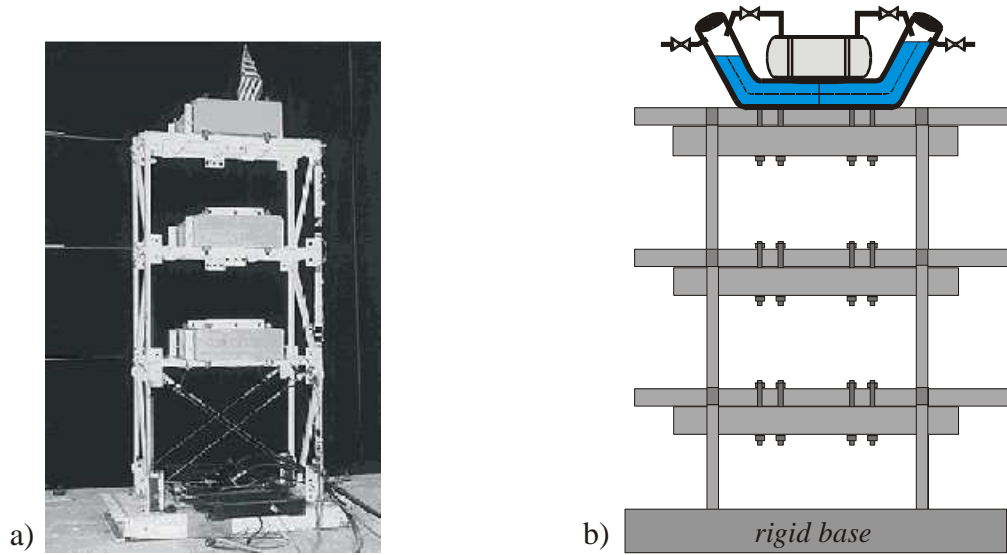


Figure 9-25: 3-DOF benchmark structure a) in active tendon configuration, see Spencer et al.¹¹
b) schematics with ATLCD installed on top floor

The mass and stiffness matrices have been provided by Prof. Soong, State University of New York at Buffalo, Department of Civil and Environmental Engineering, and they are given by

$$\mathbf{M} = \begin{bmatrix} 981 & 0 & 0 \\ 0 & 981 & 0 \\ 0 & 0 & 981 \end{bmatrix} [kg], \quad \mathbf{K} = \begin{bmatrix} 650.3 & -183.4 & 33.2 \\ -183.4 & 574.7 & -148.9 \\ 33.2 & -148.9 & 387.2 \end{bmatrix} \left[\frac{N}{m} \right]. \quad (9-10)$$

The mode shape vectors $\boldsymbol{\varphi}_1$, $\boldsymbol{\varphi}_2$ and $\boldsymbol{\varphi}_3$ are calculated from the corresponding eigenvalue problem,

$$\boldsymbol{\varphi}_1 = \begin{pmatrix} 0.0897 \\ 0.2365 \\ 0.3385 \end{pmatrix}, \boldsymbol{\varphi}_2 = \begin{pmatrix} 0.2859 \\ 0.2143 \\ -0.2255 \end{pmatrix}, \boldsymbol{\varphi}_3 = \begin{pmatrix} 0.2979 \\ -0.2769 \\ 0.1146 \end{pmatrix}. \quad (9-11)$$

Due to an inevitable reduction in scale, the ratio of model quantities to the corresponding prototype structure are: force=1:16, mass=1:16, time=1:2, displacement=1:4 and acceleration=1:1. Thus the natural frequencies of the model are approximately twice those of the prototype and they were found to be 2.27Hz , 7.33Hz , and 12.24Hz , with associated modal damping ratios given by 1%, 2%, and 3%, respectively. For the numerical study the hydraulic control actuator, connected to four pretensioned tendons, as shown in Figure 9-25a), is replaced by an ATLCD installed on top of the building, schematically displayed in Figure 9-25b). Although the real test structure is fully instrumented (acceleration and displacement transducers on each floor) to provide for a complete record of the motions undergone during testing, only absolute floor and ground acceleration measurements will be used for control purposes, since all other measurements are not directly available in a full scale implementation.

9.3.2. TLCD design

For safety reasons, the design of an ATLCD should always be based on a passive TLCD, because if the pressurisation fails, the TLCD will continue to operate properly. Therefore a conventional TLCD is designed first, starting with the determination of its geometry and mass ratio. Since the weight of dynamic absorbers (TMD or AMD) is commonly between 0.5% and 2% of the total building mass, a TLCD-building mass ratio of 1% which corresponds to about 29.5kg of water. The piping system is selected to have a constant cross sectional area, and the liquid column length is chosen to be $L_{eff} = 2.5\text{m}$, with the length of the horizontal and inclined pipe sections being $B = 1.5\text{m}$ and $H = 0.5\text{m}$, respectively. For an opening angle of $\beta = 40^\circ$ the geometry dependent coupling coefficients become (see Eq.(4-9) and Eq.(4-33)), $\kappa = \bar{\kappa} = \frac{2H \cos \beta + B}{L_{eff}} = 0.91$. Having

defined the basic geometry, the determination of the absorber tuning ω_A and the equivalent viscose damping is possible, by minimising a performance criterion, which is defined in the frequency domain, see Eq.(7-21) and Section 7.2.1,

$$J = \sum_{i=1}^N \int_{\nu_{\min}}^{\nu_{\max}} s_i |h_i(\nu)|^2 d\nu \rightarrow \text{minimum}, \quad (9-12)$$

It is minimised with respect to δ and ζ_A , and for the sake of simplicity, an infinite frequency range $-\infty \leq \nu \leq \infty$ is considered. If the reduction of the floor displacements and velocities is desired, then h_i will represent those response quantities of interest, and the performance index can be rewritten as

$$J = \int_{-\infty}^{\infty} \mathbf{z}_s^T(\nu) \mathbf{S} \mathbf{z}_s(\nu) d\nu, \quad (9-13)$$

where the weighting factors are grouped in the diagonal matrix $\mathbf{S} = \text{diag}(10, 10, 10, 1, 1, 1)$, and \mathbf{z}_s represents the host structure's state vector, $\mathbf{z}_s(\nu) = [w_1(\nu), w_2(\nu), w_3(\nu), \dot{w}_1(\nu), \dot{w}_2(\nu), \dot{w}_3(\nu)]^T$. Although no TLCD quantities, e.g. displacement or velocity, enter the performance index directly, its influence is hidden in the system dynamics and thus in structural response vector \mathbf{z}_s . Having defined a suitable performance criterion its numerical minimisation is performed with respect to ω_A and ζ_A , and the initial values of $\omega_A = \Omega_s$ and $\zeta_A = 0.1$, where Ω_s denotes the fundamental frequency of the benchmark model. Again the numerical optimisation was performed with the very robust *fminsearch* procedure available in the Matlab Optimisation Toolbox⁴, see explanations in Section 9-1. Calling *fminsearch* without any special options and with the initial parameter given above immediately renders the optimal tuning frequency and damping ratio, $f_A = \omega_A / 2\pi = 2.23 \text{ Hz}$ and $\zeta_A = 6.32\%$, respectively, corresponding to a tuning ratio of $\delta = \omega_A / \Omega_s^1 = 0.984$. Figure 9-26 illustrates the influence of the properly designed TLCD on the

weighted sum of the amplitude response function $\sum_{i=1}^6 s_i |z_i(\nu)|$ plotted in the decibel scale,

$x[\text{dB}] = 20 \log x$, to allow for variations in the response function in the order of several orders of magnitude. Apparently the TLCD mitigates vibrations near the fundamental frequency of the structure, and a response reduction of a factor of 10 ($=20\text{dB}$) is achieved at resonance.

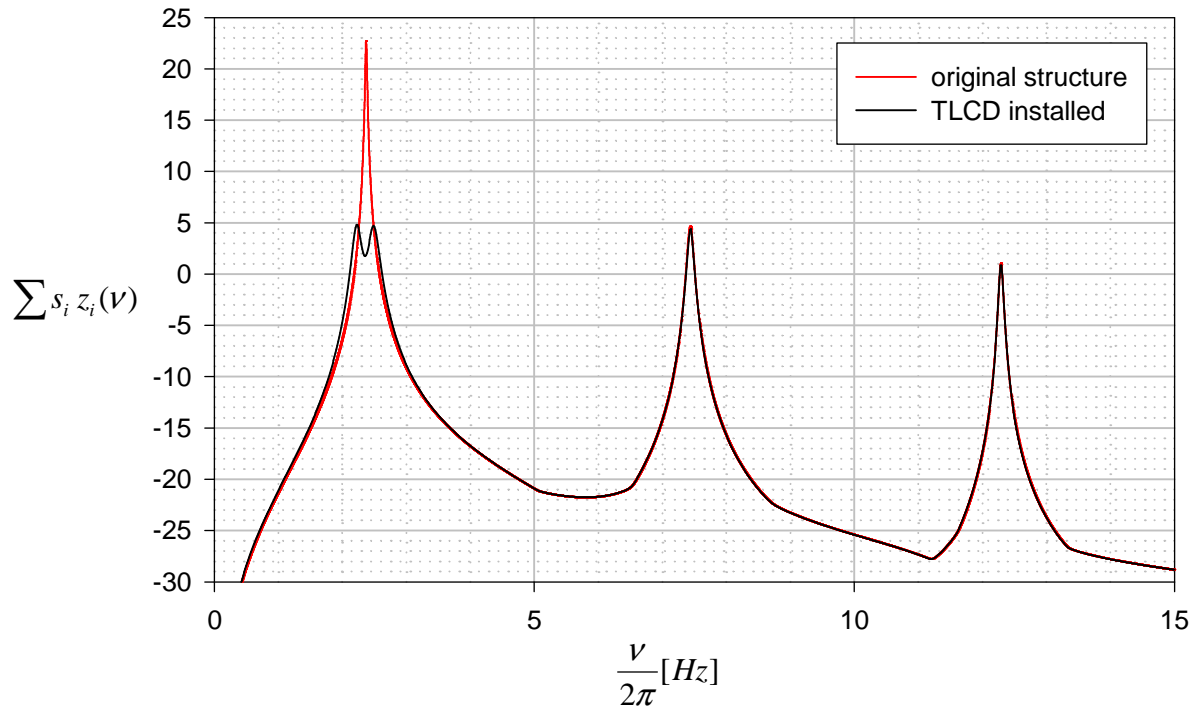


Figure 9-26: Performance index for 3-DOF benchmark structure

According to Eq.(4-10), the passive TLCD without the air-spring effect incorporated would need an effective length of about $0.064m$ to oscillate with natural frequency of $2.23Hz$. Thus it is inevitable to use the TLCD in the passive air-spring configuration. If the compression/expansion of the air inside the piping system (initially at atmospheric pressure $p_0 = 1bar$), is described by an

adiabatic process ($n = \kappa_a = \frac{c_p}{c_v} = 1.4$), then h_{eff} is found from Eq.(4-41),

$$h_{eff} = \frac{2 n p_0}{\rho (L_{eff} \omega_A^2 - 2 g \sin \beta)} = 0.58m. \quad (9-14)$$

Consequently, the maximum liquid displacement is limited by $0.5m$. Having finished the TLCD design, it is possible to perform numerical simulations to estimate the influence of the passive TLCD on the structural response. A comparison between the original structure and the one with the TLCD installed is given in Table 9-9 and Table 9-10, if the historical 1940 El Centro NS acceleration record is applied as ground excitation input. The El Centro earthquake acceleration record is presented in Figure 9-5 in its original scale with a peak ground acceleration of

$$\ddot{w}_{g,max} = 3.417 \frac{m}{s^2} = 0.35g.$$

Because the system under consideration is a scaled model, the time scale of the acceleration input is increased by a factor of 2, e.g., the earthquake occurs in $1/2$ the recorded time, thus the sampling time is reduced to $\Delta t = 0.01s$, but since the acceleration scale=1:1 the ground acceleration intensity is not modified. The response criteria considered are the floor displacement w_i with respect to the basement, the relative interstory drifts, w_i^r , the absolute accelerations of the floors, $\ddot{w}_i + \ddot{w}_g$, as well as the base shear force Q_{base} . Furthermore, the TLCD response is characterised by its maximal displacement u_{max} . For all response quantities the peak as well as the RMS are calculated.

	<i>peak response</i>				<i>RMS response</i>			
	w_i, u [cm]	w_i^r [cm]	$\ddot{w}_i + \ddot{w}_g$ [m/s ²]	Q_{base} [kN]	w_i, u [cm]	w_i^r [cm]	$\ddot{w}_i + \ddot{w}_g$ [m/s ²]	Q_{base} [kN]
floor 1	1.45	1.45	5.42		0.50	0.50	1.49	
floor 2	3.89	2.46	9.93		1.30	0.81	2.98	
floor 3	5.87	1.89	14.76		1.86	0.56	4.18	
Base				23.55				8.05

Table 9-9: Peak and RMS response of original model due to the properly scaled El Centro earthquake input

	<i>peak response</i>				<i>RMS response</i>			
	w_i, u [cm]	w_i^r [cm]	$\ddot{w}_i + \ddot{w}_g$ [m/s ²]	Q_{base} [kN]	w_i, u [cm]	w_i^r [cm]	$\ddot{w}_i + \ddot{w}_g$ [m/s ²]	Q_{base} [kN]
floor 1	0.96	0.96	5.31		0.20	0.20	1.07	
floor 2	2.35	1.55	7.21		0.53	0.33	1.36	
floor 3	3.60	1.25	9.76		0.76	0.24	1.80	
Base				16.12				3.34
TLCD	18.71				7.39			

Table 9-10: Peak and RMS response of model with TLCD attached due to the properly scaled El Centro earthquake input

Apparently, the vibration reduction achieved is about 35%, even for critical response quantities like interstory drifts and base shear. A graphical representation of the base shear and the 3rd floor interstory drift is given in Figure 9-29 and Figure 9-30 where it is clearly visible that the passive TLCD needs several vibration cycles before operating properly.

9.3.3. Implementation of an active pressure control

In order to reduce the peak responses in the transient vibration regime, the active air spring concept of Section 8.4, is applied to improve the passive TLCD. Based on a classical linear quadratic state space control design, an active pressure input is applied, and modified to a simple bang-bang controller which will turn out to work quite efficiently. To make the simulation as realistic as possible, the following control implementation constraints are placed on the system:

- The only vibration measurements directly available for use in determination of the control action are the absolute floor accelerations.
- Each of the measured responses contains an RMS noise of 0.01V, which is approximately 0.3% of the full span of the A/D converters. The measurement noise is modelled as a Gaussian rectangular pulse process.
- The controller for the structure is digitally implemented with a sampling rate of 0.01s.

If a state space representation of the structural model is known, the design of a linear quadratic controller is straightforward, because it is readily available in several control Toolboxes, e.g. the *lqr* command in the Control Toolbox of MatLab⁶. It designs linear-quadratic (LQ) state-feedback regulators for continuous plant, and calculates the optimal gain matrix $\mathbf{K} = \mathbf{S}^{-1}\mathbf{E}_a^T\mathbf{P}$, see Eq.(8-20) such that the state-feedback law $\mathbf{u}_a = -\mathbf{K}\mathbf{z}$ minimised the quadratic cost function defined by

$$\text{Eq.(8-11), } J = \int_0^{\infty} \mathbf{z}^T \mathbf{Q} \mathbf{z} + \mathbf{u}_a^T \mathbf{S} \mathbf{u}_a dt \text{ for the continuous-time state space model } \mathbf{z} = \mathbf{A}_r \mathbf{z} + \mathbf{E}_a \mathbf{u}_a.$$

Apparently the system matrix \mathbf{A}_r , the input matrix \mathbf{E}_a , as well as the state- and input-weighting matrices \mathbf{Q} and \mathbf{S} are required. Given the state vector $\mathbf{z} = [w_1, w_2, w_3, u, \dot{w}_1, \dot{w}_2, \dot{w}_3, \dot{u}]^T$ of the coupled system, the following weighting matrices were chosen in an iterative trial and error process: $\mathbf{Q} = \text{diag}(10, 10, 10, 1, 10, 10, 10, 0)$ and $\mathbf{S} = 5 \cdot 10^{-5}$. An alternative to applying the *lqr* command is to solve the Riccati Equation, Eq. (8-18), and obtain the feedback control as given by Eq.(8-20). This can e.g. be accomplished by calling the Matlab control toolbox function *care* (Continuous time Algebraic Riccati Equation), which computes the unique solution \mathbf{P} of Eq.(8-19), based on the algorithm described in Arnold¹³. Since the *lqr* command also calls *care*, both commands yield the same results. However, the full state vector has to be known for the control implementation, and measurements are restricted to accelerations only. Thus a standard Luenberger estimator, see e.g. Luenberger¹⁴ is used to estimate the state vector \mathbf{z} . It is well

known, that the design of a state estimator requires some experience since one has to compromise between accuracy, robustness, and sensitivity to noisy measurements. After a tedious trial and error process, a good state estimation has been achieved by measuring the ground and top floor acceleration as well as the pressure input, and choosing the estimator only slightly faster than the structural model. Since the acceleration input (disturbance, from a control engineer's point of view) can be measured accurately, it is sufficient to design the state estimating filter (observer) twice as fast as the structural model, thus the complex filter poles (observer) p_{filter} are defined through the structural poles p_{struct} , $\text{Re}(p_{filter}) = \text{Re}(2 p_{struct})$ and $\text{Im}(p_{filter}) = \text{Im}(2 p_{struct})$. The generation of the observing filter is supported by the functions *acker* or *place* of the Matlab Control Toolbox⁶, which designs an observing filter such that its pole location corresponds to the desired values, see e.g. Ackermann¹⁵ or Kautsky et al.¹⁶ for details. Knowing an estimation \bar{z} (output of the observing filter) of the actual state, the continuous pressure control $\mathbf{u} = -\mathbf{S}^{-1}\mathbf{E}_a^T\mathbf{P}\bar{z}$ is applied to the ATLCD, and the closed loop system can be simulated using the *lsim* command. For comparison, another controller is investigated. Based on the continuous controller control law, $\mathbf{u} = -\mathbf{S}^{-1}\mathbf{E}_a^T\mathbf{P}\bar{z}$ obtained from calling the *lqr* function, the bang-bang control, given by Eq.(8-34) is applied, and the maximum pressure difference is limited by $\Delta p_a = 1.25 \cdot 10^5 \text{ N/m}^2 = 1.25 \text{ bar}$. In addition it is assumed that the actuator dynamics can be modelled as a first order low pass process, with a cut-off frequency of $\omega_c = 30 \text{ rad/s}$, thus the actual pressure input to the ATLCD is defined by the desired bang-bang pressure input filter through a first order low pass filter, defined by $f(s) = \frac{\omega_c}{\omega_c + s}$ in the Laplace domain. For detailed information on filtering techniques see e.g. Dorf¹⁷. The application of the filtering function allows to account for the time it takes to build up the pressure. Since it is not necessary to activate the control if the passive system is working properly, activation and switch off levels are chosen according to Figure 8-5, where the ATLCD started to operate if the sum of the relative kinetic and strain energy exceeded 70 J . The ATLCD is switched off if the TLCD displacement exceeds 0.3 m . Again, the properly scaled historical 1940 El Centro NS acceleration record is applied to the frame structure and Table 9-11 and Table 9-12 summarise important response quantities.

The bang-bang controlled structure is simulated using Simulink¹⁸, a powerful tool for model construction analysis and simulation. Simulink is smoothly integrated into the Matlab scientific computing environment, and allows complex nonlinear models to be generated interactively. Thus the nonlinearity caused by switching bang-bang control law can be implemented

straightforwardly. The simulation is still based on the linear time invariant structural model used before. For the nonlinear bang-bang control a fixed time step ($\Delta t = 0.01s$) third order time integration scheme (Bogacki-Shampine) is selected to obtain a numerical solution of the dynamic system. The block diagram of the Simulink model is given in Figure 9-27

	<i>peak response</i>				<i>RMS response</i>			
	w_i, u [cm]	w_i^r [cm]	$\ddot{w}_i + \ddot{w}_g$ [m/s ²]	Q_{base} [kN]	w_i, u [cm]	w_i^r [cm]	$\ddot{w}_i + \ddot{w}_g$ [m/s ²]	Q_{base} [kN]
floor 1	0.38	0.38	3.72		0.08	0.08	0.59	
floor 2	0.99	0.67	4.78		0.20	0.12	0.63	
floor 3	1.52	0.64	5.07		0.29	0.10	0.62	
Base				6.59				1.29
TLCD	48.02				9.45			

Table 9-11: Simulated peak and RMS response of the frame structure with a continuous time controller (*lqr*), due to the properly scaled El Centro earthquake input, simulation tool Matlab *lsim* command

	<i>peak response</i>				<i>RMS response</i>			
	w_i, u [cm]	w_i^r [cm]	$\ddot{w}_i + \ddot{w}_g$ [m/s ²]	Q_{base} [kN]	w_i, u [cm]	w_i^r [cm]	$\ddot{w}_i + \ddot{w}_g$ [m/s ²]	Q_{base} [kN]
floor 1	0.64	0.64	5.23		0.15	0.15	0.96	
floor 2	1.43	0.92	6.12		0.38	0.23	1.17	
floor 3	2.10	0.77	8.40		0.53	0.17	1.52	
TLCD	50.07				11.03			
Base				11.37				2.45

Table 9-12: Simulated peak and RMS response of the frame structure with ATLCD and bang-bang control strategy applied, due to the El Centro earthquake input, simulation with Simulink¹⁸

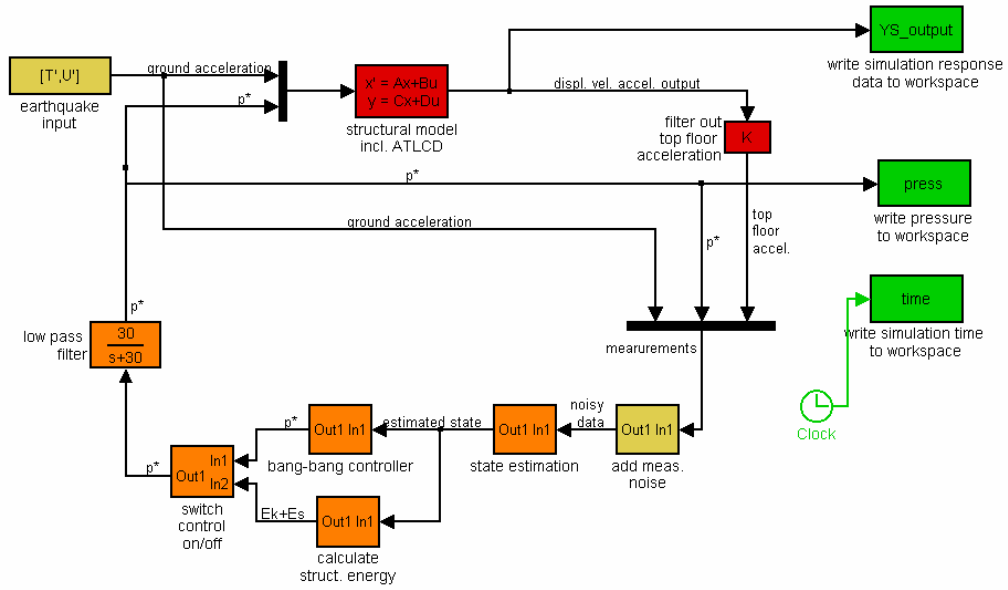


Figure 9-27: Simulink block diagram of bang-bang controlled structural system

The additional pressure difference Δp_a applied to ATLCD is shown in Figure 9-28. The major difference between the control strategies applied is: The bang-bang control law only operates for short periods and applies the maximum pressure, whereas the standard linear quadratic regulator is operating during the entire excitation period. However, since the passive TLCD is always operating it is sufficient to apply the active pressure input for peak response reduction only, thereby saving a lot of energy.

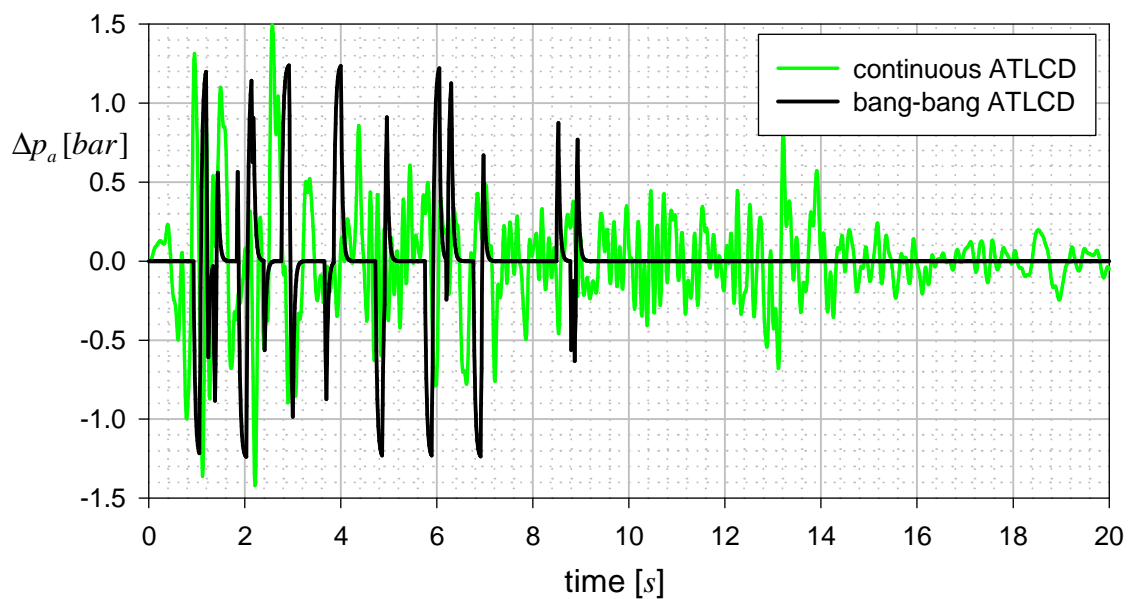


Figure 9-28: Pressure input for different control strategies

Figure 9-29 displays the base shear force for the simulated benchmark structure. The advantage of the ATLCD becomes apparent when inspecting the beginning of the excitation period, where the passive system takes several cycles before being effective in decreasing the shear force. As desired, both active configurations react much faster and avoid exceeding base shear. This main difference between active and passive systems can be found for all response quantities, see e.g. Figure 9-30, where the same effect is visible for the relative displacement of the 3rd floor with respect to the basement. From a mechanical point, this phenomenon can be explained by the fact that during the first vibration cycles, the TLCD is not oscillating at all, thus does not create counteracting forces which dissipate energy.

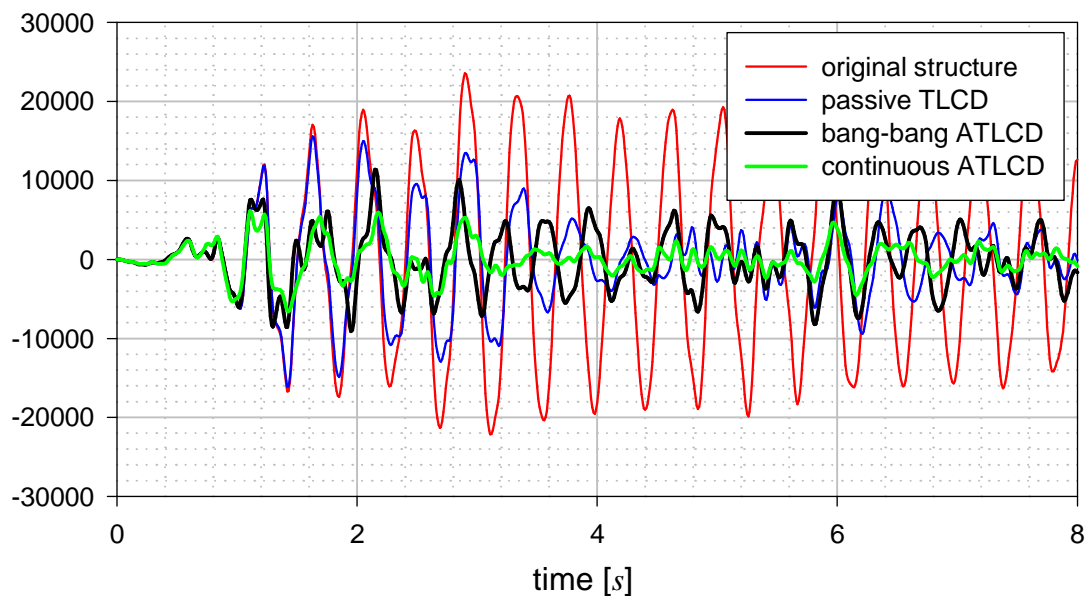


Figure 9-29: Base shear force for the benchmark structure and different TLCD configurations during the first earthquake impact

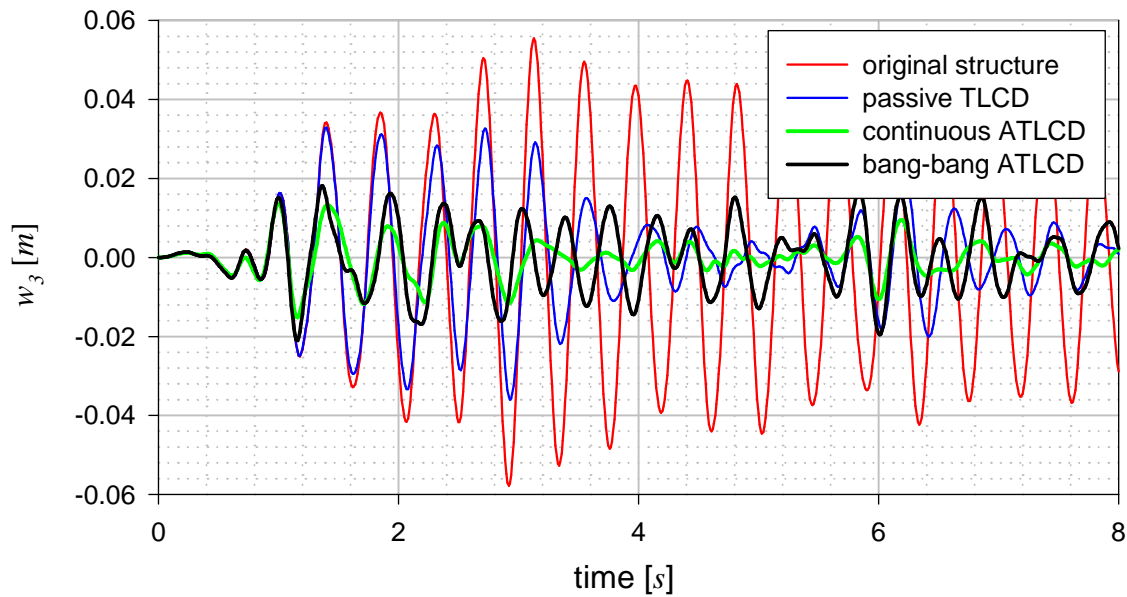


Figure 9-30: relative displacement of 3rd floor for different TLCDs configurations

An excellent visual comparison of the structural response is given in Figure 9-31, where a graphical representation of Table 9-9 - Table 9-12 is given. Again it becomes apparent, that the passive TLCD improves the structural response substantially. Nevertheless, further response reduction is achieved by an ATLCD. For peak response reductions both active control strategies perform well, but a difference can be found in the RMS responses: because the bang-bang control is switched off to save energy, its RMS response is comparable to the one obtained by the passive TLCD configuration, whereas the continuous application of pressure adaptation also reduces the RMS response substantially.

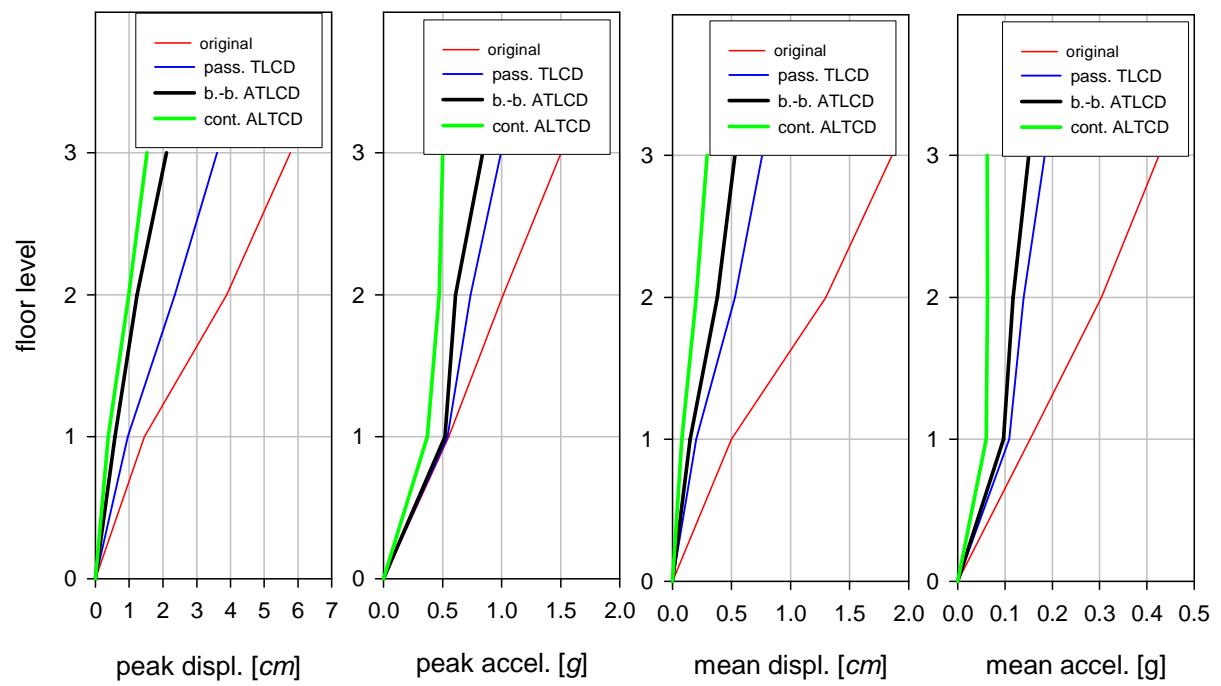


Figure 9-31: Peak and RMS responses for floor displacements and accelerations

9.4. 76-story benchmark structure

The building considered for this study is taken from another benchmark problem, see Yang et al.², where the dynamic response of a 76-story, 306 meters reinforced concrete office tower, proposed for the city of Melbourne, Australia, is studied for strong wind excitation. All relevant structural analyses and design has been completed, but due to an economic recession it has never been built. The reinforced concrete structure is slender with a height to width ratio of 7.3 and thus quite wind sensitive.

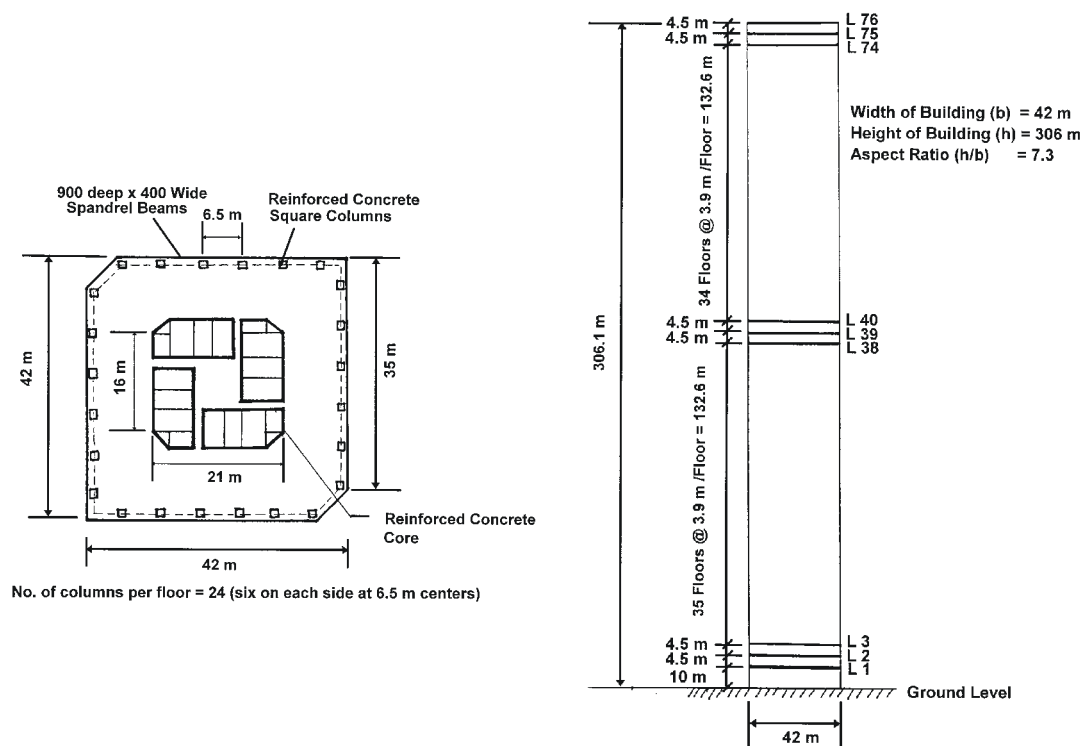


Figure 9-32: Plan view and elevation view of 76-story building, see Yang et al.²

Figure 9-32 illustrates the plan and elevation view of the office tower. It has a square cross-section with chamfers at two corners, and a total mass of 153.000 metric tons, resulting in a typical concrete structure mass density of 300 kg/m^3 for the overall building. The perimeter dimension for the centre reinforced concrete core is $21 \text{ m} \times 21 \text{ m}$. There are 24 columns on each level with 6 columns on each side of the building. Column sizes, core wall thickness and floor mass vary along the height. The building has six plant rooms, one is situated on top of the structure.

Wind force data acting on the benchmark building were determined from wind tunnel tests at the Department of Civil Engineering at the University of Sydney, Australia, where a rigid model of the

76-story benchmark building (model height 76cm) was constructed and tested in a boundary layer wind tunnel facility, see again Yang et al.². Along-wind and across-wind forces were measured in the open circuit type wind tunnel, with a working section of $2.4\text{ m} \times 2.0\text{ m}$ and a working length of 20 m , see e.g. Figure 9-33, where the schematics of a typical boundary layer wind tunnel test section is given. An appropriate model of the natural wind over a suburban terrain was established, using the augmented growth method, which included a combination of vorticity generators spanning the start of the working section and roughness blocks laid over a 12 m fetch length of the working section.

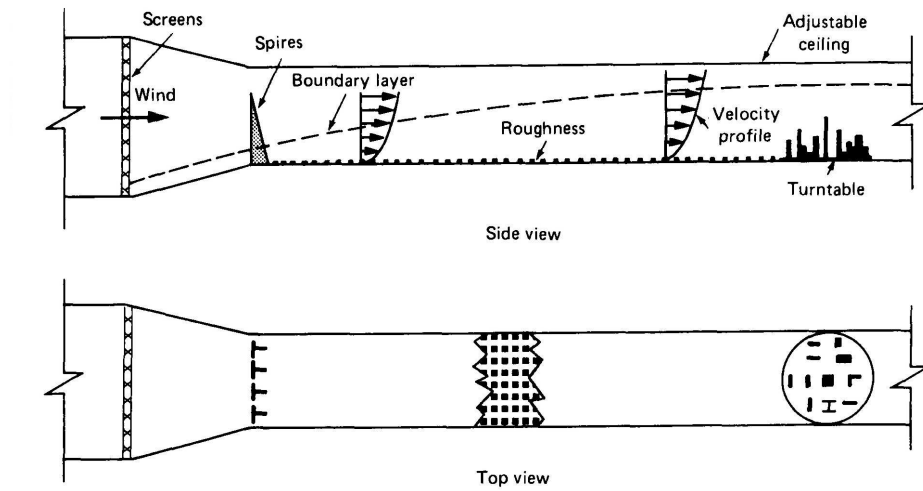


Figure 9-33: Test section of a boundary layer wind tunnel, see Liu¹⁰

The model to prototype scale for the building was 1:400 and the velocity scale was 1:3, resulting in a time scale of approximately 1:133. The pressure measurements were recorded for 27s representing approximately 1 hour of prototype data. Since the data acquisition system had a sampling rate 300Hz, corresponding pressure fluctuation of about 2.25Hz are available for the real building. If the wind velocity profile in the atmospheric boundary layer is describe by the power law, see e.g. Sockel⁸, p. 83,

$$v(z) = v_{10} \left(\frac{z}{10} \right)^\alpha, \quad (9-15)$$

and a mean wind speed of $v_{10} = 13.5\text{ m/s}$ (no. 5 on Beaufort wind scale) at a height of 10 m , then the mean wind velocity at the top of the building is approximately $v(306\text{ m}) = 47.25\text{ m/s}$, assuming a power law exponent of $\alpha = 0.365$, which is typical for city centres. If the wind data are altered to simulate higher or smaller wind speeds, the measured time history must be scaled by

$(v/47.45)^2$, where v denotes the desired mean wind speed at the top of the building. Figure 9-34 displays the time history and the power spectral density (PSD) of the wind forces for the 30th, 50th and 76th floor. The time history of the wind data for each floor was made available in a digital format by the coordinator of the wind bench mark problem, and it can be downloaded together with the benchmark definition paper and the structural model data from the WebPages of the Structural Dynamics and Control - Earthquake Engineering Laboratory at the University of Notre Dame, Notre Dame, Indiana 46556, USA, <http://www.nd.edu/~quake/>. The PSD was calculated by the author using the *psd* function of Matlab⁶, which estimates the power spectral density of a discrete-time signal. It reveals that the wind excitation spectrum has low pass characteristics with a cut-off frequency of about 0.07Hz . Consequently only the fundamental mode of vibration will have a significant contribution to the overall structural response.

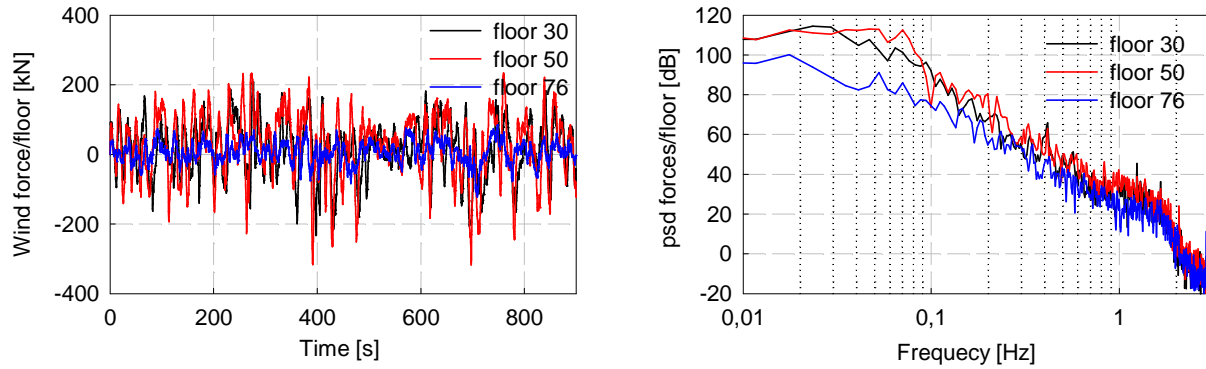


Figure 9-34: Time history and spectrum of wind load at floors 30, 50 and 76 for a top floor RMS wind speed of 47.25 m/s , time history available from Yang et al.²

In Yang et al.² a finite element model of the building is constructed by considering the portion of the building between two adjacent floors as a classical beam of uniform thickness, leading to 76 translational and 76 rotational degrees of freedom. Subsequently all rotational degrees of freedom are removed by the method of static condensation, see Section 6.5. This results in 76 degrees of freedom, representing the displacement of each floor in the horizontal direction. Thus the equations of motion can be given in the standardised form of

$$\mathbf{M}\ddot{\mathbf{w}} + \mathbf{C}\dot{\mathbf{w}} + \mathbf{K}\mathbf{w} = \mathbf{f}(t), \quad (9-16)$$

where the \mathbf{M} , \mathbf{K} and \mathbf{C} are also available in a digital format from Yang et al.², who assumed a proportional (76×76) modal damping matrix. Analysis of the model performed by the author has

revealed, that the first twelve (undamped) natural frequencies are 0.16, 0.77, 1.99, 3.79, 6.40, 9.46, 13.25, 17.52, 22.83, 28.23, 34.55 and 41.28 Hz , respectively.

9.4.1. Response of original building

The wind tunnel tests have shown that the building response quantities due to across-wind loads are much higher than that due to along-wind loads, and, as the coupled flexural-torsional motion is neglected, only the across-wind loading is considered in this investigation, see Yang et al.². From wind tunnel data generated for about an hour, a duration of 900 seconds is chosen to establish the stationary response properties. Given the mass, stiffness and damping matrix as well as the wind loading, the response of the proposed high rise structure can be calculated by solving Eq.(9-16). However, 76 degrees of freedom result in a state space representation of order 152, which makes the numerical integration rather time consuming and thus another model reduction is applied.

The author applied the modal truncation method, discussed in Chapter 6, to obtain a reduced 12DOF model (order 24). The reduced order model is generated by keeping the first 12 vibration modes, and discarding all higher order contributions. The resultant 12 DOF system is rearranged such that the state vector $\mathbf{z} = [\mathbf{w}, \dot{\mathbf{w}}]^T$ contains the floor displacements and velocities at the following floor levels (for details see Section 6.6): 1, 10, 16, 23, 30, 50, 55, 60, 65, 70, 75 and 76. Due to the frequency content of the wind excitation, the fundamental mode is expected to dominate the structural response, and 12 vibration modes have proven to be more than sufficient for accurate results. The amplitude and phase response of the 50-th and 76-th floor have been calculated by the author and are displayed for the full order model and for the reduced order model in Figure 9-35 to Figure 9-38. Comparison reveals that an identical behaviour can be expected for frequencies up to 40 Hz . Although the wind load varies with floor level and time, a constant (time averaged) spatial distribution \mathbf{b}_w of the wind has been introduced by the author to calculate the response curves. Thus, for the numerical optimisation the wind load is approximated by $\mathbf{p}_w(t) = \mathbf{b}_w f(t)$, where $f(t)$ denotes a scalar wind pressure function, and $\mathbf{b}_w = \sqrt{E[\mathbf{f}(t)^2]}$.

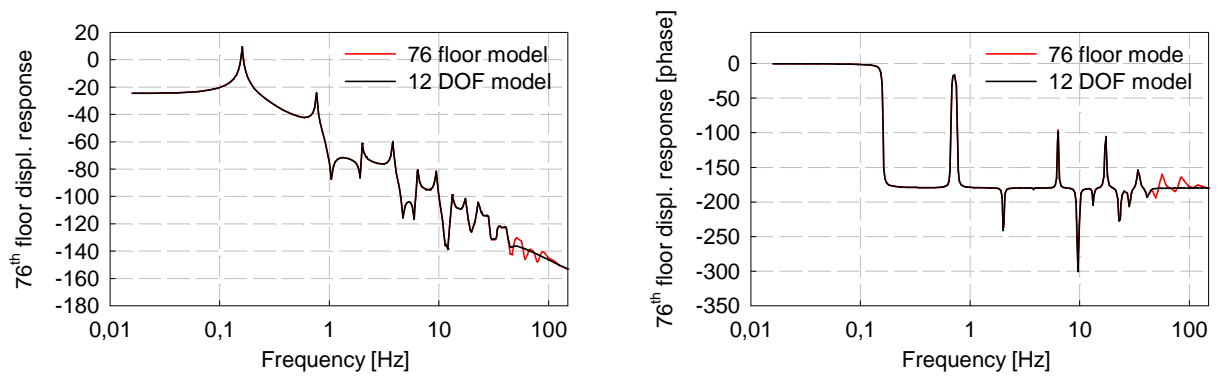


Figure 9-35: Amplitude and phase response function of top floor displacement for 76 DOF model when compared to 12 DOF structural model

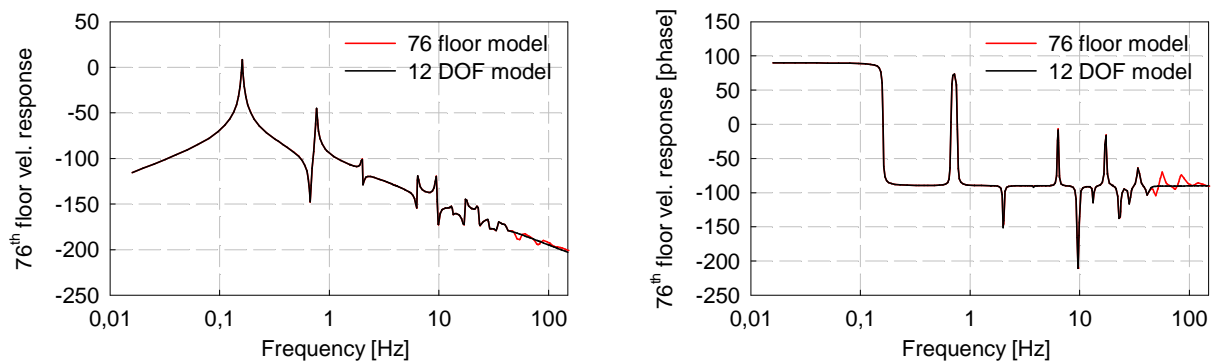


Figure 9-36: Amplitude and phase response function of top floor acceleration for 76 DOF model when compared to 12 DOF structural model

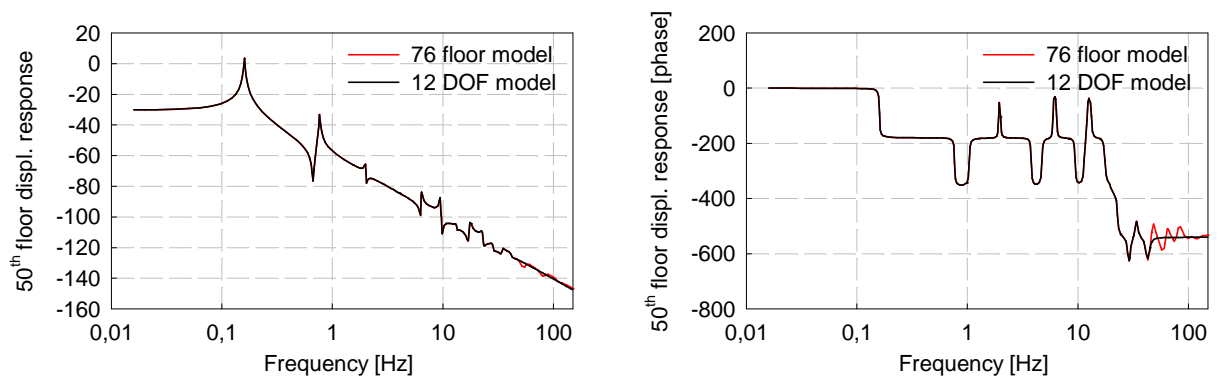


Figure 9-37: Amplitude and phase response function of 50-th floor displacement for 76 DOF model when compared to 12 DOF structural model

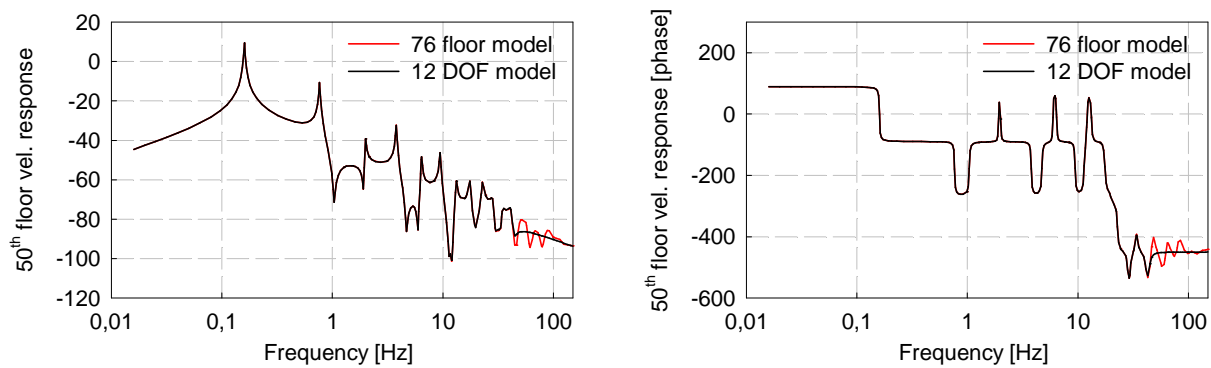


Figure 9-38: Amplitude and phase response function of 50-th floor acceleration for 76 DOF model when compared to 12 DOF structural model

The response of the full and the reduced order system has been calculated using the *lsim* command of Matlab⁶, see Section 9.1 for details. The *lsim* command is quite universal and powerful, and simulates the dynamic response of linear time invariant systems due to any excitation when properly described in the time domain. It is not necessary to specify any integration options, since *lsim* will e.g. resample the excitation input to avoid intersample oscillations. Comparison by the author has revealed, that the response errors of the reduced order model are negligible, when compared to the full order system, see Table 9-13, where RMS response quantities are given for selected floor levels. All response data are given for a top floor RMS wind speed of 47.25 m/s , which corresponds to a wind speed of $v_{10} = 13.5 \text{ m/s}$ (no. 5 on Beaufort wind scale).

Floor no.	76 DOF Model		12 DOF Model	
	$\sigma_{w_i} [\text{cm}]$	$\sigma_{\dot{w}_i} [\text{cm/s}^2]$	$\sigma_{w_i} [\text{cm}]$	$\sigma_{\dot{w}_i} [\text{m/s}^2]$
1	0.021	0.023	0.021	0.023
30	2.68	2.49	2.68	2.49
50	6.50	5.88	6.50	5.89
75	12.34	11.23	12.34	11.25
76	12.62	11.50	12.62	11.52

Table 9-13: RMS Response Quantities of the 76-Story Building subject to across-wind loads and comparison with the simplified model

The time histories and the spectral distribution of the original building, calculated by the author using Matlab's *psd* and *lsim* command, are shown in Figure 9-39 and Figure 9-40 for selected floor displacements and accelerations.

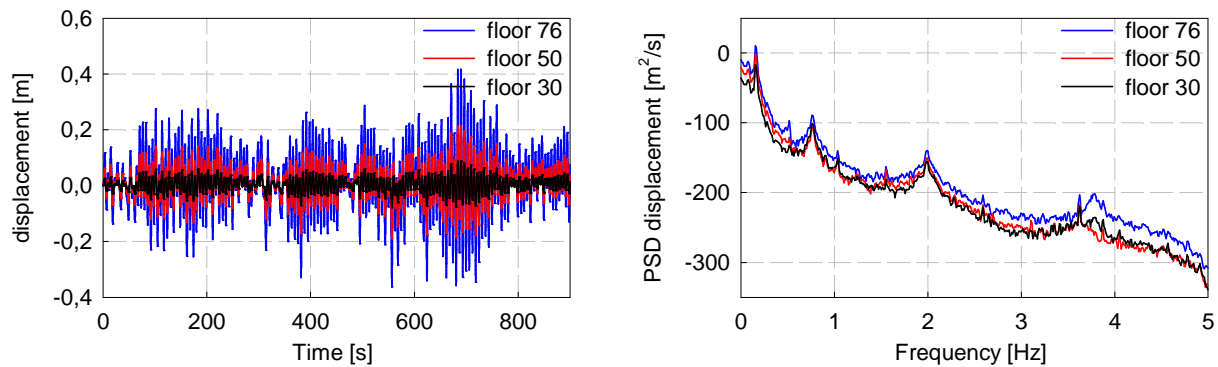


Figure 9-39: Time history and spectrum of displacement response at floors 30, 50 and 76

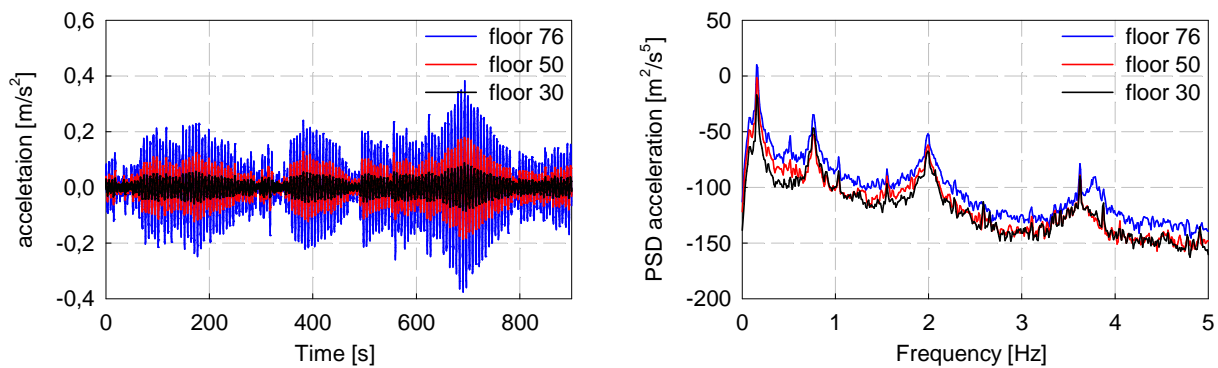


Figure 9-40: Time history and spectrum of the acceleration response at floors 30, 50 and 76

Again it is evident that the fundamental mode contribution dominates the overall structural response, and hence, a TLCD tuned to the fundamental frequency is expected to reduce the overall response substantially. However, from Figure 9-39 it is apparent, that the floor displacements also contain very low frequency response, which are due to a quasi-static wind load, and which cannot be influenced by dynamic vibration absorbers.

9.4.2. Passive TLCD

In the benchmark problem an absorber with a total mass of 500 metric tons is proposed for both passive TMD and ATMD design, and installed on the top floor, see Yang et al.². Thus, a tuned liquid column damper with an equivalent liquid mass is installed on the top of the building for comparison. The absorber-mass-ratio is about 45% of the top floor mass, which is 0.327% of the total building mass. Applying the TMD-TLCD analogy it is rather easy to determine the optimal

absorber frequency and damping ratio. According to Den Hartog's approach, minimal amplitude response functions are obtained for the analogue TMD-system, see Table 2-1,

$$\delta^* = (1 + \mu^*)^{-1}, \quad (9-17)$$

$$\zeta^* = \sqrt{\frac{3\mu^*}{8(1+\mu^*)}}.$$

Back transformation into the TLCD regime yields, see Eqs.(5-12) and (5-13),

$$\delta = \frac{\sqrt{1 + \mu(1 - \kappa\bar{\kappa})}}{1 + \mu}, \quad (9-18)$$

$$\zeta = \sqrt{\frac{3\kappa\bar{\kappa}\mu}{8(1+\mu)}}, \quad (9-19)$$

and the optimal TLCD parameter are given at once by $\omega_A = 0.158Hz$ and $\zeta_A = 6.66\%$, with a mass ratio of $\mu = 1.32\%$, under the assumption that $\kappa\bar{\kappa} = 0.92$, the geometry factors for the final TLCD geometry. For comparison, the undamped natural frequency and damping ratios of the passive device were also calculated from the following performance index

$$J = \int_{-\infty}^{\infty} \mathbf{z}_S^T(\nu) \mathbf{S} \mathbf{z}_S(\nu) d\nu, \quad (9-20)$$

where the diagonal weighting matrix $\mathbf{S} = \mathbf{I}$ is equal to the identity matrix. \mathbf{z}_S represents the host structure's state vector given by $\mathbf{z}_S(\nu) = [w_1(\nu), \dots, w_{12}(\nu), \dot{w}_1(\nu), \dots, \dot{w}_{12}(\nu)]^T$. The minimisation of J is performed numerically by calling the function *fminsearch* of the Matlab Optimisation Toolbox. *fminsearch* finds the minimum of the scalar function J of several variables, starting at an initial estimate, given by Eqs.(9-18) and (9-19). For details on *fminsearch* see Section 9.1. As the wind excitation has low pass (coloured noise) characteristics, see Figure 9-34, the reduced order dynamic model was extended according to Section 7.5, to integrate a third order Butterworth lowpass filter with a cut-off frequency of $0.1Hz$. For ideal filter parameter see, e.g. Dorf¹⁷ or the signal processing toolbox of Matlab¹⁹.

From the numerical optimisation (*fminsearch*) the optimal tuning frequency and the ideal damping ratio were determined to be $0.158 Hz$ and 5.46% , respectively. Comparing this result to the TMD-analogy almost the same parameter are obtained, since the TLCD performance is rather

insensitive to variations in ζ_A , see e.g. Section 9.2. For the subsequent investigations, the parameter obtained from the gradient method are used, since they account for the multiple degrees of freedom. The effective liquid column length is fixed to $L_{eff} = 35m$ for a piping system with uniform cross sectional area, and the horizontal pipe section is $B = 30m$ and $\beta = 45^\circ$, allowing for peak liquid displacements of $2.5m$. The system response was simulated by the author using the Matlab's *lsim* command (without calling any options) for a $15min$ wind load segment (provided by Yang et al.², displayed in Figure 9-34), and is shown in Figure 9-41 and Figure 9-42.

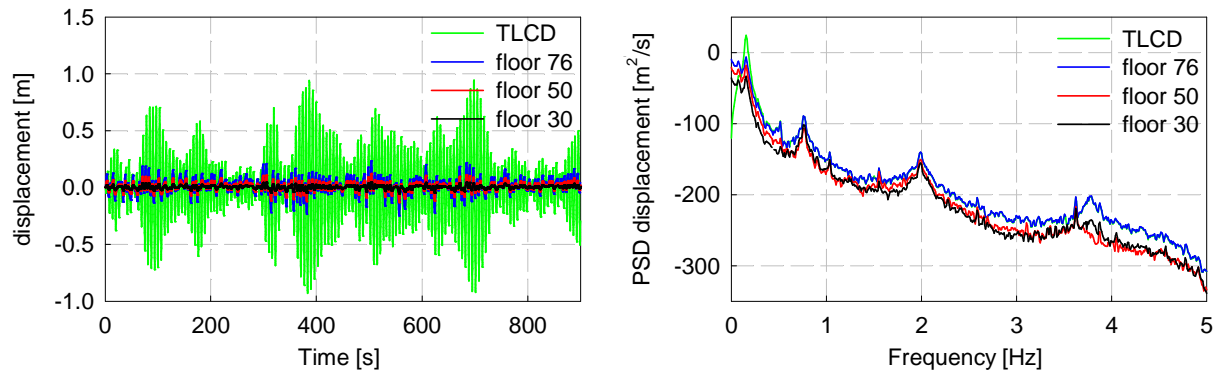


Figure 9-41: Time history and spectrum for the displacement response at floors 30, 50 and 76, with a $500t$ TLCD installed

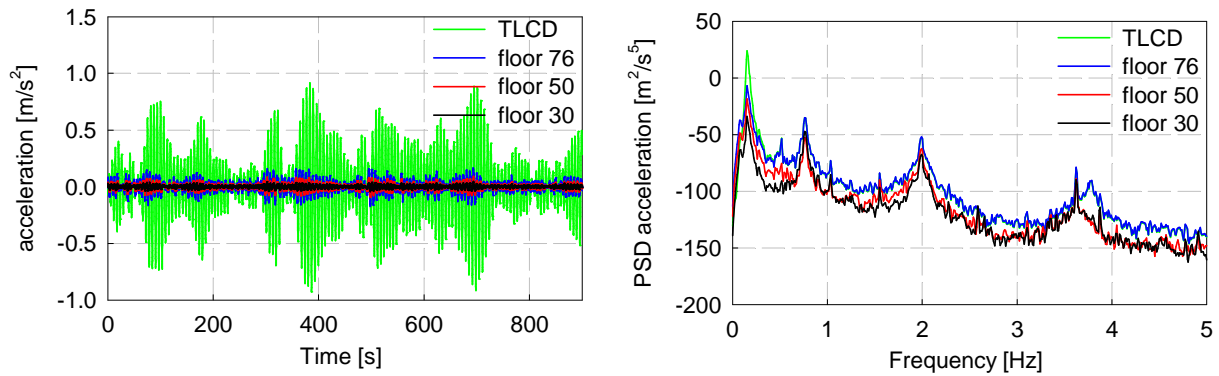


Figure 9-42: Time history and spectrum for the acceleration response at floors 30, 50 and 76, with a $500t$ TLCD installed

The RMS top floor displacement is reduced from $12.51cm$ to $7.54cm$ and similarly, the RMS top floor acceleration is reduced from $11.51cm/s^2$ to $5.26cm/s^2$, respectively. The maximum water level displacement lies well within the limits and is less than $1m$. Apparently a good vibration

reduction can be achieved with the passive device, see Table 9-14 and Table 9-15, where the peak and RMS responses of several floors are listed. The TMD result, taken from Yang et al.², is scaled to compensate for different wind force input levels.

	original building,		TMD, taken from Yang et al. ² scaled by 123%		TLCD	
Floor no.	σ_{w_i} [cm]	$\sigma_{\ddot{w}_i}$ [cm/s ²]	σ_{w_i} [cm]	$\sigma_{\ddot{w}_i}$ [cm/s ²]	σ_{w_i} [cm]	$\sigma_{\ddot{w}_i}$ [cm/s ²]
1	0.02	0.02	0.01	0.07	0.01	0.03
30	2.68	2.49	1.81	1.52	1.63	1.23
50	6.50	5.88	4.40	3.46	3.93	2.66
75	12.34	11.23	8.33	6.42	7.42	5.11
76	12.62	11.50	8.52	6.76	7.58	5.24

Table 9-14: Comparison of RMS-responses of original building, and the building equipped with TLCD and TMD

	original building,		TMD, taken from Yang et al. ² , scaled by 123%		TLCD	
Floor no.	w_i^{\max} [cm]	\ddot{w}_i^{\max} [cm/s ²]	w_i^{\max} [cm]	\ddot{w}_i^{\max} [cm/s ²]	w_i^{\max}	\ddot{w}_i^{\max} [m/s ²]
1	0.07	0.24	0.05	0.26	0.04	0.24
30	8.80	8.77	7.34	5.77	5.04	4.47
50	21.33	18.18	16.46	11.45	12.20	8.85
75	40.61	37.30	30.66	24.43	23.14	16.50
76	41.52	38.45	31.33	25.33	23.66	17.19

Table 9-15: Comparison of peak responses of original building, and the building equipped with TLCD and TMD

Since the TLCD considered has a total mass of 500 tons it must be split into several individual TLCD, e.g. six pipes with a cross section of $2.38m^2$ each. If several TLCD, forming a multiple TLCD (MTLCD), are installed they should be arranged symmetrically with respect to the building's principal axis. However, in such a situation the author has found that slightly altered TLCD design parameter give better results than six identical TLCD, a result which is also reported in several publications on MTLCD, see e.g. Chang et al.²⁰, Gao et al.²¹, Sadek et al.²² or Yalla et al.²³. Assuming that each of the three symmetrically arranged pairs of TLCD has its individual natural frequency and damping ratios the numerical optimisation is repeated. This time three sets of TLCDs are installed, and the numerical optimisation is performed with respect to the six free parameter ω_1 , ω_2 , ω_3 , ζ_1 , ζ_2 and ζ_3 , where initially all natural frequencies and damping ratios were chosen to be $\omega_i = 0.158Hz$ and $\zeta_i = 5.46\%$, representing the optimal parameter of a single

TLCD. The weighting matrix of Eq.(9-20) remains $\mathbf{S} = \mathbf{I}$, and the optimisation routine *fminsearch* is called three times, before the numerical optimisation converged to the final TLCD parameter $\omega_1 = 0.9483 \text{ rad/s}$, $\omega_2 = 0.9985 \text{ rad/s}$, $\omega_3 = 1.055 \text{ rad/s}$, $\zeta_1 = 2.52\%$, $\zeta_2 = 2.52\%$, $\zeta_3 = 2.68\%$. In Figure 9-43 the sum of the floor level amplitude response functions $\sum_{i=1}^{24} |z_i(\nu)|$ is used for a performance measure, and it clearly shows that the original resonant peak is reduced to two or more resonant peaks, depending on the number of TLCD applied.

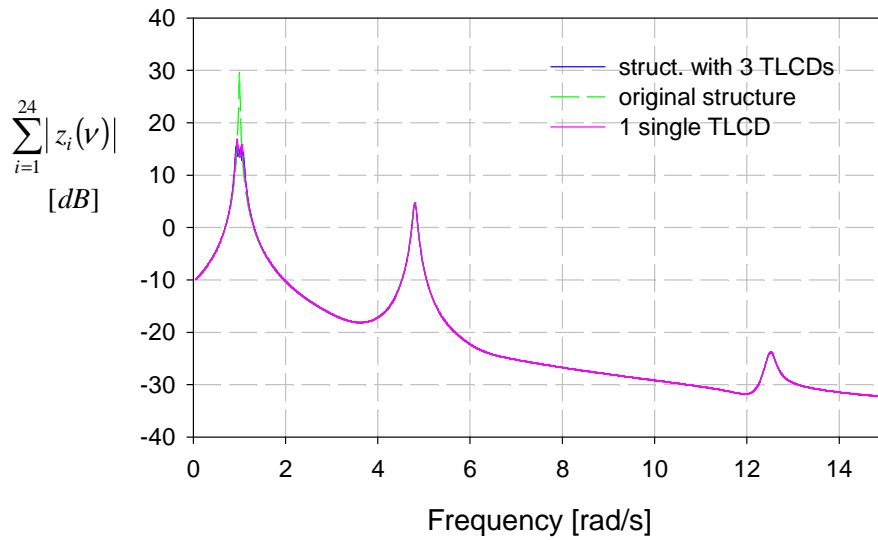


Figure 9-43a): Performance index of original structure equipped with one single and 3 pairs of TLCDs, frequency range 0-15rad/s

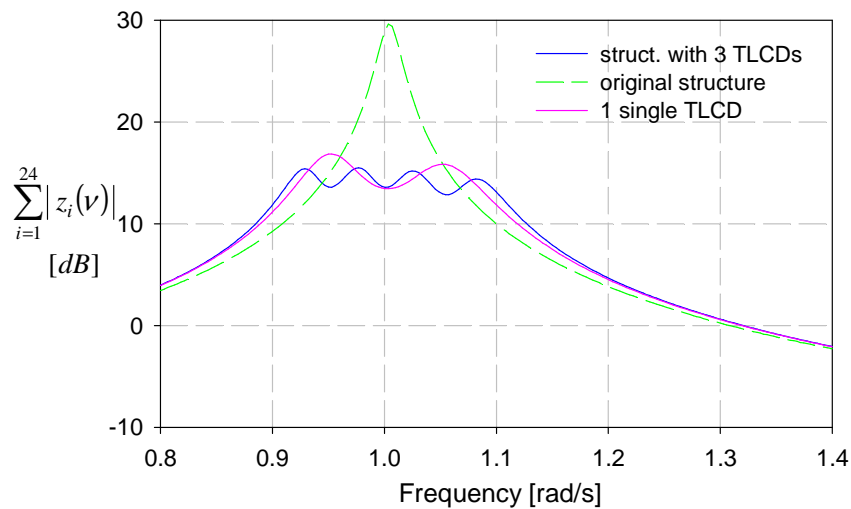


Figure 9-43b): Performance index of original structure equipped with one single and 3 pairs of TLCDs, critical frequency range

If the structural parameter (stiffness or mass matrix) are known exactly, then there is only very little difference between a single and a multiple tuned liquid column damper (MTLCD) of equal mass. However, if there is some uncertainty in the structural model, the MTLCD will perform more robust, see again Chang et al.²⁰, Gao et al.²¹, Sadek et al.²² or Yalla et al.²³. Assuming that the structural stiffness matrix can vary by $\Delta K = \pm 15\%$, a slightly modified performance index, accounting for the uncertainty in the structure, should be defined. A straightforward approach to robust optimisation is to define the overall performance index as the sum of the performance indices of the individual structure (with varying parameter), equipped with the same dynamic absorber. Thus $J = \sum J_i$, where J_i denotes the performance index of the i -th structure equipped with the TLCD arrangement, still given by Eq.(9-4). For an uncertainty in stiffness of $\Delta K = \pm 15\%$, a possible choice of J is

$$J = J_{\Delta K=0} + J_{\Delta K=+15\%} + J_{\Delta K=-15\%}, \quad (9-21)$$

With this new performance index the (robust) optimisation (using the *fminsearch* function) is repeated with respect to the damping ratios and natural frequencies of the three pairs of TLCD. The initial values were again chosen to be equal for all TLCDs, $\omega_i = 0.9922 \text{ rad/s}$ and $\zeta_i = 5.46\%$, respectively. Since no numerical problems were encountered, the optimisation converged after calling *fminsearch* three times, and the optimal natural frequencies and damping ratios for the set of TLCDs are 0.186Hz , 0.157Hz , 0.131Hz and 3.00% , 3.23% and 3.41% , respectively. The advantage of the robust optimisation becomes apparent in Figure 9-44 where the weighed sum of the amplitude response functions, $\sum_{i=1}^{24} |z_i(\nu)|$, is plotted for three different structures ($\Delta K = 0\%$, $\Delta K = \pm 15\%$) and for three absorber configurations. When compared to a single TLCD the vibrations are reduced about 4dB at the critical resonance frequency, because the peaks arising from detuning are lessened again.

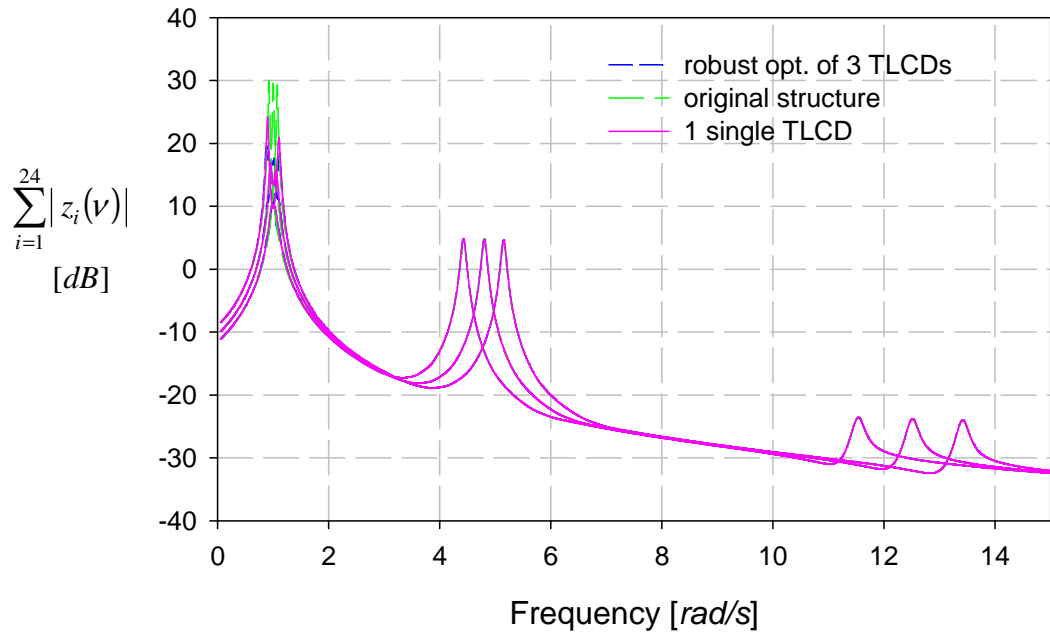


Figure 9-44a): Performance index of original and uncertain structures ($\Delta K = \pm 15\%$), equipped with one single and 3 multiple TLCDs, frequency range from 0-15 rad/s

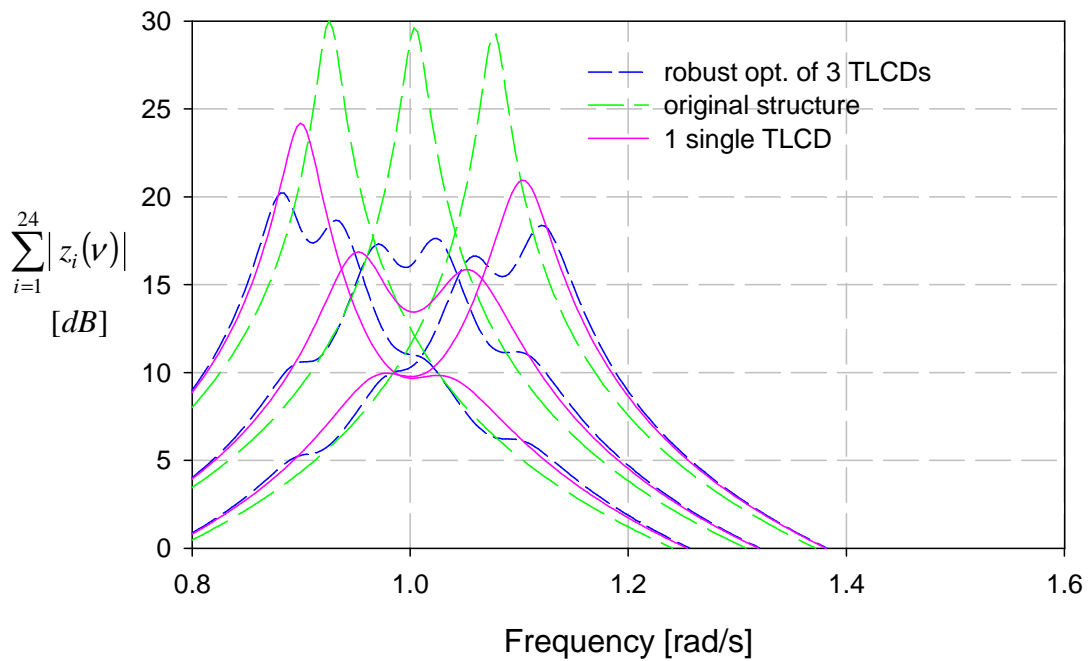


Figure 9-44b): Performance index of original and uncertain structures ($\Delta K = \pm 15\%$), equipped with one single and 3 multiple TLCDs, critical frequency range

From Figure 9-43 and Figure 9-44, it can already be concluded, that the passive TLCD can reduce the dominant resonant peak, and a high vibration reduction can be achieved. Besides the floor displacements and accelerations, which are all recorded in Table 9-19-Table 9-24 for reference, several other non-dimensional performance measures are given by Yang et al.², and they are discussed in the next section.

9.4.3. Performance criteria

The main objective of the installation of vibration absorbers is to alleviate the occupant's discomfort, and a main indicator of the TLCD's performance is to reduce the maximum floor RMS-accelerations, which can be measured by a nondimensional criterion given by, see Yang et al.² for the definition of J_1 (and all following performance measures),

$$J_1 = \max(\sigma_{\ddot{w}1}, \sigma_{\ddot{w}30}, \sigma_{\ddot{w}50}, \sigma_{\ddot{w}55}, \sigma_{\ddot{w}60}, \sigma_{\ddot{w}65}, \sigma_{\ddot{w}70}, \sigma_{\ddot{w}75}) / \sigma_{\ddot{w}75o}, \quad (9-22)$$

where $\sigma_{\ddot{w}i}$ is the RMS acceleration of the i -th floor, and $\sigma_{\ddot{w}75o} = 12.34m/s^2$ is the RMS acceleration of the 75th floor without control. In the performance criterion J_1 , accelerations up to the 75th floor are considered because the 76th floor is the top of the building and it is not used by the occupants. The second criterion is the average performance of acceleration for selected floors above the 49th floor, i.e.,

$$J_2 = \frac{1}{6} \sum_i (\sigma_{\ddot{w}i} / \sigma_{\ddot{w}io}), \quad \text{for } i = 50, 55, 60, 65, 70 \text{ and } 75, \quad (9-23)$$

in which $\sigma_{\ddot{w}io}$ is the RMS acceleration of the i -th floor of the original building. The third and fourth nondimensional evaluation criteria describe the ability of the controllers to reduce the top floor displacements,

$$J_3 = \sigma_{w76} / \sigma_{w76o}, \quad (9-24)$$

$$J_4 = \frac{1}{7} \sum_i (\sigma_{wi} / \sigma_{wio}), \quad \text{for } i = 50, 55, 60, 65, 70, 75 \text{ and } 76, \quad (9-25)$$

where σ_{wi} and σ_{wio} are the RMS displacements of the i -th floor with and without absorber, respectively, and $\sigma_{w76o} = 12.62\text{cm}$, see Table 9-14, is the RMS displacement of the 76th floor of the uncontrolled building.

The TLCD will be compared to a ATMD, designed in Yang et al.², whose actuator force $u(t)$ and piston stroke $w_m(t)$ is constrained by $\max|u(t)| \leq 300\text{ kN}$ and $\max|w_m(t)| \leq 95\text{ cm}$, respectively. Further constraints are a limitations for the RMS control force σ_u and actuator displacements σ_{wm} , $\sigma_u \leq 100\text{ kN}$ and $\sigma_{wm} \leq 30\text{ cm}$, respectively. In addition, the control effort requirements of a proposed control design should be evaluated in terms of the following non-dimensional actuator stroke and average power

$$J_5 = \sigma_{wm} / \sigma_{w76o} ; \quad (9-26)$$

$$J_6 = \sigma_P = \left\{ \frac{1}{T} \int_0^T [\dot{w}_m(t) u(t)]^2 dt \right\}^{1/2} \quad (9-27)$$

where $\dot{w}_m(t)$ denotes the actuator velocity, T is the total time of observation and σ_P denotes RMS control power.

In addition to the RMS performance, the performance in terms of the peak response quantities are considered by a set of nondimensional performance criteria,

$$J_7 = \max(\ddot{w}_{p1}, \ddot{w}_{p30}, \ddot{w}_{p50}, \ddot{w}_{p55}, \ddot{w}_{p60}, \ddot{w}_{p65}, \ddot{w}_{p70}, \ddot{w}_{p75}) / \ddot{w}_{p75o} , \quad (9-28)$$

$$J_8 = \frac{1}{6} \sum_i (\ddot{w}_{pi} / \ddot{w}_{pio}) , \quad \text{for } i = 50, 55, 60, 65, 70 \text{ and } 75 \quad (9-29)$$

$$J_9 = w_{p76} / w_{p76o} , \quad (9-30)$$

$$J_{10} = \frac{1}{7} \sum_i (w_{pi} / w_{pio}) , \quad \text{for } i = 50, 55, 60, 65, 70, 75 \text{ and } 76 \quad (9-31)$$

where w_{pi} and w_{pio} are the peak displacements of i -th floor with and without control, \ddot{w}_{pi} and \ddot{w}_{pio} are the peak acceleration of i -th floor with and without absorber. In addition, the proposed control designs should be evaluated for the following control capacity criteria

$$J_{11} = w_{pm} / w_{p760} \quad (9-32)$$

$$J_{12} = P_{\max} = \max_t |\dot{w}_m(t) u(t)| \quad (9-33)$$

where w_{pm} and P_{\max} denote the peak stroke of actuator and the peak control power, respectively.

From the performance criteria defined above, it is observed that the better the performance of the controller, the smaller the values of performance indices J_1, J_2, \dots, J_{12} . All performance criteria have been evaluated for the single TLCD and MTLCD, after calculating the dynamic response using the *lsim* function of Matlab. The results are listed in Table 9-16 and Table 9-17 for the nominal buildings as well as the structure with an altered stiffness. It has to be mentioned, that, according to the benchmark definition paper by Yang et al.², it is always the nominal structure which is used to calculate the performance indices. Furthermore, the performance criteria for the ATMD, also proposed in the benchmark definition paper, is given in Table 9-18. Comparing the ATMD and the passive TLCDs, the passive system achieves a similar level of vibration reduction, and thus it is superior to TMD and ATMD for the benchmark problem investigated, since it is cheaper, more robust and independent of any maintenance.

RMS responses STLCD				Peak responses STLCD			
Criteria	$\Delta K = 0\%$	$\Delta K = 15\%$	$\Delta K = -15\%$	Criteria	$\Delta K = 0\%$	$\Delta K = 15\%$	$\Delta K = -15\%$
J_1	0.4548	0.5372	0.5610	J_7	0.4424	0.5986	0.6383
J_2	0.3403	0.4040	0.4204	J_8	0.4490	0.5934	0.6391
J_3	0.6009	0.5519	0.8040	J_9	0.5697	0.5479	0.7124
J_4	0.6027	0.5538	0.8040	J_{10}	0.5707	0.5474	0.7081
J_5	3.2169	2.008	2.3971	J_{11}	2.2751	1.8893	2.5728
$J_6, \text{ kNm/s}$	-	-	--	$J_{12}, \text{ kNm/s}$	-	-	-
$\sigma_u, \text{ kN}$	-	-	-	$\max u(t) , \text{ kN}$	-	-	-
$\sigma_{xm}, \text{ cm}$	30.97	25.34	30.31	$\max x_m , \text{ cm}$	94.47	78.45	106.83

Table 9-16: Evaluation criteria for single TLCD (STLCD) and for varying stiffness matrix

RMS responses MTLCD				Peak responses MTLCD			
Criteria	$\Delta K = 0\%$	$\Delta K = 15\%$	$\Delta K = -15\%$	Criteria	$\Delta K = 0\%$	$\Delta K = 15\%$	$\Delta K = -15\%$
J_1	0.4844	0.5034	0.5070	J_7	0.4866	0.5815	0.5782
J_2	0.3631	0.3782	0.3792	J_8	0.4752	0.5517	0.5812
J_3	0.6174	0.5338	0.7556	J_9	0.5652	0.5014	0.6251
J_4	0.6193	0.5358	0.7571	J_{10}	0.5655	0.5009	0.6266
J_5	3.2169	2.5492	3.2872	J_{11}	3.1079	2.4974	3.1744
J_6 , kNm/s	-	-	--	J_{12} , kNm/s	-	-	-
σ_u , kN	-	-	-	$\max u(t) $, kN	-	-	-
σ_{xm} , cm	42.48	41.47	32.16	$\max x_m $, cm	167.67	198.15	141.03

Table 9-17: Evaluation criteria for multiple TLCDs (MTLCD) and for varying stiffness matrix

RMS responses ATMD				Peak responses ATMD			
Criteria	$\Delta K = 0\%$	$\Delta K = 15\%$	$\Delta K = -15\%$	Criteria	$\Delta K = 0\%$	$\Delta K = 15\%$	$\Delta K = -15\%$
J_1	0.369	0.365	0.387	J_7	0.381	0.411	0.488
J_2	0.417	0.409	0.438	J_8	0.432	0.443	0.539
J_3	0.578	0.487	0.711	J_9	0.717	0.607	0.770
J_4	0.580	0.489	0.712	J_{10}	0.725	0.614	0.779
J_5	2.271	1.812	2.709	J_{11}	2.300	1.852	2.836
J_6 , kn./s	11.99	8.463	16.61	J_{12} , kNm/s	71.87	52.68	118.33
σ_u , kN	34.07	28.29	44.32	$\max u(t) $, kN	118.24	105.58	164.33
σ_{wm} , cm	23.03	18.37	27.46	$\max w_m $, cm	74.29	59.83	91.60

Table 9-18: Evaluation criteria for ATMD (see Yang et al.²) for varying stiffness matrix

	displacements nominal structure $\Delta K = 0\%$							
	mean displacements [cm]				peak displacements [cm]			
	original building	1 TLCD 500t	3 TLCD 166t each	3 TLCD robust 166t each	original building	1 TLCD 500t	3 TLCD 166t each	3 TLCD robust 166t each
floor 1	0,02	0,01	0,01	0,01	0,07	0,04	0,04	0,04
floor 10	0,42	0,26	0,25	0,26	1,38	0,78	0,75	0,78
floor 16	0,91	0,56	0,55	0,57	2,99	1,71	1,61	1,69
floor 23	1,69	1,03	1,01	1,06	5,54	3,17	2,97	3,13
floor 30	2,68	1,63	1,61	1,68	8,80	5,04	4,69	4,97
floor 50	6,50	3,93	3,87	4,04	21,33	12,20	11,35	12,06
floor 55	7,60	4,59	4,53	4,72	24,97	14,27	13,27	14,12
floor 60	8,74	5,28	5,20	5,42	28,73	16,41	15,25	16,25
floor 65	9,91	5,97	5,88	6,14	32,60	18,60	17,29	18,44
floor 70	11,11	6,68	6,58	6,87	36,53	20,83	19,35	20,66
floor 75	12,34	7,42	7,30	7,62	40,61	23,14	21,49	22,96
floor 76	12,62	7,58	7,46	7,79	41,52	23,66	21,97	23,47
TLCD1		30,97	33,98	30,15		94,47	111,93	99,18
TLCD2			49,36	54,23			150,17	167,67
TLCD3			50,53	37,37			159,70	120,30

Table 9-19: Displacement response for nominal structure

	accelerations nominal structure $\Delta K = 0\%$							
	mean accelerations [cm/s^2]				peak accelerations [cm/s^2]			
	original building	1 TLCD 500t	3 TLCD 166t each	3 TLCD robust 166t each	original building	1 TLCD 500t	3 TLCD 166t each	3 TLCD robust 166t each
floor 1	0,03	0,03	0,03	0,03	0,24	0,24	0,24	0,24
floor 10	0,43	0,27	0,27	0,28	1,86	1,28	1,29	1,30
floor 16	0,90	0,52	0,52	0,54	3,64	2,48	2,52	2,54
floor 23	1,61	0,86	0,85	0,90	6,19	3,65	3,71	3,76
floor 30	2,49	1,23	1,21	1,30	8,77	4,47	4,56	4,65
floor 50	5,88	2,66	2,59	2,84	18,18	8,85	8,69	9,02
floor 55	6,88	3,08	3,01	3,29	21,20	9,78	9,73	10,03
floor 60	7,91	3,54	3,45	3,78	24,22	10,92	10,85	11,34
floor 65	8,98	4,02	3,91	4,29	27,33	11,83	12,27	12,65
floor 70	10,08	4,53	4,42	4,84	32,11	13,48	13,64	14,89
floor 75	11,23	5,11	4,98	5,44	37,30	16,50	16,40	18,15
floor 76	11,50	5,24	5,11	5,58	38,45	17,19	17,08	18,87
TLCD1		30,66	36,94	33,37		91,38	124,17	111,13
TLCD2			45,68	53,84			137,83	162,54
TLCD3			50,51	33,79			155,54	111,37

Table 9-20: Acceleration response for nominal structure

	weak structure $\Delta K = -15\%$							
	mean displacements [cm]				peak displacements [cm]			
	original building	1 TLCD 500t	3 TLCD 166t each	3 TLCD robust 166t each	original building	1 TLCD 500t	3 TLCD 166t each	3 TLCD robust 166t each
floor 1	0,02	0,02	0,02	0,02	0,05	0,05	0,05	0,04
floor 10	0,40	0,34	0,34	0,32	1,10	0,95	0,98	0,87
floor 16	0,87	0,74	0,73	0,69	2,40	2,07	2,12	1,89
floor 23	1,62	1,36	1,35	1,29	4,46	3,83	3,91	3,50
floor 30	2,57	2,17	2,15	2,04	7,10	6,11	6,18	5,56
floor 50	6,21	5,24	5,20	4,93	17,30	14,98	14,81	13,42
floor 55	7,26	6,12	6,08	5,76	20,28	17,59	17,30	15,68
floor 60	8,35	7,04	6,99	6,62	23,36	20,30	19,86	18,01
floor 65	9,47	7,98	7,93	7,50	26,54	23,10	22,49	20,42
floor 70	10,60	8,93	8,88	8,40	29,77	25,95	25,17	22,86
floor 75	11,77	9,92	9,86	9,32	33,12	28,92	27,94	25,39
floor 76	12,04	10,14	10,08	9,53	33,87	29,58	28,56	25,96
TLCD1		30,24	25,02	20,22		106,83	89,81	67,74
TLCD2			59,29	39,17			203,32	129,55
TLCD3			40,31	65,01			134,55	198,15

Table 9-21: Displacement response for the weak structure

	weak structure $\Delta K = -15\%$							
	mean accelerations [cm/s^2]				peak accelerations [cm/s^2]			
	original building	1 TLCD 500t	3 TLCD 166t each	3 TLCD robust 166t each	original building	1 TLCD 500t	3 TLCD 166t each	3 TLCD robust 166t each
floor 1	0,03	0,03	0,03	0,03	0,23	0,23	0,23	0,23
floor 10	0,37	0,31	0,31	0,30	1,51	1,21	1,20	1,20
floor 16	0,74	0,61	0,60	0,58	3,01	2,35	2,22	2,28
floor 23	1,28	1,02	1,00	0,95	5,14	3,90	3,51	3,69
floor 30	1,93	1,48	1,46	1,37	7,45	5,58	4,96	5,16
floor 50	4,45	3,27	3,22	2,96	15,56	11,57	10,50	10,46
floor 55	5,19	3,81	3,74	3,44	17,68	13,26	11,95	12,29
floor 60	5,96	4,37	4,30	3,94	19,92	15,36	14,04	14,08
floor 65	6,77	4,97	4,88	4,48	21,45	18,02	16,43	16,12
floor 70	7,61	5,61	5,51	5,05	23,81	20,58	18,71	18,73
floor 75	8,51	6,30	6,20	5,70	27,46	23,81	21,63	21,57
floor 76	8,72	6,46	6,36	5,84	28,29	24,59	22,36	22,23
TLCD1		26,74	24,57	20,75		98,54	89,88	73,62
TLCD2			50,61	36,37			174,31	118,82
TLCD3			37,47	53,41			127,15	170,87

Table 9-22: Acceleration response for the weak structure

	stiff structure $\Delta K = 15\%$							
	mean displacements [cm]				peak displacements [cm]			
	original building	1 TLCD 500t	3 TLCD 166t each	3 TLCD robust 166t each	original building	1 TLCD 500t	3 TLCD 166t each	3 TLCD robust 166t each
floor 1	0,01	0,01	0,01	0,01	0,04	0,04	0,04	0,03
floor 10	0,27	0,23	0,24	0,23	0,86	0,74	0,71	0,67
floor 16	0,59	0,51	0,52	0,49	1,87	1,61	1,56	1,47
floor 23	1,09	0,94	0,97	0,91	3,46	2,99	2,89	2,73
floor 30	1,73	1,50	1,54	1,45	5,49	4,77	4,60	4,36
floor 50	4,19	3,61	3,70	3,50	13,17	11,65	11,19	10,66
floor 55	4,90	4,22	4,32	4,09	15,38	13,65	13,09	12,49
floor 60	5,63	4,85	4,97	4,69	17,65	15,72	15,05	14,39
floor 65	6,38	5,49	5,62	5,31	19,97	17,85	17,06	16,34
floor 70	7,15	6,14	6,29	5,94	22,33	20,01	19,09	18,31
floor 75	7,93	6,81	6,98	6,59	24,77	22,25	21,20	20,36
floor 76	8,11	6,96	7,13	6,73	25,32	22,75	21,67	20,82
TLCD1		25,34	43,43	42,62		78,45	148,18	141,03
TLCD2			29,83	32,22			96,70	92,43
TLCD3			36,76	21,64			106,11	77,64

Table 9-23: Displacement response for the stiff structure

	stiff structure $\Delta K = 15\%$							
	mean accelerations [cm/s^2]				peak accelerations [cm/s^2]			
	original building	1 TLCD 500t	3 TLCD 166t each	3 TLCD robust 166t each	original building	1 TLCD 500t	3 TLCD 166t each	3 TLCD robust 166t each
floor 1	0,03	0,03	0,03	0,03	0,22	0,22	0,22	0,22
floor 10	0,32	0,28	0,29	0,27	1,39	1,33	1,33	1,27
floor 16	0,65	0,56	0,58	0,54	2,61	2,38	2,44	2,25
floor 23	1,13	0,95	0,99	0,91	4,37	4,02	4,03	3,79
floor 30	1,72	1,42	1,49	1,34	6,03	5,67	5,65	5,27
floor 50	3,94	3,15	3,33	2,95	13,07	10,60	11,10	9,59
floor 55	4,60	3,67	3,88	3,43	15,48	12,55	13,28	11,25
floor 60	5,29	4,21	4,46	3,94	17,95	14,59	15,82	13,27
floor 65	6,00	4,78	5,06	4,47	20,62	16,42	17,94	15,21
floor 70	6,75	5,38	5,69	5,04	23,34	18,75	20,24	18,18
floor 75	7,55	6,03	6,37	5,66	26,14	22,33	23,49	21,69
floor 76	7,73	6,19	6,53	5,80	26,77	23,14	24,33	22,49
TLCD1		28,73	52,26	52,00		90,80	174,34	167,64
TLCD2			30,60	34,66			101,77	100,82
TLCD3			40,16	21,50			118,62	72,93

Table 9-24: Acceleration response for the stiff structure

9.5. Benchmark control problem for seismically excited structure

Based on a benchmark problem published by Ohtori et al.³ which provides a problem definition and guidelines for the investigation of seismically excited structures for a 3-, 9- and 20-story building, the efficiency of TLCD in mitigating earthquake loads is investigated. The high rise, 20-story structure used in this numerical study was fully designed but actually not constructed. It meets the seismic code for the Los Angeles, California region, and represents a typical high-rise building, see Ohtori et al.³. The benchmark structure, depicted in Figure 9-25, is $30.48m$ by $36.58m$ in plan, and $80.77m$ in elevation. The bays are $6.10m$ on centre, in both directions, with five bays in the north-south (N-S) direction and six bays in the east-west (E-W) direction. The building's lateral load-resisting system is comprised of steel moment-resisting frames (MRFs). The interior bays of the structure contain simple framing with composite floors. The mass of the structure is composed of various components of the structure, including the steel framing, floor slabs, ceiling/flooring, roofing and a penthouse located on the roof. The mass, including both N-S MRFs, of the ground level is $532t$, for the first level is $563t$, for the second level to 19th level is $552t$, and for the 20th level is $584t$. The mass of the above ground levels of the entire structure is $11.100t$. The building has two basement levels, and typical floor to floor heights are $3.96m$ for all levels except the ground floor, whose height is $5.49m$.

This benchmark study focuses on an in-plane (2D) analysis of the benchmark structure. The frames considered in the development of the numerical evaluation model are the N-S MRFs, the short, or weak direction of the building. Based on the physical description of the building, a 2D finite element model has been developed by Ohtori et al.³, including the beams and columns which are modelled as plane frame elements with a distinct mass and stiffness corresponding to each element. Since every node has three degrees of freedom, the structure is described by 414 DOF prior to the application of the boundary conditions. Besides the kinematic constraints, all floors are supposed to be rigid in horizontal direction, forcing all nodes at a certain floor to have equal horizontal displacements.

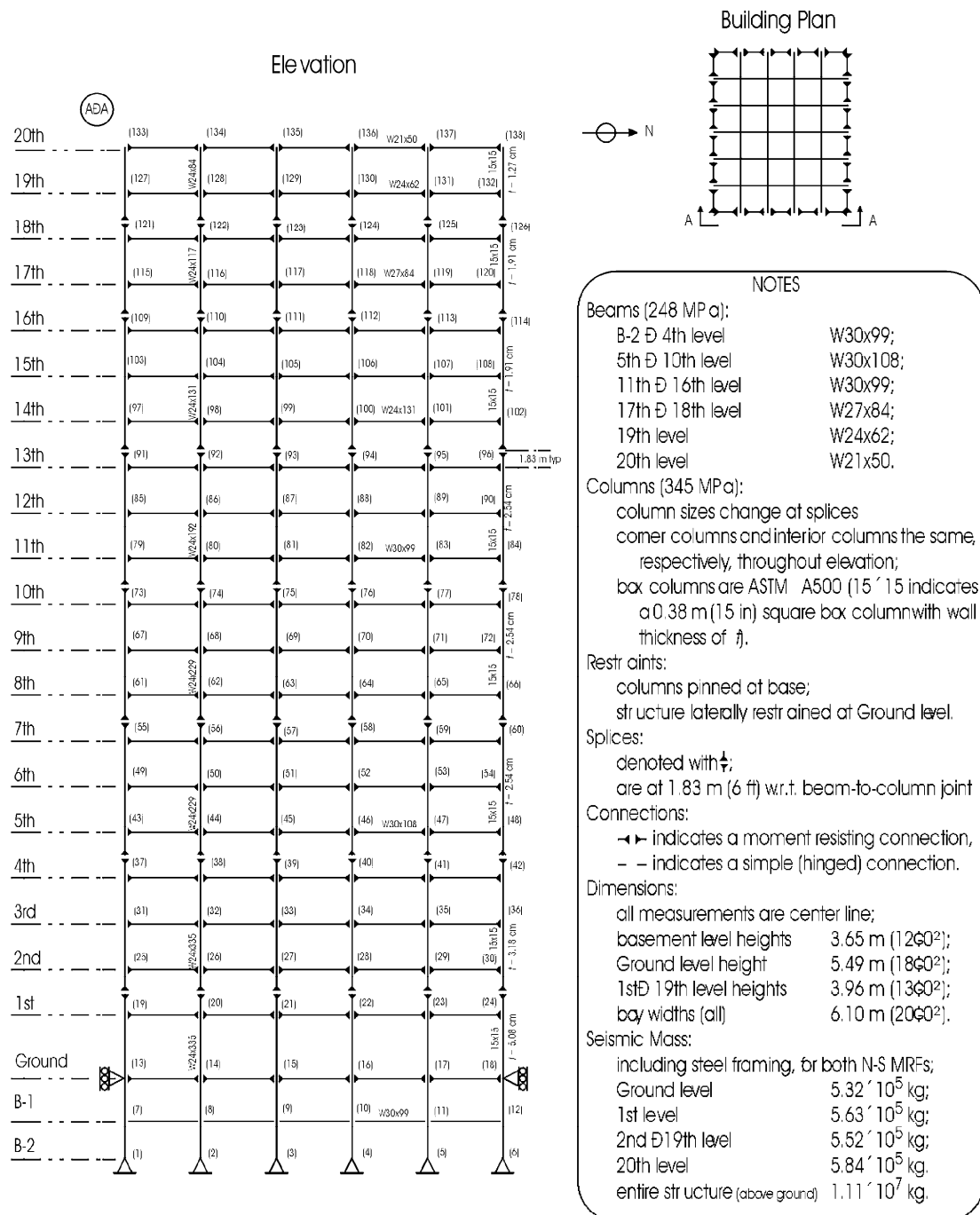


Figure 9-45: 20 DOF benchmark structure N-S direction, Moment Resisting Frame (MSR), see Ohtori et al.³

These assumption allow to decrease the degrees of freedom to 291 by means of the static condensation method. The first 10 natural frequencies of the resulting model are given in Ohtori et al.³: 0.261, 0.753, 1.30, 1.83, 2.40, 2.44, 2.92, 3.01, 3.63 and 3.68Hz, respectively. The

corresponding damping is obtained under the restricting assumption of Rayleigh damping (Eq.1-42), see Figure 9-46. Although this damping model is very controversial amongst scientist, it is kept for the subsequent analysis, for comparison's sake.

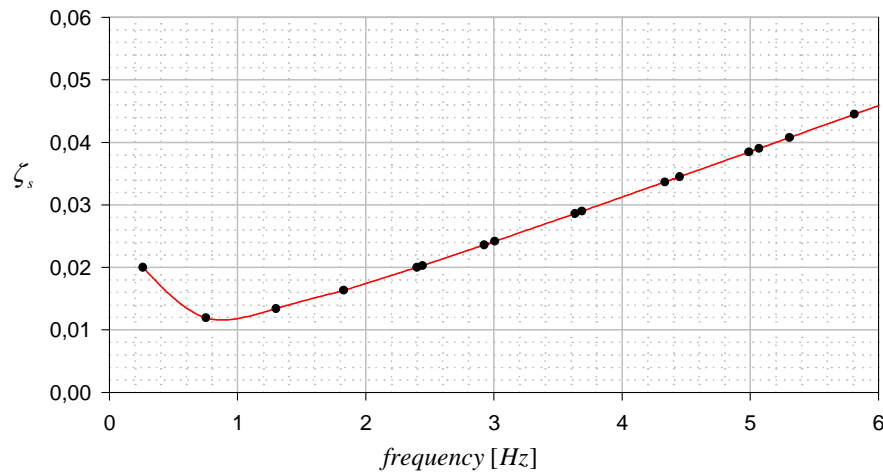


Figure 9-46: Damping coefficients for the first 10 modes, see Ohtori et al.³

In order to evaluate proposed control strategies, two far-field and two near-field historical records are selected, as required in Ohtori et al.³ (available at Structural Dynamics and Control - Earthquake Engineering Laboratory at the University of Notre Dame, Notre Dame, Indiana 46556, USA, <http://www.nd.edu/~quake/>): *El Centro*: the N-S component recorded at the Imperial Valley Irrigation on Mai 18, 1940, with the maximum (measured) of acceleration 0.35g, and digitally available with a sampling time of 0.02s. The El Centro earthquake represents a typical broad band excitation occurring under hard soil (rock) conditions. *Hachinohe*: the N-S component recorded at Hachinohe City, Japan, during the Tokachioki earthquake of May 16, 1968, with a maximum acceleration of 0.23g, and a sampling time of 0.01s. *Northridge*: the N-S component recorded at Sylmar County Hospital parking lot in Sylmar, California, on January 17, 1994, with a peak acceleration of 0.84g, and a sampling time of 0.02s. *Kobe*: the N-S component recorded at the Kobe Japanese Meteorological Agency (JMA) station during the Hyogoken Nanbu earthquake of January 17, 1995, with a peak acceleration of 0.83g and a sampling time of 0.02s. Both, Northridge and Kobe earthquake are typical near field records with an impulse (hammer) like excitation, similar to the earthquake in Skopje, Macedonia in 1963. The earthquake records are shown in Figure 9-47.

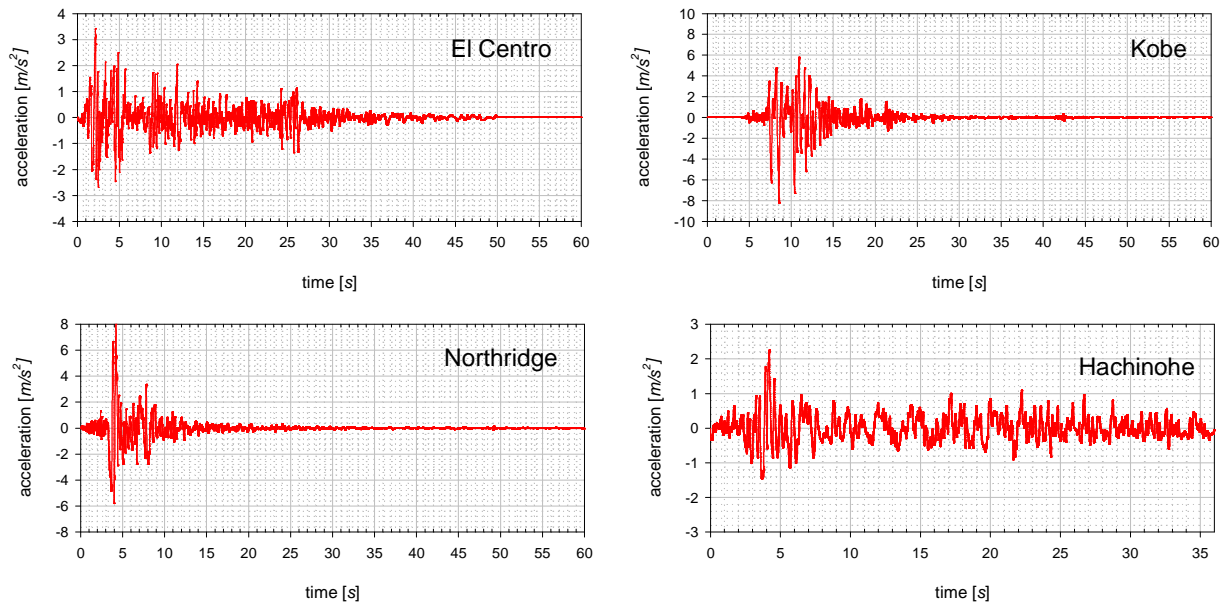


Figure 9-47: Ground acceleration of the earthquakes used in this numerical study, digitally available at WebPages of the Structural Dynamics and Control - Earthquake Engineering Laboratory at the University of Notre Dame, Notre Dame, Indiana 46556, USA, <http://www.nd.edu/~quake/>.

9.5.1. TLCD Design

It has already been mentioned that the mathematical description of the 20-story building left 291 DOF. Although it is possible to perform simulations with high order systems it is cumbersome to design and optimise TLCDs, since important physical information is hidden behind the numerous equations. Thus the author performed a model reduction to 20 degrees of freedom using the method of modal truncation, such that structural motion is characterised by the floor displacements, see Eq.(6-14) in Section 6.6 The vibration modes kept are shown in Figure 9-48.

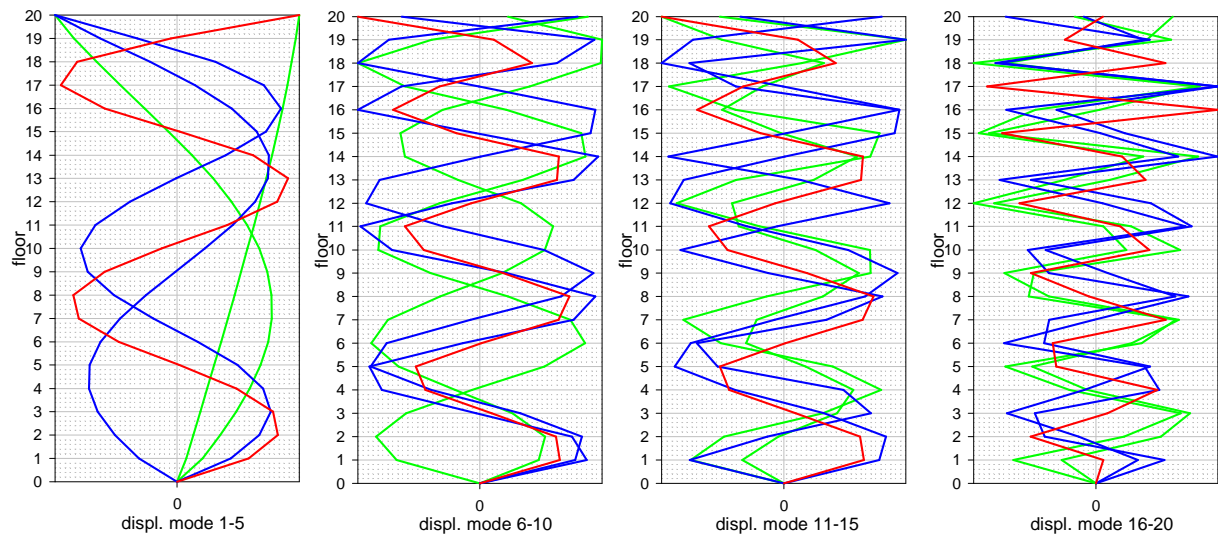


Figure 9-48: Vibration mode shapes of the 20 DOF reduced order model

It has to be mentioned, that the influence of the participation factor was taken into account, thus only the vibration mode shapes with the highest participation factors were kept for the analysis. Comparison of the full order model has shown that, similar to the wind benchmark problem, Section 9.4, the model reduction does not deteriorate the numerical results (for a linear study). Thus all subsequent results are based on the 20 DOF model. To decide in advance how many TLCD should be installed in the high rise building is difficult. From the distribution of the damping coefficients, see Figure 9-46, it is expected that the vibration modes two to four will be vibration prone, since they are lightly damped. But also the fundamental mode, whose damping ratio is 2%, may turn out to be vibration sensitive. It would be certainly best to have a TLCD dedicated to each vibration mode, but from a practical point of view, this is absolutely not feasible. To keep the number of TLCD reasonably small it is decided that three absorber will be distributed in the structure to mitigate the vibrations. It has been derived in Section 5.2, that the efficiency of the TLCD is proportional to the horizontal displacement of the floor level to which it is attached. Additionally, it will be necessary, that a single TLCD mitigates the vibrations of two or more vibration modes. The top floor is certainly ideal for installing TLCDs, but on the other hand a distribution of the absorber weight over the building height is preferable from a loading point of view. Thus the following configuration, illustrated in Figure 9-49, is considered ideal: One 50-ton-TLCD is installed on top of the structure to mitigate the fundamental and second vibration mode. Vibration modes three and four are damped by a second 40-ton-TLCD which is installed at floor

resonant vibration peak of the fundement mode seems to dominate the frequency response. However, this is only true for the steady state situation, and in the transient vibration regime, the performance will be improved dramatically by the application of an active air spring. Furthermore the tuning to the fundamental mode would cause large liquid displacements (due to the low frequency), which should be avoided.

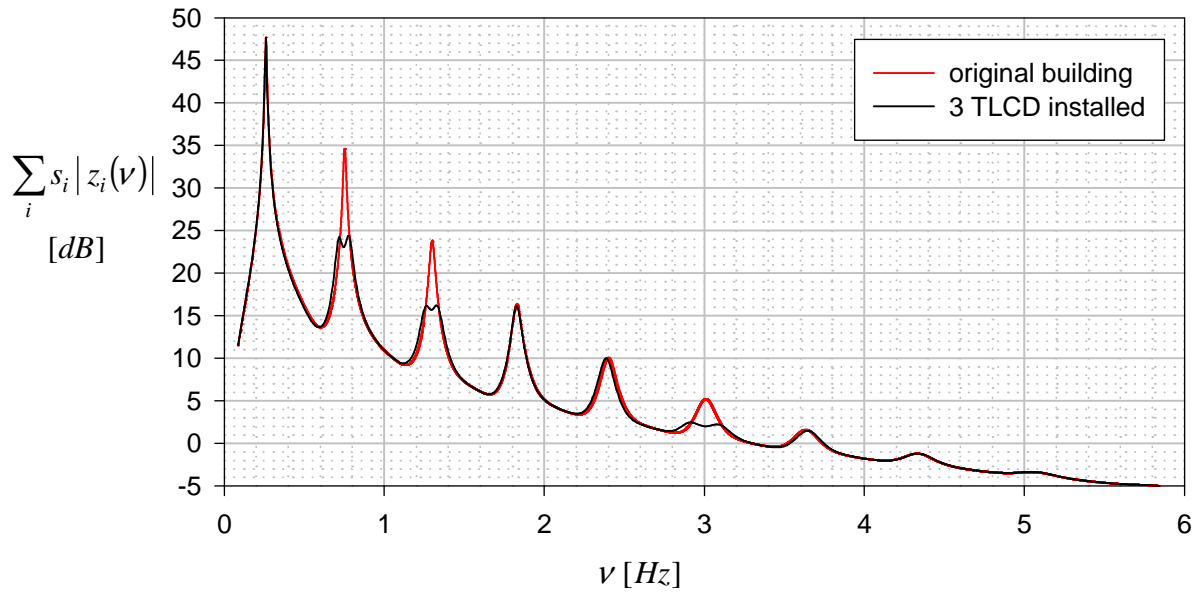


Figure 9-50: weighted frequency response function of building with and without TLCD

9.5.2. Active control

For the active control the pressure input to the active TLCDs is modelled as a first order low pass process with cut-off frequencies of 1Hz, 2Hz, 3Hz, to avoid that e.g. the first TLCD, which is designed to mitigate the first two vibration modes starts to operate at higher frequencies. The idea behind is that in order to achieve high pressure inputs at high frequencies the control input $\mathbf{u}(t)$

must be high, and accordingly the performance index $J = \frac{1}{2} \int_0^{\infty} \mathbf{z}^T \mathbf{Q} \mathbf{z} + \mathbf{u}^T \mathbf{S} \mathbf{u} dt$, Eq.(8-11), is

increased. Thus the minimisation of J will automatically create a control law which avoids high frequency pressure input, and the frequency contents of the pressure input will be limited.

The weighing matrix \mathbf{Q} must be chosen to minimise the response quantities of interest, e.g. the interstory drifts and the accelerations in this study. Since the elements of the state vector do not include floor accelerations, a modification of the linear quadratic optimal control, called the linear

quadratic regulator design with output weighting (LQRY) is applied to calculate the state feedback gain which is still of the form of Eq.(8-20), $\mathbf{u} = -\mathbf{S}^{-1}\mathbf{E}_a^T\mathbf{P}\mathbf{z}$, see e.g. Levine²⁴. The modification allows to optimise a performance index given by $J = \frac{1}{2} \int_0^\infty \mathbf{y}^T \mathbf{Q} \mathbf{y} + \mathbf{u}^T \mathbf{S} \mathbf{u} dt$, where the output vector \mathbf{y} contains interstory drifts and absolute accelerations.

The control toolbox of Matlab⁶ allows to design a linear-quadratic regulator with output weighting directly by using its *lqry* function, and the matrix \mathbf{P} is returned immediately. The application of an LQRY is also discussed in the benchmark definition paper, see Ohtori et al.³. The following weighing was used during the LQRY design with Matlab: The weights of structural interstory drifts were $\mathbf{w}_{drift} = [10, 5, 1, 1, 1, 1, 1, 1, 1, 1, 1, 1, 1, 1, 1, 1, 10, 1]$, and the TLCD displacements weight was $\mathbf{w}_{TLCD} = [0.10, 0.01, 0.01]$, whereas the weight of the floor accelerations was given by $\mathbf{w}_{accel} = [1, 2, 1, 1, 1, 1, 1, 1, 1, 1, 1, 1, 1, 1, 1, 1, 10, 8]$. The weight of the active pressure input Δp_a^* was chosen to be $\mathbf{S} = \text{diag}([0.001, 0.0015, 0.002])$. It has to be mentioned, that the selection of the weighing coefficients \mathbf{w}_{drift} , \mathbf{w}_{TLCD} , \mathbf{w}_{accel} and \mathbf{S} is always based on trial and error. Thus the design of the active control law is an iterative process, where the system's response has to be simulated repeatedly (using *lsim*), until a desirable behaviour is obtained. With the weighing coefficients given above, the optimal feedback control is calculated (using *lqry*), and a numerical simulation with four earthquake ground accelerations is performed. However, for the following numerical studies the knowledge of the full state vector is assumed, and furthermore the control pressure Δp_a^* is assumed to be applied continuously, according to Eq.(8-20). Simulations with the linear elastic model have been performed using Matlab's *lsim* command⁶, and the results are presented graphically in Figure 9-51-Figure 9-54 were the interstory drift ratio, the ratio of the relative floor displacement w_i^{rel} over the story height h_i , w_i^{rel}/h_i , and the absolute floor acceleration for both, peak and RMS responses are displayed.

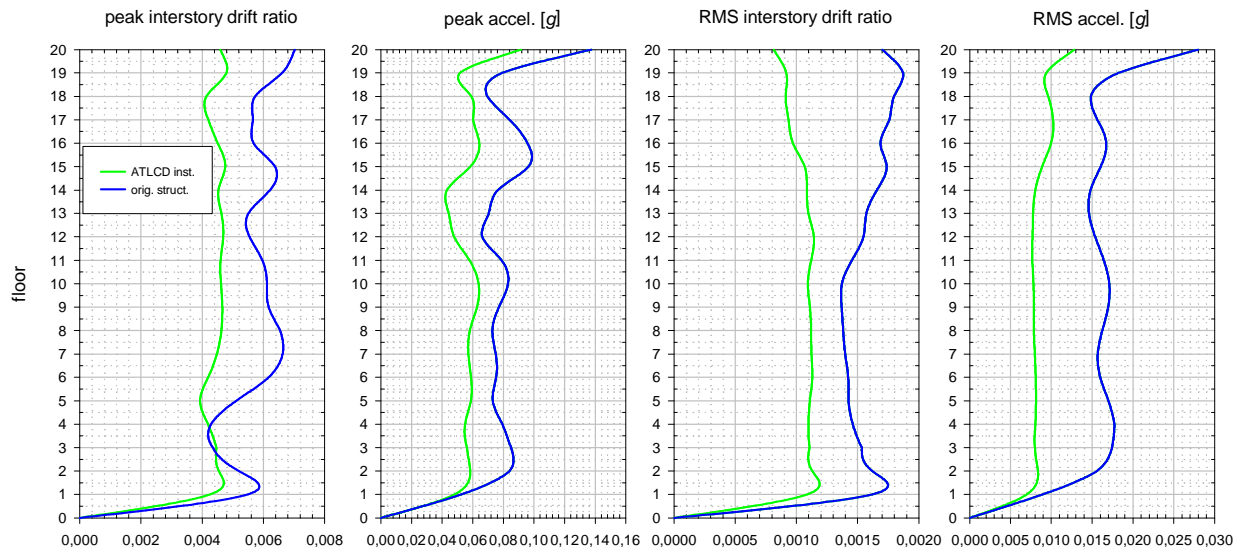


Figure 9-51a: Interstory drift ratio and absolute floor accelerations for the El Centro earthquake record

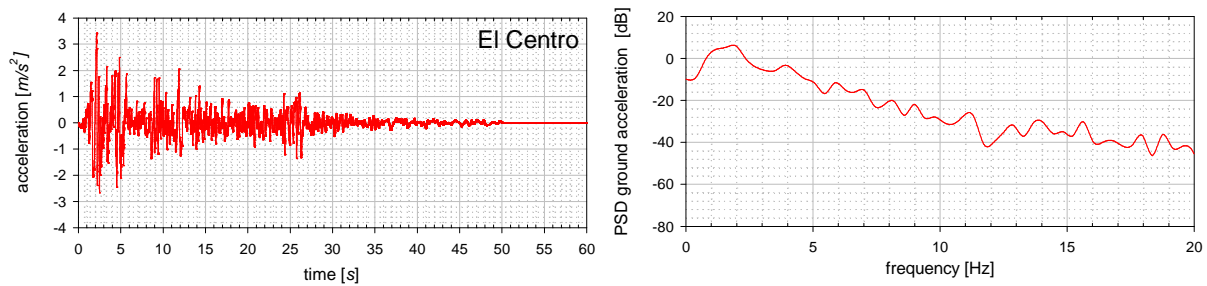


Figure 9-51b: Time history and power spectral density of the El Centro earthquake acceleration record

Apparently, the level of vibration reduction achieved is slightly less than in the previous numerical examples, presented in Section 9.1-9.4. The main reason for this is the fact that no dominating vibration modes exist, since the assumption of the Rayleigh damping generates several lightly damped modes, and thus vibration prone mode shapes. Furthermore, the operating range of the ATLCD has been limited in the frequency domain (to remain as realistic as possible), reducing the efficiency of the absorber for broad band excitation. The vibration reduction achieved is, however, very competitive when compared to the active tendon sample control problem given in the benchmark definition paper Ohtori et al.³. Nevertheless, for the building considered under

earthquake excitation, ATLCDs cannot develop their full vibration reduction capability, and thus alternative energy dissipating devices or concepts might be investigated for further improved vibration reduction.

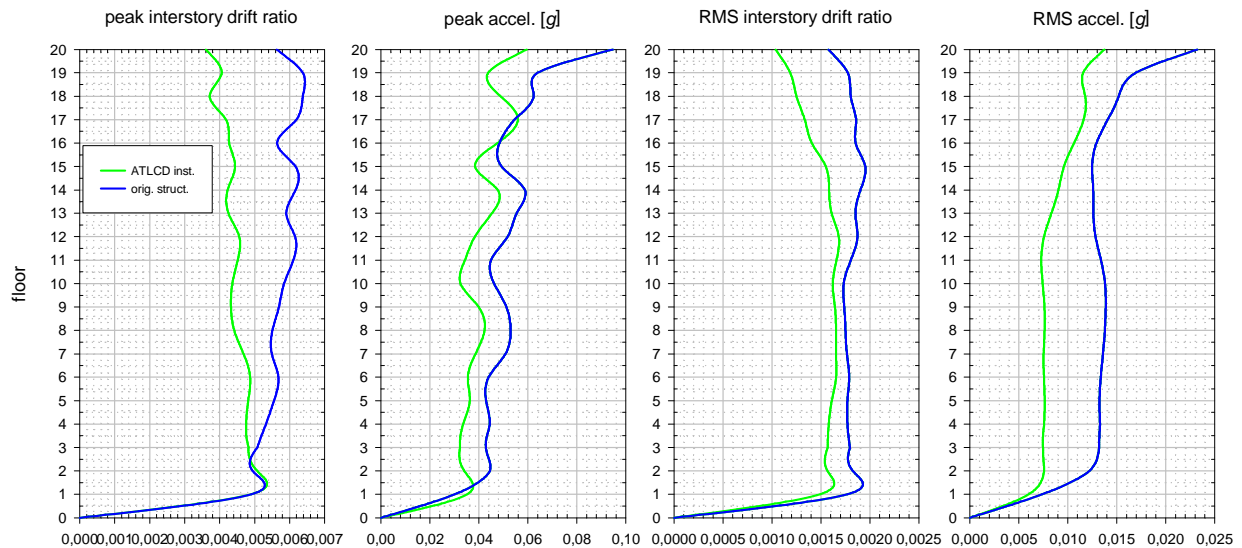


Figure 9-52a: Interstory drift ratio and absolute floor accelerations for the Hachinohe earthquake record

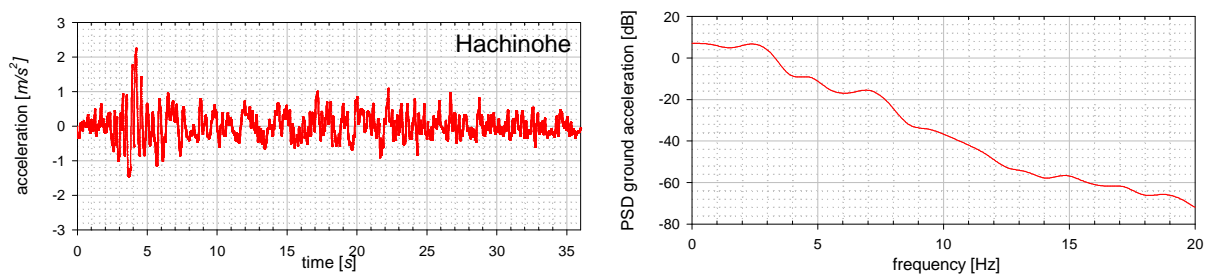


Figure 9-52b: Time history and power spectral density of the Hachinohe earthquake acceleration record

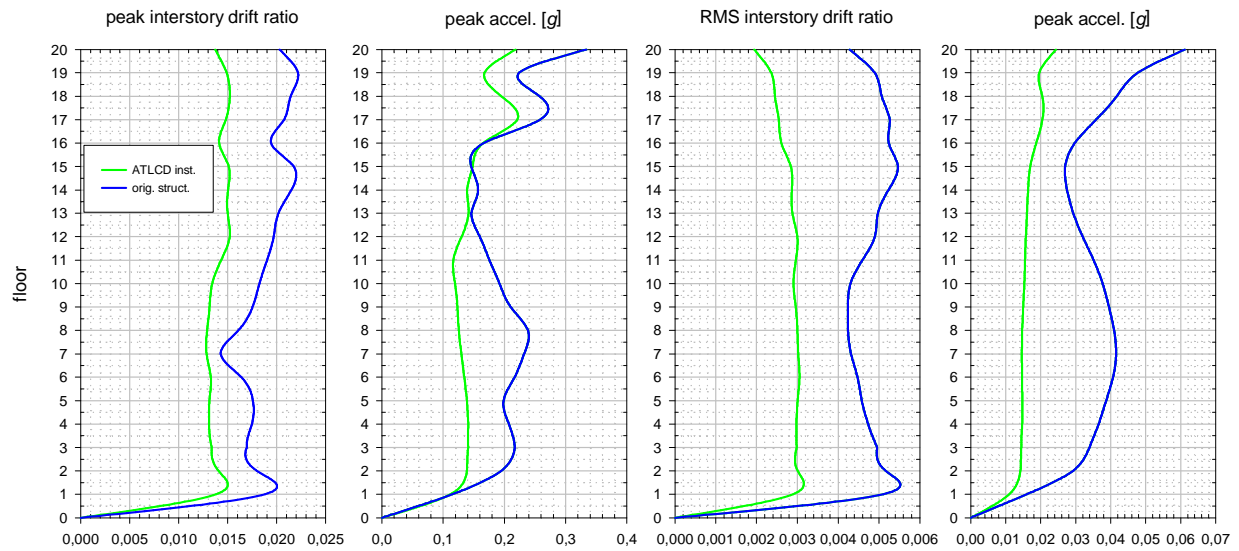


Figure 9-53a: Interstory drift ratio and absolute floor accelerations for the Northridge earthquake record

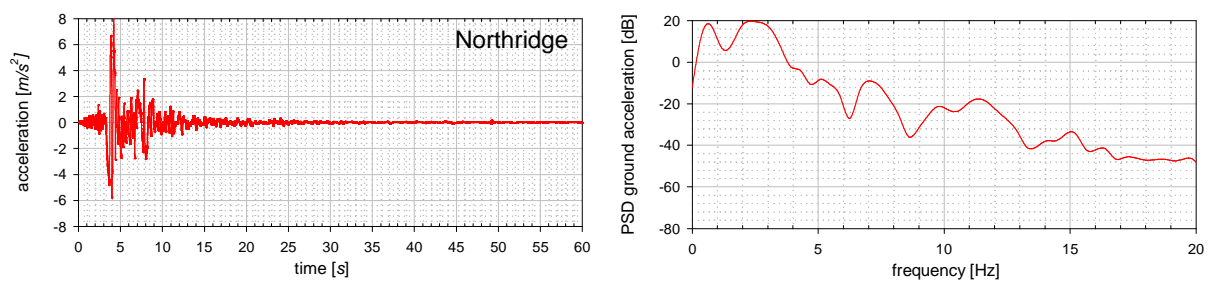


Figure 9-53b: Time history and power spectral density of the Northridge earthquake acceleration record

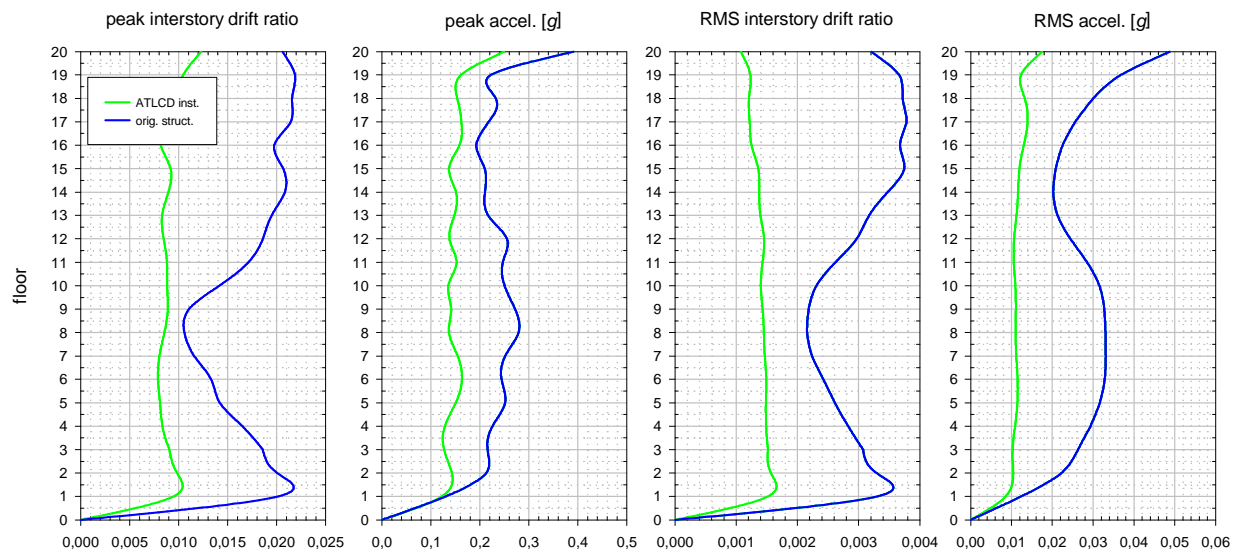


Figure 9-54a: Interstory drift ratio and absolute floor accelerations for the Kobe earthquake record

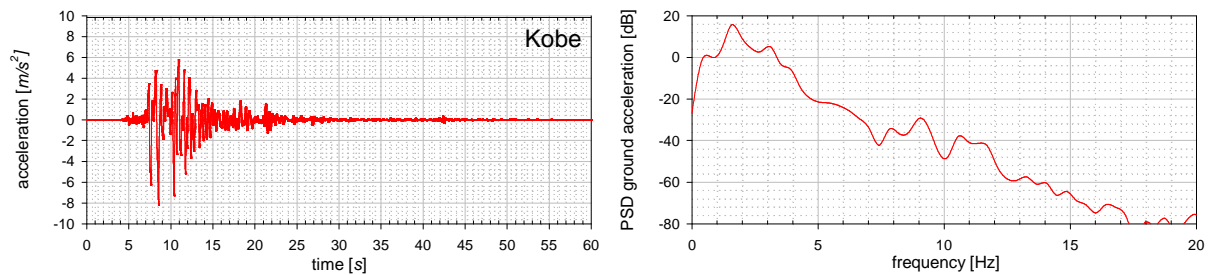


Figure 9-54b: Time history and power spectral density of the Kobe earthquake acceleration record

9.6. References

- ¹ Spencer, B.F.Jr., Dyke, S.J., Deoskar, H.S., Benchmark Problems in Structural Control, Part II: Active Tendon System, Proc. of the 1997 ASCE Structures Congress, Portland, Oregon, April 13-16, 1997, also available: <http://www.nd.edu/~quake/>
- ² Yang J.N., Agrawal, A.K., Samali, B., Wu, J.C., *A Benchmark Problem For Response Control of Wind-Excited Tall Buildings*, 2nd Europ. Conference on Structural Control, July 2000, Paris, France

- ³ Ohtori, Y., Christenson, R.E., Spencer, B.F.Jr, Dyke, S.J., Benchmark Control Problems for Seismically Excited Nonlinear Buildings, <http://www.nd.edu/~quake/>
- ⁴ The MathWorks Inc., *MATLAB, Optimization Toolbox*, 1984-2001, campus license TU-Vienna
- ⁵ Lagarias, J.C., J.A. Reeds, M.H. Wright, P.E. Wright, *Convergence Properties of the Nelder-Mead Simplex Algorithm in Low Dimensions*, to appear in the SIAM Journal of Optimization.
- ⁶ The MathWorks Inc., *MATLAB, Control Toolbox*, 1984-2001, campus license TU-Vienna
- ⁷ Franklin, G.F., J.D. Powell, and M.L. Workman, *Digital Control of Dynamic Systems*, Second Edition, Addison-Wesley, 1990
- ⁸ Sockel, H., *Aerodynamik der Bauwerke*, Fr. Vieweg & Sohn, Braunschweig, 1984
- ⁹ Soong, T.T., Reinhorn, A.M., Tuned Mass Damper/Active Mass Damper Feasibility Study for a Tall Flexible Building, NCEER/EERC Short Course on Passive Energy Dissipation, New York, NY, Sept.26-28,1996
- ¹⁰ Liu, H., *Wind Engineering, A Handbook for Structural Engineers*, Prentice Hall, Englewood Cliffs, New Jersey, 1991
- ¹¹ Spencer, B.F.Jr., Dyke, S.J., Deoskar, H.S., Benchmark Problems in Structural Control, Part II: Active Tendon System, Proc. of the 1997 ASCE Structures Congress, Portland, Oregon, April 13-16, 1997, also available: <http://www.nd.edu/~quake/>
- ¹² Chung, L.L., Lin, R.C., Soong, T.T. and Reinhorn, A.M., *Experiments on Active Control for MDOF Seismic Structures*, J. of Engrg. Mech., ASCE, vol.115(8), pp. 1609-27, 1989
- ¹³ Arnold, W.F., Laub, A.J. *Generalized Eigenproblem Algorithms and Software for Algebraic Riccati Equations*, Proc. IEEE, 72, pp. 1746-1754, 1984
- ¹⁴ Luenberger, D.G., *Introduction to Dynamic Systems*, John Wiley&Sons, New York, 1979
- ¹⁵ Ackermann, J., *Abtastregelung*, 3rd edition, Springer Verlag Berlin, 1983
- ¹⁶ Kautsky, J., Nichols, N.K., *Robust Pole Assignment in Linear State Feedback*, Int. J. Control, 41, pp.1129-1155,1985
- ¹⁷ Dorf, R.C.(ed.), *The Electrical Engineering Handbook*, CRC-Press, 1997
- ¹⁸ Matlab, *Simulink, Version 3.0.1*, The MathWorks Inc., 1984-2001, campus license TU-Vienna
- ¹⁹ Matlab, *Signal Processing Toolbox*, The MathWorks Inc., 1984-2001, campus license TU-Vienna
- ²⁰ Chang, C.C., Hsu, C.T., Swei, S.M., *Control of buildings using single and multiple tuned liquid column dampers*, Structural Engineering and Mechanics, vol.6(1),pp.77-93, 1998
- ²¹ Gao, H., Kwok, K.S.C., Samali, B., *Characteristics of multiple tuned liquid column dampers in suppressing structural vibration*, *Engineering Structures*, vol.21, pp.316-331, 1999
- ²² Sadek, F., Mohraz, B., Lew, H.S., *Single and multiple-tuned liquid column dampers for seismic applications*, Earthquake Engineering and Structural Dynamics, vol.27, pp.439-463, 1998
- ²³ Yalla, S.K., Kareem, A., *Optimum Absorber Parameter for Tuned Liquid Column Dampers*, Journal of Structural Engineering, pp.906-915, vol.126, 2000
- ²⁴ Levine, W.S. ed., *The Control Handbook*, CRC Press, IEEE Press, 1996

Appendix

A. Equivalent Linearisation

The linearisation of nonlinear differential equations is important in the course of this dissertation. Especially the nonlinear turbulent damping term $\delta_L |\dot{u}| \dot{u}$ must be converted into an equivalent viscous damping $2\zeta \omega_0 \dot{u}$ for the sake of simple investigation of the resulting dynamic system. Since the nonlinearity appears in a single differential equation, a straightforward approach is to apply the method of harmonic balance, e.g. see Ziegler¹, p.619, Magnus², or Föllinger³, pp.11-158:

Considering the dynamic system

$$\ddot{u} + f(u, \dot{u}) = 0 \quad (\text{A-1})$$

whose free vibrations can be approximated by the time harmonic motion $u(t) = A \sin(\omega t)$, then the equivalent linearised system is described by the linear differential equation

$$\ddot{u} + b\dot{u} + au = 0, \quad (\text{A-2})$$

where the Fourier coefficients a and b are determined by

$$a = \frac{1}{A\pi} \int_0^{2\pi} f(A \cos(\omega t), -A\omega \sin(\omega t)) \cos(\omega t) d(\omega t), \quad (\text{A-3})$$

$$b = \frac{1}{\omega A\pi} \int_0^{2\pi} f(A \cos(\omega t), -A\omega \sin(\omega t)) \sin(\omega t) d(\omega t) \quad (\text{A-4})$$

Evaluation of these coefficients for the nonlinear turbulent damping term

$$f(\dot{u}, u) = \delta_L |\dot{u}| \dot{u} + \omega_0^2 u \quad (\text{A-5})$$

renders

$$a = \frac{1}{A\pi} \int_0^{2\pi} \delta_L \left(\left| -A\omega \sin(\omega t) \right| A\omega \sin(\omega t) + \omega_0^2 A \cos(\omega t) \right) \cos(\omega t) d\omega t = \omega_0^2 \quad (\text{A-6})$$

$$b = \frac{1}{\omega A\pi} \int_0^{2\pi} \delta_L \left(\left| -A\omega \sin(\omega t) \right| A\omega \sin(\omega t) + \omega_0^2 A \cos(\omega t) \right) \sin(\omega t) d\omega t = \frac{8 \delta_L A \omega}{3\pi}. \quad (\text{A-7})$$

Thus the linearised equation is given by

$$\ddot{u} + 2\zeta \omega_0 \dot{u} + \omega_0^2 u = 0, \quad (\text{A-8})$$

$$\zeta = \frac{4A\delta_L}{3\pi},$$

where ζ denotes the equivalent viscous damping, and the amplitude dependence is preserved. Exactly the same result is obtained by demanding that the dissipated energy during one cycle (vibration period T_0) must be equal for the linearised and the nonlinear system, thus

$$E = \int_0^{T_0} |f(u, \dot{u}) \dot{u}| dt = \int_0^{T_0} |2\zeta \omega \dot{u} \dot{u}| dt, \text{ which also renders the equivalent viscous damping}$$

$$\zeta = \frac{4A\delta_L}{3\pi}.$$

B. Lyapunov Equation

For linear time invariant systems of the form $\dot{\mathbf{z}} = \mathbf{A} \mathbf{z} + \mathbf{B} \mathbf{u}$, the integral expression

$$\int_0^{\infty} \mathbf{z}^T \mathbf{Q} \mathbf{z} dt \quad (\text{B-1})$$

is of ultimate importance for optimisation and control, as it acts as a kind of performance index which should be minimal for optimal system performance. Assuming free motion of a linear time invariant system, the homogenous solution of the state variables is given by $\mathbf{z}(t) = e^{\mathbf{A}t} \mathbf{z}_0$. Insertion into (B-1) yields

$$\mathbf{z}_0^T \int_0^{\infty} e^{\mathbf{A}^T t} \mathbf{Q} e^{\mathbf{A} t} dt \mathbf{z}_0 = \frac{1}{2} \mathbf{z}_0^T \mathbf{P} \mathbf{z}_0 \quad (\text{B-2})$$

where the unknown matrix \mathbf{P} is defined by

$$\mathbf{P} = \int_0^{\infty} e^{\mathbf{A}^T t} \mathbf{Q} e^{\mathbf{A} t} dt \quad (\text{B-3})$$

Solving for \mathbf{P} by partial integration yields

$$\mathbf{P} = \left[e^{\mathbf{A}^T t} \mathbf{Q} \mathbf{A}^{-1} e^{\mathbf{A} t} \right]_0^{\infty} - \int_0^{\infty} \mathbf{A}^T e^{\mathbf{A}^T t} \mathbf{Q} \mathbf{A}^{-1} e^{\mathbf{A} t} dt. \quad (\text{B-4})$$

For infinite time and stable systems, the first term of Eq.(B-4) reduces to $-\mathbf{Q} \mathbf{A}^{-1}$ and due to the fact that $\mathbf{A}^{-1} e^{\mathbf{A}t} = e^{\mathbf{A}t} \mathbf{A}^{-1}$, Eq.(B-4) can be rewritten as

$$\mathbf{P} = -\mathbf{Q} \mathbf{A}^{-1} - \mathbf{A}^T \int_0^{\infty} e^{\mathbf{A}^T t} \mathbf{Q} e^{\mathbf{A} t} dt \mathbf{A}^{-1} = -\mathbf{Q} \mathbf{A}^{-1} - \mathbf{A}^T \mathbf{P} \mathbf{A}^{-1} \quad (\text{B-5})$$

where the integral equals again \mathbf{P} . Right-multiplication with \mathbf{A} renders the well known Lyapunov matrix equation, which can be solved efficiently by several numerical methods, see e.g. the Matlab Control Toolbox⁴

$$\mathbf{A}^T \mathbf{P} + \mathbf{P} \mathbf{A} + \mathbf{Q} = \mathbf{0}. \quad (\text{B-6})$$

c. Notation

\mathbf{a}	absolute acceleration
\mathbf{a}_g	guiding acceleration
\mathbf{a}'	relative acceleration
$\mathbf{A}_d(\omega), \mathbf{A}_v(\omega), \mathbf{A}_a(\omega)$	amplitude transfer function for displacement, velocity, acceleration
\mathbf{A}, \mathbf{A}_r	system matrix
A_p	area enclosed by TTLCD
A_B	cross sectional area of horizontal TLCD section
A_H	cross sectional area of inclined TLCD section
B	width of horizontal TLCD section
\mathbf{B}	system (TLCD) input matrix
c, C, \mathbf{C}	damping factor, damping matrix, output matrix
$\mathbf{D}, \mathbf{D}_a, \mathbf{D}_{eff}$	feed-through matrix
E_{kin}	kinetic energy
E_D	dissipative energy
E_S	strain energy
E_{pot}	potential energy
E_I	external input energy
E_p	dissipative energy
$\mathbf{e}_x, \mathbf{e}_y, \mathbf{e}_z, \mathbf{e}_t$	cartesian unit vectors, unit vector in tangential direction
$\mathbf{E}_a, \mathbf{E}_{eff}$	active pressure, effective force influence vector
\mathbf{F}	force vector
\mathbf{f}_{eff}	effective force loading
\mathbf{f}_A, f_x, f_z	absorber interaction forces
f, \mathbf{f}	external force, e.g. wind

$f_{eff}, \mathbf{f}_{eff}$	effective force
g	constant of gravity
\mathbf{H}'_A	angular momentum vector with respect to A
H	length of inclined TLCD section
$\mathbf{H}(s), \mathbf{h}(s), h(t)$	complex frequency transfer function, impulse response function
h_{eff}	effective height
\mathbf{I}	momentum vector, identity vector
J	performance index
K, k, \mathbf{K}	stiffness, stiffness matrix
K_t	tangent modulus
\mathbf{k}_t	body force
\mathbf{L}	position matrix
L, L_{eff}	length of liquid column, effective length
\mathbf{M}_A	interaction moment with respect to A
M, \mathbf{M}	mass, mass matrix
m_f, m^*	fluid mass, conjugate mass
N	maximal index, number of DOF of structure
n	number of TLCDs, polytropic index
α	rotation about Z-axis
$w_{xy} = a\alpha$	rotation about Z-axis
$p, \Delta p, \Delta p_L$	pressure, pressure difference, pressure loss
Δp_a	active pressure input
Δp_a^*	normalised active pressure input
\mathbf{P}	solution of Lyapunov equation
\mathbf{P}_I	observability Gramian
q_i, \mathbf{q}	modal coordinate, modal vector
Q_u	generalised force
\mathbf{Q}	weighing matrix

\mathbf{Q}_I	controlability Gramian
\mathbf{r}	position vector
\mathbf{r}'	relative position vector
\mathbf{R}	TLCD parameter matrix
\mathbf{R}_S	static influence matrix
\mathbf{r}_S	static influence vector
s	coordinate of relative streamline
\mathbf{S}, s_i	weighing matrix
S_x	power spectral density of x
$\mathbf{T}, \bar{\mathbf{T}}$	transformation matrices
T_0	natural period of vibration
u	relative liquid displacement
\dot{u}	relative flow velocity
\mathbf{v}	velocity vector
\mathbf{v}_g	guiding velocity
\mathbf{v}'	relative velocity vector
V	Lyapunov function
V_0	gas volume inside TLCD
w_g, \ddot{w}_g	horizontal ground displacement, ground acceleration
$w, \mathbf{w}, \bar{\mathbf{w}}$	floor displacement, displacement vector
w_x, w_y	displacement in X- or Y-direction
$\mathbf{z} = [\mathbf{w}, \mathbf{u}, \dot{\mathbf{w}}, \dot{\mathbf{u}}]^T$	state space vector
α_i	damping coefficient
β	TLCD opening angle
ζ, ζ_S, ζ_A	damping ratio of structure/absorber
δ_{ij}	Kronecker symbol
δ	tuning ratio
δ_L	head loss factor
$\boldsymbol{\varphi}$	mode shape vector

Φ	modal matrix
ϕ	phase angle
γ, γ_g	frequency ratio
$\Gamma(s), \Gamma(t)$	transition matrix
$\kappa, \bar{\kappa}, \bar{\bar{\kappa}}$	geometry factors
λ	loss factor
λ	costate vector
μ	absorber-structure mass ratio
ν	circular forcing frequency
ρ	mass density of fluid
Σ^2	covariance matrix
σ^2	variance
ω_0	undamped natural frequency
Ω	rotation vector
Ω_S	diagonal matrix with the structural circular frequencies
ω_A	undamped circular frequency of TLCD
ξ_g	ground excitation participation factor
$(\cdot)_\Psi$	index Ψ denotes filter quantities
$(\cdot)^*$	superscript $*$ denotes corresponding quantity in analogue TMD system

References

¹ Ziegler, F., *Mechanics of Solids and Fluids*, 2nd reprint of second edition, Springer, 1999.

² Magnus, K., Popp, K., *Schwingungen*, 5th edition, Teubner, Stuttgart, 1997

³ Föllinger, O., *Nichtlineare Regelungen*, Oldenburg Verlag, München, 1993

⁴ The MathWorks Inc., *MATLAB, Control Toolbox*, 1984-2001, campus license TU-Vienna

References

- Abé, M., Kimura, S., Fujino, Y., *Control laws for semi-active tuned liquid column damper with variable orifice openings*, 2nd International Workshop on Structural Control, 18-21 December 1996, Kong Kong, pp.5-10, 1996, [3]55, [8]145
- Ackermann, J., *Abtastregelung*, 3rd edition, Springer Verlag Berlin, 1983, [9]194
- Adam, C., Hruska, A., Kofler, M., *Elastic Structures with tuned liquid column dampers*, XVI IMEKO World Congress, Vienna, Austria, September 25-28, 2000, [3]56
- Adhikari, R., Yamaguchi, H., Yamazaki, T., *Modal Space Sliding-Mode Control of Structures*, Earthquake Engineering and Structural Dynamics, vol.27(11), pp.1303-1314, 1998, [8]158
- Agrawal, A.K., Yang, J.N., Wu, J.C., *Application of optimal polynomial control to a benchmark problem*, Earthquake Engng. Struct. Dyn. 27, 1291-1302, 1998, [8]155
- Arnold, W.F., Laub, A.J. *Generalized Eigenproblem Algorithms and Software for Algebraic Riccati Equations*, Proc. IEEE, 72, pp. 1746-1754, 1984, [9]193
- Balendra, T., Wang, C.M., Cheong, H.F., *Effectiveness of tuned liquid column dampers for vibration control of towers*, Engineering Structures, vol.17(9), pp.668-675, 1995, [3]56, [4]82
- Balendra, T., Wang, C.M., Rakesh, G., *Effectiveness of TLCD on various structural systems*, Engineering Structures, vol.21, pp.291-305, 1999, [3]57
- Balendra, T., Wang, C.M., Rakesh, G., *Vibration Control of tapered buildings using TLCD*, Journal of Wind Engineering and Industrial Aerodynamics, 77&78, pp.245-257, 1998, [3]57
- Balendra, T., Wang, C.M., Rakesh, G., *Vibration control of various types of building using TLCD*, Journal of wind engineering and industrial aerodynamics, vol.83, pp.197-208, 1999, [3]57
- Balendra, T., Wang, C.M., Yan, N., *Control of wind-excited towers by active tuned liquid column damper*, Engineering Structures vol.23, pp.1054-1067, 2001, [3]58
- Banerji, P., Murudi, M., Shah, A.H., Popplewell, N., *Tuned liquid dampers for controlling earthquake response of structures*, Earthquake Engineering and Structural Dynamics, vol.29, pp. 587-602, 2000, [3]55
- Bauer, H.F., *Oscillations of Immiscible Liquids in Rectangular Container: A New Damper for Excited Structures*, Journal of Sound and Vibration, 1984, vol.92(1), 117-133, [2]31, [3]55
- Blevins, R.D., *Applied Fluid Dynamics Handbook*, reprint, Kireger Publ., 1992, [4]73
- Burton, A.B., Makris, N., Konstantopoulos, I., Antsaklis, P.J., *Modeling the Response of ER Damper: Phenomenology and Emulation*, Journal of Engineering Mechanics, vol.122(9), pp. 897-906, 1996, [8]145, [2]51
- Cady, W.G., *Piezoelectricity*, McGraw-Hill, New York, 1946, [2]49
- Cai, G., Huang, J., Sun, F., Wang, C., *Modified sliding-mode bang-bang control for seismically excited linear structures*, Earthquake Engineering and Structural Dynamics, vol.29, p.1647-1657, 2000, [8]158
- Casciati, F.; Faravelli, L., *Coupling SMA and steel in seismic control devices*, book article in: Analysis multiechelle et systemes physiques couples, Presses de l'Ecole nationale des ponts et chaussees, Paris, 1997, [2]49
- Chang, C.C., Gu, M., *Suppression of vortex-excited vibration of tall buildings using tuned liquid dampers*, Journal of Wind Engineering and Industrial Aerodynamics, vol.83, pp.225-237, 1999, [3]55

- Chang, C.C., Hsu, C.T., Control performance of liquid column vibration absorbers, *Engineering Structures*, vol.20(7), pp.580-586, 1998, [3]58, [4]82
- Chang, C.C., Hsu, C.T., Swei, S.M., *Control of buildings using single and multiple tuned liquid column dampers*, *Structural Engineering and Mechanics*, vol.6(1), pp.77-93, 1998, [3]58, [9]209
- Chang, C.C., *Mass dampers and their optimal designs for building vibration control*, *Engineering Structures*, vol.21, pp.454-463, 1999, [3]58, [3]65
- Chang, C.C., Qu, W.L., *Unified dynamic absorber design formulas for wind-induced vibration control of tall buildings*, *The Structural Design of Tall Buildings*, vol.7, pp.147-166, 1998, [3]58
- Chase, G.J., Smith, A.H., H_{∞} -Control for Vibration Control of Civil Structures in Seismic Zones, Report No. 116, The J. Blume Earthquake Engineering Center, Stanford University, September 1995, [8]142
- Chen, Y.H., Chao, C.C., *Optimal damping ratio of TLCDs*, *Structural Engineering and Mechanics*, vol.9(3), p.227-240, 2000, [3]59
- Chiampi, V., *Use of Energy Dissipation Devices, based on yielding of steel, for earthquake protection of structures*, *Proceedings of International Meeting on Earthquake Protection of Buildings*, pp.14/D-58/D, 1991, [2]25
- Chopra, A.K., *Dynamics of structures*, Prentice Hall, 1995, [1]1, [2]31, [5]106
- Chung, L.L., Lin, R.C., Soong, T.T. and Reinhorn, A.M., *Experiments on Active Control for MDOF Seismic Structures*, *J. of Engrg. Mech.*, ASCE, vol.115(8), pp. 1609-27, 1989, [9]188
- Chwalla, E., *Introduction to Structural Mechanics, in German*, Stahlbau Verlag, Köln, 1954, [1],6
- Clark, P., *Response of Base Isolated Buildings*, WWW-publication, National Information Service for Earthquake Engineering, sponsored by the National Science Foundation and the University of California, Berkeley, 1997, WWW-address: <http://www.nd.edu/~quake/>, [2]36
- Clough, R.W., Penzien, J., *Dynamics of Structures*, 2nd ed., McGraw-Hill, New York, 1993, [1]1, [7]136, [6]112
- Constantinou, M.C., Soong, T.T., Dargush, G.F., *Passive Energy Dissipation Systems for Structural Design and Retrofit*, Multidisciplinary Center for Earthquake Engineering Research, Monograph Series, 1998, [2]45
- DeCarlo, R.A., Zak, S.H., Mathews, G.P., *Variable Structure Control of Nonlinear Multivariable Systems: A Tutorial*, *Proceedings of the IEEE*, vol.76(3), p.212-232, 1988, [8]157
- DenHartog, J.P., *Mechanical Vibrations*, reprint of 4th ed. McGrawHill 1956, [2]37, [3]55, [5]101
- Doetsch, G., *Anleitung zum praktischen Gebrauch der Laplace Transformation*, Oldenburg, 1956, [1]20
- Dolce, M., Cardone, D., Marnetto, R., *Implementation and testing of passive control devices based on shape memory alloys*, *Earthquake Engineering and Structural Dynamics*, vo.29(7), p.945-968, 2000, [2]49
- Dorf, R.C.(ed.), *The Electrical Engineering Handbook*, CRC-Press, 1997, [9]194
- Dyke, S.J., Spencer, B.F.Jr., Sain, M.K., Carlson, J.D., *Experimental verification of Semi-active Structural Control Strategies Using Acceleration Feedback*, *Proc. 3rd Int. Conference on Motion and Vibration Control*, Chiba, Japan, vol. III, pp- 291-296, 1996, [8]145
- EERC (Earthquake Engineering Research Centre), *Worldwide Applications of Tuned Mass Dampers*, WWW-publication, National Information Service for Earthquake Engineering, Berkeley, 1995, [2]47
- Flotow, von A, *Damping of Structural Vibrations with Piezoelectric Materials and Passive Electrical Networks*, *Journal of Sound and Vibration*, 1991, 146(2), 243-268, [2]50
- Föllinger, O., *Nichtlineare Regelungen*, Oldenburg Verlag, München, 1993, [A]233
- Föllinger, O., *Optimale Regelung und Steuerung*, 3rd edition, Oldenbourg Verlag, 1994, [8]150

- Frahm, H. *Device for Damped Vibrations of Bodies*, U.S. Patent No. 989958, 1909, [2]37
- Franklin, G.F., J.D. Powell, and M.L. Workman, *Digital Control of Dynamic Systems*, Second Edition, Addison-Wesley, 1990, [9]168
- Fried, E., Idelchik, I., *Flow Resistance: a Design Guide for Engineers*, Hemisphere, 1989, [4]73
- Fujino, Y., Sun, L.M., *Vibration Control by Multiple Tuned Liquid Dampers (MTLDs)*, Journal of Structural Engineering, vol.112(12), pp.3482-3502, 1993, [3]55
- Gao, H., Kwok, K.C.S., Samali, B., *Optimization of tuned liquid column dampers*, Engineering Structures, vol.19(6), pp.476-486, 2007, [3]59, [4]82
- Gao, H., Kwok, K.S.C., Samali, B., *Characteristics of multiple tuned liquid column dampers in suppressing structural vibration*, Engineering Structures, vol.21, pp.316-331, 1999, [3]59, [3]65, [9]209
- Gavin, H.P. Hanson, R.D., Filisko, F.E. *Electrorheological Dampers, Part I: Analysis and Design*, J. Appl. Mech., ASME vol. 63 (3), pp.669-675, 1996, [8]145
- Gavin, H.P. Hanson, R.D., Filisko, F.E. *Electrorheological Dampers, Part II: Testing and Modeling*, J. Appl. Mech., ASME vol. 63 (3), pp.676-682, 1996, [8]145
- Graesser, E.J.; Cozzarelli, F.A., *Shape-memory alloys as new materials for aseismic isolation*, Journal of Engineering Mechanics, vo.117(11), p.2590-2608, 1991, [2]49
- Hagenauer, K, Irschik, H. Ziegler, F., *An Exact Solution for Structural Shape Control by Piezoelectric Actuation*, VDI-Fortschrittberichte: Smart Mechanical Systems - Adaptronics, Reihe 11, vol.244, pp.93-98, VDI Verlag 1997, [2]50
- Haroun, M.A., Pires, J.A., Won, A.Y.J., *Suppression of environmentally-induced vibrations in tall buildings by hybrid liquid column dampers*, The structural Design of Tall Buildings, vol.5, pp.45-54, 1996, [3]56, [8]145
- Harris, M., Crede, C.E., *Shock and Vibration Handbook*, McGraw-Hill, 1961, [1],12
- Hasenzagl, R., Irschik, H., Ziegler, F., *Design Charts for Random Vibrations of Elasto-plastic Oscillators Subjected to Kanai-Tajimi Spectra*, Reliability Engineering and System Safety, vol.23, pp.109-126, 1988, [7]138
- Haßlinger, L., Heuer, R., Ziegler, F., *Dynamische Wirkung eines Dachschwimmbeckens auf einen harmonisch erregten Stockwerkrahmen (mit Modellversuchen)*, ÖIAZ, vol.130, 1985, [2]31
- Hayek, H., *Räumliche Bebenerrregte Schwingungen eines Hochbehälters, rechnerische und experimentelle Untersuchungen*, (in German), Master Thesis, TU-Vienna, 1985, [2]31
- Heuer, R., *Dynamische Wirkung eines Dach-Schwimmbeckens*, (in German), Master Thesis, TU-Vienna, 1984, [2]31
- Hitchcock, P.A., Glanville, M.J., Kwok, K.C.S., Watkins, R.D., Samali, B., *Damping properties and wind-induced response of a steel frame tower fitted with liquid column vibration absorbers*, Journal of wind engineering and industrial aerodynamics, 83, pp.183-196, 1999, [4]88
- Hitchcock, P.A., Kwok, K.C.S., Watkins, R.D., Samali, B., *Characteristics of liquid column vibration (LCVA)-I*, Engineering Structures, vol.19(2), pp.126-134, 1997, [3]60, [4]82
- Hitchcock, P.A., Kwok, K.C.S., Watkins, R.D., Samali, B., *Characteristics of liquid column vibration (LCVA)-II*, Engineering Structures, vol.19(2), pp.135-144, 1997, [3]60
- Hochrainer, M.J., Adam, C., *Dynamics of shear frames with tuned liquid column dampers*, ZAMM vol.80 supplement 2, pp.283-284, 2000, [3]61

- Hochrainer, M.J., Adam, C., Ziegler, F., *Application of tuned liquid column dampers for passive structural control*, Proc. 7th International Congress on Sound and Vibration, 4.July-7.July 2000, Garmisch-Partenkirchen, Germany, 2000, CD-Rom paper, also available at: Inst. f. Allgemeine Mechanik (E201), TU-Wien, Wiedner Hauptstr. 8-10/E201, 1040 Wien, Austria, [3]61
- Hochrainer, M.J., *Dynamisches Verhalten von Bauwerken mit Flüssigkeitstilgern*, ZAMM vol.81, supplement 2, pp.191-192, Göttingen Germany, 2000, [3]61, [5]104
- Hochrainer, M.J., *Dynamisches Verhalten von Bauwerken mit aktiven und passiven Flüssigkeitstilgern*, Jahrestagung GAMM 2001, CD-Rom paper, Zürich, available at: Inst. f. Allgemeine Mechanik (E201), TU-Wien, Wiedner Hauptstr. 8-10/E201, 1040 Wien, Austria, [3]62
- Hochrainer, M.J., *Investigation of active and passive tuned liquid column damper for structural control*, 8th International Congress on Sound and Vibration, 2.-6. July 2001, Hong Kong, China, 2001, also available at: Inst. f. Allgemeine Mechanik (E201), TU-Wien, Wiedner Hauptstr. 8-10/E201, 1040 Wien, Austria, [3]62
- Höllinger, F., Ziegler, F., *Stationäre Zufallsschwingungen einer elastischen Gewichtsmauer bei beliebig geformtem Becken*, ZAMM, vol.63, pp.49-54, 1983, [7]137
- Holmes, J.D., *Listing of installations*, *Engineering Structures*, vol.17(9), pp.676-678, 1995, [2]47
- Housner G.W., Bergman, L.A., Caughey, T.K., Chassiakos, A.G., Claus, R.O., Masri, S.F., Skelton, R.E., Soong, T.T., Spencer, B.F., Yao, J.T.P., *Structural Control: Past, Present, and Future*, *Journal of Engineering Mechanics*, vol.123(9), pp.897-971, [2]29, [8]141
- Hruska, A., *Elastische Rahmentragwerke mit U-rohrförmigen Flüssigkeitsdämpfern – eine computergesteuerte Modelluntersuchung* (in German), Master Thesis, Technical University of Vienna, Austria, 1999, [3]56
- Hütte, *Die Grundlagen der Ingenieurwissenschaften*, 29th edition Springer Verlag, 1991, [1]16
- Ibrahim R.A., Pilipchuk, V.N., *Recent advances in liquid sloshing dynamics*, *Applied Mechanics Reviews*, vol.54(2), 2001, [3]55
- Idelchick; I.E., *Handbook of hydraulic resistance*, Hemisphere Publishing Corporation, 1986, [4]71
- Irschik, H., Krommer, M., Pichler, U., *Shaping Distributed Piezoelectric Self-Sensing Layers for Static Shape Control of Smart Structures*, *Journal of Structural Control*, vol.7, pp.173-189, 2000, [2]50
- Irschik, H., Krommer, M., *Piezothermoelastic Behaviour of Shear Deformable Composite Shallow Shells*, Proc. of the Euromech 373 Colloquium Modelling and Control of Adaptive Mechanical Structures, Magdeburg, VDI-Fortschrittberichte, Reihe 11, vol.268, pp.229-238, VDI Verlag 1998, [2]50
- Kagawa, K., Yoshimura, Y., Fujita, K., Yamasaki, Y., Ayabe, S., *Semi-active and Passive Vibration Control of Structure by Fluid System*, PVP-Vol.289, Active and Passive Control of Mechanical Vibration, pp.41-48, ASME, New York, 1994, [3]62
- Kautsky, J., Nichols, N.K., *Robust Pole Assignment in Linear State Feedback*, *Int. J. Control*, 41, pp.1129-1155, 1985, [9]194
- Kelly, J.M., *Base Isolation: Origins and Development*, WWW-publication, National Information Service for Earthquake Engineering, sponsored by the National Science Foundation and the University of California, Berkeley, 1998, [2]36
- Kobori, T., *Future Direction on Research and Development of Seismic-Response-Controlled Structure*, Proc. 1st World Conf. on Struct. Control, Los Angeles, California, USA, Panel 19-31, August 1994, [8]140

- Kofler, M., Master Thesis, *Eine experimentelle und numerische Modelluntersuchung von ebenen Rahmentragwerken mit U-rohrförmigen Flüssigkeitsdämpfern*, Technical University of Vienna, Austria, 2000, [3]56
- Koike, Y., Murata, T., Tanida, K., Kobori, T., Ishii, K., Takenaka, Y., *Development of V-Shaped Hybrid Mass Damper and its Application to High Rise Buildings*, Proc. 1st World Conference on Structural Control, Los Angeles, California, pp.FA2:3-12, August 1994, [8]143
- Krommer, M., Irschik, H., *An Eletromechanically Coupled Theory for Piezoelastic Beams Taking into account the Charge Equation of Electrostatics*, Acta Mechanica, accepted for publication, 2001, [2]50
- Kugi, A., Schlacher, K., Irschik, H., *H_∞ control of Random Structural Vibrations with Piezoelectric Actuators*, Computers and Structures, vol.67, pp.137-145, 1997, [8]144
- Kugi, A., Schlacher, K., Irschik, H., *Nonlinear H_∞ -control of Earthquake Excited High Raised Buildings*, Third International Conference on Motion and Vibration Control, pp36-41, Chiba, Sept. 1-6, 1996, [8]144
- Kwock, K.C.S., Samali, B., *Performance of tuned mass dampers under wind loads*, Engineering Structures, vol.17(9), pp.655-667, 1995, [2]47
- Lagarias, J.C., J.A. Reeds, M.H. Wright, P.E. Wright, *Convergence Properties of the Nelder-Mead Simplex Algorithm in Low Dimensions*, to appear in the SIAM Journal of Optimization, [9]166
- Lei, Y., *Sure and Random Vibrations of Simple Dissipative Civil Engineering Steel Structures*, Dissertation and Report, Institute of Rational Mechanics, TU-Vienna, A-1040 Wien, Austria, 1994, [1]12, [2]26, [8]145
- Lei, Y., Ziegler, F., *Random Response of Friction Damped Braced Frames under Severe Earthquake Excitation*, Fifth U.S. Nat. Conference on Earthquake Engineering, Chicago, Illinois, July 10-14, 1994, pp.683-692, Earthquake Research Institute, ISBN 0-943198-46-1, [2]26, [8]145
- Leipholz, H.H.E.(ed.), *The Proceedings of the IUTAM Symposium on Structural Control*, Waterloo, Ontario, Canada, 4-7 June 1979), North-Holland Publishing Company, Amsterdam-New York-Oxford, 1980, [8]140
- Levine, W.S. (ed.), *The Control Handbook*, CRC Press 1995, [7]129, [7]131, [8]150, [9]227
- Lewis, F.L., Syrmos, V.L., *Optimal Control*, John Wiley&Sons, 1995, [8]150
- Lin, Y.K., Cai, G.Q., *Probabilistic Structural Dynamics*, McGraw-Hill, 1995, [7]132, [7]133
- Liu, H., *Wind Engineering, A Handbook for Structural Engineers*, Prentice Hall, Englewood Cliffs, New Jersey, 1991
- Lou, J.Y.K., Lutes, L.D., Li, J.J., *Active tuned liquid damper for structural control*, 1st World Conference on Structural Control, 3-5 August 1994, Los Angeles, California, USA, pp.TP1.70-TP1.79, 1994, [3]55
- Ludyk, G., *Theoretische Regelungstechnik 1*, Springer, 1995, [1]21
- Ludyk, G., *Theoretische Regelungstechnik 2*, Springer Lehrbuch, 1995, [7]129
- Luenberger, D.G., *Introduction to Dynamic Systems*, John Wiley&Sons, New York, 1979, [9]193
- Lücke, H.D., *Signalübertragung*, Springer, 6th edition, 1995, [7]131
- Magnus, K., Popp, K., *Schwingungen*, 5th edition, Teubner, Stuttgart, 1997, [1]1, [A]233
- Makris N., Constantinou, M.C., *Fractional-Derivative Maxwell Model for Viscous Dampers*, Journal of Structural Engineering, vol.117(9), pp.2708-2724, 1991, [2]28
- Martinez-Romero, E., *Experiences on the Use of Supplemental Energy Dissipators on Building Structures*, Earthquake Spectra, vol.9(3), pp.581-625, 1993, [2]25
- Matlab, *Signal Processing Toolbox*, The MathWorks Inc., 1984-2001, campus license TU-Vienna, [9]207
- Matlab, *Simulink, Version 3.0.1*, The MathWorks Inc., 1984-2001, campus license TU-Vienna, [9]194

- Matlab, *User Guide, Control Toolbox*, MathWorks Inc., Version 5.3.1, 1984-2001, [7]127, [7]129, [9]168, [A]235
- Matlab, *User Guide, Optimisation Toolbox*, MathWorks Inc., 1984-2001, [7]138, [9]166
- McKelvey, A.L., Ritchie, R.O., *Fatigue-crack propagation in Nitinol, a shape-memory and superelastic endovascular stent material*, Journal of Biomedical Materials Research, vol.47(3), pp.301-308, 1999, [2]48
- Modi, V.J., Welt, F., Seto, M.L., *Control of wind-induced instabilities through application of nutation dampers: a brief overview*, Engineering Structures, vol.17(9), pp.626-638, 1995, [2]31
- Moore, B.C., *Principal Component Analysis in Linear Systems: Controllability, Observability, and Model Reduction*, IEEE Transaction on Automatic Control, Vol. AC26(1), pp.17-32, 1981, [6]118
- Müller, K., *Entwurf robuster Regelungen*, Teubner Stuttgart, 1996, [7]129
- Müller, P.C. *Stabilität und Matrizen*, Springer Verlag Berlin, 1977, [1]16, [1]21, [6]118, [7]127
- Müller, P.C., Schiehlen, W.O., *Lineare Schwingungen*, Akademische Verlagsgesellschaft, Wiesbaden, 1976, [6]119
- Naeim, F., Kelly, J.M., *Design of Seismic Isolated Structures*, J Wiley, 1999, [2]33
- Newland, D.E., *Random Vibrations, Spectral and Wavelet Analysis*, Longman 1993, [2]39, [7]132, [7]133
- Ohtori, Y., Christenson, R.E., Spencer, B.F.Jr, Dyke, S.J., Benchmark Control Problems for Seismically Excited Nonlinear Buildings, <http://www.nd.edu/~quake/>, [9]162
- Pall, A.S., Pall, R., *Friction-dampers for seismic control of buildings "A Canadian Experience"*, 11th world conference on earthquake engineering, paper no.497, Acapulco, Mexico 1996, [2]26
- Parkus, H., *Random Processes in Mechanical Sciences*, CISM Courses and Lectures, Springer Verlag, 1969, [2]39, [7]132, [7]133
- Perry, C.L., Fierro, E.A., Sedarat, H., Scholl, R.E., *Seismic Upgrade in San Francisco Using Energy Dissipation Devices*, Earthquake Spectra, vol.9(3), pp.559-579, 1993, [2]25
- Pichler, U., Irschik, H., Krommer, M., Hagenauer, K., *Experimental Verification of a new Piezoelectric Sensor for Beam Deflections*, Proc. of the 15th Symposium "Danubia-Adria" on Experimental Methods in Solid Mechanics, Bertinoro 1998 (R.Beer, ed.), pp. 173-174, [2]50
- Rammerstorfer, F.G., Scharf, K., Fischer, F.D., *Storage tanks under earthquake loading*, Applied Mechanics Reviews, vol.43(11), pp.261-282, 1990, [2]31, [4]85
- Reed, D., Yu, J., Harry, Y., Gardarsson, S., *Investigation of Tuned Liquid Dampers under Large Amplitude Excitation*, ASCE Journal of Engineering Mechanics, vol.124(4), pp.405-413, 1998, [3]55
- Ribakov, Y., Gluck, J., *Active Control of MDOF Structures with Supplemental Electrorheological Fluid Dampers*, Earthquake Engineering and Structural Dynamics, vol.28, pp.143-156, 1999, [8]145
- Richter, H., *Rohrhydraulik*, Springer, Berlin 1934, [4]71
- Roberson, R.E., Synthesis of a Non-linear Dynamic Vibration Absorber, J. Franklin Inst., vol.254, pp.205-220, 1952, [2]36
- Sadek, F., Mohraz, B., Lew, H.S., *Single and multiple-tuned liquid column dampers for seismic applications*, Earthquake Engineering and Structural Dynamics, vol.27, pp.439-463, 1998, [3]63, [9]209
- Sakai, F., Takaeda, S., Tamaki, T., *Tuned liquid column damper – new type device for suppression of building vibrations*, Proceedings International Conference on Highrise Buildings, Nanjing, China, pp.926-931, 1989, [3]55

- Sakamoto, M., Kobori, T., Yamada, T., Takahashi, M., *Practical Applications of Active and Hybrid Response control Systems and their Verifications by Earthquake and Strong Wind Observations*, 1st World Conf. on Struct. Control, Los Angeles, California, USA, pp.WP2:90-99, Los Angeles, published by International Association for Structural Control, August 1994, [8]140
- Samali, B., Kwok, K.C.S., *Use of viscoelastic dampers in reducing wind- and earthquake-induced motion of building structures*, Engineering Structures, vol.17(9), pp.639-654, 1995, [2]27
- Schlacher, K., Irschik, H., Kugi, A., *Aktiver Erdbebenschutz für mehrstöckige Gebäude*, e&i - ÖVE Verbandszeitschrift Elektrotechnik und Informationstechnik, 114.Jg. pp.85-91, 1997, [8]144
- Schlacher, K., Kugi, A., Irschik, H., *Control of earthquake excited nonlinear shear-wall-type structures using input-output linearization*, 10th European Conference on Earthquake Engineering, Duma(ed), 1995, Balkema, Rotterdam, ISBN 90 5410 528 3, [8]144
- Schlacher, K., Kugi, A., Irschik, H., *Control of Earthquake Excited Nonlinear Structures Using a Differentialgeometric Approach*, Computers and Structures, vol.67, pp.83-90, 1998, [8]144
- Schlacher, K., Kugi, A., Irschik, H., *Nonlinear control of earthquake excited high raised buildings by appropriate disturbance decoupling*, Acta Mechanica 125, pp.49-62, 1997, [8]144
- Shinozuka, M., Schueller, G.I., *Stochastic Methods in Structural Dynamics*, Martinus Nijhoff Publishers, 1987, [7]136
- Skinner, R.I., Tyler, R.G., Heine, A.J., Robinson, W.H., *Hysteretic Dampers for the Protection of Structures from Earthquakes*, Bulletin New Zealand Society of Earthquake Engineering, vol.13(1), pp.22-36, 1980, [2]25
- Snowdown, J.C., *Dynamic Vibration Absorbers that have Increased Effectiveness*, J. Eng. for Ind., ASME, Paper No.74-DE-J, pp.940-945, 1960, [2]37
- Socket, H., *Aerodynamik der Bauwerke*, Fr. Vieweg & Sohn, Braunschweig, 1984, [9]171
- Soong, T.T., *Active Structural Control – Theory and Practice*, Longman Scientific&Technical, 1990, [8]150
- Soong, T.T., Dargush, G.F., *Passive Energy Dissipation Systems in Structural Engineering*, Wiley, Chichester England, 1997, [1]1, [1]18, [2]37, [2]38, [2]46, [5]105
- Soong, T.T., Reinhorn, A.M., *Tuned Mass Damper/Active Mass Damper Feasibility Study for a Tall Flexible Building*, NCEER/EERC Short Course on Passive Energy Dissipation, New York, NY, Sept.26-28,1996, [9]176
- Spanos, P.D., *Random Vibration and Statistical Linearisation*, John Wiley & Sons, 1990, [7]133
- Spencer, B.F. Jr., Christenson, R. Dyke, S.J., *Next Generation Benchmark Problem*, Proceedings of the Second World Conference on Structural Control, Kyoto, Japan, 1998, also www-publication: <http://www.nd.edu/~quake/>, [5]106, [6]122
- Spencer, B.F. Jr., Dyke, S.J., Doeskar, H.S., *Part I: Active Mass Driver System, Part II: Active Tendon System*, Special issue of Earthquake Engineering and Structural Dynamics, vol.27(11), pp.1127-1148, 1998, [6]122
- Spencer, B.F. Jr., Sain, M.K., *Controlling Buildings: A New Frontier in Feedback*, Special Issue of the IEEE Control Systems Magazine on Emerging Technology, vol. 17 (6), pp.19-35, 1997, [8]141
- Spencer, B.F., Dyke, S.J., Sain, M.K., Carlson, J.D., *Phenomenological Model for Magnetorheological Dampers*, Journal of Engineering Mechanics, vol.123(3), pp.230-238, 1997, [2]51

- Spencer, B.F.Jr., Dyke, S.J., Deoskar, H.S., Benchmark Problems in Structural Control, Part II: Active Tendon System, Proc. of the 1997 ASCE Structures Congress, Portland, Oregon, April 13-16, 1997, also available: <http://www.nd.edu/~quake/>, [9]162, [9]188
- Stengel, R.F., *Optimal Control and Estimation*, Dover Publications, New York 1993, [8]150
- Stoer J., Burlisch R., *Numerische Mathematik 2*, 3rd edition, Springer Verlag, 1990, [1]15
- Sun, L.M., Fujino, Y., Chaiseri, P., Pacheco, B.M., *The Properties of Tuned Liquid Dampers using a TMD Analogy*, Earthquake Engineering and Structural Dynamics, vol24, pp. 967-976, 1995, [3]55
- Sun, L.M., Fujino, Y., Koga, K., *A model of tuned liquid damper for suppressing pitching motions of structures*, Earthquake Engineering and Structural Dynamics, vol.24, pp.625-636, 1995, [3]55
- Tamura, Y., Fujii, K., Ohtsuki, T., Wakahara, T., Koshaka, R., *Effectiveness of Tuned Liquid Column Dampers in Tower-like Structures*, *Engineering Structures*, 1995, 17(9), 609-621, [2]31, [3]55
- Taylor, D.P., Constantinou, M.C., *Development and Testing of an Improved Fluid Damper Configuration for Structures having High Rigidity*, WWW-publication, Taylor Devices, Inc., www.taylordevices.com, [2]28
- Teramura, A., Yoshida, O., *Development of vibration control system using U-shaped water tank*, Elsevier Science Ltd. 11th World Conference on Earthquake Engineering (edited by Sociedad Mexicana de Ingenieria Sismica, A.C.), paper no. 1343, 1996, [3]63
- Tsai, C.S., Lee, H.H., *Applications of Viscoelastic Dampers to High-Rise Buildings*, Journal of Structural Engineering, vol.119(4), pp.1222-1233, 1993, [2]27
- Walker, J.S., *Fast Fourier Transform*, CRC Press, 1991, [1]11
- Warburton G.B., *Optimum Absorber Parameter for Simple Systems*, Earthquake Engineering and Structural Dynamics, vol.8, pp.197-217, 1980, [2]45
- Warburton, G.B., *Optimum Absorber Parameters for minimising vibration response*, Earthquake Engineering and Structural Dynamics, vol.9, pp.251-262, 1981, [5]104
- Wen, Y.K., *Methods of random vibration for inelastic structures*, Applied Mechanics Reviews, vol.42(2), 1989, [2]24
- Wilde, K., *Base isolation system with shape memory alloy device for elevated highway bridges*, Engineering Structures, vo.22(3), p.222-229, 2000, [2]49
- Wirsching P.H., Paez, T.L., Orith, K., *Random Vibrations*, John Wiley 1995, [7]132, [7]133
- Won, A.J., Pires, J.A., Haroun, M.A., *Stochastic seismic performance evaluation of tuned liquid column dampers*, Earthquake Engineering and Structural Dynamics, vol.25, pp.1259-1274, 1996, [3]65
- Won, A.Y.J., Pires, J.A., Haroun, M.A., *Performance assessment of tuned liquid column dampers under seismic loading*, Int. J. of Non-Linear Mechanics, vol.32(4), pp.745-758, 1997, [3]65
- Wu, J.C., Yang, J.N., Agrawal, A.K., *Applications of Sliding Mode Control to Benchmark Problems*, Earthquake Engineering and Structural Dynamix, vol27(11), pp.1247-1266, 1998, [8]158
- Wu, Z., Soong, T.T., Gattulli, V., Lin, R.C., *Nonlinear Control Algorithms for Peak Response Reduction*, Technical Report NCEER-95-0004, NCEER Buffalo, USA, [8]155
- Xu, Y.L., Samali, B., Kwok, K.C.S., *Control of Along-Wind Response of Structures by Mass and Liquid Dampers*, ASCE Journal of Engineering Mechanics, vol.118(1), 1992, [3]66
- Xue, S.D., Ko, J.M., Xu, Y.L., *Tuned liquid column damper for suppressing pitching motion of structures*, Engineering Structures, vol.23, pp.1538-1551, 2000, [3]66

- Yalla, S.K., Kareem, A., *Optimum Absorber Parameter for Tuned Liquid Column Dampers*, Journal of Structural Engineering, pp.906-915, August 2000, [3]65, [9]209
- Yamazaki, S., Nagata, N., Abiru, H., *Tuned Active Dampers installed in the Miratu Minai (MM) 21 Landmark Tower in Yokohama*, J. Wind Engineering and Indust. Aerodyn., vol 43, pp.1937-1948, 1992, [8]143
- Yang J.N., Agrawal, A.K., Samali, B., Wu, J.C., *A Benchmark Problem For Response Control of Wind-Excited Tall Buildings*, 2nd Europ. Conference on Structural Control, July 2000, Paris, France, [9]162
- Yang, J.N., Akbarpour, A., Ghaemmaghami, P., *Instantaneous Optimal Control Algorithms for Tall Buildings under Seismic Excitations*, Multidisciplinary Center for Earthquake Engineering Research, Buffalo, N.Y., USA, NCEER-87-0007, 1987, [3]56, [8]151
- Yang, J.N., Akbarpour, A., Ghaemmaghami, P., *New Optimal Control Algorithms for Structural Control*, ASCE Journal of Engineering Mechanics, vol.113(9), pp.1369-1386, 1987, [3]56
- Yang, J.N., Li, Z., Danielians, A., Liu, S.C., *Aseismic Hybrid Control of Nonlinear and Hysteretic Structures I*, ASCE Journal of Engineering Mechanics, vol.118(8), pp.1423-1440, 1992, [3]56
- Yang, J.N., Li, Z., Danielians, A., Liu, S.C., *Aseismic Hybrid Control of Nonlinear and Hysteretic Structures II*, ASCE Journal of Engineering Mechanics, vol.118(8), pp.1441-1456, 1992, [3]56
- Yang, J.N., Li, Z., Liu, S.C., *Stable Controllers for Instantaneous Optimal Control*, ASCE Journal of Engineering Mechanics, vol.118(7), pp.1612-1630, 1992, [3]56
- Yang, J.N., Wu, J.C., Agrawal, A.K., HSU, S.Y., *Sliding Mode Control with Compensator for Wind and Seismic Response Control*, Earthquake Engineering and Structural Dynamics, vol.26, pp. 1137-1156, 1997, [8]158
- Yang, J.N., Wu, J.C., Agrawal, A.K., *Sliding Mode Control for Seismically Excited Linear Structures*, Journal of Engineering Mechanics, vol.121(12), pp.1386-1390, 1995, [8]158
- Yang, J.N., Wu, J.C., Reinhorn, A.M., Riley, M., *Control of Sliding Isolated Buildings Using Sliding-Mode Control*, J. of Struct. Engrg., ASCE, vol. 122 (2) pp.179-186, 1996, [8]144
- Yang, C.Y., *Random Vibrations of Structures*, John Wiley 1986, [7]132
- Yeung, N., Pan, A.D.E., *The effectiveness of viscous-damping walls for controlling wind vibrations in multi-story buildings*, Journal of Wind Engineering and Industrial Aerodynamics, vol.77&78, pp.337-348, 1998, [2]29
- Yu, J., Sakahara, T., Reed, D., *A non-linear numerical model of the tuned liquid damper*, Earthquake Engineering and Structural Dynamics, vol.28, pp.671-686, 1999, [3]55
- Zhang, R., Soong, T.T., Mahmoodi, P., *Seismic Response of Steel Frame Structures with Added Viscoelastic Dampers*, Earthquake Engineering and Structural Dynamics, vol.18, pp. 389-296, 1989, [2]27
- Ziegler, F., *Mechanics of Solids and Fluids*, 2nd reprint of second edition, Springer, New York, Vienna, 1998, [1]1, [1]8, [4]73, [4]74, [4]78, [4]79, [8]146, [A]233
- Ziegler, F., *Random Vibrations: A spectral method for linear and nonlinear structures*, Probabilistic Eng. Mech., vol.2(2), 1987, [7]137
- Ziegler, F., *Vorlesungen über Baudynamik*, lecture notes, Technical University of Vienna, 1979, [1]2

Curriculum Vitae

Name: **Hochrainer**

First name: **Markus**

Middle name: **Johannes**

8.3.1973: Born in Schaerding, Austria

10.6.1991: A-level exam

1992-1996: Studies at Johannes Kepler University of Linz
Course: Mechatronik

10.9.1996: Final examination
Diploma thesis: Natural Frequencies of Thin Layered Shells

1996-1997: Postgraduate studies at Loughborough University, UK
Course: Mechatronics and Optical Engineering
Master thesis: Repair of Femoral Neck Fractures, passed with distinction

1997-1998: Postgraduate research assistant in the department of Mechanical Engineering, Prof. H. Irschik, University of Linz, Austria

1998-present: Assistant of Professor F. Ziegler at the Technical University of Vienna, Institute of Rational Mechanics

Research Visits:

Summer 1995: University of Dundee, GB
Department of Applied Physics and Electronic & Mechanical Engineering

Summer 1999: University of Southampton, GB
Institute of Sound and Vibration Research (ISVR)

Summer 2000: State University of New York at Buffalo, NY, USA
Department of Civil, Structural and Environmental Engineering